



HAL
open science

Influence of chain length and crystallinity on the molecular mobility of polylactide and its oligomers

Sareh Mahmoudian Moghaddam

► **To cite this version:**

Sareh Mahmoudian Moghaddam. Influence of chain length and crystallinity on the molecular mobility of polylactide and its oligomers. Other [cond-mat.other]. Normandie Université, 2020. English. NNT : 2020NORMR039 . tel-03473747

HAL Id: tel-03473747

<https://theses.hal.science/tel-03473747>

Submitted on 10 Dec 2021

HAL is a multi-disciplinary open access archive for the deposit and dissemination of scientific research documents, whether they are published or not. The documents may come from teaching and research institutions in France or abroad, or from public or private research centers.

L'archive ouverte pluridisciplinaire **HAL**, est destinée au dépôt et à la diffusion de documents scientifiques de niveau recherche, publiés ou non, émanant des établissements d'enseignement et de recherche français ou étrangers, des laboratoires publics ou privés.



Normandie Université

THESE

Pour obtenir le diplôme de doctorat
Spécialité : Physique
Préparée au sein de l'Université de Rouen Normandie

Influence de la longueur de chaîne et de la cristallinité sur la mobilité moléculaire du polylactide et de ses oligomères

Présentée et soutenue par
Sareh MAHMOUDIAN MOGHADDAM

Thèse soutenue publiquement le 10th Novembre 2020 devant le jury composé de		
M. Eric DANTRAS	MCF-HDR / CIRIMAT, Université Paul Sabatier, Toulouse III, France	Rapporteur
M. Cyrille SOLLOGOUB	Pr. / PIMM, École Nationale Supérieure d'Arts et Métiers, Paris, France	Rapporteur
M. Loïc LE PLUART	Pr. / LMCT, ENSICAEN, Université de Caen Normandie	Examinateur
Mme. Emeline DUDOGNON	MCF / UMET, Université de Lille I, France	Examinatrice
Mme. Elisa PASSAGLIA	Directrice de Recherche/ CNR-ICCOMUOS, Pise, Italie	Examinatrice
Mme. Allisson SAITER	Pr. / GPM, Université de Rouen Normandie	Examinatrice
M. Stefano FIORI	Dr. / Condensia Química S.A., Barcelone, Espagne	Invité
M. Nicolas DELPOUVE	MCF/ GPM, Université de Rouen Normandie	Co-encadrant de thèse
M. Laurent DELBREILH	MCF-HDR / GPM, Université de Rouen Normandie	Directeur de thèse

Thèse dirigée par Dr. Laurent DELBREILH et co-encadrée par Dr. Nicolas DELPOUVE, Groupe de Physique des Matériaux (GPM), UMR 6634





Normandie Université

PhD THESIS

In partial fulfillment of the requirements for the degree of
Doctor of Philosophy in Science
Specialty: Physics
Submitted to the University of Rouen Normandie

Influence of chain length and crystallinity on the molecular mobility of polylactide and its oligomers

Presented and defended by
Sareh MAHMOUDIAN MOGHADDAM

Defended on November 10, 2020 in the presence of the dissertation committee composed of		
Mr. Eric DANTRAS	MCF-HDR / CIRIMAT, University of Paul Sabatier, Toulouse III, France	Reviewer
Mr. Cyrille SOLLOGOUB	Pr. / PIMM, École Nationale Supérieure d'Arts et Métiers, Paris, France	Reviewer
Mr. Loïc LE PLUART	Pr. / LMCT, ENSICAEN, University of Caen Normandie	Examiner
Mrs. Emeline DUDOGNON	MCF / UMET, University of Lille I, France	Examiner
Mrs. Elisa PASSAGLIA	Directrice de Recherche/ CNR-ICCOMUOS, Pisa Italy	Examiner
Mrs. Allisson SAITER	Pr. / GPM, University of Rouen Normandie	Examiner
Mr. Stefano FIORI	Dr. / Condensia Química S.A., Barcelona, Spain	invited
Mr. Nicolas DELPOUVE	MCF/ GPM, University of Rouen Normandie	PhD co-supervisor
Mr. Laurent DELBREILH	MCF-HDR / GPM, University of Rouen Normandie	PhD supervisor

Thesis directed by Dr. Laurent DELBREILH and co-supervised by Dr. Nicolas DELPOUVE, Group of Materials Physics (GPM), UMR 6634



ACKNOWLEDGMENTS

The following manuscript deals with the entire work performed during my PhD thesis. It would be egotistic to think that this work comes only from my own efforts. First of all, I would like to thank my great God that everything human has is due to his generosity.

During my thesis I had the chance to benefit the knowledge of many people with different specialities. I would like give my sincere thanks to my supervisor Dr. Laurent DELBREIL and co-supervisor Dr.Nicolas DELPOUVE who gave me the chance to work with EIRCAP group, I plenty used their constructive advices to improve my knowledge. I would like to thank for all availability, kindness, interest, support, passion, trust and friendship of many people I interacted with them in GPM (Groupe de Physique des Matériaux) during my thesis. Sincere thanks for all juries and reviewers for their fruitful discussion during the defense.

Honestly, I should also appreciate from many people who supported and encouraged me to continue my education in France. When I came to France and started my studies in different domains at the master's level, I had several opportunities to interact with kind people and benift their experiences, advices and knowledge. Here, I would like to thank my dear Dr. Genevieve ROLLET, Dr. Laura HERNANDEZ, Dr.Stéphane PONS, Dr.Sergio VLAIC and all the ones that I dealt with them in Cergy-Pontoise university, Paris VI (Pierre-et-Marie-Curie) university, INSA (Institut des NanoSciences de Paris), ESPCI Paris(PSL).

Finally, I give sincerely this dissertation to my lovely parents with deep gratitude for all their supports since my birth. I love you (momy and dady) so much...

Special thanks to:

Pr. Eric DARGENT, Dr. Allison SAITER, Dr. Antonella ESPOSITO, Marie-Rose GARDA, Eric DONTZOFF, Pr. Cyrille SOLLOGOUB, Dr. Elisa PASSAGLIA, Dr. Stefano FIORI, Alain GUINAULT, Pr. Philippe PAREIGE , Dr. Heideh BOOSTANDOOST, Clément DEMAREST, Dr. Steven ARAUJO, Dr. Xavier MONNIER, Dr. Bienvenu ATAWA, Dr. Yoga Sugama SALIM, Dr. Vincent TOGNETTI, Dr. Rakibul ISLAM, Dr. Aurélie BOURDET, Dr. Nagihan Varol, Clément FOSSE, Alexandre MORVAN, Dr. Benjamin SCHAMMÉ, Blandine QUELENNEC, Tasnim MISSAOU, Dr. Quentin LOZAY, Dr. Lindor DIALLO, Dr. Jorge Arturo SOTO PUENTE, Germain MARTIGNY, Coleen BOOST, Dr. Zahra ASGHARI,...

Table of contains

Introduction.....	1
--------------------------	----------

Chapter 1: Bibliography review

1- Glassy and supercooled liquid state.....	9
1-1 The Dependence of T_g with the cooling rate.....	11
2- Molecular dynamics of glass-forming systems.....	11
2-1 Relaxation phenomenon above T_g in liquid state.....	12
2-2 Relaxation phenomenon below T_g in glassy-state.....	14
3- Models of glass transition.....	15
3-1 Adam-Gibbs's model.....	15
3-2 Free-volume model.....	16
4- Concept of fragility.....	17
5- Cooperativity.....	19
6- Donth's approach.....	21
7- Structural relaxation.....	21
7-1 Fictive temperature.....	22
7-2 Calculation of fictive temperature.....	23
8- Crystallization.....	25
8-1 Crystallization of polymers.....	25
8-2 Three-phase mode.....	26
9- Confinement.....	27
9-1 Finite size effect.....	27
9-2 Chain confinement effects.....	28
9-3 Molecular Weight and chemical structure dependence of T_g and fragility.....	29

10- Different types of confinement.....	32
10-1 Polymer blends.....	32
10-2 Thin films or nanolayers.....	33
10-3 Free surface.....	35
10-4 Multilayer films.....	36
10-5 Semi-crystalline polymers.....	38
Bibliography.....	41

Chapter 2: Materials and experimental techniques

1- Poly (lactic acid) and its oligomers.....	61
2- Thermogravimetric analysis (TGA)	62
3- Differential scanning calorimetry (DSC)	63
3-1 Heat-flux DSC.....	64
3-1-1 Conventional DSC.....	65
3-1-2 Modulated temperature DSC.....	65
3-2 Power-compensated DSC.....	68
4- Fast Scanning Calorimetry (FSC)	68
5- Dielectric Relaxation Spectroscopy (DRS)	70
5-1 Basic principle of DRS.....	70
5-2 Analysis of dielectric spectra.....	73
Bibliography.....	75

Chapter3: Molecular dynamics of Poly Lactic Acid (PDLLA) and its oligomers (OLAs) in amorphous state

1- Fictive temperature.....	81
1-1 Dependence of fictive temperature on cooling rate.....	82
1-2 Thermal lag correction corrections in Flash DSC.....	83
1-3 Non-Arrhenius behavior of fictive temperature's variation.....	84
2- Dielectric relaxations in 3D curves.....	86
3- Conduction effect in DRS data.....	87
4- Normal mode and α-relaxation.....	88
4-1 Shape parameters α_{HN}, β_{HN}	89
4-2 Dielectric relaxation strength $\Delta\epsilon$	90
5- Relaxation map for α-relaxation.....	91
6- Combination of DRS and Flash DSC techniques.....	93
7- Variation of T_g and fragility with molecular weight.....	94
8- Activation energy of α-relaxation.....	96
9- Secondary relaxations.....	97
9-1 Arrhenius behavior of secondary relaxations.....	99
9-2 Activation energy.....	99
9-3 Shape parameters $\alpha_{HN}, \beta_{HN} = 1$	100
Conclusion.....	101
Bibliography.....	103

Chapter4: Crystallization of OLA2700 investigated by Flash DSC and Dielectric Relaxation Spectroscopy (DRS)

1- Flash DSC results.....	111
1-1 Crystallization protocol.....	111
1-2 Normalized heat flow of amorphous and semi-crystalline sample.....	112
1-3 Variation of glass transition temperature T_g	113
1-4 Variation of heat capacity step ΔC_p	114
1-5 Melting temperature T_m and melting enthalpy ΔH_m	117
1-6 Two-phase and/or three-phase model.....	118
2-Dielectric Relaxation Spectroscopy (DRS) results.....	122
2-1 Crystallization protocol.....	122
2-2 Dielectric relaxation in 3D curves.....	122
2-3 Segmental relaxation (α -relaxation)	123
2-3-1 Fragility and glass transition.....	124
2-3-2 Shape parameters α_{HN}, β_{HN}	125
2-3-3 Dielectric relaxation strength $\Delta\varepsilon_\alpha$	126
2-3-4 Activation energy of α -relaxation.....	127
2-4 Secondary relaxations.....	127
2-4-1 Activation energy of secondary relaxations.....	129
2-4-2 Shape parameters $\alpha_{HN}, \beta_{HN} = 1$	129
Conclusion.....	131
Bibliography.....	133
Conclusion and perspectives.....	137
Abbreviations List.....	139

Introduction

When a glass-forming liquid is cooled fast enough, crystallization can be prevented, thus a glass is formed. The transition from liquid to glass is characterized by a brutal increase of both viscosity and relaxation time. A temperature, called glass transition temperature (T_g) is classically defined as the temperature at which the relaxation time attains to 100 seconds (or the viscosity reaches to value 10^{12} Pa.s). The associated dynamics phenomenon is called α -relaxation. Despite almost 100 years of research on the liquid/glass transition, it is not yet clear which molecular mechanisms are responsible for the unique slow-down in molecular dynamics¹.

Molecular dynamics is a critical factor for the development of materials requiring structural flexibility^{2,3} or requesting complicated performances at the molecular level, such as in actuators and sensors^{4,5}. In polymers, various investigations have been done to characterize the structural dependence of molecular dynamics as a function of time and temperature. In recent years, specifically in our group EIRCAP (GPM), molecular dynamic characterizations have been reported for nano-composite polymers⁶, multilayer polymers^{7,8}, plasticized polymers^{9,10} and crystallized polymers¹¹⁻¹³.

Polymeric glass formers have complex architectures in which macromolecules are randomly structured with many entanglements. Thus, there is a real interest in investigating how the average length of the chain influences the molecular dynamics. As previous results seem to suggest, the α -relaxation in polymers (which is related to dynamic glass transition) is strongly correlated to the nature and number of intermolecular interactions between the macromolecules. In this work, we investigate how reducing the chain length (or molecular weight) and crystallization impact the molecular dynamics in our systems such as fragility, glass transition temperature and etc.

The chosen systems are low-molecular-weight polyesters that are oligomers of D/L lactic acid series with different dispersity. They were synthesized and supplied in company "Condensia Química" placed in Spain, by collaboration with Dr. E. Passaglia in "Istituto di Chimica dei Composti Organometallici (ICCOM)"¹⁴ which is based in Italy and Dr. S. Fiori in "Condensia Química". Besides, PDLLA (grade 4042D) which is a well-studied biodegradable and a linear thermoplastic polymer is used in this work.

The fundamental concepts which are needed to understand the different aspects of glassy physics and to interpret the molecular dynamics as well as the relaxation phenomena involved in the polymer glasses are explained in **Chapter1**. More details about the relaxation phenomena, models of glass transition, fragility, cooperativity, crystallization, confinement effects etc. are written in **Chapter1**.

In **Chapter2**, the experimental techniques used in this work are illustrated. For thermal analysis the different types of Differential Scanning Calorimetry (DSC) techniques such as Modulated Temperature DSC (MT-DSC), Hyper DSC and Fast Scanning Calorimetry (Flash DSC) were used. Calorimetry techniques offer a wide dynamic range regarding heating and cooling rates, including isothermal and temperature modulated operation. They allow a

qualitative and quantitative determination of the thermal phenomena accompanying a phase transformation or structural evolution for a broad range of materials¹⁵⁻¹⁷. Besides, in order to study the molecular dynamics of our samples, the Dielectric Relaxation Spectroscopy (DRS) was applied, which is a powerful technique due to a very broad frequency range from milihertz to megahertz¹⁸. DRS allows probing multiple dipolar fluctuations in a variety of structures, such as local molecular fluctuations at low temperatures or the dynamic glass transition (α -relaxation) due to cooperative molecular motions at high temperatures. Details of the all samples are assigned in this chapter.

Chapter3 is focused on the systematic study of the effect of molecular weight on molecular dynamics in amorphous oligomers of lactic acid and PDLLA through calorimetric techniques and Dielectric Relaxation Spectroscopy (DRS). The effect of molecular weight on glass transition temperature and fragility was studied for several polymers¹⁹⁻²¹ specially polystyrene²² but oligomers of lactic acid can give us a new insight for evolution of molecular dynamics with decreasing molecular weight. By using calorimetry techniques we will also investigate the effect of the cooling rates on glass transition especially thanks to Flash DSC which allows exploring thermal properties of materials over a broad range of heating and cooling rates, complementary to rates usually used with DSC. In parallel using Dielectric Relaxation Spectroscopy (DRS) technique over a wide range of temperature and frequency leads to observe several relaxations for samples. From both techniques the glass transition temperature (T_g) and fragility index (m) will be obtained and compared. The temperature dependence of the cooling rate obtained by Flash DSC will be compared to the temperature dependence of the relaxation times obtained from DRS.

In **Chapter4**, the molecular dynamics in semi-crystalline oligomer of lactic acid with $\bar{M}_w = 2700$ g/mol is investigated. This work is in continuity of previous studies performed in EIRCAP (GPM)²³⁻²⁶ and that will be contribute to increase the knowledge about amorphous phase dynamics in semi-crystalline systems by investigating semi-crystalline oligomers, which has not been done yet in EIRCAP. The glass transition and fragility can be affected by crystals in semi-crystalline polymers, however the discussion about the influence of the crystalline phase on the fragility index (m) is still intense²⁷. Some authors associate the variation of fragility index in semi-crystalline polymers to the establishment of the RAF^{28,29} (Rigid Amorphous Fraction) whereas other people suggest that if the polymer backbone is less flexible the fragility is more affected due to confined amorphous phase^{30,31}. No global law has been established till now, as the variation of fragility index with the crystallization conditions depends on the considered polymer³². So semi-crystalline polymers create a worthy model to study the dynamic behavior of polymeric chains²⁷.

Bibliography

- (1) Arrow, K. J. Through the Glass Lightly. *Science* **1995**, *267* (5204), 1617–1618. <https://doi.org/10.1126/science.267.5204.1617-f>.
- (2) Eggeman, A. S.; Illig, S.; Troisi, A.; Siringhaus, H.; Midgley, P. A. Measurement of Molecular Motion in Organic Semiconductors by Thermal Diffuse Electron Scattering. *Nat. Mater.* **2013**, *12* (11), 1045–1049. <https://doi.org/10.1038/nmat3710>.
- (3) Bath, J.; Turberfield, A. J. DNA Nanomachines. *Nat. Nanotechnol.* **2007**, *2* (5), 275–284. <https://doi.org/10.1038/nnano.2007.104>.
- (4) Dhotel, A.; Chen, Z.; Delbreilh, L.; Youssef, B.; Saiter, J.-M.; Tan, L. Molecular Motions in Functional Self-Assembled Nanostructures. *Int. J. Mol. Sci.* **2013**, *14* (2), 2303–2333. <https://doi.org/10.3390/ijms14022303>.
- (5) Pei, Z.; Yang, Y.; Chen, Q.; Terentjev, E. M.; Wei, Y.; Ji, Y. Mouldable Liquid-Crystalline Elastomer Actuators with Exchangeable Covalent Bonds. *Nat. Mater.* **2014**, *13* (1), 36–41. <https://doi.org/10.1038/nmat3812>.
- (6) Couderc, H. Nanocomposites: Polyester Amorphe-Montmorillonite. Influence Des Nanoparticules Sur Les Dynamiques Des Relaxations Moléculaires. PhD thesis, France, 2008.
- (7) Fernandes Nassar, S. Understanding of the Relationship between the Microstructure of Polylactide, Its Macromolecular Mobility and Its Barrier Properties for the Creation of Packaging from Tomorrow's Renewable Resources. PhD thesis, Paris-Saclay, France, 2017.
- (8) Arabeche, K. Etude de La Mobilité Moléculaire Dans Les Systèmes Amorphes Complexes : Multicouches de Polycarbonates de Bisphénol A (PC) / Polyméthacrylate de Méthyle (PMMA) de l'échelle Microscopique à l'échelle Nanoscopique. PhD thesis, Rouen, Normandy, France, 2011.
- (9) Araujo, S.; Delpouve, N.; Domenek, S.; Guinault, A.; Golovchak, R.; Szatanik, R.; Ingram, A.; Fauchard, C.; Delbreilh, L.; Dargent, E. Cooperativity Scaling and Free Volume in Plasticized Polylactide. *Macromolecules* **2019**, *52* (16), 6107–6115. <https://doi.org/10.1021/acs.macromol.9b00464>.
- (10) Burgos, N.; Tolaguera, D.; Fiori, S.; Jiménez, A. Synthesis and Characterization of Lactic Acid Oligomers: Evaluation of Performance as Poly(Lactic Acid) Plasticizers. *J. Polym. Environ.* **2014**, *22* (2), 227–235. <https://doi.org/10.1007/s10924-013-0628-5>.
- (11) Monnier, X. Molecular Dynamics in Complex Polymer Systems : From Anisotropy to Confinement Effects. PhD thesis, Rouen, Normandy, France, 2017.
- (12) Delpouve, N. Etude de La Microstructure et Des Phénomènes de Relaxation Dans Un Biopolyester : Le Poly(Acide Lactique). PhD thesis, Rouen, Normandy, France, 2009.
- (13) Hamonic, F. Etude de La Mobilité Moléculaire Dans Des Polyesters Synthétiques: Mise En Évidence de l'anisotropie. PhD thesis, Rouen, Normandy, France, 2012.
- (14) Cicogna, F.; Coiai, S.; De Monte, C.; Spiniello, R.; Fiori, S.; Franceschi, M.; Braca, F.; Cinelli, P.; Fehri, S. M. K.; Lazzeri, A.; Oberhauser, W.; Passaglia, E. Poly(Lactic Acid) Plasticized with Low-Molecular-Weight Polyesters: Structural, Thermal and Biodegradability Features: PLA Plasticized with Low-Molecular-Weight Polyesters. *Polym. Int.* **2017**, *66* (6), 761–769. <https://doi.org/10.1002/pi.5356>.
- (15) Wunderlich, B. *Thermal Analysis of Polymeric Materials*; Springer, Berlin, Heidelberg, 2005.
- (16) Reading, M.; Craig, D. Q. M. *Thermal Analysis of Pharmaceuticals*; CRC Press, 2006.

- (17) Höhne, G. W. H.; Hemminger, W. F.; Flammersheim, H.-J. *Differential Scanning Calorimetry*; Springer Berlin Heidelberg: Berlin, Heidelberg, 2003. <https://doi.org/10.1007/978-3-662-06710-9>.
- (18) Lunkenheimer, P.; Loidl, A. Dielectric Spectroscopy of Glass-Forming Materials: α -Relaxation and Excess Wing. *Chem. Phys.* **2002**, *284* (1–2), 205–219. [https://doi.org/10.1016/S0301-0104\(02\)00549-9](https://doi.org/10.1016/S0301-0104(02)00549-9).
- (19) Elfadl, A. A.; Herrmann, A.; Hintermeyer, J.; Petzold, N.; Novikov, V. N.; Rössler, E. A. Molecular Weight Dependence of Fragility in Polymers. *Macromolecules* **2009**, *42* (17), 6816–6817. <https://doi.org/10.1021/ma900666z>.
- (20) Beevers, R. B.; White, E. F. T. Physical Properties of Vinyl Polymers. Part 1.—Dependence of the Glass-Transition Temperature of Polymethylmethacrylate on Molecular Weight. *Trans Faraday Soc* **1960**, *56* (0), 744–752. <https://doi.org/10.1039/TF9605600744>.
- (21) Baker, D. L.; Reynolds, M.; Masurel, R.; Olmsted, P. D.; Mattsson, J. Chain-Length, Flexibility and the Glass Transition of Polymers. *ArXiv191113278 Cond-Mat Physicsphysics* **2019**.
- (22) Santangelo, P. G.; Roland, C. M. Molecular Weight Dependence of Fragility in Polystyrene. *Macromolecules* **1998**, *31* (14), 4581–4585. <https://doi.org/10.1021/ma971823k>.
- (23) Delpouve, N.; Saiter, A.; Mano, J. F.; Dargent, E. Cooperative Rearranging Region Size in Semi-Crystalline Poly(L-Lactic Acid). *Polymer* **2008**, *49* (13–14), 3130–3135. <https://doi.org/10.1016/j.polymer.2008.04.045>.
- (24) Saiter, A.; Delpouve, N.; Dargent, E.; Saiter, J. M. Cooperative Rearranging Region Size Determination by Temperature Modulated DSC in Semi-Crystalline Poly(L-Lactide Acid). *Eur. Polym. J.* **2007**, *43* (11), 4675–4682. <https://doi.org/10.1016/j.eurpolymj.2007.07.039>.
- (25) Delpouve, N.; Saiter, A.; Dargent, E. Cooperativity Length Evolution during Crystallization of Poly(Lactic Acid). *Eur. Polym. J.* **2011**, *47* (12), 2414–2423. <https://doi.org/10.1016/j.eurpolymj.2011.09.027>.
- (26) Esposito, A.; Delpouve, N.; Causin, V.; Dhotel, A.; Delbreilh, L.; Dargent, E. From a Three-Phase Model to a Continuous Description of Molecular Mobility in Semicrystalline Poly(Hydroxybutyrate-*Co*-Hydroxyvalerate). *Macromolecules* **2016**, *49* (13), 4850–4861. <https://doi.org/10.1021/acs.macromol.6b00384>.
- (27) Ngai, K. L.; Roland, C. M. Intermolecular Cooperativity and the Temperature Dependence of Segmental Relaxation in Semicrystalline Polymers. *Macromolecules* **1993**, *26* (11), 2688–2690. <https://doi.org/10.1021/ma00063a008>.
- (28) Arnoult, M.; Dargent, E.; Mano, J. F. Mobile Amorphous Phase Fragility in Semi-Crystalline Polymers: Comparison of PET and PLLA. *Polymer* **2007**, *48* (4), 1012–1019. <https://doi.org/10.1016/j.polymer.2006.12.053>.
- (29) Brás, A. R.; Malik, P.; Dionísio, M.; Mano, J. F. Influence of Crystallinity in Molecular Motions of Poly(L-Lactic Acid) Investigated by Dielectric Relaxation Spectroscopy. *Macromolecules* **2008**, *41* (17), 6419–6430. <https://doi.org/10.1021/ma800842a>.
- (30) Napolitano, S.; Wübbenhorst, M. Slowing Down of the Crystallization Kinetics in Ultrathin Polymer Films: A Size or an Interface Effect? *Macromolecules* **2006**, *39* (18), 5967–5970. <https://doi.org/10.1021/ma061304u>.
- (31) Lan, T.; Torkelson, J. M. Fragility-Confinement Effects: Apparent Universality as a Function of Scaled Thickness in Films of Freely Deposited, Linear Polymer and Its

- Absence in Densely Grafted Brushes. *Macromolecules* **2016**, *49* (4), 1331–1343. <https://doi.org/10.1021/acs.macromol.5b02489>.
- (32) Hamonic, F.; Miri, V.; Saiter, A.; Dargent, E. Rigid Amorphous Fraction versus Oriented Amorphous Fraction in Uniaxially Drawn Polyesters. *Eur. Polym. J.* **2014**, *58*, 233–244. <https://doi.org/10.1016/j.eurpolymj.2014.06.014>.

Chapter 1: Bibliography review

This chapter introduced some critical concepts in order to understand the different aspects of glassy physics and interpret the molecular dynamics as well as the relaxation phenomena involved in the polymer glasses. Focus is also done on the effect of covalent backbone length on the molecular mobility in amorphous and crystalline polymers and oligomers.

In this work, the influence of molecular weight and crystallization can be considered as a confinement effect, where confining a system to a scale comparable to its characteristic length (for macromolecules, gyration radius for example) results in significant deviations of the structural, dynamical and thermo-dynamical properties with respect to the bulk. Many studies demonstrate effects of different types of confinement on the dynamic properties around glass transition behavior¹⁻⁴.

1- Glassy and supercooled liquid states

We have been producing glass for more than 5000 years. Examples include tools to hunt, packaging to preserve our food, transparent panels to isolate us from cold, and thin layers where the simple touch of our fingers is transformed into information. All of these are glass. Under this generic name, we identify a class of materials showing a solid-like response, though lacking (like liquids) the long-range order of crystals.

Glasses are prepared by quickly cooling or pressurizing a liquid, which induces a slow-down in molecular motion. When these operations are performed at a constant rate, the timescale of structural relaxation eventually exceeds the time allowed for equilibration (the inverse of the cooling/pressuring rate). This brings the system out of equilibrium and is referred to glass transition. Once a liquid is cooled down fast enough to avoid crystallization, it will turn into a disorder. Such materials are called glass-formers which exhibit very different chemical nature and can be formed in many ways⁵. Glass formers include oxides⁶, chalcogenide⁷, halides⁸, organic components⁹, polymers¹⁰ and etc.

Despite almost 100 years of research on the liquid/glass transition, it is not yet clear which molecular mechanisms are responsible for the unique slow-down in molecular dynamics. As Nobel Laureate P. W. Anderson¹¹ stated, glass transition is the "...most interesting unsolved problem in solid state theory...

When a glass-forming liquid is cooled fast enough, its viscosity reach to value 10^{12} Pa.s or relaxation time attain to 100 seconds at a temperature which is called glass transition temperature T_g ¹². The associated dynamics phenomenon is called α -relaxation. The more crucial question is: what kind of changes at the molecular level induce such a tremendous increase in relaxation time in a liquid as it approaches to glass transition? Many models and theories can explain the nature of glass transition phenomenon in different glass formers such as thermodynamics models¹³, mode coupling theory¹⁴, Adam and Gibbs theory¹⁵, free volume approach¹⁶ and etc.

The thermodynamic properties (volume, enthalpy, entropy...) of the glass formed going through glass transition leave the equilibrium, so a glass is then a non-equilibrium state.

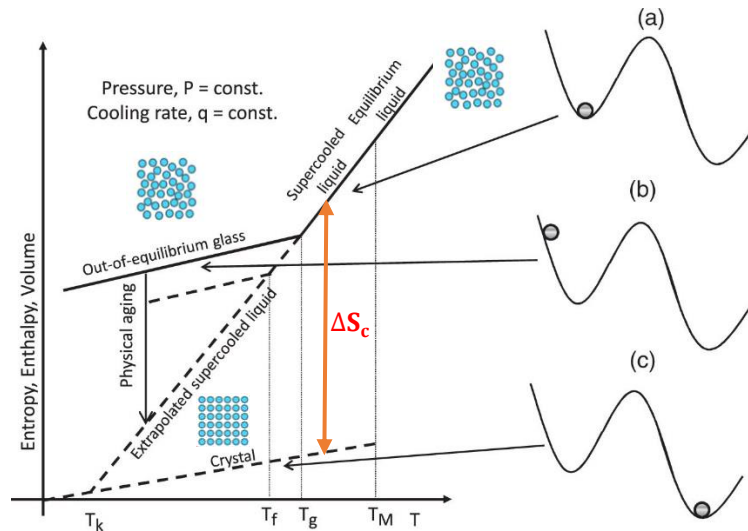


Figure1-1 Schematic picture of the temperature dependence of a thermodynamics properties of a glass forming liquid. (According to D. Cangialosi's article¹⁷.) T_K : Kauzmann's temperature. T_g : glass transition temperature. T_M : melting temperature. ΔS_c : configurational entropy $\Delta S_c = S_{\text{liquid}} - S_{\text{crystal}}$.

Figure1-1 depicts the variation of thermodynamic properties in glass-forming systems at constant pressure as a function of temperature leading to the formation of an amorphous solid, namely a glass. In **Figure1-1**, following temperatures are indicated:

- (i) T_M , is the melting temperature. At this temperature an abrupt discontinuity of the thermodynamic properties turn crystals into liquid state through a first order transition. At high temperature in the liquid state, the glass-forming liquid is in equilibrium. The viscosity is low ($\sim 10^{-1} \text{Pa}\cdot\text{s}$) and the molecular motion is high. Upon sufficient cooling rate to avoid crystallization, the system is in metastable state below melting temperature what is called supercooled liquid.
- (ii) T_g , is the temperature for which the supercooled liquid transforms into a glass at the cooling rate of the experiment. On the other word, the intersection of the liquid and glassy lines defines glass transition temperature T_g . Upon cooling, the viscosity increases and the molecular mobility decreases. The thermodynamic properties gradually decrease up to change in slope at glass transition temperature where the glass-forming liquid vitrifies. Comparing with melting, vitrification occurs relatively over a wide range of temperature.
- (iii) T_f , is fictive temperature. There is a common way to define the thermodynamic state of a glass, that was long ago introduced by Tool¹⁸; that is, the temperature at which a glass in a certain thermodynamic state would be at equilibrium.
- (iv) T_K , Kauzmann temperature, is the temperature at which the entropy of the supercooled liquid equal with the corresponding crystal.

Right part of **Figure1-1** shows the stability plots for (a) the metastable supercooled liquid; (b) the out of equilibrium glass and (c) the stable crystal.

1-1 The Dependence of T_g with the cooling rate

The kinetic nature of glass transition is well established by dependence of T_g with cooling rate^{19,20} which is defined as $\beta_c = \frac{dT}{dt}$. If the cooling process is viewed as a series of temperature steps, then cooling rate shows the time t spent at each temperature T ($t = \frac{T}{\beta_c}$). This allows us to introduce the notion of relaxation time τ which is the time required for the system to reach equilibrium after external perturbation. Thus the liquid falls out of equilibrium when t is smaller than the relaxation time τ , on the other hand the system can not stay in equilibrium by lack of time, so this shows the temperature dependence of relaxation time.

As you see in **Figure1-2**, fast cooling rate leads to high glass transition temperature while slowing down cooling rate will reduce the glass transition temperature because by applying high cooling rate the rearrangement of molecules will be low so molecules will be frozen more quickly.

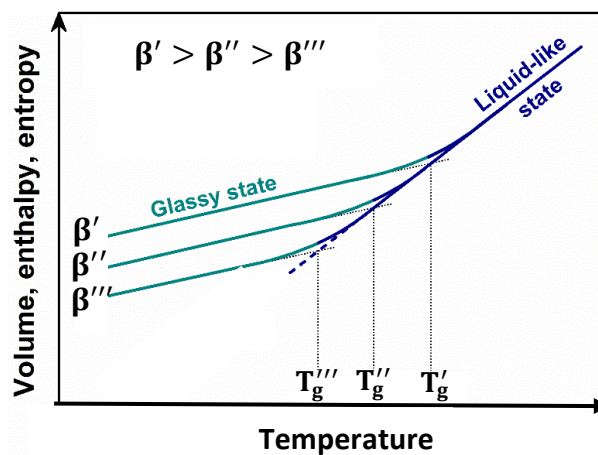


Figure1-2 Schematic picture of the temperature dependence of the thermodynamic properties of a glass forming liquid for different cooling rates.

2- Molecular dynamics of glass-forming systems

In glass-forming materials different atomic and molecular motions exist above and below glass transition. Upon cooling from a liquid, molecular motions are slowed down as approaching the supercooled liquid state. This slowing down extends from picoseconds to almost one hundred seconds in the glass transition area. For polymers, different relaxation processes exist depending on the size of the molecular segments involve in the movement. Generally we can distinguish two major types of molecular motions:

(i) Molecular mobility around glass transition which is called "segmental motion", since it is cooperative and involves the movement of long chain segments of polymers. Such molecular dynamics is also identified as α -relaxation because of its typical appearance at a

lower frequency in a dielectric relaxation profile and is characterized by an Arrhenius to a non-Arrhenius dependence of the relaxation time when reaching glass transition²¹.

(ii) Molecular mobility below the vicinity of glass transition which is called “localized motion”, since it involves the local movement of group of molecules within the macromolecule chain segment of polymers. When the temperature is decreased from the vicinity of the glass transition towards below, α -relaxation process is becoming slow and so its relaxation time will be often longer than the time scale of experimental observation. Thus, fast local motions of individual molecules or parts of molecules may occur, designated as secondary relaxation processes (beta, gamma, delta,...). Fast local motions take place at different scales and the temperature dependence of their relaxation time is characterized by an Arrhenius behavior. These processes may have inter and/or intra molecular origin.

Among different secondary relaxation phenomena, the slowest one is called Johari-Goldstein (JG) relaxation, which has an intermolecular origin. It is assumed that this process is related to rotation of entire molecules²². In the 1970s scientists Johari and Goldstein demonstrated the existence of a secondary relaxation in completely rigid molecules²³. Today, Johari-Goldstein relaxation is believed to be a universal feature of all glass formers and serves as the precursor of the primary α -relaxation²⁴. Other secondary relaxations (generally faster than the JG relaxation) exist and originate from intramolecular reorientations of some flexible parts of the molecules.

In polymers, chain motions may be affected by molecular weight, geometric factors, polarity, crystallization and etc. Thus the molecular motions and the relaxation maybe arise from different interaction: (1) Covalent bonds along the main macromolecular chains which are strong. (2) Weak bonds which have less energy.

2-1 Relaxation phenomenon above T_g in liquid-state

The combination of relaxation phenomena is still a challenge in order to understand the molecular dynamics in glass-forming liquids. However, according to their chemical nature or their structures, glass-forming liquids can display a deviation more or less from Arrhenius to the non-Arrhenius behavior. One of the most challenging is the explanation of the Arrhenius to non- Arrhenius temperature dependence of α -relaxation as approaching the glass transition. In the supercooled liquid state ($T > T_g$), the segmental relaxation corresponds to the relaxation process which is associated to the molecular rearrangement.

By using experimental technique like dielectric spectroscopy, the characteristic relaxation times (τ) of α -relaxation are measured as a function of temperatures, so glass transition is observed by assuming that, it occurs when the segmental relaxation time reaches 100s.

The simplest model relevant for the description of the relaxation time dependence above the glass transition temperature in the supercooled liquid state is the Arrhenius activation model. The Arrhenius like behavior law is given by the following equation:

$$\tau(T) = \tau_{\infty} \exp\left(\frac{E_a}{k_B T}\right) \quad (1.1)$$

Here, τ_∞ is the relaxation time at infinite temperature, E_a is the activation energy which is related to the energy needed to overcome the barrier leading to molecular motions. k_B is Boltzmann constant. Motions associated to δ and γ -relaxations display low activation energies due to their localized nature, whereas α and β -relaxations present higher activation energies.

Generally, from very high temperatures toward cross over temperature T_c , which has been predicted by the mode coupling theory²⁵ (**Figure1-3**), most of glass-forming liquids exhibit an exotic temperature dependence of molecular mobility, the secondary relaxations (β, γ, δ) still describe an Arrhenius behavior whereas the slowing down of the α -relaxation cannot be outlined by an Arrhenius tendency. The observed non-Arrhenius behavior can be described by the empirical Vogel-Fulcher-Tamman^{26,27} (VFT) equation:

$$\tau(T) = \tau_\infty \exp\left(\frac{DT_V}{T-T_V}\right) \quad (1.2)$$

Where τ_∞ , T_V and D are fitting parameters. D is the strength parameter (related to fragility, introduced in next section) and T_V is a characteristic temperature below T_g which is called Vogel temperature. T_V is a hypothetical thermodynamic temperature at which cooperative molecular mobility is regarded to be close to zero.

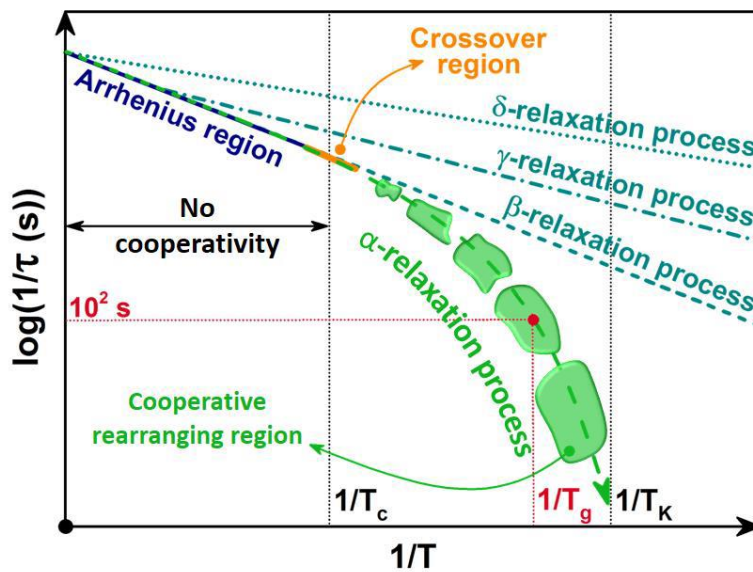


Figure1-3 Schematic plot of the temperature dependence of relaxation processes for a glass-forming liquid upon cooling²⁸. T_c corresponds to the cross-over temperature where α and β -relaxation merge. T_g is the glass transition temperature where relaxation time reach hundred seconds. T_k defines Kauzmann's temperature. Plot was taken from the thesis of Xavier Monnier²⁸.

In the liquid state, because of the strong coupling between the primary and secondary processes, it is very difficult to characterize secondary relaxation times. In this case, the temperature dependence of the secondary relaxation times can be more complex (a single VFT equation is not sufficient). Ngai²⁹ indicated that most of glass forming liquids, including polymers, present a crossover between two differentiated temperature dependence of the relaxation time at a temperature T_c . From very high temperatures to T_c , the relaxation times related to $\alpha, \beta, \gamma, \delta$ relaxations upon cooling shows and Arrhenius behavior (**Figure1-3**). At T_c

the α -relaxation becomes cooperative, that was introduced by Adam and Gibbs 's theory (will be explained in section4), so α -relaxation exhibits non-Arrhenius behavior. In order to provide a good fit for relaxation data in the temperature range between T_c to T_g , two VFT equations are required (one at high and one at low temperature).

2-2 Relaxation phenomenon below T_g in glassy-state

Upon cooling, structure of the liquid becomes "frozen" and the system reaches the glassy state. Far from equilibrium, the time scale of structural relaxation below T_g is extremely long. Nowadays, only predictions of the α -relaxation times may be conducted. Thus, in the glassy state, usually just secondary relaxations coming from some local molecular motions are experimentally measured. Although, τ_α is an undetermined quantity below the glass transition, but knowledge of the time scale of the α -relaxation below T_g is crucial to select suitable storage conditions of amorphous materials against a potential crystallization and chemical instability. Consequently, estimation of τ_α in the glassy state is substantial.

One of the main characteristic features of secondary relaxations is that they can be observed at very low temperatures, far below T_g . Hence, they are considered as the main source of motion in the glassy state. The temperature dependence of these secondary relaxation times in the glassy state is usually described by Arrhenius equation (**Eq.1.1**).

Sometimes, identification of the nature of secondary relaxations is very complex due to their distinct dielectric spectra appearance. For example, Johari-Goldstein (JG) relaxation process is assumed to have much lower magnitude than the structural α -relaxation, therefore, secondary relaxation of intermolecular nature may not be visible in the dielectric spectra. By contrast with a well pronounced relaxation peak, the high-frequency α -peak shows an excess wing (high frequency wing). This excess wing which is demonstrated in **Figure1-4** can be well described by a power law:

$$\varepsilon'' \sim \vartheta^{-b} \quad (1.3)$$

As you see in **Figure1-4**, at higher frequencies than secondary relaxation processes, some other feature appears like a peak which is called boson peak which reflects the vibrational properties of systems.

Already, the excess wing was interpreted as an inseparable part of the α -relaxation³⁰. Nowadays, the excess wing is believed to be an unresolved JG relaxation, concealed by the most intense α -peak (**Figure1-5**). The interpretation of both the excess wing and nature of secondary relaxations can be resolved by performing dielectric studies at elevated pressure³¹.

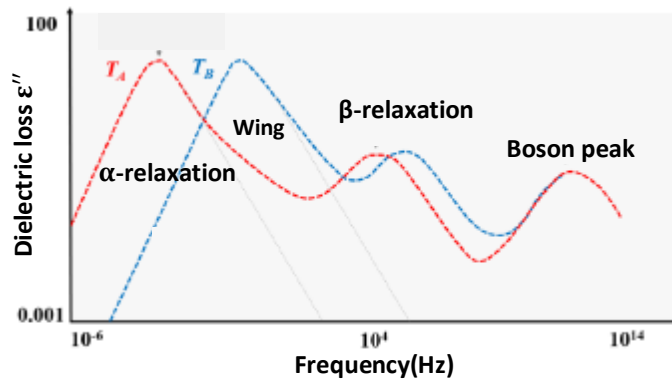


Figure1-4 schematic view of dielectric loss process as function of frequency at two temperatures T_A and T_B displaying the α -relaxation, the β -relaxation and an inflection in the high frequency flank of the α -process called excess wing. At frequencies higher than the β -process, a boson peak could be visible, reflecting vibrational properties of the system.(Adapted from F. Kremer's article³².)

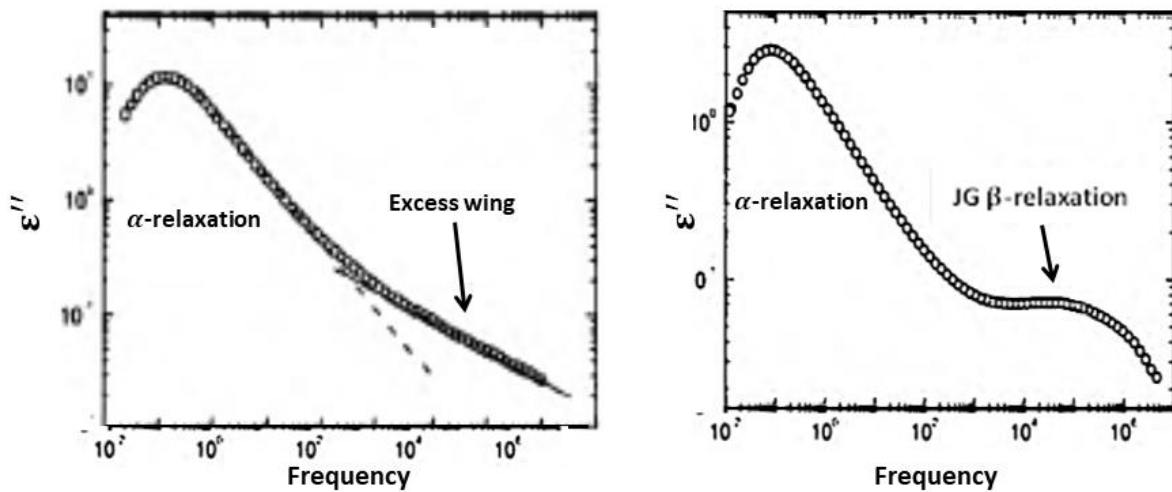


Figure1-5 Dielectric spectra of glass-forming systems (Adapted from K. L. Ngai 's article²⁴). (a) Solid line shows the additional power law with a weaker slope compared to the α -relaxation peak. (b) shows JG- β relaxation.

3-Models of glass transition

Numerous theories, models and approaches^{13,33-35} have been proposed to explain the fundamental nature of glass transition in glass-forming liquids. The validity of different theoretical descriptions have been widely studied^{5,12,36}. However there is no general accepted theoretical model which can describe all aspects of glass transition. In this chapter we confine briefly our consideration on two models: Adam-Gibbs's model and free-volume model.

3-1 Adam-Gibbs's model

Adam and Gibbs in 1965¹⁵ proposed a theory in which the configurational entropy S_c determines the rate of α -relaxation. In fact the central idea of entropy based systems arises from the slowing down of relaxation dynamics upon cooling, coming from the decline of

configurational entropy and consequently the amount of available configurations. Adam and Gibbs's approach is the most popular entropy based model. They suggested that relaxation processes involved in glass-forming liquids upon cooling take place through cooperative rearrangements of molecular groups. In other words, the motion of such groups are only possible if a given number of neighboring molecular groups are also in motion. They discussed that the number of molecular groups involved in those cooperative rearrangements grows by decreasing temperature.

The size of cooperative rearranging region (CRR), is defined as the smallest region which can be subjected to a new configuration without requiring any simultaneous configurational change on and outside its limit. Those subsystems are assumed to relax independently of the others. The CRR size increases as temperature decreases, namely the configurational entropy S_c decreases. Thus, by assuming that the energy barrier to overcome in order to relax is proportional to the size of the region, the temperature dependence of the relaxation times τ of glass-forming liquids approaching the glass transition is then described by the following equation:

$$\tau(T) = \tau_0 \exp\left(\frac{C}{TS_c}\right) \quad (1.4)$$

Where τ_0 and C are constant. This equation states the relationship between relaxation time and configurational entropy of a glass-forming liquid when approaching glass transition.

3-2 Free-volume model

The concept of free volume V_f , and the idea that the mobility of molecules at any temperature is primarily controlled by the free volume, was proposed by Doolittle³⁷ in explaining the non-Arrhenius temperature dependence of the viscosity η , of liquids of low molecular weight. The free volume V_f , is defined as the difference between the total specific volume V and occupied volume V_0 . The Doolittle equation is:

$$\ln \eta(T) = \ln A + B(V - V_f(T))/V_f(T) \quad (1.5)$$

Where A , B are constants, describes well the temperature dependence of the viscosity. The physical basis for free volume can be understood from the theory of Turnbull and Cohen³⁴. According to them, motion of a molecule can occur only a void having volume greater than a certain critical value is available for it to move into. The voids are created by fluctuations or the redistribution of free volume coming from the collective or cooperative motion of molecules. On cooling, the glass transition region begins when the free volume falls below some value at which the molecular mobility is low enough that the material cannot reach equilibrium.

In other words Turnbull and Cohen assumed that, the free volume in viscous liquid is continuously redistributed without any expense of local free energy and molecular mobility is associated with movement of atoms or molecules into voids of approximately equal or greater than that of molecular dimensions. Motion of molecules lead to redistribution of the free volume V_f .

The free-volume model can be used to describe the temperature dependence of relaxation process (such as α -relaxation) or viscosity. However the model does not address the temperature dependence of the viscoelastic response of motion on the longer-length scales in polymers.

4- Concept of fragility

Different supercooled liquids can be classified on the basis of the temperature dependence of dynamic and (or) thermodynamic quantities by concept of fragility. The fragility concept, in its modern form, has been introduced and developed by Angell³⁸⁻⁴⁰. This parameter describes, in its kinetic (dynamic) version, how fast the α -relaxation time (τ_α) increases with decreasing temperature on approaching the glass transition temperature, T_g , defined as the temperature where τ_α becomes equal to 100s. In fact kinetic fragility index (m), characterizes the dynamic properties of a liquid and changes in the molecular mobility as approaching glass transition temperature. This parameter is defined as:

$$m = \left. \frac{d(\log \tau)}{d\left(\frac{T_g}{T}\right)} \right|_{T=T_g} \quad (1.6)$$

The value of relaxation time depends on experimental techniques and is rather difficult to access when the value of τ_α is large, so for these reasons, in non-polymeric liquids, the fragility is usually defined through the temperature dependence of the shear viscosity η ³⁹.

Glass-forming liquids can be classified into three categories by using the fragility index m ³⁹: “fragile”, “intermediate” and “strong”. “Strong” systems have low values of fragility (m is close to 16) and show a weak temperature dependence of τ_α , that can be described by an Arrhenius law, while “fragile” systems have high value of index m (up to 200-250) and show (close to T_g) a much faster temperature dependence of τ_α , which is described by non-Arrhenius behavior (**Figure1-6**). Thus, “strong” glass-formers are considered more physically stable than “fragile” one. In The other words, in a fragile material physical properties change abruptly as it approaches T_g , whereas in strong materials they show a strong resistance to change with temperature, undergoing a relatively smooth transition from the rubbery state to the glassy state. Hence, fragility of a glass-forming liquid was proposed to be a measure of structural stability, and thus an important parameter to characterize glass formation.

Understanding the structural parameters of polymers that control their fragility and differentiate them from other glass-forming systems remains a challenge. The flexibility of side groups relative to the flexibility of the backbone is the most important factor controlling fragility in polymers^{41,42}. Already, Ngai et al.⁴³ related fragility of polymers to chain stiffness and side group bulkiness. Usually, polymers with stiff backbones such as polycarbonates (PC)⁴² and polymers with flexible backbones but bulky side groups, such as polystyrene (PS) show high fragility^{42,44,45}, whereas polymers with flexible backbones and no side groups have low fragility. For the most common type of polymeric structure, C-C or Si -O containing side groups, the fragility increases with increasing relative stiffness of side groups versus the backbone⁴¹. Other studies reveal that oligomers usually exhibit low or intermediate fragility ($m \sim 60-90$), similar to that of small molecular weight liquids with van der Waals

interactions⁴⁶. Generally an increase in chain length leads to an increase in fragility in most polymers^{47,48}, but in some polymers with flexible backbones such as polydimethylsiloxane (PDMS) and polyisoprene (PIP) with increase in chain length there is no (or very weak) change in fragility^{42,44}. Beside structural parameters of polymers that control their fragility, the presence and amount of crystals in polymers can affect on value of fragility⁴⁹.

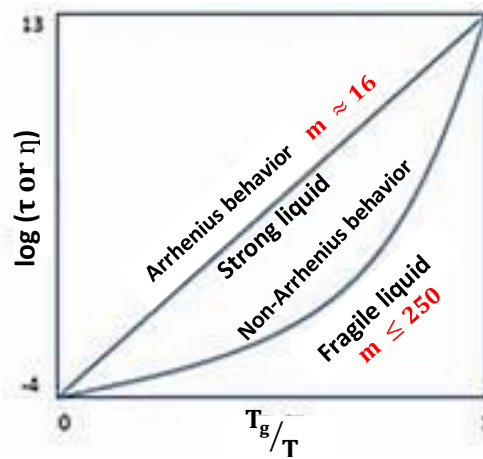


Figure1-6 Angell's plot showing the variations of relaxation time τ , or viscosity η , as a function of normalized temperature T_g/T .

According to many studies, there is a correlation between the value of the fragility and other properties of the supercooled liquids, such as the stretching of the decay of the correlation functions at the glass transition temperature^{50,51}, the temperature dependence of the shear elastic modulus in liquids (shoving mode)⁵²⁻⁵⁴, the vibrational properties of the glass at $T \rightarrow 0$ ⁵⁵ and etc. Other researchers have tried to extract physical information on the nature of the glass transition from the existence of these correlations^{56,57}.

Similar to the kinetic fragility that emerges from the Angell's plot, the concept of thermodynamic fragility (m_T) can be present by the drop in excess entropy $\Delta S_{ex}(T)$ approaching T_g . $\Delta S_{ex}(T)$ is defined as the difference between the entropy of the liquid and the entropy of the stable crystal:

$$m_T = \left. \frac{d\left(\frac{\Delta S_{ex}(T_g)}{\Delta S_{ex}(T)}\right)}{d\left(\frac{T_g}{T}\right)} \right|_{T=T_g} \quad (1.7)$$

Eq.1.7 gives a plot very similar to the Angell plot. This quantity naturally appears when the Adam-Gibbs's relation is used to work out a link between kinetic and thermodynamic fragility. The Adam and Gibbs model¹⁵, provided the first quantitative relation between the thermodynamic and kinetic properties of a liquid. Several approaches to correlate the kinetic fragility of supercooled liquids with thermodynamic behaviors have been used, they have mainly concentrated on changes in heat capacity⁴⁵ and entropy⁵⁸⁻⁶⁰. The kinetic fragility index can reflect nontrivial thermodynamic properties. In one of these approaches, Angell and co-workers have argued that the dynamic fragility, should be related to the rate of configurational entropy variation, because the relaxation time of the α -relaxation process is

correlated to the configurational entropy of the glass-former which is the consequence of the Adam and Gibbs assumption¹⁵:

$$\tau(T) = \tau_0 \exp\left(\frac{\Delta\mu s_c^*}{k_B T S_c}\right) = \tau_0 \exp\left(\frac{C}{T S_c}\right) \quad (1.8)$$

Where k_B is the Boltzmann constant, T is the temperature, S_c is the configurational entropy, $\Delta\mu$ is the energy barrier per particle over which a cooperative rearranging group must overcome, s_c^* is the configurational entropy associated to such a rearrangement, and τ_0 is the relaxation time at infinite temperature. s_c^* and $\Delta\mu$ are assumed to be independent of temperature.

In the relevant range of application of the Adam and Gibbs's equation⁶¹⁻⁶⁴, the liquid entropy in excess to the corresponding crystal has been used since access to configurational entropy data for glass forming liquids is impossible experimentally. Under this assumption, **Eq.1.8** can be rewritten as:

$$\tau(T) = \tau_0 \exp\left(\frac{C'}{T S_{ex}}\right) \quad (1.9)$$

Where S_{ex} is the excess entropy and C' is proportional to C , defined in **Eq.1.8**. According to similar definition proposed by speedy⁶⁵, the kinetic (dynamic) fragility can be written as:

$$m = \frac{d\left[\frac{\ln(\tau(T)/\tau_0)}{\ln(\tau(T_g)/\tau_0)}\right]}{d\left(\frac{T_g}{T}\right)} \Bigg|_{T=T_g} \quad (1.10)$$

With insertion of **Eq.1.9** in **Eq.1.10** a connection between the kinetic fragility and thermodynamic properties is obtained:

$$m = 1 - S_{ex}(T_g)^{-1} \left[\frac{dS_{ex}(T)}{dT} \right] \left[\frac{dT}{d\left(\frac{T_g}{T}\right)} \right] \Bigg|_{T=T_g} \quad (1.11)$$

This equation is independent of C (C') on the material because of using the definition of dynamic fragility provided by **Eq.1.10**. Now, by rearranging **Eq.1.11**, a correlation between the dynamic fragility and the excess entropy (S_{ex}) and heat capacity (ΔC_p) is obtained:

$$m = 1 + \frac{\Delta C_p(T_g)}{S_{ex}(T_g)} \quad (1.12)$$

5- Cooperativity

One concept, which is often used in the description of glass transition dynamics, is the idea of cooperative motion. The basic idea behind the approach, first introduced empirically by Adam and Gibbs¹⁵, is that as the temperature in a glass forming material is brought near the glass transition temperature, individual particle motion is frozen out. The result is that the only structural rearrangements, which may occur must involve the collective movement of many particles, and the length scale for cooperative dynamics must be temperature dependent, increasing as the temperature is lowered.

In the vitreous polymer, relaxation processes are known to be cooperative phenomena and the molecule motions depend on neighbor's motions: The rearranging movement of one structural unit is only possible if a certain number of neighboring structural units is in motion.

In fact when a glass forming liquid is cooled down towards glass transition, viscosity and the structural relaxation times increase dramatically. This phenomenon can be interpreted assuming a cooperative behavior of the relevant molecular motions. Adam and Gibbs¹⁵ have introduced the notion of the Cooperative Rearranging Region (CRR) which is defined as the smallest amorphous domain where a conformational rearrangement may occur without causing rearrangements in the surrounding. It means if the total volume of a system is divided into equal "Adam–Gibbs volumes", the density ρ , the temperature T , the entropy S , and the energy E are somewhat different in each sub-volume and the mean square fluctuations $\langle \Delta\rho^2 \rangle$, $\langle \Delta T^2 \rangle$, $\langle \Delta S^2 \rangle$ and $\langle \Delta E^2 \rangle$ are given by standard relations of statistical thermodynamics⁶⁶.

One specific characteristic of glass former is non-Arrhenius dependence of the structural relaxation time τ . The deviation from the Arrhenius behavior has been traditionally related to an increase of cooperativity in the relaxation process of interest (**Figure1-3**) and it can be quantified by the fragility index which is a material dependent parameter. Even if the non-Arrhenius behavior of the temperature dependence of relaxation time has been usually attributed to cooperativity of the process, establishing a quantitative relationship between the size of CRR and the fragility is not clear since many other physical and chemical parameters must be considered, such as density, macromolecular organization microstructural organization, backbone rigidity, inter and intramolecular interactions and etc.⁶⁷⁻⁷⁰. In experiments we should pay attention to study the variation of fragility and CRR size by changing few and selected parameters. Hong et al.⁷¹ tried to explain that, there is no consistency between cooperativity and fragility. For this purpose they separated the fragility into two contributions: (1) the isochoric fragility m_V (energetic component) corresponding to the temperature dependence of the segmental relaxation time at a constant volume (2) and $m - m_V$, associated with the volume contribution. According to this assumption, the fragility can be expressed as:

$$m = m_V + \frac{\Delta V^*}{\text{Ln}(10)k_B} \frac{\alpha_T}{\kappa} \quad (1.13)$$

Where, k_B is Boltzmann constant, κ is the compressibility and α_T is the coefficient of thermal expansion of the supercooled liquid at T_g . ΔV^* is the activation volume for a single unit to relax and is equal to approximately 4% of the cooperativity volume. So, just the parameter $m - m_V$, is directly correlated to the cooperativity at the glass transition. Thus, fragility changes accordingly with cooperativity only when m_V remains constant. In this representation, according to works of Araujo et al.^{72,73}, $m - m_V$ depends on interchain interactions while the stiffness of the backbone mainly influences m_V . In other words, it can be assumed that structural changes impacting only the interchain interactions without any influence on the polymer backbone stiffness should lead to ideal variations of fragility with cooperativity.

6- Donth's approach

Besides VFT equation and Angell's fragility concept, which characterize Arrhenius to non-Arrhenius behavior of the α -relaxation process, in order to estimate the size or the number of structural units involved in the cooperative rearrangements, numerous approaches exist⁷⁴⁻⁷⁶. One of the popular one is the approach of Donth⁷⁷. This approach is based on the theory of Adam and Gibbs: the configurational-entropy theory^{15,78}.

Cooperative Rearranging Region (CRR) is an independent and distinct subsystem with own relaxation time, relaxation temperature and glass transition temperature. So, going through glass transition, the glass-forming liquid displays a broad distribution of relaxation times and dynamic glass transition temperatures related to each CRR. The main idea of Donth et al.^{79,80} was to relate the statistical thermodynamic relations to the width of relaxation time distribution of the so-called α process. Each sub-volume (called CRR) with a specific size equal to $V = \xi^3$ can be then considered as a thermodynamic system in metastable equilibrium with fluctuating variables having a Gaussian distribution.

According to Donth's approach the cooperativity volume at the average dynamic glass transition can be obtained by this formula:

$$V_\alpha = \xi_\alpha^3 = \frac{\Delta(\frac{1}{C_p})}{\rho(\delta T)^2} k_B T_\alpha^2 = \frac{(1/C_p)_{\text{glass}} - (1/C_p)_{\text{liquid}}}{\rho(\delta T)^2} k_B T_\alpha^2 \quad (1.14)$$

Where ξ_α is the characteristic length of dynamic glass transition (T_α), δT is mean temperature fluctuation related to dynamic glass transition of one CRR⁸¹, k_B is Boltzmann constant, ρ is density of relaxing system and C_p is heat capacity at a constant pressure. The number of structural units in one average CRR with volume V_α is obtained from:

$$N_\alpha = \frac{\rho N_\alpha V_\alpha}{M_0} = N_A \frac{\Delta(\frac{1}{C_p})}{M_0(\delta T)^2} k_B T_\alpha^2 \quad (1.15)$$

Where M_0 is the weight for a whole molecule, or monomer unit for polymers and N_A is Avogadro number. The Cooperative Rearranging Region (CRR) can be estimated from Temperature Modulated Differential Scanning Calorimetry (TMDSC) and Dielectric relaxation spectroscopy (DRS)⁸² and can be changed by structural constraints such as confinement⁸² or plasticization in polymers⁸³.

7- Structural relaxation

Beside the temperature dependence of α -relaxation process in glass-forming liquids through Arrhenius to non-Arrhenius behavior by increasing the cooperative rearrangement sizes upon cooling, there is another phenomenon while approaching glass transition (and below), which is known structural relaxation.

Structural relaxation or structural recovery refers to a process by which thermodynamic variables (for ex. volume, enthalpy and etc.) evolve in an effort to reach the equilibrium, when held isothermally at temperatures below T_g . The change in mechanical properties of glass-forming liquids as a consequence of structural recovery is known as structural

relaxation⁸⁴. Such phenomenon is clearly visible through the concept of physical aging⁸⁵ (**Figure1-7**). Study physical aging is a main subject in order to perceive the structural relaxation processes on the evolution of physical properties. From free-volume model³⁷, it has been proposed from several investigations that the driving forces of the physical aging, which is leading to the decrease of thermodynamic properties towards equilibrium are related to a free volume hole diffusion towards surfaces⁸⁶. Those surfaces may be the external ones of the system or the internal ones tied to the creation of low density regions induced by the cooling rate. Thus, through structural relaxation, molecular motions can be studied.

Kinetics features of physical aging can be observed by heating the material from the glassy state to the equilibrium liquid-state with using calorimetric techniques. The response observed on heating depends on the previous thermal history of material. The lower energetic state (lower enthalpy) reached delays to recovery the liquid-like state upon subsequent heating. Therefore, when material is held isothermally below the glass transition temperature, the subsequent heating will show a peak superimposed to the glass transition by means of calorimetric techniques like Differential Scanning Calorimetry (DSC) and Flash DSC. The delay leads to an overshoot peak which is related to the enthalpy recovery and gives intuition on the excess of energy released upon aging for an aging time.

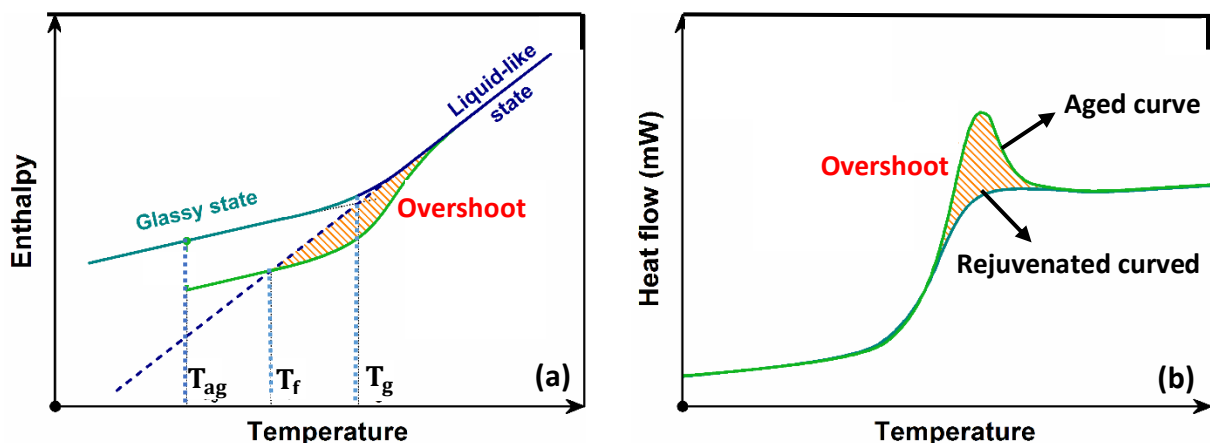


Figure1-7: (a) Schematic plot of enthalpy of a glass-forming liquid upon physical aging and (b) the respective DSC heat flow as a function of temperature. T_g is glass transition temperature and T_{ag} is aging temperature.

7-1 Fictive temperature

The evolution of structure during the relaxation process can be examined by the concept of fictive temperature T_f , which has been introduced by Tool in 1931¹⁸. The fictive temperature is the temperature at which the non-equilibrium value of the macroscopy property reach the equilibrium. This temperature is defined as the intersection of the glass and liquid lines obtained on heating and is also used in order to investigate the kinetic nature of the glass transition through the cooling rate dependence of glass-forming liquids. In the case of an unaged glass, T_f is termed the limiting fictive temperature T_f' . The importance of T_f' is its equivalence to T_g ^{87,88}. The enthalpy (or specific volume) response

observed on heating of the material after cooling at various rates is shown in **Figure1-8**. The glass line overshoots the equilibrium liquid line when the heating rate is higher than cooling rate due to lower mobility in the glassy state. The enthalpy overshoot shifts to higher temperatures and grows in magnitude with decreasing cooling rate⁸⁸. Higher the difference between the cooling and the heating rates, higher the magnitude of the overshoot. However, if the heating rate is lower than the cooling rate, the relaxation will happen along the glassy line leading to an undershoot⁸⁹.

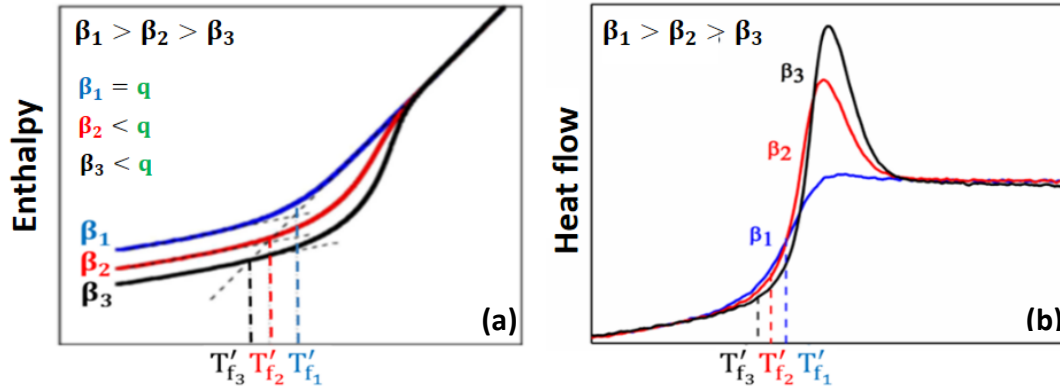


Figure1-8: Variation of (a) enthalpy (adapted from article of Simon L.¹⁹) and (b) normalized heat flow, versus temperature when heating at the same rate (q) after cooling at different rates $\beta_1, \beta_2, \beta_3$, where $\beta_1 > \beta_2 > \beta_3$. The limiting fictive temperature results in $T'_{f_1} > T'_{f_2} > T'_{f_3}$ and the overshoot shifts to higher temperatures for lower cooling rates.

In **Figure1-8**, first, a glass is formed at β_1 , then, by heating at the same rate $\beta_1 = q$, the enthalpy recovers the equilibrium in the liquid-like state on the same line, but when a glass is formed at β_2 lower than β_1 , the limiting fictive temperature shows a lower value. The glass transition measured on heating immediately after cooling at a given rate can be characterized by using limiting fictive temperature. As for physical aging, the effect of structural relaxation related to the difference between the cooling and the heating rates is a peak superimposed to the glass transition upon heating when investigated by calorimetric techniques.

7-2 Calculation of fictive temperature

Tool-Narayanaswamy-Moynihan (TNM)'s model allows to describe the enthalpy relaxation by using the concept of fictive temperature T_f . From calorimetric measurement, fictive temperature T_f can be calculated by Moynihan's equation^{90,91} (also called areas matching method).

$$\int_{T_f}^{T_2} (C_{p,l} - C_{p,g}) dT = \int_{T_1}^{T_2} (C_p - C_{p,g}) dT \quad (1.16)$$

Where, $C_{p,g}$ and $C_{p,l}$ are heat capacities of the glass and liquid respectively. C_p is the heat capacity of the material, T_2 is an arbitrary temperature above the range of thermal glass transition at which C_p is equal to $C_{p,l}$ and T_1 is a temperature below the range of thermal glass transition at which C_p is equal to $C_{p,g}$. In the liquid state $T_f(T) = T$, whereas in glassy state $T_f(T) = T'_f$ (limiting fictive temperature). The limiting value of T_f , noted T'_f , is obtained

when the extrapolation is performed from a point far in the glassy state after cooling at a given rate. **Figure1-9** depicts the procedure to estimate the fictive temperature based on the conventional area-matching method as proposed by Moynihan et al.⁹⁰

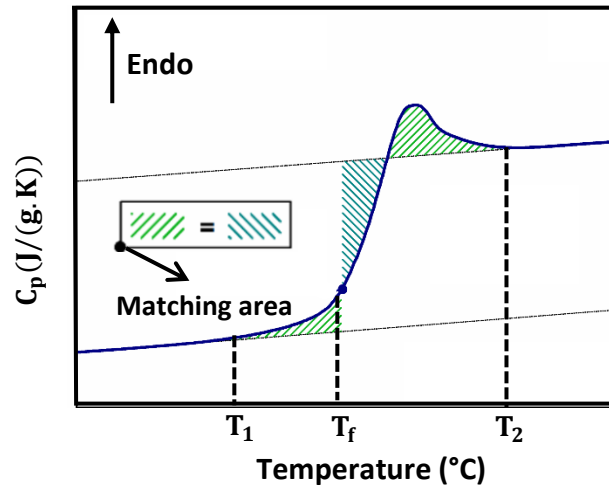


Figure1-9: Schematic plot of the heat capacity as a function of temperature for the determination of the fictive temperature.

As described in previous section the structural relaxation occurs below glass transition. The kinetics of structural recovery have been well formulated through Tool-Narayanaswamy-Moynihan (TNM)'s model⁹⁰. This model can describe both temperature and structure dependence of the relaxation time. Narayanaswamy⁹² described the relaxation time by this expression:

$$\tau = A \exp\left(\frac{H_g}{RT} + \frac{H_s}{RT_f}\right) \quad (1.17)$$

Where A , H_g , and H_s are material-dependent constants, and R is ideal gas constant. The thermal and the structural contribution to the segmental relaxation phenomenon is described by two terms depending on the temperature T and fictive temperature T_f . In the case where the system is at thermodynamic equilibrium ($T_f = T$), this equation is reduced to an Arrhenius equation with activation energy $H_g + H_s$. Subsequently, a partition parameter x has been introduced⁹³ to account for a thermal and structural contribution:

$$\tau = \tau_0 \exp\left(\frac{x \cdot \Delta h^*}{RT} + \frac{(1-x) \cdot \Delta h^*}{RT_f}\right) \quad (1.18)$$

where τ_0 is the relaxation time in equilibrium at an infinitely high temperature, T is the temperature, Δh^* is the activation energy of the relaxation phenomena and x is a constant of the material ($0 \leq x \leq 1$) defining the relative contributions of temperature and structure to the relaxation time. The equation shows the non-linearity of the relaxation time, as already observed from the Arrhenius to non-Arrhenius behavior of the α -relaxation.

From configurational-entropy theory⁹⁴, each Cooperative Rearranging Region (CRR) has its own characteristic relaxation time. Therefore, a broad distribution of relaxation times is available, and is well described through a stretched exponential function Φ , also known as Kohlraush-Williams-Watt (KWW) function⁹⁵:

$$\Phi(t) = \exp\left(-\left(t/\tau_{KWW}\right)^{\beta_{KWW}}\right) \quad (1.19)$$

Where, τ_{KWW} is the relaxation time and β_{KWW} is the stretch exponent which generally ranges between 0 and 1, It is inversely proportional to the width of a corresponding distribution of relaxation times. It means when β_{KWW} is near 0, the distribution of relaxation times is very broad, whereas for β_{KWW} close to 1 the distribution of relaxation times is characterized by a simple exponential, that is the time behavior of liquids above the melting point. Therefore, in addition of the non-linearity as a function of temperature, the relaxation times also depict a non-exponential behavior as a function of time upon isothermal annealing.

8- Crystallization

The phenomenon of crystallization can occur in glass-forming liquids, in addition of vitrification. The word “crystallization” refers to the process where a disordered phase transforms into a highly ordered phase called “crystal”. This process can occur from the melt, solution, vapor phase and amorphous state. As mentioned already, when a liquid is cooled at a temperature lower than its melting point, it enters into a supercooled liquid state. During this cooling, several phase transitions or physical changes can happen: (1) precipitation of a crystalline solid; (2) formation of a disordered solid (glass) (3) liquid-liquid separation followed by solidification of the components. Crystallization in the liquid state can occur from the melt or from the glass.

8-1 Crystallization of polymers

The crystallization phenomenon of polymers is well describe by the concept of Lauritzen-Hoffman which is based on the nucleation theory leading to the formation of stable crystal nuclei which then, are followed by their own growth^{96,97}. Usually, crystal growth is appearing between the melting temperature and the glass transition temperature but in some cases nucleation may occur in the glassy state ($T < T_g$)^{85,98}.

When polymers crystallize, macromolecular chains which are in 3D random coils conformations turn into crystalline lamellae with a thickness of nanometers scale. These lamellae are separated by amorphous regions with some folded chains which can connect them together (**Figure1-10**). Thus, following their crystallization, polymers are always semi-crystalline with different degree of crystallinity.

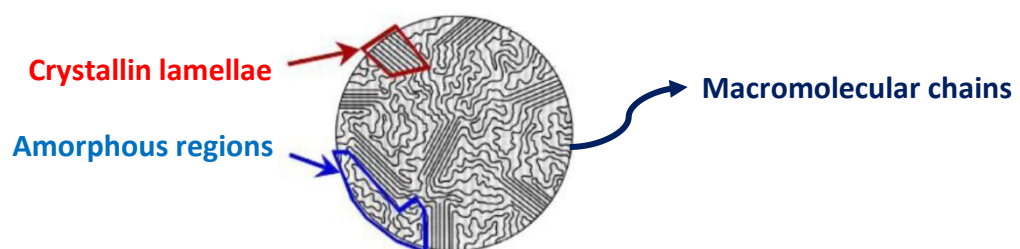


Figure1-10: Schematic view of the crystalline lamellae and the amorphous regions competition arising from quiescent crystallization.

Semi-crystalline polymers can be obtained conventionally or unconventionally. Crystallization is conventional when the process is only thermally activated (quiescent crystallization), whether performed upon cooling from the melt or upon heating from the glassy state to a given temperature^{99,100}. Quiescent crystallization is also possible in the presence of nucleating agents, which allow tailoring crystal morphology and lamellae orientation¹⁰¹. Unconventional crystallization comes from particular conditions, such as memory effect¹⁰², cross-nucleation¹⁰³ or thermo-mechanical history¹⁰⁴.

8-2 Three-phase model

The morphology of semi crystalline polymers is often described as a lamellae stack of crystalline and non-crystalline layers which is called “two-phase model”¹⁰⁵. It is successfully applied for the interpretation of X-ray diffraction as well as heat of fusion or density measurements¹⁰⁶. On the other hand, it is well known that several mechanical properties as well as the relaxation strength at glass transition cannot be described by such a two-phase approach as discussed by Gupta¹⁰⁷. From standard DSC measurements¹⁰⁸, dielectric spectroscopy¹⁰⁹, shear spectroscopy¹¹⁰, NMR¹¹¹ and other techniques probing molecular dynamics at glass transition (α -relaxation) the measured relaxation strength is always smaller than expected from the fraction of the non-crystalline phase. The difference is caused by different conformations of the chains as detected by IR and Raman spectroscopy¹¹² or due to spatial confinement because of the neighboring lamellae.

Takayanagi and coworkers¹¹³ and Wunderlich and coworkers¹⁰⁸ didn't discussed only on crystalline and non-crystalline phases in semi crystalline polymers. The non-crystalline phase has to be divided in two parts, one part contributing and a second one not contributing to the relaxation strength at glass transition. Furthermore, Wunderlich and coworkers distinguished between a mobile and a rigid fraction of the polymer. The rigid fraction consists of the crystalline phase and that fraction of the non-crystalline phase which is not contributed to the glass transition. Therefore another model was introduced for distinguishing between the crystalline (CRF), the rigid amorphous (RAF) and the mobile amorphous (MAF) fractions. This model is often called “three-phase model”¹⁰⁶ of semi crystalline polymers (**Figure1-11**).

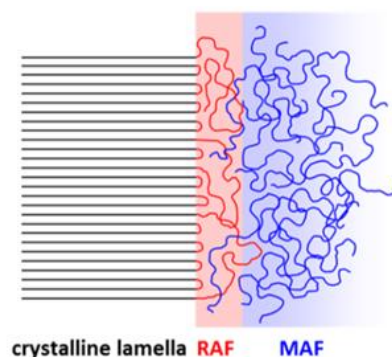


Figure1-11: Schematic views of the arrangement of crystalline, rigid amorphous and mobile amorphous fractions in semi-crystalline polymers according to three-phase model. Picture was taken from A. Esposito's article¹¹⁴.

The presence of RAF in semi-crystalline polymers can be explained by the fact that the amorphous phase appears to be constrained by the crystalline lamellae. This constraint is the effect of both a geometrical confinement and a covalent coupling between the lamellae and the non-crystalline regions through tie molecules. When this coupling is strong enough, a separate phase in nano-metric size can be created at the interface between the two phases, due to the fact that polymer chains are much longer than the typical dimensions of polymer crystal^{114,115}. Thus RAF has been so called as its mobility is drastically restricted¹¹⁶. Another fraction is unconstrained amorphous phase which is called mobile amorphous fraction (MAF). Thus a three-phase model describes well the semi crystalline structure.

In the past few years, constrained and unconstrained mobile amorphous fractions (CMAF and UCMAF), have been reported for semi-crystalline polyesters, such as PET¹¹⁷ and PLA¹¹⁸, as revealed by DSC measurements through the concept of cooperative rearranging regions¹¹⁹ as well as structural relaxation (for ex. physical aging)¹²⁰. Thus, the presence of crystals have influence on the molecular dynamics of the mobile amorphous fraction.

9- Confinement of polymers

The confinement of polymers has been widely studied by many people in more than two past decades. Jackson and Mckenna¹²¹ are pioneers in this field who studied on T_g deflection of organic liquids in nanopores. Since two decades ago, great effort has been devoted to pursuing an understanding of the glass transition temperature and associated dynamics of polymers confined to the nanoscale level, in geometries ranging from films (1D confinement), to pores (2D), to spheres (3D). In the aim of searching, a variety geometries have been proposed to confine both amorphous and semicrystalline polymers. Although, we know more about the glassy properties of confined polymers today rather than a decade ago, much of our understanding has been obtained by studies on thin polymer films, since they are easy to process and are of significant technological importance. Nevertheless, studies on polymers confined to other geometries are becoming increasingly more important as we follow questions difficult to address using thin films and as technology demands the use of confined polymers beyond thin films.

Confining a system to a scale comparable to its characteristic length (for ex. gyration radius in macromolecules and cooperative length ξ) can lead to considerable changes of the dynamical, thermodynamical and structural properties with respect to the bulk material^{15,122}. Many studies^{1-3,3,123-126} have discussed the effect of geometrical confinement on the glass transition temperature, molecular mobility, thermal properties, barrier properties etc. of amorphous polymers and it may be said that chain dynamics in confined geometries are commonly related to two main mechanisms: **(1)** finite size effect, **(2)** chain confinement.

9-1 Finite size effect

The finite size effect¹²⁷ comes from the breakdown of cooperative motion and is related to the dynamic cooperative length of the α -relaxation process. On the other hand we can say finite size is referred to pure confinement on pure geometrical effect. Such effects are

believed to play an important role when the system is confined into dimension close to the CRR size (Cooperatively Rearranging Region) for example in porous glasses¹, silicate layers¹²⁸ or ultrathin polymer films¹²⁹.

The basic idea of finite size effects is easily described. We consider the sample is confined to a size D . At high enough temperatures $\xi(T) \ll D$, the dynamics of the confined system will be the same as the bulk system. When the temperature is decreased, $\xi(T)$ increases and finally the condition $\xi(T) \approx D$, will be reached. When $\xi(T) \approx D$, the confined system will show abnormal dynamics compared to the corresponding bulk system. The way that the dynamics of the confined system will be affected depends strongly on the boundary conditions of the system. According to the concept of cooperative motion, if molecules on the boundary are held fixed (strongly attractive interaction in an experiment), then the confined system will exhibit much slower dynamics than the bulk system or may even be completely arrested, whereas if the molecules on the boundary have a high degree of freedom (in the experimental case of a free surface), then the dynamics of the confined system will be faster than that of the bulk system¹³⁰.

9-2 Chain confinement effects

Chain confinement¹³¹, related to the conformational changes of entire polymer coils induced by squeezing of the polymer chains, for example conformational changes of the polymer coil from its equilibrium size and shape.

Polymer molecules are extended objects with a characteristic size, the r.m.s. (root mean square end-to-end distance¹³²) $R_{EE} \propto N^2$, where N is the number of monomer units. This intrinsic length scale introduces the possibility of chain confinement effects as the film thickness (h) becomes smaller than the unperturbed molecular size. Such effects may be very difficult to distinguish as they can demonstrate anomalies in the dynamics without necessarily causing any changes in the structural properties. One way possible to identify chain confinement effects is that the magnitude of such an effect (for constant film thickness), should depend on the molecular size. While the existence of chain confinement effects may conceal observation of finite size effects, they are interesting in their own right as they serve as a probe of fundamental aspects of perturbations of polymer dynamics.

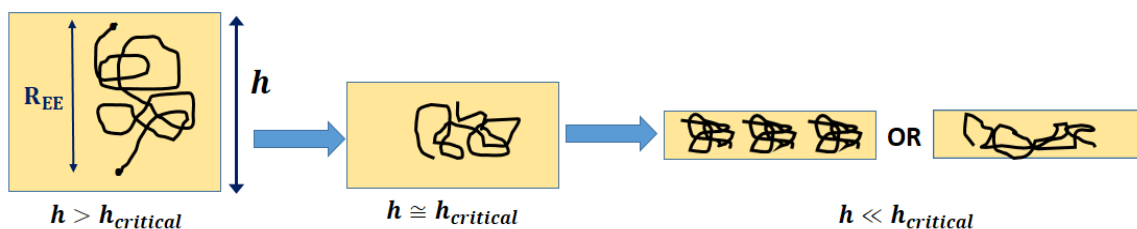


Figure1-12 Schematic view of changes in polymer's chains due to confinement.

9-3 Molecular Weight and chemical structure dependence on T_g and fragility

The molecular weight (M_w) dependence of T_g has received long-standing interest since the pioneering work by Fox and Flory^{133,134}. The relationship has been demonstrated experimentally for a number of polymers including polystyrene (PS), poly(α -methyl styrene) (PaMS), poly(vinyl chloride) (PVC), poly(ethylene terephthalate) (PET), and poly(methyl methacrylate) (PMMA)¹³⁵⁻¹⁴¹. The related T_g - M_w dependences have been noted in other studies^{46,142,143}. In general, by increasing M_w for linear polymers, the restriction on segmental mobility increases, leading to an increase in T_g . A stronger increase in T_g is observed for rigid polymers (PS, PMMA) compared to flexible polymers (PIP, PDMS) because of a much stronger restriction imposed by the chain connectivity on rigid polymers compared to flexible ones⁴⁶. This was represented in **Figure1-13**.

Several approaches and theories have been developed to account for the variation in T_g as a function of M_w . One notable approach is Fox-Flory relation^{133,134}:

$$T_g = T_{g,\infty} - K/M_n \quad (1.13)$$

Where $T_{g,\infty}$ is T_g in the limit of infinite M_w , M_n is the number-average M_w , and K is an empirical parameter for a particular polymer species.

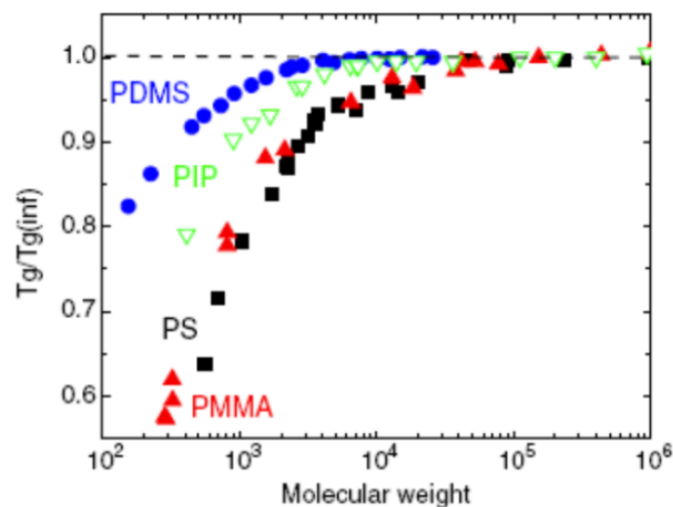


Figure1-13 The molecular weight dependence of T_g scaled by T_g at high M_w ($T_{g,\infty}$) for PS, PMMA, PIP and PDMS⁴⁶.

Although the Fox-Flory equation satisfactorily fits the M_w dependence of T_g in PS, the linear equation often predicts a stronger M_w dependence at low M_w (typically for $M_n < 5$ kg/mol). Recently L. Zhang et al.¹⁴⁴ showed for anionic PMMA, the T_g - M_w dependence becomes weaker at very low M_w , which can be reasonably fitted by another equation given by the statistical theory of Gibbs and DiMarzio¹⁴⁵.

The Fox-Flory's relation often breaks down for oligomeric systems^{13,143,146-148}. Besides the intermolecular effects¹³³, chain connectivity^{13,149} and intramolecular rearrangement¹⁵⁰ affect glass formation which leads experimentally to a complex $T_g(M_w)$ behavior. First Cowie et

al.¹⁴⁷ showed that $T_g(M_w)$ can be divided into three regions, corresponding to long-chain molecular weight M_w (region I), intermediate (region II) and oligomeric (region III) which are separated by molecular weights M^* and M^{**} , where

$$T_g \cong A_{I,II} + B_{I,II} \log_{10} M \quad (1.14)$$

in region II and III, and $T_g \cong T_{g,\infty}$ in region I.

According to the diagram of Hintermeyer J. et al.¹⁴³ (**Figure1-14**) region I, can be identified when the asymptotic value of T_g is reached for high molecular weight polymers. In this region systems show T_g which are essentially constant and independent of molecular weight (or chain length). Region II covers the range of molecular weight where T_g decreases slowly with decreasing molecular weight. If the range of molecular weights is sufficiently wide, region III can be identified at very low molecular weight where the decrease in T_g is even more pronounced than in Region II.

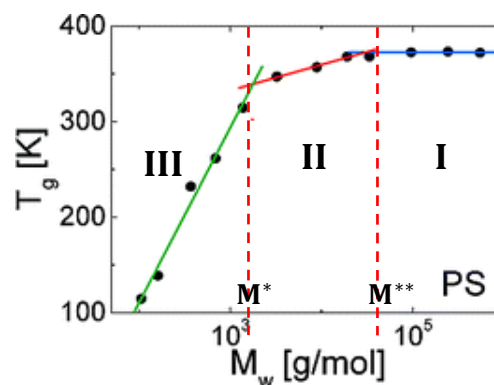


Figure1-14 Variation of T_g with molecular weight in logarithmic scale for Polystyrene (work of J. Hintermeyer et al.¹⁵¹) which indicate clearly three separate regions.

Recently, Baker L. et al. showed the behavior of $T_g(M)$ according to rigidity of some polymers. They observed that for relatively rigid polymers such as PS and PMMA which have carbon-based backbones and bulky side groups T_g values vary significantly with M , whereas for more flexible polymers like PDMS which has Si-O backbone and low rotational barriers variation of T_g is much smaller, so in contrary to PS and PMMA, variation of T_g with molecular weight for PDMS can be described by Fox-Flory relation. It means that for most flexible polymers the region II is less visible.

On supported polystyrene (PS) films, two reviews^{130,152} have found extensive agreement for T_g nano confinement effect across many measurement methods: when scaled according to the bulk T_g as $T_g / T_{g,bulk}$ the thickness dependence of T_g has been found to be approximately independent of PS molecular weight M_w ^{130,153} over a M_w range of 3600-2 900 000 g/mol.

Most organic polymers with van der Waals interactions exhibit fragility much higher than their small molecular weight counterparts. As shown in **Figure1-15**, the fragility of most monomers or oligomers is within the range of 60-90, similar to small molecules with Van der Waals interactions. However, as the chain length increases, most polymers exhibit an increase in fragility. The fragility of many high molecular weight polymers is over 100^{154,155}. It has been speculated that the nature of this specific behavior may be related to chain connectivity⁴⁶. However, the causes behind such large differences in the fragility of polymers versus small molecules are not completely understood.

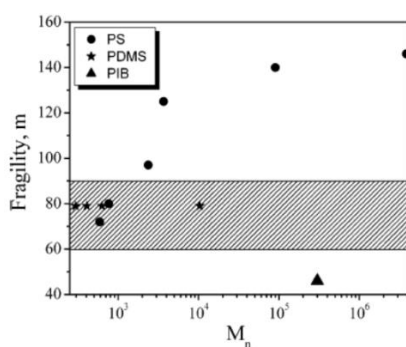


Figure1-15 Molecular weight dependence of fragility index m for PS, PDMS, and PIB. Shaded area marks the fragility range of small molecules with Van der Waals interactions¹⁵⁶.

In addition of molecular weight, polymers with different chemical structures show different dependences of fragility and T_g on chain length. According to theoretical predictions¹⁵⁷⁻¹⁵⁹ T_g and fragility for linear monodisperse chains is only expected to increase with molecular weight. With advancements in chemistry that have enabled the synthesis of an array of polymer architectures, there has been a growing interest in examining the effect of confinement as a function of molecular architecture¹⁶⁰⁻¹⁶³. Compared to films of linear precursor chains, films of cross-linked PS made directly from films of precursor chains exhibit a larger T_g confinement effect¹⁶⁰. Multiarm star PS reportedly exhibits enhanced T_g and reduced physical aging rate with confinement¹⁶¹.

When comparing the fragilities of different chemical structures of polymers, we have taken into consideration the fragility values for molecular weights where the M_w -dependence of T_g seems to have saturated. Looking at literature data reveals that different polymers show a wide range of fragilities. The most fragile polymer known till now is polyetherimide (PEI) with $m \sim 214$ ^{42,164} which is known to have a distinctively stiff backbone structure, contributing to its higher T_g . However, some of the least fragile polymers such as polyethyleneoxide (PEO) and polyisobutylene have fragilities 23 and 46 respectively¹⁶⁵. All of the other studied polymers fall within this range and show a wide distribution of fragilities.

The work of Ellison, Kim and al.¹⁶⁶ have also shown that the effect of nano confinement on T_g of PS can be reduced or completely eliminated by adding pyrene or dioctylphthalate as plasticizers. This was attributed to the effect of reducing the cooperative nature of dynamics α -relaxation by the plasticizing molecules.

10- Different types of confinement

In general we can classify different types of confinement like below:

- Polymer blends¹⁶⁷
 - Thin films or nanolayers^{2,4,168,169}
 - Multilayer films^{82,170–172}
 - Free surfaces³
 - Droplet dispersion¹⁷³
 - Polymers infiltrated in inorganic nanotemplates¹⁷⁴
 - Self-assembled block copolymers¹⁷⁵
 - Nanocomposites¹⁷⁶
 - Semi-crystalline polymers¹⁷⁷
- etc.

In the following of this chapter, few researches and results associated to molecular dynamics in polymers are summarized for some types of confinement which are more interesting for the thesis.

10-1 Polymer blends

Polymer blending has been identified as the most versatile and economical method to produce new multiphase polymeric materials that are able to satisfy the complex demands for performance¹⁷⁸. Several types of blends including thermosets, thermoplastics, thermoplastic vulcanizates, and structured copolymers exist¹⁷⁸. Polymer blends have been often treated as a patchwork of different domains with separate properties and it is often assumed that these domains retain the bulk properties of the individual components. This assumption is adequate for blends with large domains (micron size) since the relatively small contributions of the regions near polymer-polymer interfaces between domains can be reasonably ignored. Recently polymer blends can be used to study confinement effects not only on T_g but also on chain modes¹⁷⁹. Blending of two miscible components of polymers having different glass transitions leads to change chain dynamics^{179,180}. Results for the PMMA/PEP blends in work of J. Colmenero¹⁸⁰ showed significant non-exponential behavior in the relaxations, although the confinement leads to reduced concentration fluctuations but results were interpreted to imply that the changing dynamics had to do with composition effects rather than length-scale effects. Nowadays, in order to improve material performance and blend uniformity for particular applications, several strategies have done to decrease the domain sizes below 100 nm range^{181,182} such as: synthesis of multicomponent block copolymers¹⁸³, novel cold-state processing methods¹⁸⁴ and nanolayer stacking and interweaving^{82,185}. Polymer-polymer interfaces and interfacial reaction of

polymers play an important role in the properties of nanostructured polymer blends¹⁷⁸. For example, the performance of materials used in catalysis, ion conduction, photovoltaic technologies and filtration¹⁸⁶, is dictated by the properties of the material near the polymer-polymer interfaces. According to Baglay and Roth's expression¹⁸⁷: "nanostructured polymer blends with domain sizes of a few hundred nanometers likely have no regions where the local properties remain bulk-like. Instead, nanostructured blends likely exhibit more uniform properties across the different domains and interfaces, which may explain their typically enhanced performance over more traditional blends with large micron-sized domains."

10-2 Thin films or nanolayers

An attractive sample choice for studies of finite size effects is that of thin polymer films. The experimental results^{188,189}, numerical simulations^{190,191} and theoretical approaches^{192,193} show changes in the glass transition in nanoscale films. These works showed variations in the molecular dynamics of chains during measurements when measuring relaxation times by dielectric spectroscopy^{194,195} or by calculating characteristic length of cooperativity ξ (CRR) measured by MT-DSC^{1,196}. Similarly, the study of the glass transition temperature T_g remains mainly the most characterized at this scale. Different research groups have studied glass transition temperature T_g in a confined polymer using different techniques such as Positron Annihilation Lifetime Spectroscopy (PALS)¹⁹⁷, fluorescence spectroscopy^{187,198} and ellipsometry^{199,200}. These variations in T_g value were observed for the first time for thicknesses lower than a threshold value of the order of ≤ 100 nm and this phenomenon is accentuated even for thicknesses ≤ 40 nm²⁰¹. In the general case, these variations are observed at a scale corresponding to the dimensions of the characteristic length of the chains of polymers, or on a much smaller scale corresponds to the typical length of cooperativity (ξ)²⁰².

Considering the set of confined glass-forming liquids, these variations of T_g can be both increases and decreases compared to the measured value for the massive material. These two trends are associated with two types of effects distinct:

- A free surface or weak interactions of the film with its substrate, increase the molecular mobility close to the surface, resulting in a decrease in T_g ²⁰³⁻²⁰⁵.
- Strong interactions with the substrate, immobilizing polymer chains at neighborhood of the interface cause an increase in the value of T_g ^{206,207}.

In a few cases involving copolymers with comonomer units which exhibit attractive, neutral or repulsive substrate interactions, T_g has been observed to be nearly invariant with film thickness²⁰⁸.

According to statement of McKenna G.B. in his review¹⁷⁹, in some studies, modest reduction of T_g was observed in ultrathin films supported on rigid substrates²⁰⁹ while a very large reduction of T_g was occurred in freely-standing films of polystyrene²¹⁰. It should be considered whether or not these reductions are real or potential artifacts of the experiment or sample preparation. Since in many cases, the small amount of material is used in experiments, so the potential artifact in materials at the nanometer size scale is not

negligible. From investigation of A. Serghei²¹¹ and F. Kremer²¹², the ultrathin polymer film T_g reductions are artifacts of the sample preparation and annealing treatment, when is avoided, no reduction of the glass transition temperature is observed.

The first systematic study of the T_g of supported thin films of polymers was made by Keddie, Jones and Cory²⁰⁹ on polystyrene films with thickness between 300 and 10 nm. This study reveals a remarkable decrease in T_g values measured by ellipsometry, compared to bulk samples for films thickness ≤ 40 nm. The lowest measured T_g value is observed for a film thickness of 10 nm, it is 25 °C lower than the value measured for the solid film. These results have been compared with other values obtained by different techniques such as ellipsometry^{177,213}, dielectric spectroscopy¹⁵³, X-ray²¹³, Positron Annihilation Lifetime Spectroscopy (PALS), local thermal analysis²¹⁴ and fluorescence spectroscopy²¹⁵. All of this data is grouped in **Figure1-16**.

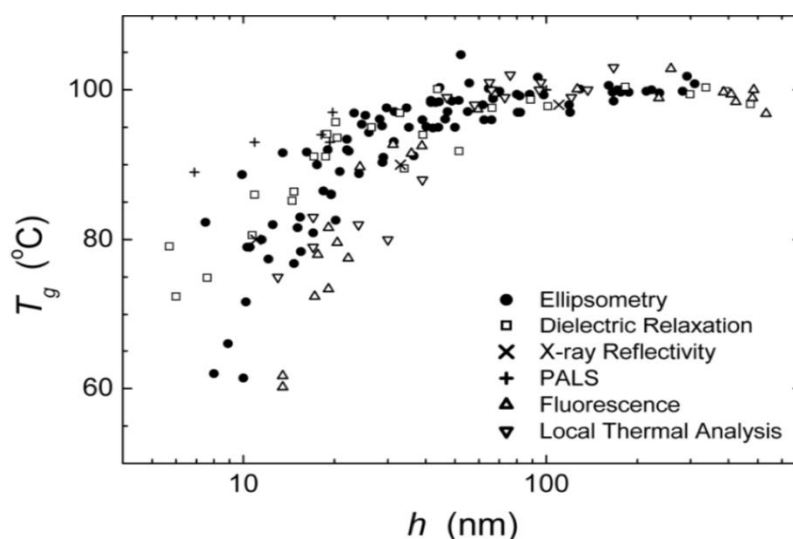


Figure1-16 Compilation of T_g measurements of polystyrene films supported on substrate using different techniques¹²².

The results are similar regardless of the technique. Variations in T_g are mainly associated with the surface effect disturbing the dynamic chains at the nanoscale. These surface effects are supposed to lead a gradual dynamic that comes from the disrupted interface. Ellison et al²¹⁵ use a multilayer fluorescence technique in which a fluorescent thin film of Polystyrene (PS) is incorporated into an unlabeled PS film. This makes it possible to measure T_g locally in different parts of the film. They get a big reduction in T_g on the free surface of PS films and a continuous attenuation of the effect when the fluorescent layer is located deeper and deeper in the film. It is possible to measure a decrease in T_g in a labeled layer up to 30 nm from the free surface of the film. The influence of substrate/liquid glass-forming interactions on the dynamics of polymer chains at the nanoscale primarily demands the implementation of films deposited on different types of substrate.

Recently, Connie B. Roth¹⁸⁷ has shown (**Figure1-17**) the local glass transition $T_g(z)$ profile of polystyrene (PS) when changing the neighboring polymer from a lower T_g material (called soft confinement) to a higher T_g material (called hard confinement). This shows that the dynamics in nanoscale layers is influenced by the adjacent area via interactions at the interface. This implies that as well as substrate and interface effects, other factors play an important role such as the chemical structure of the polymers and the nature of the cooperative movements associated with the dynamics of α -relaxation. The work of Priestley, Campbell et al.^{216,217} is evidence of the role of size, flexibility of monomer units and side group which seems to influence the behavior of T_g . This suggests that the dynamics of cooperative segments play a role in T_g behavior.

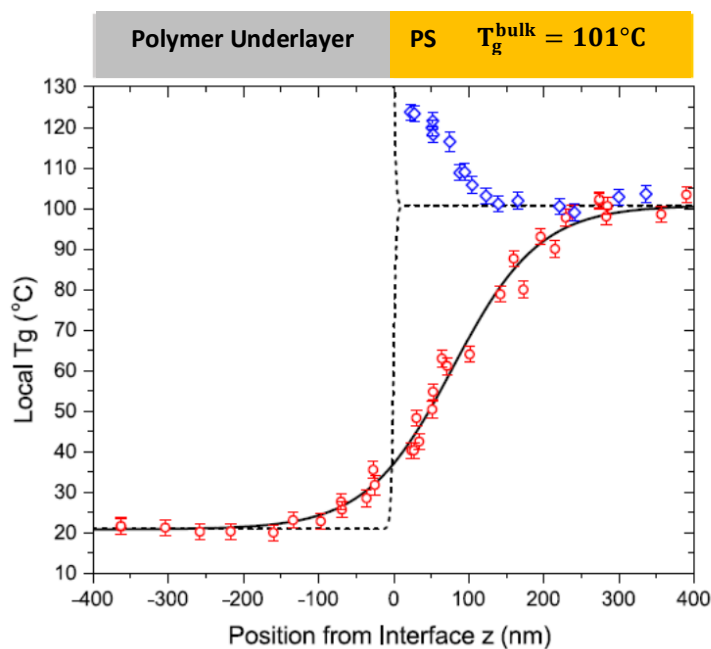


Figure1-17 Experimentally measured local $T_g(z)$ profile of PS/PSF (open blue diamonds), compared with that PS/PnBMA (open red circles), as a function of z . In the PS/PSF (polysulfone) system, the PS layer is rubbery relative to PSF undergoing hard confinement, while in the PS/PnBMA (poly isobutyl methacrylate) system, and the PS layer is glassy relative to PnBMA undergoing soft confinement. Connie B. Roth¹⁸⁷

10-3 Free surface

In the domain of confinement in polymers, the controversy concerning the effect of the substrate in thin film on T_g prompted studies of free-standing films which can be considered as free surface.

The first and most measurements of T_g value in free-standing films were the BLS (Brillouin light scattering)¹⁷⁷ studies of PS films with thickness(h) between 200 and 2000 Å²¹⁸. Forest et al.²¹⁸ measured T_g values in the free-standing films which exhibited reductions below the bulk value. These values were much greater in magnitude than those reported for supported films; with a 200 Å film having a T_g value reduced by 70K below the bulk value. For comparison, a supported film of the same thickness exhibits a T_g reduction of only 10 K.

Consistent with this larger magnitude of T_g anomalies, was the fact that T_g reductions were observed for much larger values of the film thickness; up to 700 Å. An extension of BLS studies to a second value of molecular weight M_w , revealed a strong M_w dependence of T_g value¹⁷⁷, in contrast to the observations for supported films. The strong M_w dependence observed in these studies revealed the importance of chain confinement effects for high M_w , in free surface.

In general, the presence of a free surface tends to speed up the local mobility, while the presence of a substrate interface can slow down the local dynamics, typically depending on whether attractive interactions, such as hydrogen bonding, are present between the polymer and substrate interface in question¹³⁶. Studies have shown that the perturbations originating from the free surface (“the free-surface effect”) can propagate several tens of nanometers into the film interior^{219,220} and have a strong dependence on the time scale employed to probe cooperative relaxation dynamics²²¹.

Besides it is now known that the α -relaxation (the molecular dynamics associated with the glass transition) in polymers is strongly correlated to the nature and number of intermolecular interactions between macromolecules. Reduction of polymer’s chain length in amorphous system, can offer the opportunity to restrict the volume engaged in the α -relaxation, leading to an effect approaching the free confinement classically investigated in thin layers. It means the reduction of polymers ‘s chain like reducing the thickness in polymer thin films, lead to less intermolecular interaction (Van der Waals interaction). For this purpose during my thesis we study Oligomers of Lactic Acid (OLA) with different molecular weight and dispersity.

This thesis is focused on systematic study of the effect of molecular weight on molecular dynamics in Oligomers of Lactic Acid (OLAs) which act as free surface and were synthesized and supplied in the company “Condensia Química SA” placed in Spain by collaboration with Dr. E. Passaglia from “Istituto di Chimica dei Composti Organometallici (ICCOM)” in Italy and Dr. S. Fiori from “Condensia Química SA”. Dielectric Relaxation Spectroscopy (DRS), Hyper Differential Scanning Calorimetry (Hyper-DSC) and Fast scanning calorimetry (FSC) have been used to study the segmental dynamics of amorphous OLAs with varying molecular weights.

10-4 Multilayer films

There are many techniques used to confine polymers at the nanoscale including spin coating thin films onto a substrate^{222,223}, block copolymers containing a crystallizing block^{224,225}, layer-by-layer depositing²²⁶ and more recently nano layer multiplying co-extrusion^{222,223}. The layer multiplying co-extrusion offers the huge advantage of being able to produce objects at large scale and to be transferable to the industry for the fabrication of commodity materials.

Multilayer coextrusion, can be used to obtain materials with enhanced macroscopic properties²²⁷. It is derived from classical coextrusion and its industrial potential has already been demonstrated by Dow which patented it close to 40 years ago²²⁸. Using this technique help us to produce materials with enhanced properties, in particular optical properties²²⁹, mechanical properties²³⁰, gas barrier properties²³¹. Those improvements were shown to

arise from the multiplication of the interfaces and/or the confinement, induced by the process (named 'forced-assembly'). The layer multiplying co-extrusion offers the huge advantage of being able to produce objects at large scale and to be transferable to the industry for the fabrication of commodity materials.

This process combines two or three polymers into a continuous alternating layered structure with hundreds or thousands of layers. This can decrease the layer thickness of each individual layer to about 10 nm. However, the confinement effect in the whole volume of the material can only be reached when perfectly continuous multi-nanolayer structures are created with a homogenous layer thickness.

For semi-crystalline polymers, this innovative technique has been recognized as an effective way to induce one-dimensional confined crystallization of polymers²³²: when the polymer layer thickness decreases, the crystalline morphology is gradually altered from a three-dimensional spherulitic morphology into one-dimensional crystalline lamellae.

In Multilayered polymer films, the influencing of thickness reduction on the glass transition temperature and cooperatively rearranging region(CRR) size can be investigated by several thermal analysis techniques⁸² and also dielectric relaxation spectroscopy.

Studying multilayer samples with thicknesses ranging from micro- to nano-scale allows us to highlight two types of constraints influencing molecular mobility in the amorphous materials:

- 1)** Increase the number of layers in films and so, reduction the thickness down to the nanoscale, implies a constraint on the mobility of chains by reducing the dimensionality of the system accessible to relaxation.
- 2)** Vicinity of two polymers with very different chemical structures raises the question of the influence of interfacial zones on the dynamics of the chains in conditions of geometrical confinement.

In EIRCAP group (GPM laboratory) several people investigated molecular dynamics in multilayered polymer films^{122,172,233}. Fernandes Nassar S. et al.¹⁷⁰ observed, the confinement of PLLA in PS/PLLA induced a change in the molecular mobility, evidenced by a drop of Cooperative Rearranging Region (CRR) size at the glass transition. They showed annealing of confined PLLA layers reveals slower crystallization kinetics and two-dimensional crystalline growth geometry. Furthermore, the annealing of PLLA in confined layers allowed a decoupling between the amorphous and crystalline phase, evidenced by the absence of a rigid amorphous fraction (RAF). In bulk polymers, where the level of coupling between amorphous and crystals is high, the glass transition temperature increased significantly whereas the CRR size fell. It is deduced that the glass transition dynamics in semicrystalline polymers is strongly related to the mobility landscape at the interface with crystals. In the work of Arabeche Kh. et al.¹⁷² on amorphous PC/PMMA multilayer samples (**Figure 1-18**), the effect of the layer thickness reduced down to 12 nm has been shown to have very different influence on glass transition parameters of the two polymers. Polycarbonate has exhibited a huge sensitivity to such geometric scale modifications whereas no modification has been

observed for PMMA. A large decrease of fragility index (m), has been observed for PC. This modification is proportional to length scale variations of molecular cooperative motions at T_g , $\xi(T_g)$. In regard to the molecular structure of each polymer, results showed that this correlation between fragility index (m) and $\xi(T_g)$ is mainly associated to modifications of intermolecular interactions and local density.

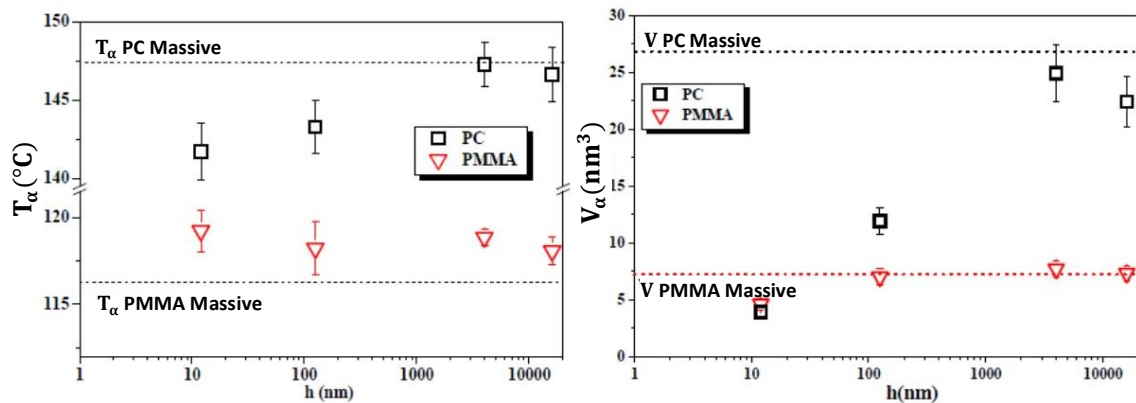


Figure1-18(a) Variation of the dynamic vitreous transition (T_α) of each component of multilayer films PC/PMMA depending on the thickness of the layers (h). (b) Evolution of the average volume, V_α , of Cooperative Rearrangement Region (CRR) around the glass transition for each component of multilayer films PC/PMMA depending on the thickness of the layers (h).

Casalini et al.¹⁸⁵ studied the dynamics of PMMA in multilayer films with polycarbonate and compared bulk films with films having layer thickness of 25nm, 8nm and 4nm. They observed a small effect on the amorphous phase dynamics comparing bulk PMMA with confined PMMA layers of 25 nm thickness. Interestingly, they showed absence of confinement effects on the cooperativity length comparing the most confined PMMA (8nm and 4nm) to the bulk properties. Indeed, the values of ξ were equal to or smaller than the layer thickness of PMMA. Thus, they concluded that the dynamic correlation length did not appear to be limited by the geometrical confinement. Another interesting aspect of this study is the increase in T_g when thickness layers decreases, which was explained by interfacial interactions between PMMA and PC.

10-5 Semi-crystalline polymers

The semi-crystalline polymers consist of a crystalline phase, and amorphous phase and tie molecules in both phases. It is popular that the amorphous parts will be placed in the spherulitic structures and confined between the crystalline lamellae²³⁴. Polymeric chains display a conformational dynamics different from the bulk when the amorphous regions are confined in geometry with length scales of some nanometers by crystalline part¹³⁰. Thus, semi-crystalline polymers form a worthy model to study the dynamic behavior of polymeric chains in nano-confined conditions²³⁵.

This type of confinement which is observed in semi-crystalline polymers can affect molecular dynamics, and especially cooperativity which depend on the molecular interactions between the macromolecular chains. These interactions depend also on the environment or the structural hindrances of the system. For example crystallization of PLA²³⁶

and PET²³⁷ display a decrease of the cooperativity due to the confinement effects of the crystals. Some authors showed correlations between crystallinity degree and CRR size (cooperative rearranging region), they observed that the CRR volume and number of monomer units per CRR decreases with increasing crystallinity degree^{76,238–240}. Many studies show that the more confined the amorphous phase, the smaller the average size of CRR^{196,241}.

Thus, the glass transition temperature is also affected by crystals in semi-crystalline polymers. For example Dionísio M. et al. observed a consistent shift of glass transition temperature T_g to higher value in the case of semi-crystalline PLLA²⁴². However Fitz and Andjelic²⁴³ observed a shift to lower T_g in PLLA at similar conditions but in partial constrained situation. In another study, Mijović and Sy did not observed any change of T_g during crystallization of PLLA at 80°C²⁴⁴. So understanding the attribution of changes occurring in the glass transition dynamics during crystalline development is complicated.

In semi-crystalline polymers, the discussion about the influence of the crystalline phase on the fragility value (m) is still intense. Ngai and Roland²³⁵ showed that for various materials the fragility value is unchanged with respect to the one measured in the fully amorphous. According to the work of Arnoult M. et al.⁴⁹ for semi-crystalline PLLA there is no significant variation of the fragility index compare to amorphous one, whereas for PET the fragility index decreases obviously during crystallization, so it goes from a fragile to strong material as soon as it becomes semi-crystalline. Some authors associate the variation of fragility index in semi-crystalline polymers to the establishment of the RAF^{49,245} which was explained in **section 7-2**. Other people suggested that if the polymer backbone is less flexible the fragility is more affected due to confined amorphous phase^{221,246}. No global law has been established till now, as the variation of m with the crystallization conditions depend on the considered polymer^{236,247,248}.

In this work, we investigate also the molecular dynamics in semi-crystalline oligomer of lactic acid with $\bar{M}_w = 2700$ g/mol. However in EIRCAP group (GPM laboratory) several people studied molecular dynamics in semi-crystalline polymers^{49,114,119,239,249}, but nobody considered the molecular mobility in oligomers especially by using Flash DSC instrument.

Bibliography

- (1) Schick, C. Glass Transition under Confinement-What Can Be Learned from Calorimetry. *Eur. Phys. J. Spec. Top.* **2010**, *189* (1), 3–36. <https://doi.org/10.1140/epjst/e2010-01307-y>.
- (2) Kipnusu, W. K.; Elsayed, M.; Krause–Rehberg, R.; Kremer, F. Glassy Dynamics of Polymethylphenylsiloxane in One- and Two-Dimensional Nanometric Confinement— A Comparison. *J. Chem. Phys.* **2017**, *146* (20), 203302. <https://doi.org/10.1063/1.4974767>.
- (3) Dhotel, A.; Chen, Z.; Sun, J.; Youssef, B.; Saiter, J.-M.; Schönhals, A.; Tan, L.; Delbreilh, L. From Monomers to Self-Assembled Monolayers: The Evolution of Molecular Mobility with Structural Confinements. **2014**. <https://doi.org/10.1039/c4sm01893a>.
- (4) Kremer, F.; Tress, M.; Mapesa, E. U. Glassy Dynamics and Glass Transition in Nanometric Layers and Films: A Silver Lining on the Horizon. *J. Non-Cryst. Solids* **2015**, *407*, 277–283. <https://doi.org/10.1016/j.jnoncrsol.2014.08.016>.
- (5) Angell, C. A. Formation of Glasses from Liquids and Biopolymers. *Science* **1995**, *267* (5206), 1924–1935. <https://doi.org/10.1126/science.267.5206.1924>.
- (6) Shakhmatkin, B. A.; Vedishcheva, N. M.; Shultz, M. M.; Wright, A. C. The Thermodynamic Properties of Oxide Glasses and Glass-Forming Liquids and Their Chemical Structure. *J. Non-Cryst. Solids* **1994**, *177*, 249–256. [https://doi.org/10.1016/0022-3093\(94\)90538-X](https://doi.org/10.1016/0022-3093(94)90538-X).
- (7) Chebli, K.; Saiter, J. M.; Grenet, J.; Hamou, A.; Saffarini, G. Strong-Fragile Glass Forming Liquid Concept Applied to GeTe Chalcogenide Glasses. *Phys. B Condens. Matter* **2001**, *304* (1–4), 228–236. [https://doi.org/10.1016/S0921-4526\(01\)00501-4](https://doi.org/10.1016/S0921-4526(01)00501-4).
- (8) Mackenzie, J. D.; Murphy, W. K. Structure of Glass-Forming Halides. II. Liquid Zinc Chloride. *J. Chem. Phys.* **1960**, *33* (2), 366–369. <https://doi.org/10.1063/1.1731151>.
- (9) Schammé, B.; Mignot, M.; Couvrat, N.; Tognetti, V.; Joubert, L.; Dupray, V.; Delbreilh, L.; Dargent, E.; Coquerel, G. Molecular Relaxations in Supercooled Liquid and Glassy States of Amorphous Quinidine: Dielectric Spectroscopy and Density Functional Theory Approaches. *J. Phys. Chem. B* **2016**, *120* (30), 7579–7592. <https://doi.org/10.1021/acs.jpcc.6b04242>.
- (10) Priestley, R. D.; Ellison, C. J.; Broadbelt, L. J.; Torkelson, J. M. Structural Relaxation of Polymer Glasses at Surfaces, Interfaces, and In Between. *Science* **2005**, *309* (5733), 456–459. <https://doi.org/10.1126/science.1112217>.
- (11) Arrow, K. J. Through the Glass Lightly. *Science* **1995**, *267* (5204), 1617–1618. <https://doi.org/10.1126/science.267.5204.1617-f>.
- (12) Ediger, M. D.; Angell, C. A.; Nagel, S. R. Supercooled Liquids and Glasses. *J. Phys. Chem.* **1996**, *100* (31), 13200–13212. <https://doi.org/10.1021/jp953538d>.
- (13) Gibbs, J. H.; DiMarzio, E. A. Nature of the Glass Transition and the Glassy State. *J. Chem. Phys.* **2004**, *28* (3), 373. <https://doi.org/10.1063/1.1744141>.
- (14) Götze, W. *Complex Dynamics of Glass-Forming Liquids, A Mode-Coupling Theory*, OUP Oxford.; 2008.
- (15) Adam, G.; Gibbs, J. H. On the Temperature Dependence of Cooperative Relaxation Properties in Glass-Forming Liquids. *J. Chem. Phys.* **2004**, *43* (1), 139. <https://doi.org/10.1063/1.1696442>.
- (16) Turnbull, D.; Cohen, M. H. Free-Volume Model of the Amorphous Phase: Glass Transition. *J. Chem. Phys.* **2004**, *34* (1), 120. <https://doi.org/10.1063/1.1731549>.

- (17) Cangialosi, D. Dynamics and Thermodynamics of Polymer Glasses. *J. Phys. Condens. Matter* **2014**, *26* (15), 153101. <https://doi.org/10.1088/0953-8984/26/15/153101>.
- (18) Tool, A. Q.; Eicitlin, C. G. VARIATIONS CAUSED IN THE HEATING CURVES OF GLASS BY HEAT TREATMENT1. *J. Am. Ceram. Soc.* **1931**, *14* (4), 276–308. <https://doi.org/10.1111/j.1151-2916.1931.tb16602.x>.
- (19) Gao, S.; Simon, S. L. Measurement of the Limiting Fictive Temperature over Five Decades of Cooling and Heating Rates. *Thermochim. Acta* **2015**, *603*, 123–127. <https://doi.org/10.1016/j.tca.2014.08.019>.
- (20) Weyer, S.; Huth, H.; Schick, C. Application of an Extended Tool–Narayanaswamy–Moynihan Model. Part 2. Frequency and Cooling Rate Dependence of Glass Transition from Temperature Modulated DSC. *Polymer* **2005**, *46* (26), 12240–12246. <https://doi.org/10.1016/j.polymer.2005.10.097>.
- (21) Rault, J. Origin of the Vogel–Fulcher–Tammann Law in Glass-Forming Materials: The α – β Bifurcation. *J. Non-Cryst. Solids* **2000**, *271* (3), 177–217. [https://doi.org/10.1016/S0022-3093\(00\)00099-5](https://doi.org/10.1016/S0022-3093(00)00099-5).
- (22) Rodrigues, A. C.; Viciosa, M. T.; Danède, F.; Affouard, F.; Correia, N. T. Molecular Mobility of Amorphous S -Flurbiprofen: A Dielectric Relaxation Spectroscopy Approach. *Mol. Pharm.* **2014**, *11* (1), 112–130. <https://doi.org/10.1021/mp4002188>.
- (23) Johari, G. P.; Goldstein, M. Viscous Liquids and the Glass Transition. II. Secondary Relaxations in Glasses of Rigid Molecules. *J. Chem. Phys.* **2003**, *53* (6), 2372. <https://doi.org/10.1063/1.1674335>.
- (24) Ngai, K. L.; Paluch, M. Classification of Secondary Relaxation in Glass-Formers Based on Dynamic Properties. *J. Chem. Phys.* **2004**, *120* (2), 857–873. <https://doi.org/10.1063/1.1630295>.
- (25) Gotze, W.; Sjogren, L. Relaxation Processes in Supercooled Liquids. *Rep. Prog. Phys.* **1992**, *55* (3), 241–376. <https://doi.org/10.1088/0034-4885/55/3/001>.
- (26) Fulcher, G. S. ANALYSIS OF RECENT MEASUREMENTS OF THE VISCOSITY OF GLASSES. *J. Am. Ceram. Soc.* **1925**, *8* (6), 339–355. <https://doi.org/10.1111/j.1151-2916.1925.tb16731.x>.
- (27) Cyrot, M. A Possible Origin for the Vogel-Fulcher Law. *Phys. Lett. A* **1981**, *83* (6), 275–278. [https://doi.org/10.1016/0375-9601\(81\)90982-8](https://doi.org/10.1016/0375-9601(81)90982-8).
- (28) Monnier, X. Molecular Dynamics in Complex Polymer Systems : From Anisotropy to Confinement Effects. PhD thesis, Rouen, Normandy, France, 2017.
- (29) Ngai, K. L. *Relaxation and Diffusion in Complex Systems; Partially Ordered Systems*; Springer New York: New York, NY, 2011. <https://doi.org/10.1007/978-1-4419-7649-9>.
- (30) Dixon, P. K.; Wu, L.; Nagel, S. R.; Williams, B. D.; Carini, J. P. Scaling in the Relaxation of Supercooled Liquids. *Phys. Rev. Lett.* **1990**, *65* (9), 1108. <https://doi.org/10.1103/PhysRevLett.65.1108>.
- (31) Floudas, G.; Paluch, M.; Grzybowski, A.; Ngai, K. L. New Physics Gained by the Application of Pressure in the Study of Dynamics of Glass Formers. *Mol. Dyn. Glass-Form. Syst.* **2011**, 89–120. https://doi.org/10.1007/978-3-642-04902-6_4.
- (32) Kremer, F. Dielectric Spectroscopy – Yesterday, Today and Tomorrow. *J. Non-Cryst. Solids* **2002**, *305* (1–3), 1–9. [https://doi.org/10.1016/S0022-3093\(02\)01083-9](https://doi.org/10.1016/S0022-3093(02)01083-9).
- (33) Glarum, S. H. Dielectric Relaxation of Isoamyl Bromide. *J. Chem. Phys.* **2004**, *33* (3), 639. <https://doi.org/10.1063/1.1731229>.
- (34) Cohen, M. H.; Turnbull, D. Molecular Transport in Liquids and Glasses. *J. Chem. Phys.* **2004**, *31* (5), 1164. <https://doi.org/10.1063/1.1730566>.

- (35) Stillinger, F. H.; Weber, T. A. Dynamics of Structural Transitions in Liquids. *Phys. Rev. A* **1983**, *28* (4), 2408. <https://doi.org/10.1103/PhysRevA.28.2408>.
- (36) Cavagna, A. Supercooled Liquids for Pedestrians. *Phys. Rep.* **2009**, *476* (4–6), 51–124. <https://doi.org/10.1016/j.physrep.2009.03.003>.
- (37) Doolittle, A. K. Studies in Newtonian Flow. II. The Dependence of the Viscosity of Liquids on Free-Space. *J. Appl. Phys.* **2004**, *22* (12), 1471. <https://doi.org/10.1063/1.1699894>.
- (38) Angell, C. A. Spectroscopy Simulation and Scattering, and the Medium Range Order Problem in Glass. *J. Non-Cryst. Solids* **1985**, *73* (1–3), 1–17. [https://doi.org/10.1016/0022-3093\(85\)90334-5](https://doi.org/10.1016/0022-3093(85)90334-5).
- (39) Angell, C. A. Relaxation in Liquids, Polymers and Plastic Crystals — Strong/Fragile Patterns and Problems. *J. Non-Cryst. Solids* **1991**, *131–133*, 13–31. [https://doi.org/10.1016/0022-3093\(91\)90266-9](https://doi.org/10.1016/0022-3093(91)90266-9).
- (40) Böhmer, R.; Ngai, K. L.; Angell, C. A.; Plazek, D. J. Nonexponential Relaxations in Strong and Fragile Glass Formers. *J. Chem. Phys.* **1993**, *99* (5), 4201–4209. <https://doi.org/10.1063/1.466117>.
- (41) Kunal, K.; Robertson, C. G.; Pawlus, S.; Hahn, S. F.; Sokolov, A. P. Role of Chemical Structure in Fragility of Polymers: A Qualitative Picture. *Macromolecules* **2008**, *41* (19), 7232–7238. <https://doi.org/10.1021/ma801155c>.
- (42) Qin, Q.; McKenna, G. B. Correlation between Dynamic Fragility and Glass Transition Temperature for Different Classes of Glass Forming Liquids. *J. Non-Cryst. Solids* **2006**, *352* (28–29), 2977–2985. <https://doi.org/10.1016/j.jnoncrysol.2006.04.014>.
- (43) Ngai, K. L.; Roland, C. M. Chemical Structure and Intermolecular Cooperativity: Dielectric Relaxation Results. *Macromolecules* **1993**, *26* (25), 6824–6830. <https://doi.org/10.1021/ma00077a019>.
- (44) Roland, C. M.; Santangelo, P. G.; Ngai, K. L. The Application of the Energy Landscape Model to Polymers. *J. Chem. Phys.* **1999**, *111* (12), 5593–5598. <https://doi.org/10.1063/1.479861>.
- (45) Huang, D.; McKenna, G. B. New Insights into the Fragility Dilemma in Liquids. *J. Chem. Phys.* **2001**, *114* (13), 5621–5630. <https://doi.org/10.1063/1.1348029>.
- (46) Sokolov, A. P.; Novikov, V. N.; Ding, Y. Why Many Polymers Are so Fragile. *J. Phys. Condens. Matter* **2007**, *19* (20), 205116. <https://doi.org/10.1088/0953-8984/19/20/205116>.
- (47) Santangelo, P. G.; Roland, C. M. Molecular Weight Dependence of Fragility in Polystyrene. *Macromolecules* **1998**, *31* (14), 4581–4585. <https://doi.org/10.1021/ma971823k>.
- (48) Williams, M. L.; Landel, R. F.; Ferry, J. D. The Temperature Dependence of Relaxation Mechanisms in Amorphous Polymers and Other Glass-Forming Liquids. *J. Am. Chem. Soc.* **1955**, *77* (14), 3701–3707. <https://doi.org/10.1021/ja01619a008>.
- (49) Arnoult, M.; Dargent, E.; Mano, J. F. Mobile Amorphous Phase Fragility in Semi-Crystalline Polymers: Comparison of PET and PLLA. *Polymer* **2007**, *48* (4), 1012–1019. <https://doi.org/10.1016/j.polymer.2006.12.053>.
- (50) Ngai, K. L. Dynamic and Thermodynamic Properties of Glass-Forming Substances. *J. Non-Cryst. Solids* **2000**, *275* (1–2), 7–51. [https://doi.org/10.1016/S0022-3093\(00\)00238-6](https://doi.org/10.1016/S0022-3093(00)00238-6).
- (51) Böhmer, R.; Angell, C. A. Correlations of the Nonexponentiality and State Dependence of Mechanical Relaxations with Bond Connectivity in Ge-As-Se

- Supercooled Liquids. *Phys. Rev. B* **1992**, *45* (17), 10091–10094. <https://doi.org/10.1103/PhysRevB.45.10091>.
- (52) Hall, R. W.; Wolynes, P. G. The Aperiodic Crystal Picture and Free Energy Barriers in Glasses. *J. Chem. Phys.* **1987**, *86* (5), 2943–2948. <https://doi.org/10.1063/1.452045>.
- (53) Dyre, J. C.; Olsen, N. B.; Christensen, T. Local Elastic Expansion Model for Viscous-Flow Activation Energies of Glass-Forming Molecular Liquids. *Phys. Rev. B* **1996**, *53* (5), 2171–2174. <https://doi.org/10.1103/PhysRevB.53.2171>.
- (54) Dyre, J. C. Source of Non-Arrhenius Average Relaxation Time in Glass-Forming Liquids. *J. Non-Cryst. Solids* **1998**, *235–237*, 142–149. [https://doi.org/10.1016/S0022-3093\(98\)00502-X](https://doi.org/10.1016/S0022-3093(98)00502-X).
- (55) Scopigno, T. Is the Fragility of a Liquid Embedded in the Properties of Its Glass? *Science* **2003**, *302* (5646), 849–852. <https://doi.org/10.1126/science.1089446>.
- (56) Xia, X.; Wolynes, P. G. Fragilities of Liquids Predicted from the Random First Order Transition Theory of Glasses. *Proc. Natl. Acad. Sci.* **2000**, *97* (7), 2990–2994. <https://doi.org/10.1073/pnas.97.7.2990>.
- (57) Buchenau, U.; Wischnewski, A. Fragility and Compressibility at the Glass Transition. *Phys. Rev. B* **2004**, *70* (9), 092201. <https://doi.org/10.1103/PhysRevB.70.092201>.
- (58) Martinez, L.-M.; Angell, C. A. A Thermodynamic Connection to the Fragility of Glass-Forming Liquids. *Nature* **2001**, *410* (6829), 663–667. <https://doi.org/10.1038/35070517>.
- (59) Ngai, K. L.; Yamamuro, O. Thermodynamic Fragility and Kinetic Fragility in Supercooling Liquids: A Missing Link in Molecular Liquids. *J. Chem. Phys.* **1999**, *111* (23), 10403–10406. <https://doi.org/10.1063/1.480394>.
- (60) Ito, K.; Moynihan, C. T.; Angell, C. A. Thermodynamic Determination of Fragility in Liquids and a Fragile-to-Strong Liquid Transition in Water. *Nature* **1999**, *398* (6727), 492–495. <https://doi.org/10.1038/19042>.
- (61) Angell, C. A.; Borick, S. Specific Heats C_p , C_v , C_{conf} and Energy Landscapes of Glassforming Liquids. *J. Non-Cryst. Solids* **2002**, *307–310*, 393–406. [https://doi.org/10.1016/S0022-3093\(02\)01500-4](https://doi.org/10.1016/S0022-3093(02)01500-4).
- (62) Prevosto, D.; Lucchesi, M.; Capaccioli, S.; Casalini, R.; Rolla, P. A. Correlation between Configurational Entropy and Structural Relaxation Time in Glass-Forming Liquids. *Phys. Rev. B* **2003**, *67* (17), 174202. <https://doi.org/10.1103/PhysRevB.67.174202>.
- (63) Prevosto, D.; Capaccioli, S.; Lucchesi, M.; Leporini, D.; Rolla, P. Pressure and Temperature Dependence of Structural Relaxation Dynamics in Polymers: A Thermodynamic Interpretation. *J. Phys. Condens. Matter* **2004**, *16* (36), 6597–6608. <https://doi.org/10.1088/0953-8984/16/36/025>.
- (64) Corezzi, S.; Comez, L.; Fioretto, D. Can Experiments Select the Configurational Component of Excess Entropy? *Eur. Phys. J. E* **2004**, *14* (2), 143–147. <https://doi.org/10.1140/epje/i2003-10145-0>.
- (65) Speedy, R. J. Relations between a Liquid and Its Glasses. *J. Phys. Chem. B* **1999**, *103* (20), 4060–4065. <https://doi.org/10.1021/jp983830w>.
- (66) Lifshitz, E. M.; Pitaevski, L. P. *Statistical Physics, Theory of the Condensed State*, first edition.; Elsevier, 1980.
- (67) Crétois, R.; Delbreilh, L.; Dargent, E.; Follain, N.; Lebrun, L.; Saiter, J. M. Dielectric Relaxations in Polyhydroxyalkanoates/Organoclay Nanocomposites. *Eur. Polym. J.* **2013**, *49* (11), 3434–3444. <https://doi.org/10.1016/j.eurpolymj.2013.07.009>.

- (68) Saiter, A.; Hess, M.; D'Souza, N. A.; Saiter, J. M. Entropy and Fragility in Vitreous Polymers. *Polymer* **2002**, *43* (26), 7497–7504. [https://doi.org/10.1016/S0032-3861\(02\)00631-6](https://doi.org/10.1016/S0032-3861(02)00631-6).
- (69) Saiter, A.; Devallencourt, C.; Saiter, J. M.; Grenet, J. Thermodynamically “Strong” and Kinetically “Fragile” Polymeric Glass Exemplified by Melamine Formaldehyde Resins. *Eur. Polym. J.* **2001**, *37* (6), 1083–1090. [https://doi.org/10.1016/S0014-3057\(00\)00242-1](https://doi.org/10.1016/S0014-3057(00)00242-1).
- (70) Hamonic, F.; Saiter, A.; Prevosto, D.; Dargent, E.; Saiter, J. M. Temperature Dependence of Structural Relaxation Time in Drawn Polymers: Which Is the Role of Cooperativity?; Ischia, Italy, 2012; pp 211–213. <https://doi.org/10.1063/1.4738446>.
- (71) Hong, L.; Novikov, V. N.; Sokolov, A. P. Is There a Connection between Fragility of Glass Forming Systems and Dynamic Heterogeneity/Cooperativity? *J. Non-Cryst. Solids* **2011**, *357* (2), 351–356. <https://doi.org/10.1016/j.jnoncrysol.2010.06.071>.
- (72) Araujo, S.; Batteux, F.; Li, W.; Butterfield, L.; Delpouve, N.; Esposito, A.; Tan, L.; Saiter, J.-M.; Negahban, M. A Structural Interpretation of the Two Components Governing the Kinetic Fragility from the Example of Interpenetrated Polymer Networks: A Structural Interpretation of the Two Components Governing the Kinetic Fragility from the Example of Interpenetrated Polymer Networks. *J. Polym. Sci. Part B Polym. Phys.* **2018**, *56* (20), 1393–1403. <https://doi.org/10.1002/polb.24722>.
- (73) Araujo, S.; Delpouve, N.; Domenek, S.; Guinault, A.; Golovchak, R.; Szatanik, R.; Ingram, A.; Fauchard, C.; Delbreilh, L.; Dargent, E. Cooperativity Scaling and Free Volume in Plasticized Polylactide. *Macromolecules* **2019**, *52* (16), 6107–6115. <https://doi.org/10.1021/acs.macromol.9b00464>.
- (74) Hong, L.; Gujrati, P. D.; Novikov, V. N.; Sokolov, A. P. Molecular Cooperativity in the Dynamics of Glass-Forming Systems: A New Insight. *J. Chem. Phys.* **2009**, *131* (19), 194511. <https://doi.org/10.1063/1.3266508>.
- (75) Ediger, M. D.; Harrowell, P. Perspective: Supercooled Liquids and Glasses. *J. Chem. Phys.* **2012**, *137* (8), 080901. <https://doi.org/10.1063/1.4747326>.
- (76) Hempel, E.; Hempel, G.; Hensel, A.; Schick, C.; Donth, E. Characteristic Length of Dynamic Glass Transition near T_g for a Wide Assortment of Glass-Forming Substances. *J. Phys. Chem. B* **2000**, *104* (11), 2460–2466. <https://doi.org/10.1021/jp991153f>.
- (77) Donth, E. The Size of Cooperatively Rearranging Regions at the Glass Transition. *J. Non-Cryst. Solids* **1982**, *53* (3), 325–330. [https://doi.org/10.1016/0022-3093\(82\)90089-8](https://doi.org/10.1016/0022-3093(82)90089-8).
- (78) Adam, G.; Gibbs, J. H. On the Temperature Dependence of Cooperative Relaxation Properties in Glass-Forming Liquids. *J. Chem. Phys.* **1965**, *43* (1), 139–146. <https://doi.org/10.1063/1.1696442>.
- (79) Fischer, E. W.; Donth, E.; Steffen, W. Temperature Dependence of Characteristic Length for Glass Transition. *Phys. Rev. Lett.* **1992**, *68* (15), 2344. <https://doi.org/10.1103/PhysRevLett.68.2344>.
- (80) Moynihan, C. T.; Schroeder, J. Anomalous Light Scattering in the Glass Transition Region. *J. Non-Cryst. Solids* **1993**, *161*, 148–151. [https://doi.org/10.1016/0022-3093\(93\)90687-S](https://doi.org/10.1016/0022-3093(93)90687-S).
- (81) Donth, E. Characteristic Length of Glass Transition. *J. Non-Cryst. Solids* **1991**, *131*–*133*, 204–206. [https://doi.org/10.1016/0022-3093\(91\)90300-U](https://doi.org/10.1016/0022-3093(91)90300-U).

- (82) Arabeche, K.; Delbreilh, L.; Adhikari, R.; Michler, G. H.; Hiltner, A.; Baer, E.; Saiter, J.-M. Study of the Cooperativity at the Glass Transition Temperature in PC/PMMA Multilayered Films: Influence of Thickness Reduction from Macro- to Nanoscale. *Polymer* **2012**, *53* (6), 1355–1361. <https://doi.org/10.1016/j.polymer.2012.01.045>.
- (83) Monnier, X.; Delpouve, N.; Basson, N.; Guinault, A.; Domenek, S.; Saiter, A.; Mallon, P. E.; Dargent, E. Molecular Dynamics in Electrospun Amorphous Plasticized Polylactide Fibers. *Polymer* **2015**, *73*, 68–78. <https://doi.org/10.1016/j.polymer.2015.07.047>.
- (84) Cangialosi, D. Glass Transition and Physical Aging of Confined Polymers Investigated by Calorimetric Techniques. In *Handbook of Thermal Analysis and Calorimetry*; Elsevier, 2018; Vol. 6, pp 301–337. <https://doi.org/10.1016/B978-0-444-64062-8.00013-9>.
- (85) Hutchinson, J. M. Physical Aging of Polymers. *Prog. Polym. Sci.* **1995**, *20* (4), 703–760. [https://doi.org/10.1016/0079-6700\(94\)00001-I](https://doi.org/10.1016/0079-6700(94)00001-I).
- (86) Huang, Y.; Paul, D. R. Physical Aging of Thin Glassy Polymer Films Monitored by Optical Properties. *Macromolecules* **2006**, *39* (4), 1554–1559. <https://doi.org/10.1021/ma050533y>.
- (87) Richardson, M. J.; Savill, N. G. Derivation of Accurate Glass Transition Temperatures by Differential Scanning Calorimetry. *Polymer* **1975**, *16* (10), 753–757. [https://doi.org/10.1016/0032-3861\(75\)90194-9](https://doi.org/10.1016/0032-3861(75)90194-9).
- (88) Badrinarayanan, P.; Zheng, W.; Li, Q.; Simon, S. L. The Glass Transition Temperature versus the Fictive Temperature. *J. Non-Cryst. Solids* **2007**, *353* (26), 2603–2612. <https://doi.org/10.1016/j.jnoncrysol.2007.04.025>.
- (89) Gao, S.; Koh, Y. P.; Simon, S. L. Calorimetric Glass Transition of Single Polystyrene Ultrathin Films <https://pubs.acs.org/doi/abs/10.1021/ma3020036> (accessed Mar 23, 2018). <https://doi.org/10.1021/ma3020036>.
- (90) Moynihan, C. T.; Macedo, P. B.; Montrose, C. J.; Montrose, C. J.; Gupta, P. K.; DeBolt, M. A.; Dill, J. F.; Dom, B. E.; Drake, P. W.; Easteal, A. J.; Elterman, P. B.; Moeller, R. P.; Sasabe, H.; Wilder, J. A. STRUCTURAL RELAXATION IN VITREOUS MATERIALS. *Ann. N. Y. Acad. Sci.* **1976**, *279* (1 The Glass Tra), 15–35. <https://doi.org/10.1111/j.1749-6632.1976.tb39688.x>.
- (91) Moynihan, C. T.; Easteal, A. J.; Wilder, J.; Tucker, J. Dependence of the Glass Transition Temperature on Heating and Cooling Rate. *J. Phys. Chem.* **1974**, *78* (26), 2673–2677. <https://doi.org/10.1021/j100619a008>.
- (92) Narayanaswamy, O. S. A Model of Structural Relaxation in Glass. *J. Am. Ceram. Soc.* **1971**, *54* (10), 491–498. <https://doi.org/10.1111/j.1151-2916.1971.tb12186.x>.
- (93) Moynihan, C. T.; Easteal, A. J.; Bolt, M. A. D.; Tucker, J. Dependence of the Fictive Temperature of Glass on Cooling Rate. *J. Am. Ceram. Soc.* **1976**, *59* (1-2), 12–16. <https://doi.org/10.1111/j.1151-2916.1976.tb09376.x>.
- (94) Mackenzie, J. D.; Rice, S. A. *Modern Aspects of the Vitreous State. Phys. Today* **1961**, *14* (10), 62–62. <https://doi.org/10.1063/1.3057162>.
- (95) Williams, G.; C. Watts, D. Non-Symmetrical Dielectric Relaxation Behaviour Arising from a Simple Empirical Decay Function. *Trans. Faraday Soc.* **1970**, *66* (0), 80–85. <https://doi.org/10.1039/TF9706600080>.
- (96) Toda, A.; Androsch, R.; Schick, C. Insights into Polymer Crystallization and Melting from Fast Scanning Chip Calorimetry. *Polymer* **2016**, *91*, 239–263. <https://doi.org/10.1016/j.polymer.2016.03.038>.

- (97) Olmsted, P. D.; Poon, W. C. K.; McLeish, T. C. B.; Terrill, N. J.; Ryan, A. J. Spinodal-Assisted Crystallization in Polymer Melts. *Phys. Rev. Lett.* **1998**, *81* (2), 373–376. <https://doi.org/10.1103/PhysRevLett.81.373>.
- (98) Hodge, I. M. Enthalpy Relaxation and Recovery in Amorphous Materials. *J. Non-Cryst. Solids* **1994**, *169* (3), 211–266. [https://doi.org/10.1016/0022-3093\(94\)90321-2](https://doi.org/10.1016/0022-3093(94)90321-2).
- (99) Li, H.; Huneault, M. A. Effect of Nucleation and Plasticization on the Crystallization of Poly(Lactic Acid). *Polymer* **2007**, *48* (23), 6855–6866. <https://doi.org/10.1016/j.polymer.2007.09.020>.
- (100) Ammar, A. H.; Farid, A. M.; Farag, A. A. M. Non-Isothermal Kinetic Analysis of Crystallization of Vacuum Prepared Se₉₀In_{9.9}Cu_{0.1} Alloy Thin Films. *J. Non-Cryst. Solids* **2016**, *434*, 85–91. <https://doi.org/10.1016/j.jnoncrysol.2015.12.009>.
- (101) Bai, H.; Huang, C.; Xiu, H.; Zhang, Q.; Fu, Q. Enhancing Mechanical Performance of Polylactide by Tailoring Crystal Morphology and Lamellae Orientation with the Aid of Nucleating Agent. *Polymer* **2014**, *55* (26), 6924–6934. <https://doi.org/10.1016/j.polymer.2014.10.059>.
- (102) Reid, B. O.; Vadlamudi, M.; Mamun, A.; Janani, H.; Gao, H.; Hu, W.; Alamo, R. G. Strong Memory Effect of Crystallization above the Equilibrium Melting Point of Random Copolymers. *Macromolecules* **2013**, *46* (16), 6485–6497. <https://doi.org/10.1021/ma400839d>.
- (103) Cavallo, D.; Gardella, L.; Portale, G.; Müller, A. J.; Alfonso, G. C. Kinetics of Cross-Nucleation in Isotactic Poly(1-Butene). *Macromolecules* **2014**, *47* (2), 870–873. <https://doi.org/10.1021/ma402396f>.
- (104) Wang, Z.; Ma, Z.; Li, L. Flow-Induced Crystallization of Polymers: Molecular and Thermodynamic Considerations. *Macromolecules* **2016**, *49* (5), 1505–1517. <https://doi.org/10.1021/acs.macromol.5b02688>.
- (105) Strobl, G. R. *The Physics of Polymers: Concepts for Understanding Their Structures and Behavior*, 3rd. rev. and expanded ed.; Springer: Berlin ; New York, 2007.
- (106) Sharma, V.; Desai, P.; Abhiraman, A. S. Crystallinity Vis-à-vis Two-phase Models of Oriented Polymers: Inferences from an Experimental Study of Poly(Ethylene Terephthalate). *J. Appl. Polym. Sci.* **1997**, *65* (13), 2603–2612. [https://doi.org/10.1002/\(SICI\)1097-4628\(19970926\)65:13<2603::AID-APP2>3.0.CO;2-F](https://doi.org/10.1002/(SICI)1097-4628(19970926)65:13<2603::AID-APP2>3.0.CO;2-F).
- (107) Gupta, V. B. Heat Setting. *J. Appl. Polym. Sci.* **2002**, *83* (3), 586–609. <https://doi.org/10.1002/app.2260>.
- (108) Suzuki, H.; Grebowicz, J.; Wunderlich, B. Heat Capacity of Semicrystalline, Linear Poly(Oxymethylene) and Poly(Oxyethylene). *Makromol. Chem.* **1985**, *186* (5), 1109–1119. <https://doi.org/10.1002/macp.1985.021860521>.
- (109) Nogales, A.; Ezquerra, T. A.; Batallán, F.; Frick, B.; López-Cabarcos, E.; Baltá-Calleja, F. J. Restricted Dynamics in Poly(Ether Ether Ketone) As Revealed by Incoherent Quasielastic Neutron Scattering and Broad-Band Dielectric Spectroscopy. *Macromolecules* **1999**, *32* (7), 2301–2308. <https://doi.org/10.1021/ma9815758>.
- (110) Schick, C.; Dobbertin, J.; Pötter, M.; Dehne, H.; Hensel, A.; Wurm, A.; Ghoneim, A. M.; Weyer, S. Separation of Components of Different Molecular Mobility by Calorimetry, Dynamic Mechanical and Dielectric Spectroscopy. *J. Therm. Anal.* **1997**, *49* (1), 499–511. <https://doi.org/10.1007/BF01987477>.

- (111) Gabrielse, W.; Angad Gaur, H.; Feyen, F. C.; Veeman, W. S. ¹³C Solid-State NMR Study of Differently Processed Poly(Ethylene Terephthalate) Yarns. *Macromolecules* **1994**, *27* (20), 5811–5820. <https://doi.org/10.1021/ma00098a040>.
- (112) Cole, K. C.; Ajji, A.; Pellerin, É. New Insights into the Development of Ordered Structure in Poly(Ethylene Terephthalate). 1. Results from External Reflection Infrared Spectroscopy. *Macromolecules* **2002**, *35* (3), 770–784. <https://doi.org/10.1021/ma011492i>.
- (113) Ishida, Yō.; Yamafuji, K.; Ito, H.; Takayanagi, M. Effects of Degree of Crystallinity upon Dielectric Behaviors in Some Aromatic Polyesters. *Kolloid-Z. Z. Für Polym.* **1962**, *184* (2), 97–108. <https://doi.org/10.1007/BF01795078>.
- (114) Esposito, A.; Delpouve, N.; Causin, V.; Dhotel, A.; Delbreilh, L.; Dargent, E. From a Three-Phase Model to a Continuous Description of Molecular Mobility in Semicrystalline Poly(Hydroxybutyrate- Co -Hydroxyvalerate). *Macromolecules* **2016**, *49* (13), 4850–4861. <https://doi.org/10.1021/acs.macromol.6b00384>.
- (115) Androsch, R.; Wunderlich, B. The Link between Rigid Amorphous Fraction and Crystal Perfection in Cold-Crystallized Poly(Ethylene Terephthalate). *Polymer* **2005**, *46* (26), 12556–12566. <https://doi.org/10.1016/j.polymer.2005.10.099>.
- (116) Ma, Q.; Georgiev, G.; Cebe, P. Constraints in Semicrystalline Polymers: Using Quasi-Isothermal Analysis to Investigate the Mechanisms of Formation and Loss of the Rigid Amorphous Fraction. *Polymer* **2011**, *52* (20), 4562–4570. <https://doi.org/10.1016/j.polymer.2011.08.006>.
- (117) Alves, N. M.; Mano, J. F.; Balaguer, E.; Meseguer Dueñas, J. M.; Gómez Ribelles, J. L. Glass Transition and Structural Relaxation in Semi-Crystalline Poly(Ethylene Terephthalate): A DSC Study. *Polymer* **2002**, *43* (15), 4111–4122. [https://doi.org/10.1016/S0032-3861\(02\)00236-7](https://doi.org/10.1016/S0032-3861(02)00236-7).
- (118) Wang, Y.; Mano, J. F. Effect of Structural Relaxation at Physiological Temperature on the Mechanical Property of Poly(L-lactic Acid) Studied by Microhardness Measurements. *J. Appl. Polym. Sci.* **2006**, *100* (4), 2628–2633. <https://doi.org/10.1002/app.22643>.
- (119) Delpouve, N.; Saiter, A.; Mano, J. F.; Dargent, E. Cooperative Rearranging Region Size in Semi-Crystalline Poly(l-Lactic Acid). *Polymer* **2008**, *49* (13–14), 3130–3135. <https://doi.org/10.1016/j.polymer.2008.04.045>.
- (120) Wang, Y.; Gómez Ribelles, J. L.; Salmerón Sánchez, M.; Mano, J. F. Morphological Contributions to Glass Transition in Poly(L -Lactic Acid). *Macromolecules* **2005**, *38* (11), 4712–4718. <https://doi.org/10.1021/ma047934i>.
- (121) Jackson, C. L.; McKenna, G. B. The Glass Transition of Organic Liquids Confined to Small Pores. *J. Non-Cryst. Solids* **1991**, *131–133*, 221–224. [https://doi.org/10.1016/0022-3093\(91\)90305-P](https://doi.org/10.1016/0022-3093(91)90305-P).
- (122) Fernandes Nassar, S. Understanding of the Relationship between the Microstructure of Polylactide, Its Macromolecular Mobility and Its Barrier Properties for the Creation of Packaging from Tomorrow's Renewable Resources. PhD thesis, Paris-Saclay, France, 2017.
- (123) Langhe, D. S.; Murphy, T. M.; Shaver, A.; LaPorte, C.; Freeman, B. D.; Paul, D. R.; Baer, E. Structural Relaxation of Polystyrene in Nanolayer Confinement. *Polymer* **2012**, *53* (9), 1925–1931. <https://doi.org/10.1016/j.polymer.2012.02.044>.
- (124) Shakhmatkin, B. A.; Vedishcheva, N. M.; Shultz, M. M.; Wright, A. C. The Thermodynamic Properties of Oxide Glasses and Glass-Forming Liquids and Their

- Chemical Structure. *J. Non-Cryst. Solids* **1994**, *177*, 249–256. [https://doi.org/10.1016/0022-3093\(94\)90538-X](https://doi.org/10.1016/0022-3093(94)90538-X).
- (125) Kremer, F.; Tress, M.; Mapesa, E. U. Glassy Dynamics and Glass Transition in Nanometric Layers and Films: A Silver Lining on the Horizon. *J. Non-Cryst. Solids* **2015**, *407*, 277–283. <https://doi.org/10.1016/j.jnoncrysol.2014.08.016>.
- (126) Messin, T.; Follain, N.; Guinault, A.; Miquelard-Garnier, G.; Sollogoub, C.; Delpouve, N.; Gaucher, V.; Marais, S. Confinement Effect in PC/MXD6 Multilayer Films: Impact of the Microlayered Structure on Water and Gas Barrier Properties. *J. Membr. Sci.* **2017**, *525*, 135–145. <https://doi.org/10.1016/j.memsci.2016.10.039>.
- (127) Arabeche, K.; Delbreilh, L.; Adhikari, R.; Michler, G. H.; Hiltner, A.; Baer, E.; Saiter, J.-M. Study of the Cooperativity at the Glass Transition Temperature in PC/PMMA Multilayered Films: Influence of Thickness Reduction from Macro- to Nanoscale. *Polymer* **2012**, *53* (6), 1355–1361. <https://doi.org/10.1016/j.polymer.2012.01.045>.
- (128) Anastasiadis, S. H.; Karatasos, K.; Vlachos, G.; Manias, E.; Giannelis, E. P. Nanoscopic-Confinement Effects on Local Dynamics. *Phys. Rev. Lett.* **2000**, *84* (5), 915–918. <https://doi.org/10.1103/PhysRevLett.84.915>.
- (129) Mattsson, J.; Forrest, J. A.; Börjesson, L. Quantifying Glass Transition Behavior in Ultrathin Free-Standing Polymer Films. *Phys. Rev. E* **2000**, *62* (4), 5187–5200. <https://doi.org/10.1103/PhysRevE.62.5187>.
- (130) Forrest, J. A.; Dalnoki-Veress, K. The Glass Transition in Thin Polymer Films. *Adv. Colloid Interface Sci.* **2001**, *94* (1–3), 167–195. [https://doi.org/10.1016/S0001-8686\(01\)00060-4](https://doi.org/10.1016/S0001-8686(01)00060-4).
- (131) 12th International Symposium on Electrets (ISE 12). In *2005 12th International Symposium on Electrets*; IEEE: Salvador, Brazil, 2005; pp i–i. <https://doi.org/10.1109/ISE.2005.1612299>.
- (132) Root-Mean-Square End-to-End Distance in Polymers, 1/2. In *IUPAC Compendium of Chemical Terminology*; Nič, M., Jiráč, J., Košata, B., Jenkins, A., McNaught, A., Eds.; IUPAC: Research Triangle Park, NC, 2009. <https://doi.org/10.1351/goldbook.R05405>.
- (133) Fox, T. G.; Flory, P. J. Second-Order Transition Temperatures and Related Properties of Polystyrene. I. Influence of Molecular Weight. *J. Appl. Phys.* **1950**, *21* (6), 581–591. <https://doi.org/10.1063/1.1699711>.
- (134) Fox, T. G.; Flory, P. J. The Glass Temperature and Related Properties of Polystyrene. Influence of Molecular Weight. *J. Polym. Sci.* **1954**, *14* (75), 315–319. <https://doi.org/10.1002/pol.1954.120147514>.
- (135) Fox, T. G.; Flory, P. J. Second-Order Transition Temperatures and Related Properties of Polystyrene. I. Influence of Molecular Weight. *J. Appl. Phys.* **1950**, *21* (6), 581–591. <https://doi.org/10.1063/1.1699711>.
- (136) Geng, K.; Tsui, O. K. C. Effects of Polymer Tacticity and Molecular Weight on the Glass Transition Temperature of Poly(Methyl Methacrylate) Films on Silica. *Macromolecules* **2016**, *49* (7), 2671–2678. <https://doi.org/10.1021/acs.macromol.6b00108>.
- (137) Ueberreiter, K.; Kanig, G. Self-Plasticization of Polymers. *J. Colloid Sci.* **1952**, *7* (6), 569–583. [https://doi.org/10.1016/0095-8522\(52\)90040-8](https://doi.org/10.1016/0095-8522(52)90040-8).
- (138) Cowie, J. M. G.; Toporowski, P. M. The Dependence of Glass Temperature on Molecular Weight for Poly α -Methyl Styrene. *Eur. Polym. J.* **1968**, *4* (5), 621–625. [https://doi.org/10.1016/0014-3057\(68\)90060-8](https://doi.org/10.1016/0014-3057(68)90060-8).

- (139) Pezzin, G.; Zilio-Grandi, F.; Sanmartin, P. The Dependence of the Glass Transition Temperature on Molecular Weight for Polyvinylchloride. *Eur. Polym. J.* **1970**, *6* (7), 1053–1061. [https://doi.org/10.1016/0014-3057\(70\)90038-8](https://doi.org/10.1016/0014-3057(70)90038-8).
- (140) Beevers, R. B.; White, E. F. T. Physical Properties of Vinyl Polymers. Part 1.—Dependence of the Glass-Transition Temperature of Polymethylmethacrylate on Molecular Weight. *Trans Faraday Soc* **1960**, *56* (0), 744–752. <https://doi.org/10.1039/TF9605600744>.
- (141) Montserrat, S.; Colomer, P. The Effect of the Molecular Weight on the Glass Transition Temperature in Amorphous Poly(Ethylene Terephthalate). *Polym. Bull.* **1984**, *12* (2). <https://doi.org/10.1007/BF00263341>.
- (142) Agapov, A. L.; Sokolov, A. P. Does the Molecular Weight Dependence of T_g Correlate to M_e ? *Macromolecules* **2009**, *42* (7), 2877–2878. <https://doi.org/10.1021/ma9002825>.
- (143) Hintermeyer, J.; Herrmann, A.; Kahlau, R.; Goiceanu, C.; Rössler, E. A. Molecular Weight Dependence of Glassy Dynamics in Linear Polymers Revisited. *Macromolecules* **2008**, *41* (23), 9335–9344. <https://doi.org/10.1021/ma8016794>.
- (144) Zhang, L.; Torkelson, J. M. Enhanced Glass Transition Temperature of Low Molecular Weight Poly(Methyl Methacrylate) by Initiator Fragments Located at Chain Ends. *Polymer* **2017**, *122*, 194–199. <https://doi.org/10.1016/j.polymer.2017.06.054>.
- (145) Gibbs, J. H.; DiMarzio, E. A. Nature of the Glass Transition and the Glassy State. *J. Chem. Phys.* **1958**, *28* (3), 373–383. <https://doi.org/10.1063/1.1744141>.
- (146) Bershtein, V. A.; Egorov, V. M.; Podolsky, A. F.; Stepanov, V. A. Interrelationship and Common Nature of the β Relaxation and the Glass Transition in Polymers. *J. Polym. Sci. Polym. Lett. Ed.* **1985**, *23* (7), 371–377. <https://doi.org/10.1002/pol.1985.130230705>.
- (147) Cown, J. M. G. Some General Features of Relations for Oligomers and Amorphous Polymers. *Eur. Polym. J.* **1975**, *11* (4), 297–300. [https://doi.org/10.1016/0014-3057\(75\)90037-3](https://doi.org/10.1016/0014-3057(75)90037-3).
- (148) Baker, D. L.; Reynolds, M.; Masurel, R.; Olmsted, P. D.; Mattsson, J. Chain-Length, Flexibility and the Glass Transition of Polymers. *ArXiv191113278 Cond-Mat Physicsphysics* **2019**.
- (149) Mirigian, S.; Schweizer, K. S. Dynamical Theory of Segmental Relaxation and Emergent Elasticity in Supercooled Polymer Melts. *Macromolecules* **2015**, *48* (6), 1901–1913. <https://doi.org/10.1021/ma5022083>.
- (150) Colmenero, J. Are Polymers Standard Glass-Forming Systems? The Role of Intramolecular Barriers on the Glass-Transition Phenomena of Glass-Forming Polymers. *J. Phys. Condens. Matter* **2015**, *27* (10), 103101. <https://doi.org/10.1088/0953-8984/27/10/103101>.
- (151) Hintermeyer, J.; Herrmann, A.; Kahlau, R.; Goiceanu, C.; Rössler, E. A. Molecular Weight Dependence of Glassy Dynamics in Linear Polymers Revisited. *Macromolecules* **2008**, *41* (23), 9335–9344. <https://doi.org/10.1021/ma8016794>.
- (152) Kawana, S.; Jones, R. A. L. Character of the Glass Transition in Thin Supported Polymer Films. *Phys. Rev. E* **2001**, *63* (2). <https://doi.org/10.1103/PhysRevE.63.021501>.
- (153) Fukao, K.; Miyamoto, Y. Glass Transitions and Dynamics in Thin Polymer Films: Dielectric Relaxation of Thin Films of Polystyrene. *Phys. Rev. E* **2000**, *61* (2), 1743–1754. <https://doi.org/10.1103/PhysRevE.61.1743>.

- (154) Huang, D.; McKenna, G. B. New Insights into the Fragility Dilemma in Liquids. *J. Chem. Phys.* **2001**, *114* (13), 5621–5630. <https://doi.org/10.1063/1.1348029>.
- (155) Böhmer, R.; Ngai, K. L.; Angell, C. A.; Plazek, D. J. Nonexponential Relaxations in Strong and Fragile Glass Formers. *J. Chem. Phys.* **1993**, *99* (5), 4201–4209. <https://doi.org/10.1063/1.466117>.
- (156) Ding, Y.; Novikov, V. N.; Sokolov, A. P.; Dalle-Ferrier, C.; Alba-Simionesco, C.; Frick, B. Influence of Molecular Weight on Fast Dynamics and Fragility of Polymers. *Macromolecules* **2004**, *37* (24), 9264–9272. <https://doi.org/10.1021/ma0492420>.
- (157) Dudowicz, J.; Freed, K. F.; Douglas, J. F. The Glass Transition Temperature of Polymer Melts †. *J. Phys. Chem. B* **2005**, *109* (45), 21285–21292. <https://doi.org/10.1021/jp0523266>.
- (158) Saltzman, E. J.; Schweizer, K. S. Universal Scaling, Dynamic Fragility, Segmental Relaxation, and Vitrification in Polymer Melts. *J. Chem. Phys.* **2004**, *121* (4), 2001–2009. <https://doi.org/10.1063/1.1756856>.
- (159) Andreozzi, L.; Autiero, C.; Faetti, M.; Giordano, M.; Zulli, F. Dynamics, Fragility, and Glass Transition of Low-Molecular-Weight Linear Homopolymers. *Philos. Mag.* **2008**, *88* (33–35), 4151–4159. <https://doi.org/10.1080/14786430802468231>.
- (160) Jin, K.; Torkelson, J. M. Enhanced T_g -Confinement Effect in Cross-Linked Polystyrene Compared to Its Linear Precursor: Roles of Fragility and Chain Architecture. *Macromolecules* **2016**, *49* (14), 5092–5103. <https://doi.org/10.1021/acs.macromol.6b01042>.
- (161) Glynos, E.; Frieberg, B.; Oh, H.; Liu, M.; Gidley, D. W.; Green, P. F. Role of Molecular Architecture on the Vitrification of Polymer Thin Films. *Phys. Rev. Lett.* **2011**, *106* (12). <https://doi.org/10.1103/PhysRevLett.106.128301>.
- (162) Frieberg, B.; Glynos, E.; Green, P. F. Structural Relaxations of Thin Polymer Films. *Phys. Rev. Lett.* **2012**, *108* (26). <https://doi.org/10.1103/PhysRevLett.108.268304>.
- (163) He, Q.; Narayanan, S.; Wu, D. T.; Foster, M. D. Confinement Effects with Molten Thin Cyclic Polystyrene Films. *ACS Macro Lett.* **2016**, *5* (9), 999–1003. <https://doi.org/10.1021/acsmacrolett.6b00497>.
- (164) Simon, S. L.; Plazek, D. J.; Sobieski, J. W.; McGregor, E. T. Physical Aging of a Polyetherimide: Volume Recovery and Its Comparison to Creep and Enthalpy Measurements. *J. Polym. Sci. Part B Polym. Phys.* **1997**, *35* (6), 929–936. [https://doi.org/10.1002/\(SICI\)1099-0488\(19970430\)35:6<929::AID-POLB7>3.0.CO;2-C](https://doi.org/10.1002/(SICI)1099-0488(19970430)35:6<929::AID-POLB7>3.0.CO;2-C).
- (165) Cangialosi, D.; Alegría, A.; Colmenero, J. A Thermodynamic Approach to the Fragility of Glass-Forming Polymers. *J. Chem. Phys.* **2006**, *124* (2), 024906. <https://doi.org/10.1063/1.2149853>.
- (166) Kim, S.; Mundra, M. K.; Roth, C. B.; Torkelson, J. M. Suppression of the T_g - Nanoconfinement Effect in Thin Poly(Vinyl Acetate) Films by Sorbed Water. *Macromolecules* **2010**, *43* (11), 5158–5161. <https://doi.org/10.1021/ma1005606>.
- (167) Wang, T.; Li, H.; Wang, F.; Yan, S.; Schultz, J. M. Confined Growth of Poly(Butylene Succinate) in Its Miscible Blends with Poly(Vinylidene Fluoride): Morphology and Growth Kinetics. *J. Phys. Chem. B* **2011**, *115* (24), 7814–7822. <https://doi.org/10.1021/jp203680e>.
- (168) Carr, J. M.; Langhe, D. S.; Ponting, M. T.; Hiltner, A.; Baer, E. Confined Crystallization in Polymer Nanolayered Films: A Review. *J. Mater. Res.* **2012**, *27* (10), 1326–1350. <https://doi.org/10.1557/jmr.2012.17>.

- (169) Gao, S.; Koh, Y. P.; Simon, S. L. Calorimetric Glass Transition of Single Polystyrene Ultrathin Films. *Macromolecules* **2013**, *46* (2), 562–570. <https://doi.org/10.1021/ma3020036>.
- (170) Nassar, S. F.; Domenek, S.; Guinault, A.; Stoclet, G.; Delpouve, N.; Sollogoub, C. Structural and Dynamic Heterogeneity in the Amorphous Phase of Poly(L, L-Lactide) Confined at the Nanoscale by the Coextrusion Process. *Macromolecules* **2018**, *51* (1), 128–136. <https://doi.org/10.1021/acs.macromol.7b02188>.
- (171) Messin, T.; Follain, N.; Guinault, A.; Sollogoub, C.; Gaucher, V.; Delpouve, N.; Marais, S. Structure and Barrier Properties of Multinanolayered Biodegradable PLA/PBSA Films: Confinement Effect via Forced Assembly Coextrusion. *ACS Appl. Mater. Interfaces* **2017**, *9* (34), 29101–29112. <https://doi.org/10.1021/acsami.7b08404>.
- (172) Arabeche, K.; Delbreilh, L.; Saiter, J.-M.; Michler, G. H.; Adhikari, R.; Baer, E. Fragility and Molecular Mobility in Micro- and Nano-Layered PC/PMMA Films. *Polymer* **2014**, *55* (6), 1546–1551. <https://doi.org/10.1016/j.polymer.2014.02.006>.
- (173) Massa, M. V.; Dalnoki-Veress, K. Homogeneous Crystallization of Poly(Ethylene Oxide) Confined to Droplets: The Dependence of the Crystal Nucleation Rate on Length Scale and Temperature. *Phys. Rev. Lett.* **2004**, *92* (25), 255509. <https://doi.org/10.1103/PhysRevLett.92.255509>.
- (174) Shin, K.; Woo, E.; Jeong, Y. G.; Kim, C.; Huh, J.; Kim, K.-W. Crystalline Structures, Melting, and Crystallization of Linear Polyethylene in Cylindrical Nanopores. *Macromolecules* **2007**, *40* (18), 6617–6623. <https://doi.org/10.1021/ma070994e>.
- (175) Dhotel, A.; Chen, Z.; Delbreilh, L.; Youssef, B.; Saiter, J.-M.; Tan, L. Molecular Motions in Functional Self-Assembled Nanostructures. *Int. J. Mol. Sci.* **2013**, *14* (2), 2303–2333. <https://doi.org/10.3390/ijms14022303>.
- (176) Huang, H.-D.; Xu, J.-Z.; Fan, Y.; Xu, L.; Li, Z.-M. Poly(L-Lactic Acid) Crystallization in a Confined Space Containing Graphene Oxide Nanosheets. *J. Phys. Chem. B* **2013**, *117* (36), 10641–10651. <https://doi.org/10.1021/jp4055796>.
- (177) Forrest, J. A.; Dalnoki-Veress, K.; Dutcher, J. R. Interface and Chain Confinement Effects on the Glass Transition Temperature of Thin Polymer Films. *Phys. Rev. E* **1997**, *56* (5), 5705. <https://doi.org/10.1103/PhysRevE.56.5705>.
- (178) *Micro- and Nanostructured Multiphase Polymer Blend Systems: Phase Morphology and Interfaces*, 1st ed.; Harrats, C., Thomas, S., Groeninckx, G., Eds.; CRC Press, 2005. <https://doi.org/10.1201/9781420026542>.
- (179) McKenna, G. B. Ten (or More) Years of Dynamics in Confinement: Perspectives for 2010. *Eur. Phys. J. Spec. Top.* **2010**, *189* (1), 285–302. <https://doi.org/10.1140/epjst/e2010-01334-8>.
- (180) Colmenero, J. Chain Dynamics in Asymmetric Polymer Blends, Presentation 3-5 March, 2010.
- (181) Bernards, D. A.; Desai, T. A. Nanoscale Porosity in Polymer Films: Fabrication and Therapeutic Applications. *Soft Matter* **2010**, *6* (8), 1621. <https://doi.org/10.1039/b922303g>.
- (182) Leibler, L. Nanostructured Plastics: Joys of Self-Assembling. *Prog. Polym. Sci.* **2005**, *30* (8–9), 898–914. <https://doi.org/10.1016/j.progpolymsci.2005.06.007>.
- (183) Kuan, W.-F.; Roy, R.; Rong, L.; Hsiao, B. S.; Epps, T. H. Design and Synthesis of Network-Forming Triblock Copolymers Using Tapered Block Interfaces. *ACS Macro Lett.* **2012**, *1* (4), 519–523. <https://doi.org/10.1021/mz3000804>.

- (184) Tao, Y.; Kim, J.; Torkelson, J. M. Achievement of Quasi-Nanostructured Polymer Blends by Solid-State Shear Pulverization and Compatibilization by Gradient Copolymer Addition. *Polymer* **2006**, *47* (19), 6773–6781. <https://doi.org/10.1016/j.polymer.2006.07.041>.
- (185) Casalini, R.; Zhu, L.; Baer, E.; Roland, C. M. Segmental Dynamics and the Correlation Length in Nanoconfined PMMA. *Polymer* **2016**, *88*, 133–136. <https://doi.org/10.1016/j.polymer.2016.02.030>.
- (186) Jackson, E. A.; Lee, Y.; Hillmyer, M. A. ABAC Tetrablock Terpolymers for Tough Nanoporous Filtration Membranes. *Macromolecules* **2013**, *46* (4), 1484–1491. <https://doi.org/10.1021/ma302414w>.
- (187) Baglay, R. R.; Roth, C. B. Local Glass Transition Temperature Tg(z) of Polystyrene next to Different Polymers: Hard vs. Soft Confinement. *J. Chem. Phys.* **2017**, *146* (20), 203307. <https://doi.org/10.1063/1.4975168>.
- (188) Bernazzani, P.; Sanchez, R. F.; Woodward, M.; Williams, S. Determination of the Glass Transition Temperature of Thin Unsupported Polystyrene Films Using Interference Fringes. *Thin Solid Films* **2008**, *516* (21), 7947–7951. <https://doi.org/10.1016/j.tsf.2008.06.041>.
- (189) Erber, M.; Khalyavina, A.; Eichhorn, K.-J.; Voit, B. I. Variations in the Glass Transition Temperature of Polyester with Special Architectures Confined in Thin Films. *Polymer* **2010**, *51* (1), 129–135. <https://doi.org/10.1016/j.polymer.2009.11.032>.
- (190) Xu, G.; Mattice, W. L. Monte Carlo Simulation on the Glass Transition of Free-Standing Atactic Polypropylene Thin Films on a High Coordination Lattice. *J. Chem. Phys.* **2003**, *118* (11), 5241–5247. <https://doi.org/10.1063/1.1544552>.
- (191) Liu, T.; Siegel, R. W.; Ozisik, R. The Effect of Confinement in Nanoporous Polymers on the Glass Transition Temperature. *Polymer* **2010**, *51* (2), 540–546. <https://doi.org/10.1016/j.polymer.2009.11.026>.
- (192) Mittal, J.; Shah, P.; Truskett, T. M. Using Energy Landscapes To Predict the Properties of Thin Films †. *J. Phys. Chem. B* **2004**, *108* (51), 19769–19779. <https://doi.org/10.1021/jp040402j>.
- (193) Ngai, K. L. The Effects of Changes of Intermolecular Coupling on Glass Transition Dynamics in Polymer Thin Films and Glass-Formers Confined in Nanometer Pores. *Eur. Phys. J. E* **2003**, *12* (1), 93–100. <https://doi.org/10.1140/epje/i2003-10029-3>.
- (194) Wubbenhorst, M.; Murray, C. A.; Forrest, J. A.; Dutcher, J. R. Dielectric Relaxations in Ultra-Thin Films of PMMA: Assessing the Length Scale of Cooperativity in the Dynamic Glass Transition; IEEE, 2002; pp 401–406. <https://doi.org/10.1109/ISE.2002.1043027>.
- (195) Wubbenhorst, M.; Lupascu, V. Glass Transition Effects in Ultra-Thin Polymer Films Studied by Dielectric Spectroscopy - Chain Confinement vs. Finite Size Effects; IEEE, 2005; pp 87–90. <https://doi.org/10.1109/ISE.2005.1612325>.
- (196) Tran, T. A.; Saïd, S.; Grohens, Y. Compared Study of Cooperativity in PMMA Nanocomposites and Thin Films. *Compos. Part Appl. Sci. Manuf.* **2005**, *36* (4), 461–465. <https://doi.org/10.1016/j.compositesa.2004.10.003>.
- (197) DeMaggio, G. B.; Frieze, W. E.; Gidley, D. W.; Zhu, M.; Hristov, H. A.; Yee, A. F. Interface and Surface Effects on the Glass Transition in Thin Polystyrene Films. *Phys. Rev. Lett.* **1997**, *78* (8), 1524–1527. <https://doi.org/10.1103/PhysRevLett.78.1524>.

- (198) Varnik, F.; Baschnagel, J.; Binder, K. Reduction of the Glass Transition Temperature in Polymer Films: A Molecular-Dynamics Study. *Phys. Rev. E* **2002**, *65* (2). <https://doi.org/10.1103/PhysRevE.65.021507>.
- (199) Singh, L.; Ludovice, P. J.; Henderson, C. L. Influence of Molecular Weight and Film Thickness on the Glass Transition Temperature and Coefficient of Thermal Expansion of Supported Ultrathin Polymer Films. *Thin Solid Films* **2004**, *449* (1–2), 231–241. [https://doi.org/10.1016/S0040-6090\(03\)01353-1](https://doi.org/10.1016/S0040-6090(03)01353-1).
- (200) Seemann, R.; Jacobs, K.; Landfester, K.; Herminghaus, S. Freezing of Polymer Thin Films and Surfaces: The Small Molecular Weight Puzzle. *J. Polym. Sci. Part B Polym. Phys.* **2006**, *44* (20), 2968–2979. <https://doi.org/10.1002/polb.20920>.
- (201) Keddie, J. L.; Jones, R. A. L.; Cory, R. A. Size-Dependent Depression of the Glass Transition Temperature in Polymer Films. *Europhys. Lett. EPL* **1994**, *27* (1), 59–64. <https://doi.org/10.1209/0295-5075/27/1/011>.
- (202) Forrest, J. A.; Dalnoki-Veress, K.; Stevens, J. R.; Dutcher, J. R. Effect of Free Surfaces on the Glass Transition Temperature of Thin Polymer Films. *Phys. Rev. Lett.* **1996**, *77* (10), 2002–2005. <https://doi.org/10.1103/PhysRevLett.77.2002>.
- (203) Wübbenhorst, M.; Murray, C. A.; Dutcher, J. R. Dielectric Relaxations in Ultrathin Isotactic PMMA Films and PS-PMMA-PS Trilayer Films. *Eur. Phys. J. E* **2003**, *12* (S1), 109–112. <https://doi.org/10.1140/epjed/e2003-01-025-1>.
- (204) Roth, C. B.; Dutcher, J. R. Glass Transition and Chain Mobility in Thin Polymer Films. *J. Electroanal. Chem.* **2005**, *584* (1), 13–22. <https://doi.org/10.1016/j.jelechem.2004.03.003>.
- (205) Mundra, M. K.; Donthu, S. K.; Dravid, V. P.; Torkelson, J. M. Effect of Spatial Confinement on the Glass-Transition Temperature of Patterned Polymer Nanostructures. *Nano Lett.* **2007**, *7* (3), 713–718. <https://doi.org/10.1021/nl062894c>.
- (206) Grohens, Y.; Hamon, L.; Reiter, G.; Soldera, A.; Holl, Y. Some Relevant Parameters Affecting the Glass Transition of Supported Ultra-Thin Polymer Films. *Eur. Phys. J. E* **2002**, *8* (2), 217–224. <https://doi.org/10.1140/epje/i2001-10088-4>.
- (207) Ellison, C. J.; Kim, S. D.; Hall, D. B.; Torkelson, J. M. Confinement and Processing Effects on Glass Transition Temperature and Physical Aging in Ultrathin Polymer Films: Novel Fluorescence Measurements. *Eur. Phys. J. E* **2002**, *8* (2), 155–166. <https://doi.org/10.1140/epje/i2001-10057-y>.
- (208) Park, C. H.; Kim, J. H.; Ree, M.; Sohn, B.-H.; Jung, J. C.; Zin, W.-C. Thickness and Composition Dependence of the Glass Transition Temperature in Thin Random Copolymer Films. *Polymer* **2004**, *45* (13), 4507–4513. <https://doi.org/10.1016/j.polymer.2004.04.048>.
- (209) Keddie, J. L.; Jones, R. a. L.; Cory, R. A. Size-Dependent Depression of the Glass Transition Temperature in Polymer Films. *EPL Europhys. Lett.* **1994**, *27* (1), 59. <https://doi.org/10.1209/0295-5075/27/1/011>.
- (210) Dalnoki-Veress, K.; Forrest, J. A.; Murray, C.; Gigault, C.; Dutcher, J. R. Molecular Weight Dependence of Reductions in the Glass Transition Temperature of Thin, Freely Standing Polymer Films. *Phys. Rev. E* **2001**, *63* (3), 031801. <https://doi.org/10.1103/PhysRevE.63.031801>.
- (211) A. Serghei. A. Serghei, Dynamics and Phase Transitions of Confined Polymers, Presentation given at the 4th International Workshop on Dynamics in Confinement, Grenoble, France, 3–5 March (2010), 2010.

- (212) Kremer, F. Dielectric Relaxations at Nanometric Length Scales, Presentation given at the 4th International Workshop on Dynamics in Confinement, 2010.
- (213) Tsui, O. K. C.; Russell, T. P.; Hawker, C. J. Effect of Interfacial Interactions on the Glass Transition of Polymer Thin Films. *Macromolecules* **2001**, *34* (16), 5535–5539. <https://doi.org/10.1021/ma000028v>.
- (214) Fryer, D. S.; Nealey, P. F.; de Pablo, J. J. Thermal Probe Measurements of the Glass Transition Temperature for Ultrathin Polymer Films as a Function of Thickness. *Macromolecules* **2000**, *33* (17), 6439–6447. <https://doi.org/10.1021/ma0003349>.
- (215) Ellison, C. J.; Torkelson, J. M. Sensing the Glass Transition in Thin and Ultrathin Polymer Films via Fluorescence Probes and Labels. *J. Polym. Sci. Part B Polym. Phys.* **2002**, *40* (24), 2745–2758. <https://doi.org/10.1002/polb.10343>.
- (216) Priestley, R. D.; Mundra, M. K.; Barnett, N. J.; Broadbelt, L. J.; Torkelson, J. M. Effects of Nanoscale Confinement and Interfaces on the Glass Transition Temperatures of a Series of Poly(n-Methacrylate) Films. *Aust. J. Chem.* **2007**, *60* (10), 765. <https://doi.org/10.1071/CH07234>.
- (217) Campbell, C. G.; Vogt, B. D. Examination of the Influence of Cooperative Segmental Dynamics on the Glass Transition and Coefficient of Thermal Expansion in Thin Films Probed Using Poly(n-Alkyl Methacrylate)s. *Polymer* **2007**, *48* (24), 7169–7175. <https://doi.org/10.1016/j.polymer.2007.10.003>.
- (218) Forrest, J. A.; Dalnoki-Veress, K.; Stevens, J. R.; Dutcher, J. R. Effect of Free Surfaces on the Glass Transition Temperature of Thin Polymer Films. *Phys. Rev. Lett.* **1996**, *77* (10), 2002–2005. <https://doi.org/10.1103/PhysRevLett.77.2002>.
- (219) Ellison, C. J.; Torkelson, J. M. The Distribution of Glass-Transition Temperatures in Nanoscopically Confined Glass Formers. *Nat. Mater.* **2003**, *2* (10), 695–700. <https://doi.org/10.1038/nmat980>.
- (220) Pye, J. E.; Rohald, K. A.; Baker, E. A.; Roth, C. B. Physical Aging in Ultrathin Polystyrene Films: Evidence of a Gradient in Dynamics at the Free Surface and Its Connection to the Glass Transition Temperature Reductions. *Macromolecules* **2010**, *43* (19), 8296–8303. <https://doi.org/10.1021/ma101412r>.
- (221) Lan, T.; Torkelson, J. M. Fragility-Confinement Effects: Apparent Universality as a Function of Scaled Thickness in Films of Freely Deposited, Linear Polymer and Its Absence in Densely Grafted Brushes. *Macromolecules* **2016**, *49* (4), 1331–1343. <https://doi.org/10.1021/acs.macromol.5b02489>.
- (222) Guo, D.; Setter, N. Impact of Confinement-Induced Cooperative Molecular Orientation Change on the Ferroelectric Size Effect in Ultrathin P(VDF-TrFE) Films. *Macromolecules* **2013**, *46* (5), 1883–1889. <https://doi.org/10.1021/ma302377q>.
- (223) Bhandaru, N.; Das, A.; Mukherjee, R. Confinement Induced Ordering in Dewetting of Ultra-Thin Polymer Bilayers on Nanopatterned Substrates. *Nanoscale* **2016**, *8* (2), 1073–1087. <https://doi.org/10.1039/C5NR06690E>.
- (224) Burt, T. M.; Monemian, S.; Jordan, A. M.; Korley, L. T. J. Thin Film Confinement of a Spherical Block Copolymer via Forced Assembly Co-Extrusion. *Soft Matter* **2013**, *9*, 4381. <https://doi.org/10.1039/c3sm27797f>.
- (225) Burt, T. M.; Keum, J.; Hiltner, A.; Baer, E.; Korley, L. T. J. Confinement of Elastomeric Block Copolymers via Forced Assembly Coextrusion. *ACS Appl. Mater. Interfaces* **2011**, *3* (12), 4804–4811. <https://doi.org/10.1021/am201297f>.
- (226) Xu, W.; Wang, Z.; Shi, L.; Ma, Y.; Yuan, S.; Sun, L.; Zhao, Y.; Zhang, M.; Zhu, J. Layer-by-Layer Deposition of Organic–Inorganic Hybrid Multilayer on Microporous

- Polyethylene Separator to Enhance the Electrochemical Performance of Lithium-Ion Battery. *ACS Appl. Mater. Interfaces* **2015**, *7* (37), 20678–20686. <https://doi.org/10.1021/acsami.5b05457>.
- (227) Ponting, M.; Hiltner, A.; Baer, E. Polymer Nanostructures by Forced Assembly: Process, Structure, and Properties. *Macromol. Symp.* **2010**, *294* (1), 19–32. <https://doi.org/10.1002/masy.201050803>.
- (228) Schrenk, W. J. Apparatus for Multilayer Coextrusion of Sheet or Film, May 20, 1975.
- (229) Kazmierczak, T.; Song, H.; Hiltner, A.; Baer, E. Polymeric One-Dimensional Photonic Crystals by Continuous Coextrusion. *Macromol. Rapid Commun.* **2007**, *28* (23), 2210–2216. <https://doi.org/10.1002/marc.200700367>.
- (230) Kerns, J.; Hsieh, A.; Hiltner, A.; Baer, E. Mechanical Behavior of Polymer Microlayers. *Macromol. Symp.* **1999**, *147* (1), 15–25. <https://doi.org/10.1002/masy.19991470104>.
- (231) Messin, T.; Follain, N.; Guinault, A.; Miquelard-Garnier, G.; Sollogoub, C.; Delpouve, N.; Gaucher, V.; Marais, S. Confinement Effect in PC/MXD6 Multilayer Films: Impact of the Microlayered Structure on Water and Gas Barrier Properties. *J. Membr. Sci.* **2017**, *525*, 135–145. <https://doi.org/10.1016/j.memsci.2016.10.039>.
- (232) Carr, J. M.; Langhe, D. S.; Ponting, M. T.; Hiltner, A.; Baer, E. Confined Crystallization in Polymer Nanolayered Films: A Review. *J. Mater. Res.* **2012**, *27* (10), 1326–1350. <https://doi.org/10.1557/jmr.2012.17>.
- (233) Arabeche, K. Etude de la mobilité moléculaire dans des systèmes amorphes complexes : multicouches de polycarbonate de bisphénol A (PC) / polyméthacrylate de méthyle (PMMA) de l'échelle microscopique à l'échelle nanoscopique, Rouen, Normandy, France, 2011.
- (234) Ivanov, D. A.; Pop, T.; Yoon, D. Y.; Jonas, A. M. Direct Observation of Crystal–Amorphous Interphase in Lamellar Semicrystalline Poly(Ethylene Terephthalate). *Macromolecules* **2002**, *35* (26), 9813–9818. <https://doi.org/10.1021/ma011784j>.
- (235) Ngai, K. L.; Roland, C. M. Intermolecular Cooperativity and the Temperature Dependence of Segmental Relaxation in Semicrystalline Polymers. *Macromolecules* **1993**, *26* (11), 2688–2690. <https://doi.org/10.1021/ma00063a008>.
- (236) Delpouve, N.; Delbreilh, L.; Stoclet, G.; Saiter, A.; Dargent, E. Structural Dependence of the Molecular Mobility in the Amorphous Fractions of Polylactide. *Macromolecules* **2014**, *47* (15), 5186–5197. <https://doi.org/10.1021/ma500839p>.
- (237) Lixon, C.; Delpouve, N.; Saiter, A.; Dargent, E.; Grohens, Y. Evidence of Cooperative Rearranging Region Size Anisotropy for Drawn PET. *Eur. Polym. J.* **2008**, *44* (11), 3377–3384. <https://doi.org/10.1016/j.eurpolymj.2008.08.001>.
- (238) Schick, C.; Donth, E. Characteristic Length of Glass Transition: Experimental Evidence. *Phys. Scr.* **1991**, *43* (4), 423–429. <https://doi.org/10.1088/0031-8949/43/4/010>.
- (239) Saiter, A.; Delpouve, N.; Dargent, E.; Saiter, J. M. Cooperative Rearranging Region Size Determination by Temperature Modulated DSC in Semi-Crystalline Poly(L-Lactide Acid). *Eur. Polym. J.* **2007**, *43* (11), 4675–4682. <https://doi.org/10.1016/j.eurpolymj.2007.07.039>.
- (240) Donth, E.-J. *The Glass Transition: Relaxation Dynamics in Liquids and Disordered Materials*; Zunger, A., Osgood, R. M., Hull, R., Sakaki, H., Series Eds.; Springer Series in MATERIALS SCIENCE; Springer Berlin Heidelberg: Berlin, Heidelberg, 2001; Vol. 48. <https://doi.org/10.1007/978-3-662-04365-3>.

- (241) Tran, T. A.; Saïd, S.; Grohens, Y. Nanoscale Characteristic Length at the Glass Transition in Confined Syndiotactic Poly(Methyl Methacrylate). *Macromolecules* **2005**, *38* (9), 3867–3871. <https://doi.org/10.1021/ma0487296>.
- (242) Dionísio, M.; Viciosa, M. T.; Wang, Y.; Mano, J. F. Glass Transition Dynamics of Poly(L-Lactic Acid) during Isothermal Crystallisation Monitored by Real-Time Dielectric Relaxation Spectroscopy Measurements. *Macromol. Rapid Commun.* **2005**, *26* (17), 1423–1427. <https://doi.org/10.1002/marc.200500319>.
- (243) Fitz, B. D.; Andjelić, S. Real-Time Monitoring of Segmental Dynamics during Crystallization of Poly(l(-)-Lactide) by Simultaneous DRS/SALS Technique. *Polymer* **2003**, *44* (10), 3031–3036. [https://doi.org/10.1016/S0032-3861\(03\)00161-7](https://doi.org/10.1016/S0032-3861(03)00161-7).
- (244) Mijović, J.; Sy, J.-W. Molecular Dynamics during Crystallization of Poly(L -Lactic Acid) As Studied by Broad-Band Dielectric Relaxation Spectroscopy. *Macromolecules* **2002**, *35* (16), 6370–6376. <https://doi.org/10.1021/ma0203647>.
- (245) Brás, A. R.; Malik, P.; Dionísio, M.; Mano, J. F. Influence of Crystallinity in Molecular Motions of Poly(L -Lactic Acid) Investigated by Dielectric Relaxation Spectroscopy. *Macromolecules* **2008**, *41* (17), 6419–6430. <https://doi.org/10.1021/ma800842a>.
- (246) Napolitano, S.; Wübbenhorst, M. Slowing Down of the Crystallization Kinetics in Ultrathin Polymer Films: A Size or an Interface Effect? *Macromolecules* **2006**, *39* (18), 5967–5970. <https://doi.org/10.1021/ma061304u>.
- (247) Hamonic, F.; Prevosto, D.; Dargent, E.; Saiter, A. Contribution of Chain Alignment and Crystallization in the Evolution of Cooperativity in Drawn Polymers. *Polymer* **2014**, *55* (12), 2882–2889. <https://doi.org/10.1016/j.polymer.2014.04.030>.
- (248) Hamonic, F.; Miri, V.; Saiter, A.; Dargent, E. Rigid Amorphous Fraction versus Oriented Amorphous Fraction in Uniaxially Drawn Polyesters. *Eur. Polym. J.* **2014**, *58*, 233–244. <https://doi.org/10.1016/j.eurpolymj.2014.06.014>.
- (249) Delpouve, N.; Saiter, A.; Dargent, E. Cooperativity Length Evolution during Crystallization of Poly(Lactic Acid). *Eur. Polym. J.* **2011**, *47* (12), 2414–2423. <https://doi.org/10.1016/j.eurpolymj.2011.09.027>.

Chapter 2: Materials and experimental techniques

In this chapter, first of all the analyzed materials are presented, then the experimental techniques which were used to analyze these samples are described in more details.

1- Poly (lactic acid) (PDLLA) and its oligomers

Lactic acid is an organic acid. It has a molecular formula $\text{CH}_3\text{CH}(\text{OH})\text{CO}_2\text{H}$. It is a crystalline white acid in solid state and is extremely soluble in water. It is a chiral compound, as presented in **Figure2-1** which means that there are two enantiomers D and L of lactic acid. The L isomer is much more present in nature.



Figure2-1 Chemical structure of lactic acid dimers.

Lactic acid is also a monomer used for the synthesis of Poly (lactic acid) (PLA). The frequent association of two enantiomers in the form of dimers gives rise to three chemical compounds shown in **Figure2-2**: L,L-lactide, D,D-lactide and D,L-lactide.

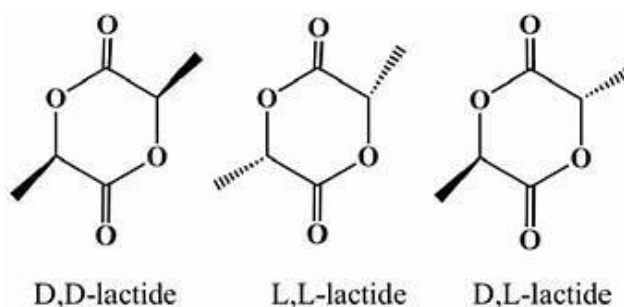


Figure2-2 Chemical structure of lactic acid dimers.

The mass production of PLA can be done by several methods of synthesis^{1,2}. The PLA pellets which are used in my work were provided by Natureworks LLC[®] who uses the ring-opening polymerization method of lactides³. In a first step, the water is removed under mild conditions and in the absence of solvent. A prepolymer is thus formed. This prepolymer is depolymerized catalytically to form a dimeric cyclic compound: lactide. The purified lactide is polymerized by ring-opening in the absence of a solvent. This polymerization is mostly catalyzed by tin complexes^{4,5}.

The PLA used in this work is PDLLA grade 4042D (having 95.7% L and 4.3% D isomers). It is a linear thermoplastic polymer. The presence D-lactic acid interferes with polymer crystallization, increases the chance to get a substantially amorphous PLA⁶. The number-average and weight-average molecular weights are $\bar{M}_n = 116$ kDa and $\bar{M}_w = 188$ kDa, respectively, as measured by gel permeation chromatography. Before making film, pellets were dried for several hours at 50°C to remove any humidity.

Different low-molecular-weight polyesters that are oligomers of D-/L-lactic acid series (Glyplast[®] OLAs, code OLA_x_y where 'x' is acid number (is a measure of the amount of free acids in a substance usually expressed as the number of milligrams of potassium hydroxide (KOH) required to neutralize one gram of the substance⁷.) and 'y' is weight average molecular weight (\bar{M}_w) have been studied herein which were synthesized and supplied by "Condensia Química SA" in collaboration with Dr. S. Fiori and Dr. E. Passaglia in "Istituto di Chimica dei Composti Organometallici (ICCOM)"⁸. Some information were summarized in **Table2-1**.

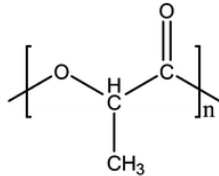
Samples	repeating unit	Acid number (mg KOH g^{-1})	\bar{M}_w (g.mol ⁻¹)
PDLLA		-	188000
OLA2.5_2700		2.5	2700
OLA2.5_1900		2.5	1900
OLA1.7_1400		1.7	1400

Table2-1-Repeating Units, Acid number and weight-average molecular weight (\bar{M}_w) of samples.

2- Thermogravimetric analysis (TGA)

TGA is a kind of thermal analysis in which the sample weight is measured either as a function of temperature and/or time, under nitrogen, helium, air, other gas, or vacuum. It gives us the information about different chemical phenomena such as thermal decomposition and physical phenomena including phase transitions, absorption and desorption⁹. It is a beneficial technique for the study of polymer materials, including thermoplastics, thermosets, elastomers, composites, fibers, and coating¹⁰.

In this work, TGA analyses were performed using a Netzsch TG209 apparatus. Sample (mass of 5 ± 0.5 mg) was placed in an open ceramic crucible. Baseline was calibrated from 25 °C to 500 °C with a scanning rate of 10 K/min. A nitrogen atmosphere with a flow rate of 15 mL/min was applied for the measurement. The Netzsch Proteus Thermal Analysis Software was used for data processing. **Figure2-3** shows thermograms and derivative curves as a function of temperature for oligomers of lactic acid (OLAs) obtained by TG209. According to **Figure2-3** there is no mass loss till 125°C, so we should be careful to apply the maximum limit of temperature in DSC because the material degradation can damage the apparatus and on the other hand in DSC all quantities are normalized to the sample weight, so during the analysis, the mass should be constant. Using TGA shows that the thermal stability decreases when the molecular weight decreases. The degradation temperature for 2% and the maximum weight loss was indicated in **Table2-1**.

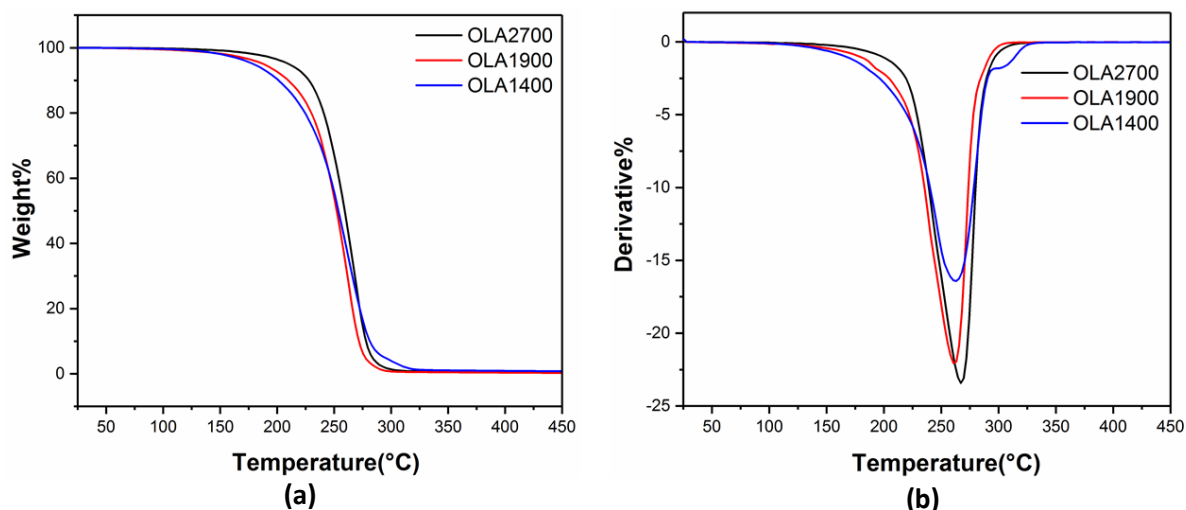


Figure2-3 TGA curves of OLAs obtained by TG209 (a) thermograms and (b) derivative curves as a function of temperature.

Samples	Temperature of 2% weight loss (°C)	Temperature of max weight loss (°C)
OLA2700	181.3	267.4
OLA1900	154.4	261.6
OLA1400	151.2	262.5

Table2-2 Degradation temperature for OLAs obtained by TG209.

3- Differential scanning calorimetry (DSC)

Understanding a material's structure properties is necessary when designing, processing, and using a product. A range of thermal analysis techniques measure the physical properties of a material with respect to temperature, time, and atmosphere. The most prevalent thermal analysis technique is Differential Scanning Calorimetry (DSC) that allows a qualitative and quantitative determination of the thermal phenomena accompanying a phase transformation or structural evolution of a broad range of materials including polymers, pharmaceuticals, foods, biologicals, organic chemicals, and inorganic materials¹¹⁻¹³. With DSC, we easily measure thermal events such as the glass transition, melting, crystallization, cure reactions, onset of oxidation, and heats of transitions (enthalpy). Then expand upon the measurement of DSC heat Flow we can determine reaction kinetics, specific heat capacity, compatibility and stability of blends and alloys, effect of aging, impact of additives on crystallization, and much more. In general two kinds of DSC exist: 1) heat-flux DSC, 2) power-compensated DSC.

3-1 Heat-flux DSC

The heat-flux DSC consists of a single furnace in which the sample and reference materials are heated or cooled together under a controlled temperature program. The measurement is based on the measure difference of heat flow between sample, reference and furnace. The sample is encapsulated in a pan (usually aluminum) and, along with an empty reference pan, sits on a thermoelectric disk surrounded by the furnace. The variation of temperature is applied to whole furnace and heat is transferred to the sample and reference (**Figure2-4**).

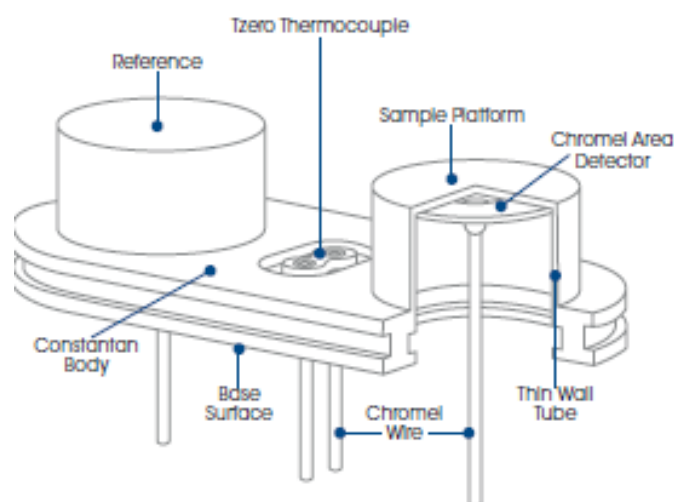


Figure2-4 Schematic view of fusion cell in heat-flux DSC based on Tzero® technology¹⁴.

A material's response in a DSC is best defined by the equation below, where the amplitude of heat flow is the sum total of a heat capacity component and kinetic component of the test material.

$$\phi = C_p \frac{dT}{dt} + f(T, t) \quad (2.1)$$

Where: $\phi = dQ/dt$ is the sample heat flow, C_p is sample specific heat capacity, $\frac{dT}{dt}$ is heating rate, and $f(T, t)$ is kinetic response at a specific temperature, time. The heat capacity component of the equation, $C_p \frac{dT}{dt}$, will express the specific heat capacity and changes in the heat capacity; this includes the glass transition observed in amorphous and semi-crystalline materials. Evaporation, cure reactions, crystallization, denaturation, and decomposition are expressed in the kinetic component, whereas melting, a latent heat, is an endothermic enthalpy change and may be expressed as a sum total of both heat capacity and kinetic components within the melting temperature range of a material.

In this work, experiments using heat-flux DSC were carried out with Thermal Analysis (TA) Instruments (DSC Q2000) based on Tzero® technology (**Figure2-5**). Such technology uses a more complex equation of heat flow. Thermal resistance and heat capacity of the sample (R_s, C_s) and reference (R_r, C_r) cell platforms are taken into account in the heat flow equation that give us the accurate real-time determination of heat flow available on any DSC. Thus by

measuring the temperature of the sample (T_s) and the reference (T_r) as a function of fixed temperature (T_0) the measured heat flow is expressed as follow¹⁴:

$$\phi = -\frac{\Delta T}{R_r} + \Delta T_0 \left(\frac{1}{R_s} - \frac{1}{R_r} \right) + (C_r - C_s) \frac{dT_s}{dt} - C_r \frac{d\Delta T}{dt} \quad (2.2)$$

Where, ΔT is a temperature difference between the sample and reference. In order to do an experiment with DSC Q2000 based on Tzero[®] technology, specific calibration is needed. First, a constant heating rate experiment was performed without sample and reference's pans. A second constant heating rate experiment was performed with sapphire disks directly placed on the sample and reference platform. These experiments figure out the resistance and capacitance of the cell platforms. In next step, the calibration in temperature and energy were carried out with using indium, by matching the melting temperature ($T_m = 156.6^\circ\text{C}$) and enthalpy ($\Delta H_m = 28.6 \text{ J.g}^{-1}$) associated. A second standard for calibration in temperature is usually benzophenone ($T_m = 48^\circ\text{C}$). The calibration has to be repeated if the scanning rate is changed. To ensure a good signal-to-noise ratio, masses of sample should be in the range of between 5 and 10mg. Scanning rate is selected to promote the resolution of investigated thermal events. All experiments are carried out under a nitrogen atmosphere.



Figure2-5 DSC Q2000 based on Tzero[®] technology

3-1-1 Conventional DSC

In conventional DSC (or classic or standard DSC), during heating, the sample and reference are subjected to a linear temperature ramp:

$$T(t) = \beta t + T_0 \quad (2.3)$$

In which T_0 is the initial temperature and β is the scanning rate.

3-1-2 Modulated temperature DSC

By using conventional DSC, during heating or cooling ramps, samples undergoes thermal reactions that changes their physical and/or chemical properties. These reactions may occur at the same time or in the same range of temperature, so the respective heat flows are overlapped and cannot be distinguished from each other by conventional DSC. In 1993, Reading M.¹⁵ has proposed to use a sinusoidal oscillation super-imposed on a linear temperature scan in the conventional DSC. This idea is the basis of modulated temperature

DSC (MDSC). The temperature modulation can be also in other forms like square wave, saw tooth wave, triangular wave and pulse wave¹⁶.

In TA's MDSC, a sinusoidal temperature oscillation is overlaid on the traditional linear ramp (**Figure2-6**). The net effect is that heat flow can be measured simultaneously with, and independently of, changes in heat capacity. In sinusoidal temperature oscillation in MDSC we can define:

$$T = \beta t + T_0 + A \sin(\omega t) \quad (2.4)$$

Where, A is the modulation amplitude and ω is the angular frequency of the temperature modulation with the period of oscillation $p = 2\pi/\omega$ which varies from 10 to 100 seconds. Thus, the modulated heat flow ϕ is expressed as follow:

$$\phi = C^*(\beta + A\omega \cos(\omega t)) \quad (2.5)$$

Herein C^* is complex heat capacity. In order to allow the sample to follow the imposed thermal oscillation and also according to the nature of the event which is investigated, the modulation amplitude (A), period of oscillation (p) and scanning rate (β) have to be chosen satisfactory¹⁷.

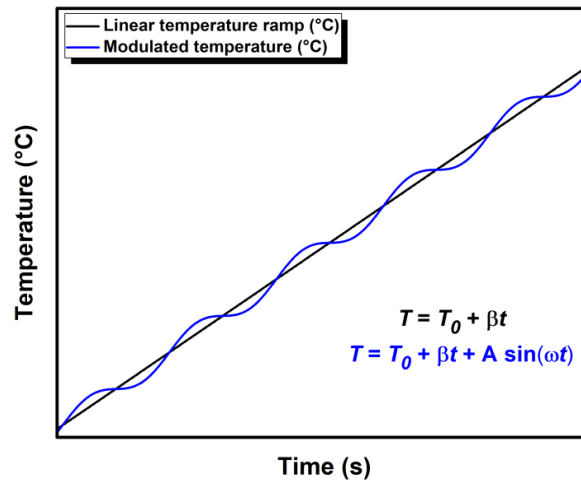


Figure2-6 Sinusoidal temperature oscillation in MDSC. Plot was taken from thesis of Nagihan Varol¹⁸.

The total heat flow signal contains the sum of all thermal transitions, just as in standard DSC. Modulated DSC separates the total heat flow into the reversing: $C_p \frac{dT}{dt}$, and non-reversing: $f(T, t)$ heat flow signals^{16,19} (**Eq.2.1**). The reversing heat flow, comprised of the heat capacity component, contains glass transition and melting transitions. The non-reversing heat flow (kinetic component), contains events like crystallization, curing, volatilization, melting, and decomposition. In **Figure2-7** the total heat flow with reversing and non-reversing signals were presented for PDLLA obtained by MDSC Q2000 with the modulation amplitude $A \approx \pm 0.32K$, period of oscillation $p = 60s$ and scanning ramp $\beta = 2K/min$ in heat-only modulation mode.

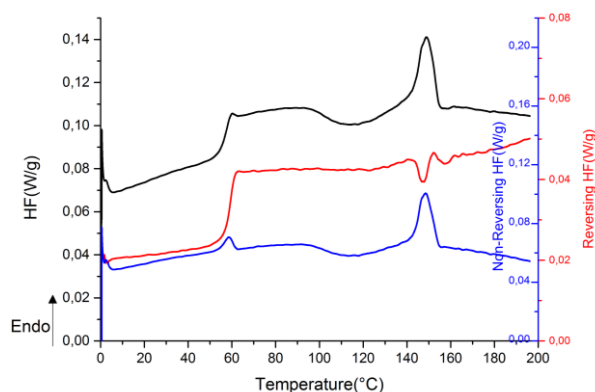


Figure2-7 Total heat flow (black curve) with separated reversing (red curve) and non-reversing (blue curve) signals obtained from MDSC Q2000 for PDLLA. The total heat flow signal contains the sum of all thermal transitions. The reversing heat flow shows the glass transition step and the small melting peak. The non-reversing heat flow shows the crystallization (exothermic reaction) and melting (endothermic peak)²⁰.

In MDSC, there are three temperature modulation modes: 1) heat-only, 2) heat-iso and 3) heat-cool. Heat-only is often used to investigate the coupling of different thermal events such as glass transition and cold crystallization and melting. Heat-iso is applied to investigate melting whereas heat-cool is used to study the glass transition and the molecular mobility in this region. In this work the heat-only and heat-cool modulation mode were selected.

The calibration of MT-DSC consists of DSC calibration and an additional step to calibrate the heat capacity. In this step a sapphire is used as a heat capacity standard because it does not undergo any transition in the temperature range scanned for polymer analysis. The heat capacity of sapphire as a function of temperature is stable and is well known (**Figure2-8**). Any change of experimental conditions such as the modulation amplitude, the scanning rate or the period of oscillation leads to do again the calibration. A calibration factor K_{C_p} can be calculated from the experimental and theoretical values of reversing heat capacity (**Eq.2.6**). This factor corrects the apparent heat capacity of the sample. This factor is averaged on the temperature range investigated.

$$K_{C_p}(T) = \frac{\text{Rev}C_p(\text{sapphire,theoretical})}{\text{Rev}C_p(\text{sapphire,experimental})} \quad (2.6)$$

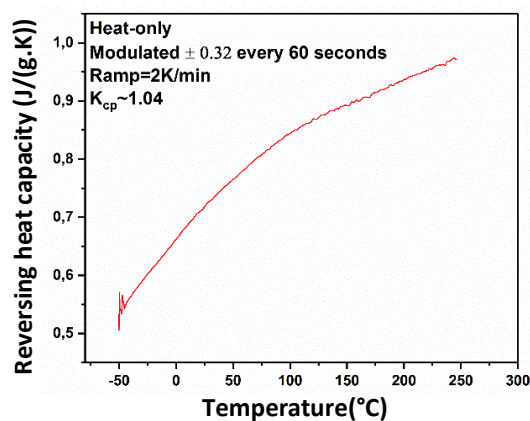


Figure2-8 Reversing heat capacity of sapphire done by DSC Q2000 in order to calibrate heat capacity.

3-2 Power-compensated DSC

In contrast to heat-flux DSC, in power-compensated DSC, sample and reference are completely isolated from each other (**Figure2-9**). Both the sample crucible and the reference crucible have their own heating element and temperature sensing element^{21,22}. With the aid of a temperature programmer, both sample and reference are heated and always controlled to have the same temperature. As soon as changes in the sample occur, extra (in the case of an endothermic reaction) or less (with an exothermic reaction) heat will be needed to maintain the set heating rate. With the aid of special electronic circuitry, extra or less power is now sent to the sample holder in order to keep the temperature difference zero. In this way power and consequently heat flow and enthalpy changes are measured. In fact the reduction of the furnace size improves the heat transfer. Moreover, in this apparatus, it is expected that the distance between the furnace and the refrigerating system is also reduced, so power compensated DSC is a worthy to work at rates ranging from 10 to 200 K/min²³. In this work power-compensated DSC measurements were performed with Hyper DSC 8500 Perkin Elmer®.

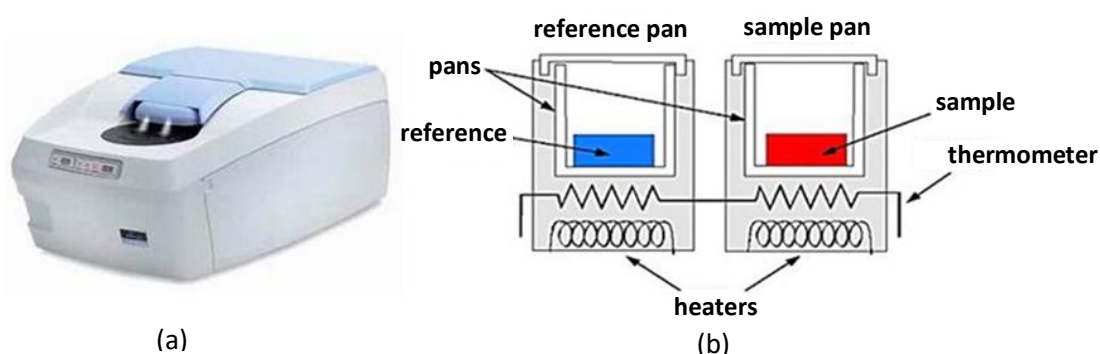


Figure2-9 (a) Hyper DSC 8500 Perkin Elmer®, **(b)** DSC power compensation principle²⁴

4- Fast Scanning Calorimetry (FSC)

Fast scanning calorimetry (FSC) is used for the measurement of phase transformations over a wide scanning rate range. Schick and Mathot²⁵ proposed to apply very high scanning rates in order to avoid or prevent thermal reactions, as well as observed very fast thermal reactions or crystallization processes by FSC.

In the past decades, the scan rate range of calorimeters has been extended strongly. According to the statement of Schick C. and Mathot V. in their book *Fast Scanning Calorimetry*²⁵, the combination of various calorimeters and the newly-developed Fast Scanning Calorimeters (FSC) now span 11 orders of magnitude, by which many processes can be mimicked according to the time scales of chemical and physical transitions occurring during cooling, heating and isothermal stays. This opens not only new areas of research on polymers, metals, pharmaceuticals and all kinds of substances with respect to glass transition, crystallization and melting phenomena, but also enables in depth study of metastability and reorganization of samples from 1 to 1000ng scale. In addition, FSC will become a crucial tool for understanding and optimization of processing methods at high speeds like injection molding.

The basic principle of FSC is to quantify the difference in amount of heat required to increase the temperature of a sample and a reference. So far, FSC measurements are only done by a power-compensated calorimeter. In this work, experiments were performed by fast scanning calorimeter Flash 1 DSC provided by Mettler Toledo[®] using calorimetric twin-type chip sensor, based on MEMS (Micro-Electro-Mechanical Systems) technology (**Figure2-10**). The MEMS chip sensor has two separated calorimeters for sample and reference and is mounted on a stable ceramic. The applied temperature is transferred by electrical thermocouples. Both sides of the chip sensor contain two thermal resistance heaters in order to apply desired temperature and the temperature resolution is determined by the time constant of the sensor (about 1 millisecond). Eight thermocouples polysilicon thermopile measure the temperature elevation of the sample area with respect to the silicon frame, which acts as heat sink. The measurement area of the chip is made of a silicon nitride and silicon dioxide coated with a thin layer of aluminum to provide homogenous temperature distribution across the sensor. FSC measurement system can support precisely cooling rates from 0.01 to 4000 K/s and heating scans up to 40.000K/s in a wide range of temperature (from -90°C up to 450°C)²⁶. Samples were continuously flushed with a 20 mL·min⁻¹ nitrogen flow gas to avoid water condensation from the environment and to optimize the program temperature which was applied.

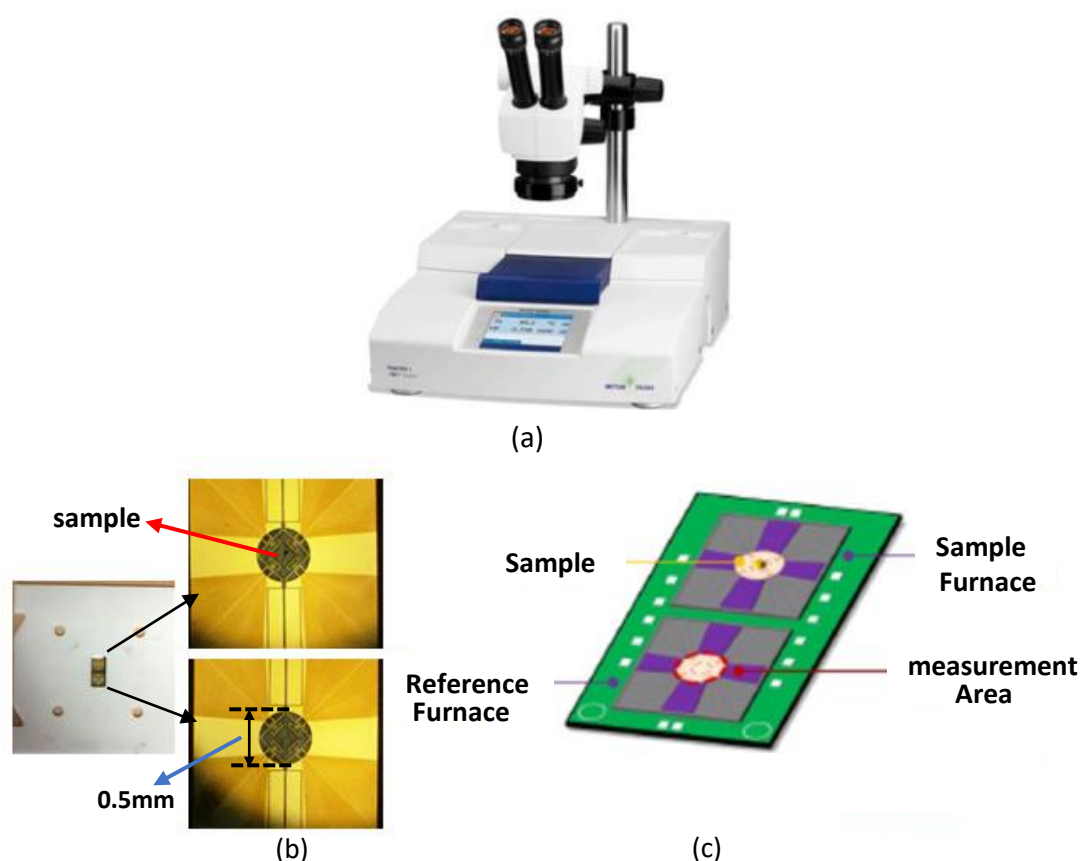


Figure2-10 (a) Flash 1 DSC provided by Mettler Toledo[®], **(b)** Twin-type MEMS chip sensor and its microscopic image with the PDLLA sample placed in the center of the sample area. **(c)** schematic view of twin-type MEMS chip sensor.

The calibration of the Flash 1 DSC consists of conditioning and correction procedures. The conditioning procedure checks the proper behavior of the sensor. Potential memory effects from its production are erased by heating the sensor to the maximum temperature (450 °C).

Then, the correction temperature is performed in order to correct the thermocouple signal with respect to the sensor support temperature. The correction is done by comparing the signal of the thermocouples with the temperature behavior of the heating resistances, which was determined during production.

In this work samples mass was estimated from the step change in heat flow at the glass transition in amorphous state, from the one obtained through Flash DSC at $|\beta_c| = |\beta_h| = 1500\text{Ks}^{-1}$ and the one obtained using Hyper DSC 8500 Perkin Elmer[®] and/or MDSC at $|\beta_c| = |\beta_h| \cong 0.16\text{Ks}^{-1}$:

$$m_{\text{FSC}}(\text{g}) = \frac{\Delta H_{\text{Flash DSC}}(\text{J.s}^{-1})}{\Delta C_{\text{p,Hyper DSC}}(\text{J.g}^{-1}.\text{K}^{-1}) \times \beta_{\text{h,Flash DSC}}(\text{K.s}^{-1})} \quad (2.7)$$

5- Dielectric Relaxation Spectroscopy (DRS)

Dielectric Relaxation Spectroscopy is a powerful technique to study molecular dynamics especially in polymers²⁷. This is partly due to the fact that a very broad frequency range from milihertz to gigahertz²⁸ can be covered by dielectric spectroscopy in its modern form routinely by a tune combination of different measurement instrumentation.

5-1 Basic principle of DRS

The basic principle of DRS is based on studying the motion of permanent dipoles present in materials by applying an alternating electric field which is created with a voltage. There are several types of polarization, such as: I) Electronic polarization (\vec{P}_e), when the external field is applied, the electron clouds of atom are displaced with respect to the heavy nuclei within the dimensions of atom. It does not depend upon temperature. II) Ionic polarization (\vec{P}_i), It occurs only in some ionic crystals. In the presence of external electric field the positive and negative ions are displaced up to the point where ionic bonding force stops this displacement. Hence dipoles get induced. They also do not depend upon temperature. III) Orientational polarization (\vec{P}_o), it applies only in polar dielectric materials. Generally, in absence of external electric field electric dipoles are so oriented randomly that their net effect becomes zero but in presence of electric field, these dipole try to rotate and align in the direction of electric field. This is known as orientation polarization which is dependent over temperature also. In case of polymer, the net dipole moment per unit volume is linked to the total vector of all molecule dipoles that exist in the repeating unit, the polymer chain and overall structure in polymer chain. The polarization observed in polymers comes from the rotational mobility of permanent dipole moments (μ). This reorientation of the permanent dipoles of molecules is used to identify the sample properties like permittivity, resistivity, energy storage etc., which give us information on molecular mobility within materials as a function of frequency and temperature²⁹⁻³¹.

In the broad range of frequency, the sample can be considered as a circuit composed of an ideal capacitor and an ohmic resistor combined in parallel or serial. The complex impedance $Z^*(\omega)$ of the circuit is measured by the spectrometer and may be defined in terms of energy dissipation or resistance $R(\omega)$, and energy storage or capacitance $C(\omega)$, where $\omega = 2\pi f$ is the angular frequency and f is the frequency. Other properties, such as electrical modulus $M^*(\omega)$, electrical conductivity $\sigma^*(\omega)$, resistivity $R^*(\omega)$, and more

particularly dielectric permittivity $\varepsilon^*(\omega)$ are directly derived from the complex electrical impedance $Z^*(\omega)$. In order to measure complex impedance $Z^*(\omega)$, a sinusoidal voltage $U^*(\omega)$ is applied to the sample at a constant frequency:

$$U^*(\omega) = U_0 \sin(\omega t) \quad (2.8)$$

Then, the current $I_s^*(\omega)$ is measured across the sample:

$$I_s^*(\omega) = U_0 \sin(\omega t + \varphi) \quad (2.9)$$

Where φ is the phase shift between the applied voltage and measured current. The value of the complex impedance $Z^*(\omega)$ is then obtained by the ratio³²:

$$Z^*(\omega) = \frac{U^*(\omega)}{I^*(\omega)} \quad (2.10)$$

The impedance is determined from the measurements of two voltages corresponding to the generated voltage applied to the sample and the voltage-converted sample current $I_s^*(\omega)$. A schematic view of an equivalent circuit is presented in **Figure2-11**. These voltages are analyzed by the Fourier transform technique to obtain information on their phases and amplitudes. The complex permittivity is consequently determined from the following equation:

$$\varepsilon^*(\omega) = \frac{1}{j\omega C_0 Z^*(\omega)} \quad (2.11)$$

Where, C_0 is the capacitance of the empty capacitor.

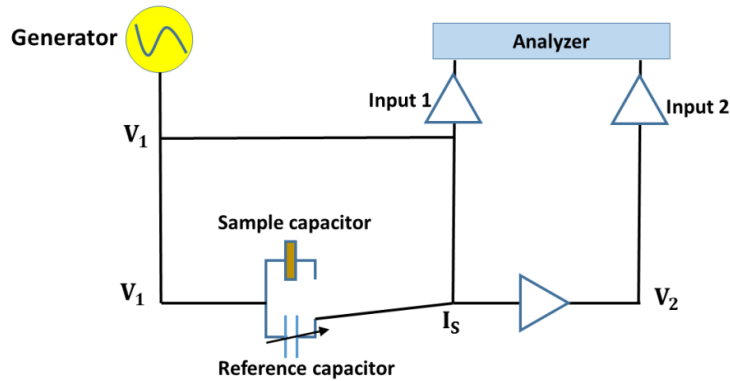


Figure2-11 Schematic view of an equivalent circuit to the spectrometer analyzer²⁷

Permittivity characterizes the ability of charges within a material to displace or reorient in the presence of an external electric field, so its determination is all important to obtain information on the capacity of dipoles within a material to move. The complex permittivity can also be written as a real and imaginary part:

$$\varepsilon^*(\omega) = \varepsilon'(\omega) - i\varepsilon''(\omega) \quad (2.12)$$

Where $\varepsilon'(\omega)$ is the real part of the permittivity related to the stored energy within the medium and $\varepsilon''(\omega)$ is the imaginary part of the permittivity related to the dissipation of energy within the medium.

In this study, DRS measurements were carried out with a Novocontrol Alpha analyzer (**Figure2-12a**). The temperature was controlled by a Quatro Novocontrol Cryosystem with temperature stability better than $\pm 0.2\text{K}$. The broadband dielectric converter (Alpha analyzer interface) allows the measurement of the complex dielectric permittivity (real and imaginary parts) in a wide frequency range (In this thesis, from 10^{-1}Hz to $2 \times 10^6\text{Hz}$ was used). In our work, parallel electrodes (for PDLLA) and interdigitated electrodes (IEs) (for OLAs) were used for dielectric measurements (**Figure2-12**). PDLLA film (prepared from PDLLA pellets) was placed between parallel electrodes, using circular gold plates having 30mm diameter. OLAs were placed on interdigitated electrodes (IEs) (BDS1410-20-150) with a sensor diameter of 20 mm and accuracy in loss factor equal to $\tan \delta = 0.001$. IE electrodes are made of two interpenetrating comb electrodes made of gold plated copper located on a silica substrate. This interdigitated configuration creates an electric field distribution mainly concentrated within a very thin layer of thickness at the interface between the substrate and sample material. Before deposition OLAs on IEs, each electrode was calibrated by measuring its respective geometric capacity (C_0) when it is empty and substrate capacity (C_{su}) through the measurement of a standard material with well-known permittivity (Silicon oil). Assuming that the electric field penetrates only in the sample and the substrate by creating two independent capacitors so the measured total capacity is given by³³:

$$C_m^* = C_0(\epsilon_s^* + \epsilon_{su}^*) \quad (2.13)$$

Where $C_m^*(\omega)$ is the complex capacity of the electrode and ϵ_s^* , ϵ_{su}^* are the complex permittivity of the sample and substrate respectively.

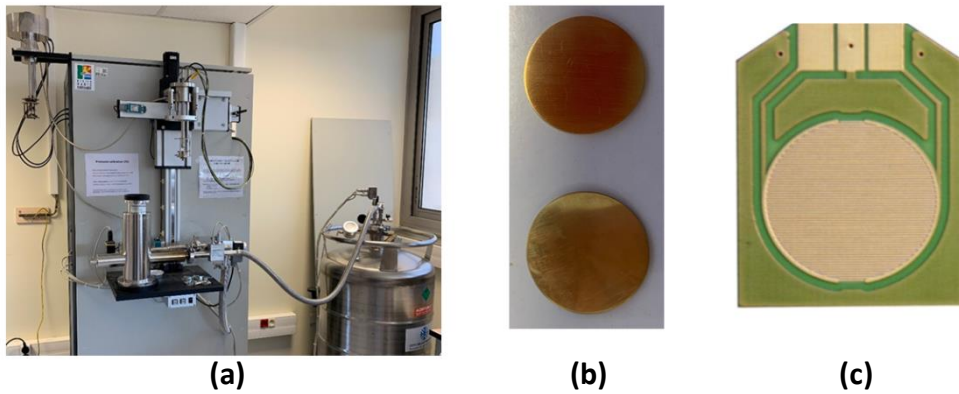


Figure2-12 (a) Dielectric Relaxation Spectroscopy (DRS) Novocontrol device, **(b)** Parallel electrodes used for PDLLA film, **(c)** Interdigitated electrodes used for OLAs samples.

DRS measurements were performed on amorphous systems. For PLLA, pellets were dried for several hours at 50°C to remove any humidity. Pellets were first melted for few minutes at 190°C and then press into molded film between steel plates under 2T (for two minutes) with manual Hydraulic press by SPECAC[®], then, the film was quenched with cold water (at room temperature) in order to avoid crystallization. For OLAs, samples have been melt and then quenched with liquid nitrogen on IE electrodes.

5-2 Analysis of dielectric spectra

In this work, we use dielectric spectroscopy in order to investigate the relaxation processes. The dielectric relaxation processes can be analyzed by different model functions²⁷. Starting from the theoretically well founded Debye function²⁷, several formulas for both the frequency and the time domain have been suggested to describe the experimentally observed spectra. The most important of these approaches are summarized below:

1) The Debye function for the frequency dependence of $\varepsilon^*(\omega)$ is given by:

$$\varepsilon^*(\omega) = \varepsilon_{\infty} + \frac{\Delta\varepsilon}{1+i\omega\tau_D} \quad (2.14)$$

Where $\Delta\varepsilon$ is the dielectric relaxation strength or intensity, ε_{∞} is the dielectric permittivity in the high frequency limit of the material and τ_D is Debye relaxation time which related to the position of maximal loss. In this case the shape of the loss peak is symmetric. The Debye model is usually suitable for simple polar liquids but rapidly becomes inappropriate in more complex systems like amorphous polymers. This is the simplest model of dipole relaxation.

2) In most cases the half width of measured loss peaks is much broader than predicted by **(Eq.2.14)** (up to six decades) and in addition their shapes are asymmetric with a high frequency tail. This is called non-Debye relaxation behavior. Broadening of the dielectric function can be described by Cole/Cole (CC) function³⁴:

$$\varepsilon_{CC}^*(\omega) = \varepsilon_{\infty} + \frac{\Delta\varepsilon}{1+(i\omega\tau_{CC})^{\beta}} \quad (2.15)$$

Where, $0 < \beta < 1$ leads to a symmetrical broadening for the relaxation function compared to **(Eq.2.14)**. For $\beta = 1$ the Debye-function is obtained. The Cole/Cole relaxation time τ_{CC} gives the position of maximal loss by $\omega = 1/\tau_{CC}$.

3) Many experimental results, especially on liquids or low molecular glass-forming materials, show that the complex dielectric function can have also an asymmetric broadening which can be described by the Cole/Davidson function³⁵ for higher frequencies:

$$\varepsilon_{CD}^*(\omega) = \varepsilon_{\infty} + \frac{\Delta\varepsilon}{(1+i\omega\tau_{CD})^{\gamma}} \quad (2.16)$$

The parameter $0 < \gamma \leq 1$ describes an asymmetric broadening of the relaxation function for frequencies $\omega > 1/\tau_{CD}$ where τ_{CD} is the Cole/Davidson relaxation time. For $\gamma = 1$ the Debye-function is recovered again. It should be noted that for an asymmetric model function like the Cole/Davidson-function the characteristic relaxation time of the model function does not coincide with the relaxation time which is related to the position of maximal loss.

4) A more general model function was introduced by Havriliak and Negami (HN-function), which is in fact a combination of the Cole/Cole- and the Cole/Davidson-function³⁶:

$$\varepsilon_{HN}^*(\omega) = \varepsilon_{\infty} + \frac{\Delta\varepsilon}{(1+(i\omega\tau_{HN})^{\alpha})^{\beta}} \quad (2.17)$$

Shape parameters α and β describe the symmetric and asymmetric broadening of the complex dielectric function, when $\alpha = 1$, $\beta = 1$ the equation is reduced to Debye function. Real and imaginary part for the HN-function are given as follows:

$$\varepsilon'(\omega) = \varepsilon_{\infty} + \Delta\varepsilon_{\text{HN}} \frac{\cos(\beta_{\text{HN}}\varphi_{\text{HN}})}{\left[1 + 2\sin\left(\frac{\pi(1-\alpha_{\text{HN}})}{2}\right)(\omega\tau_{\text{HN}})^{\alpha_{\text{HN}}} + (\omega\tau_{\text{HN}})^{2\alpha_{\text{HN}}}\right]^{\beta_{\text{HN}}/2}} \quad (2.18)$$

$$\varepsilon''(\omega) = \Delta\varepsilon_{\text{HN}} \frac{\sin(\beta_{\text{HN}}\varphi_{\text{HN}})}{\left[1 + 2\sin\left(\frac{\pi(1-\alpha_{\text{HN}})}{2}\right)(\omega\tau_{\text{HN}})^{\alpha_{\text{HN}}} + (\omega\tau_{\text{HN}})^{2\alpha_{\text{HN}}}\right]^{\beta_{\text{HN}}/2}} \quad (2.19)$$

With:

$$\varphi_{\text{HN}} = \arctan\left(\frac{(\omega\tau_{\text{HN}})^{\alpha_{\text{HN}}}\cos\left(\frac{\pi(1-\alpha_{\text{HN}})}{2}\right)}{1 + (\omega\tau_{\text{HN}})^{\alpha_{\text{HN}}}\sin\left(\frac{\pi(1-\alpha_{\text{HN}})}{2}\right)}\right) \quad (2.20)$$

The position of maximal loss $\tau_{\text{max}} = (2\pi f_{\text{max}})^{-1}$ depends on the parameters α_{HN} and β_{HN} according to³⁷:

$$\tau_{\text{max}} = \tau_{\text{HN}} \times \left[\frac{\sin\frac{\alpha_{\text{HN}}\beta_{\text{HN}}}{2+2\beta_{\text{HN}}}}{\sin\frac{\alpha_{\text{HN}}\pi}{2+2\beta_{\text{HN}}}}\right]^{1/\alpha_{\text{HN}}} \quad (2.21)$$

In practice, the dielectric spectra of a complex system do not exhibit isolated peaks, various relaxation processes and conduction effects also contribute to the dielectric spectra. The conduction effects were analyzed by adding a contribution $\sigma_{\text{cond}} = \frac{\sigma_0}{\omega^s \varepsilon_0}$ to the dielectric loss, where σ_0 is Ohmic conduction related to the mobile charge carriers. Parameter s ($0 < s \leq 1$) describes Ohmic ($s = 1$) and non-Ohmic ($s < 1$) effects in conductivity. ε_0 is dielectric permittivity of vacuum. In this work, the analysis of dielectric spectroscopy data has been performed using gratuity software. When several relaxation processes were observed in the experimental frequency range, a sum of HN functions was applied to the experimental data. The fitting procedure can be conducted on both the loss part (imaginary part) and also on the real part.

Bibliography

- (1) Hartmann, M. H. High Molecular Weight Polylactic Acid Polymers. In *Biopolymers from Renewable Resources*; Kaplan, D. L., Ed.; Springer Berlin Heidelberg: Berlin, Heidelberg, 1998; pp 367–411. https://doi.org/10.1007/978-3-662-03680-8_15.
- (2) Jamshidian, M.; Tehrany, E. A.; Imran, M.; Jacquot, M.; Desobry, S. Poly-Lactic Acid: Production, Applications, Nanocomposites, and Release Studies. *Compr. Rev. Food Sci. Food Saf.* **2010**, *9* (5), 552–571. <https://doi.org/10.1111/j.1541-4337.2010.00126.x>.
- (3) Gruber, P.; O'Brien, M. *Poly lactides "NatureWorks™ PLA" in Biopolymers in 10 Volumes, Volume 4, Polyesters III Applications and Commercial Products*.
- (4) Chen, F.; Gao, Q.; Hong, G.; Ni, J. Synthesis of Magnetite Core–Shell Nanoparticles by Surface-Initiated Ring-Opening Polymerization of L-Lactide. *J. Magn. Magn. Mater.* **2008**, *320* (13), 1921–1927. <https://doi.org/10.1016/j.jmmm.2008.02.132>.
- (5) Kricheldorf, H. R.; Meier-Haack, J. Polylactones, 22 ABA Triblock Copolymers of L-Lactide and Poly(Ethylene Glycol). *Makromol. Chem.*, *194* (1993) 715.
- (6) Delpouve, N.; Saiter, A.; Dargent, E. Cooperativity Length Evolution during Crystallization of Poly(Lactic Acid). *Eur. Polym. J.* **2011**, *47* (12), 2414–2423. <https://doi.org/10.1016/j.eurpolymj.2011.09.027>.
- (7) Definition of ACID NUMBER. <https://www.merriam-webster.com>.
- (8) Cicogna, F.; Coiai, S.; De Monte, C.; Spiniello, R.; Fiori, S.; Franceschi, M.; Braca, F.; Cinelli, P.; Fehri, S. M. K.; Lazzeri, A.; Oberhauser, W.; Passaglia, E. Poly(Lactic Acid) Plasticized with Low-Molecular-Weight Polyesters: Structural, Thermal and Biodegradability Features: PLA Plasticized with Low-Molecular-Weight Polyesters. *Polym. Int.* **2017**, *66* (6), 761–769. <https://doi.org/10.1002/pi.5356>.
- (9) Coats, A. W.; Redfern, J. P. Thermogravimetric Analysis. A Review. *The Analyst* **1963**, *88* (1053), 906. <https://doi.org/10.1039/an9638800906>.
- (10) Reyes-Labarta, J. A.; Marcilla, A. Thermal Treatment and Degradation of Cross-Linked Ethylene Vinyl Acetate–Polyethylene–Azodicarbonamide–ZnO Foams. Complete Kinetic Modeling and Analysis. *Ind. Eng. Chem. Res.* **2012**, *51* (28), 9515–9530. <https://doi.org/10.1021/ie3006935>.
- (11) Wunderlich, B. *Thermal Analysis of Polymeric Materials*; Springer, Berlin, Heidelberg, 2005.
- (12) Reading, M.; Craig, D. Q. M. *Thermal Analysis of Pharmaceuticals*; CRC Press, 2006.
- (13) Höhne, G. W. H.; Hemminger, W. F.; Flammersheim, H.-J. *Differential Scanning Calorimetry*; Springer Berlin Heidelberg: Berlin, Heidelberg, 2003. <https://doi.org/10.1007/978-3-662-06710-9>.
- (14) Differential Scanning Calorimetry (DSC) - METTLER TOLEDO.
- (15) Reading, M.; Luget, A.; Wilson, R. Modulated Differential Scanning Calorimetry. *Thermochim. Acta* **1994**, *238*, 295–307. [https://doi.org/10.1016/S0040-6031\(94\)85215-4](https://doi.org/10.1016/S0040-6031(94)85215-4).
- (16) Reading, M.; Hahn, B. K.; Crowe, B. S. Method and Apparatus for Modulated Differential Analysis. US5346306A, September 13, 1994.
- (17) Bustin, O. Relaxation Structurale Des Matériaux Vitriifiables Par Calorimétrie à Balayage Modulé. thesis, Lille 1, 1999.
- (18) Varol, N. Advanced Thermal Analysis and Transport Properties of PolyLactide Stereocomplex Materials. Thesis, Rouen, Normandy, France, 2019.

- (19) Pyda, M.; Wunderlich, B. Reversing and Nonreversing Heat Capacity of Poly(Lactic Acid) in the Glass Transition Region by TMDSC. *Macromolecules* **2005**, *38* (25), 10472–10479. <https://doi.org/10.1021/ma051611k>.
- (20) Aliotta, L.; Gazzano, M.; Lazzeri, A.; Righetti, M. C. Constrained Amorphous Interphase in Poly(L-Lactic Acid): Estimation of the Tensile Elastic Modulus. *ACS Omega* **2020**, *5* (33), 20890–20902. <https://doi.org/10.1021/acsomega.0c02330>.
- (21) Haines, P. J.; Reading, M.; Wilburn, F. W. Differential Thermal Analysis and Differential Scanning Calorimetry. In *Handbook of Thermal Analysis and Calorimetry*; Elsevier: Netherlands, 1998; Vol. 1, pp 279–361.
- (22) Zucca, N.; Erriu, G.; Onnis, S.; Longoni, A. An Analytical Expression of the Output of a Power-Compensated DSC in a Wide Temperature Range. *Thermochim. Acta* **2004**, *413* (1–2), 117–125. <https://doi.org/10.1016/j.tca.2003.10.006>.
- (23) Pijpers, T. F. J.; Mathot, V. B. F.; Goderis, B.; Scherrenberg, R. L.; van der Vegte, E. W. High-Speed Calorimetry for the Study of the Kinetics of (De)Vitrification, Crystallization, and Melting of Macromolecules †. *Macromolecules* **2002**, *35* (9), 3601–3613. <https://doi.org/10.1021/ma011122u>.
- (24) Le Parlouër, P. Thermal Analysis and Calorimetry Techniques for Catalytic Investigations. In *Calorimetry and Thermal Methods in Catalysis*; Auroux, A., Ed.; Springer Berlin Heidelberg: Berlin, Heidelberg, 2013; Vol. 154, pp 51–101. https://doi.org/10.1007/978-3-642-11954-5_2.
- (25) *Fast Scanning Calorimetry*; Schick, C., Mathot, V., Eds.; Springer, 2016.
- (26) Mathot, V.; Pyda, M.; Pijpers, T.; Vanden Poel, G.; van de Kerkhof, E.; van Herwaarden, S.; van Herwaarden, F.; Leenaers, A. The Flash DSC 1, a Power Compensation Twin-Type, Chip-Based Fast Scanning Calorimeter (FSC): First Findings on Polymers. *Thermochim. Acta* **2011**, *522* (1–2), 36–45. <https://doi.org/10.1016/j.tca.2011.02.031>.
- (27) *Broadband Dielectric Spectroscopy*; Kremer, F., Schönhals, A., Eds.; Springer Berlin Heidelberg: Berlin, Heidelberg, 2003. <https://doi.org/10.1007/978-3-642-56120-7>.
- (28) Lunkenheimer, P.; Loidl, A. Dielectric Spectroscopy of Glass-Forming Materials: α -Relaxation and Excess Wing. *Chem. Phys.* **2002**, *284* (1–2), 205–219. [https://doi.org/10.1016/S0301-0104\(02\)00549-9](https://doi.org/10.1016/S0301-0104(02)00549-9).
- (29) Yin, H.; Napolitano, S.; Schönhals, A. Molecular Mobility and Glass Transition of Thin Films of Poly(Bisphenol A Carbonate). *Macromolecules* **2012**, *45* (3), 1652–1662. <https://doi.org/10.1021/ma202127p>.
- (30) Lukichev, A. A. Graphical Method for the Debye-like Relaxation Spectra Analysis. *J. Non-Cryst. Solids* **2012**, *358* (3), 447–453. <https://doi.org/10.1016/j.jnoncrysol.2011.10.022>.
- (31) Nobukawa, S.; Urakawa, O.; Shikata, T.; Inoue, T. Dynamics of a Probe Molecule Dissolved in Several Polymer Matrices with Different Side-Chain Structures: Determination of Correlation Length Relevant to Glass Transition. *Macromolecules* **2013**, *46* (6), 2206–2215. <https://doi.org/10.1021/ma302567j>.
- (32) Kremer, F.; Schönhals, A. Broadband Dielectric Measurement Technique. In *Broadband Dielectric Spectroscopy*; Springer Berlin Heidelberg: Berlin, Heidelberg, 2003; pp 35–56.
- (33) Schaumburg, G. Novocontrol Introduces High Quality Low Cost Interdigitated Comb Electrodes. **2006**, 5–7.

- (34) Cole, K. S.; Cole, R. H. Dispersion and Absorption in Dielectrics I. Alternating Current Characteristics. *J. Chem. Phys.* **1941**, *9* (4), 341–351. <https://doi.org/10.1063/1.1750906>.
- (35) Davidson, D. W.; Cole, R. H. Dielectric Relaxation in Glycerol, Propylene Glycol, and *n*-Propanol. *J. Chem. Phys.* **1951**, *19* (12), 1484–1490. <https://doi.org/10.1063/1.1748105>.
- (36) Havriliak, S.; Negami, S. A Complex Plane Representation of Dielectric and Mechanical Relaxation Processes in Some Polymers. *Polymer* **1967**, *8*, 161–210. [https://doi.org/10.1016/0032-3861\(67\)90021-3](https://doi.org/10.1016/0032-3861(67)90021-3).
- (37) Díaz-Calleja, R. Comment on the Maximum in the Loss Permittivity for the Havriliak–Negami Equation. *Macromolecules* **2000**, *33* (24), 8924–8924. <https://doi.org/10.1021/ma991082i>.

Chapter3: Molecular dynamics of Poly Lactic Acid (PDLLA) and its oligomers (OLAs) in amorphous state

In this chapter, we study the structural relaxation and molecular dynamics of wholly amorphous PDLLA (95.7% L-lactic acid) and its oligomers (OLAs) with different molecular weight through calorimetric techniques such as MDSC, Flash DSC. Some concepts such as fictive temperature, thermal lag and structural relaxation have been studied to characterize the influence of the cooling rate on glass transition in Flash DSC. In fact, Flash DSC allows exploring thermal properties of materials over a broad range of heating and cooling rates, complementary to rates usually used with DSC.

In parallel we use Dielectric Relaxation Spectroscopy (DRS) technique over a wide range of temperature and frequency to cover global and secondary relaxations. By this technique several relaxations were observed for these samples. Beside these relaxations, α -relaxation parameters, the relaxation times, glass transition temperature (T_g), fragility and activation energy (related to each relaxation process) etc. are discussed in this chapter to investigate the effect of molecular weight on our samples. Then, the temperature dependence of the cooling rate obtained by Flash DSC is also compared to the temperature dependence of the relaxation times obtained from DRS. The comparison of these two dependencies implies a better understanding about the origin of the temperature dependence of the cooling rate.

In this chapter, we compare also results given by calorimetric and dielectric techniques regarding the influence of the molecular weight of our samples on both glass transition temperature and fragility index.

1- Fictive temperature

The phenomenon of global relaxation can be depicted using the concept of fictive temperature T_f ¹ which depends on cooling rates β_c applied in Flash DSC. This temperature allows to characterize the non-equilibrium state related to vitrification and is calculated by area matching method² which was explained in first chapter. In fact, the value obtained is limiting fictive temperature, since the fictive temperature is not a fix value and is dependent on temperature but for simplicity we used fictive temperature instead of limiting fictive temperature in this work.

Figure3-1 shows the estimation of fictive temperature with Flash DSC technique upon heating for PDLLA by area matching method proposed by Moynihan et al.², when the heating and cooling have equal rate ($\beta_h = |\beta_c| = 1500\text{K/s}$), the $T_f = 74^\circ\text{C}$ is obtained without thermal lag corrections (explained in next part) so it is higher than one obtained by DSC (at $\beta_h = |\beta_c| = 10\text{K/min} \approx 0.16\text{K/s}$) which is 57°C .^{3,4}

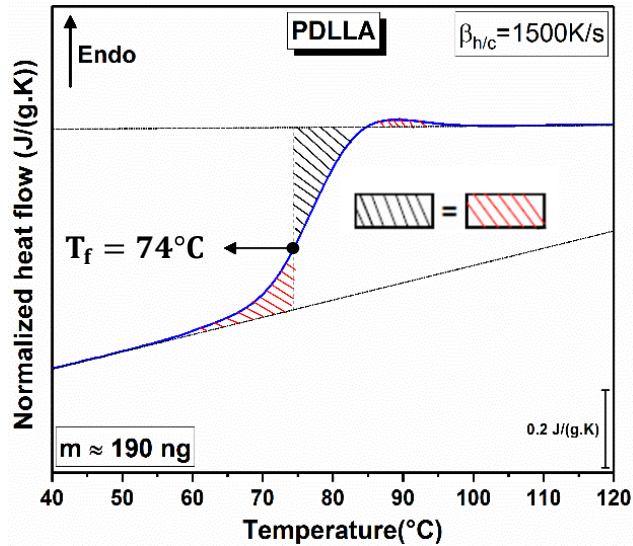


Figure3-1 Flash DSC Normalized heat flow of 190ng wholly amorphous PDLLA as a function of temperature upon heating for scanning rate $\beta_h = |\beta_c| = 1500\text{K/s}$.

1-1 Dependence of fictive temperature on cooling rate

Many studies have demonstrated that fictive temperature depends on cooling rate⁵⁻⁷ and theoretically it shouldn't depend on heating rates. Gao et al.⁶ observed no dependence of fictive temperature on a wide range of heating rates by combining Flash DSC and DSC.

In this work, the dependence of fictive temperature on cooling rates has been investigated by using Flash DSC on PDLLA and oligomers of lactic acid with different molecular weight. **Figure3-2** shows heating scans of wholly amorphous PDLLA and OLAs over five decades of cooling rates in Flash DSC. An endothermic step of specific heat capacity indicate glass transition of the material which is observed along with an endothermic relaxation peak. This relaxation peak shifts toward higher temperatures and its amplitude increases when the cooling rate is reduced. The mass of samples in Flash DSC was estimated by following equation:

$$\text{mass (g)} = \frac{\Delta H_{(\text{Flash DSC})}}{\Delta C_{p(\text{MDSC})} \beta_{h(\text{Flash DSC})}} \quad (3.1)$$

Where, $\Delta H_{(\text{Flash DSC})}$ is heat flow step at glass transition obtained from Flash DSC in Watt, $\Delta C_{p(\text{MDSC})}$ is heat capacity step obtained from MDSC in J/(g.K) and β_h (K/s) is heating rate in Flash DSC. Values of ΔC_p obtained from MDSC ($p = 60\text{s}, \tau \approx 10\text{s}$) were reported in **Table3-1**.

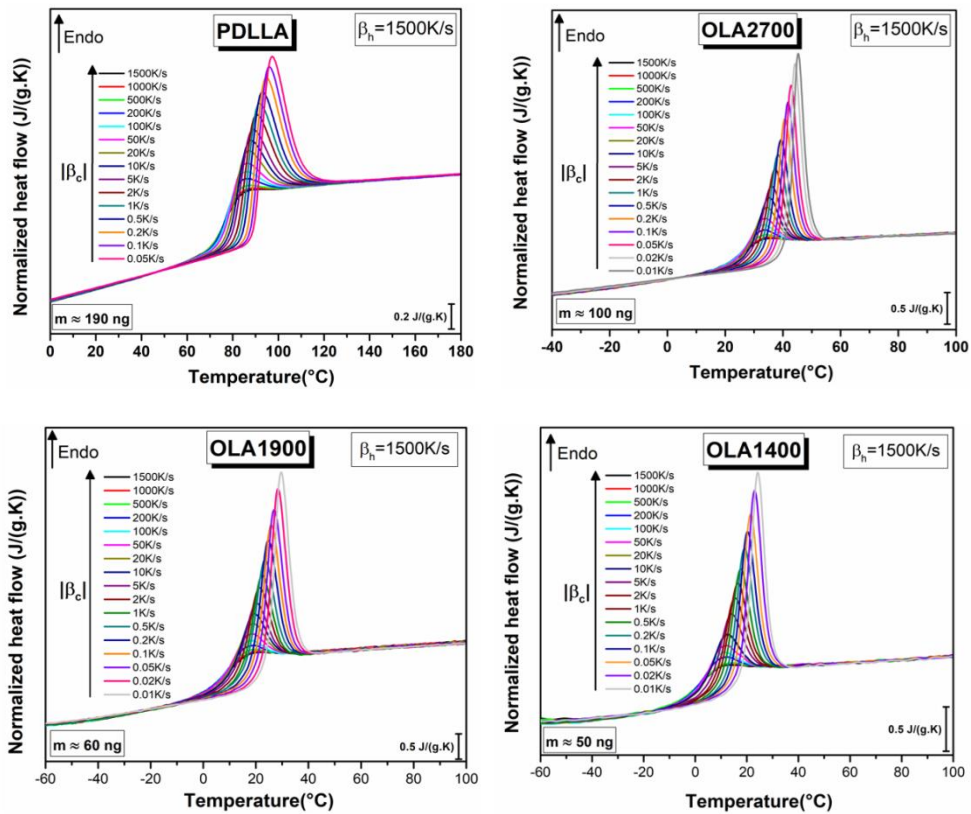


Figure3-2 Flash DSC Normalized heat flow of wholly amorphous PDLLA and its OLAs as a function of temperature upon heating for scanning rate $\beta_h = 1500\text{K/s}$. The glassy PDLLA and its OLAs were formed over five decades of cooling rates.

Samples	PDLLA	OLA2700	OLA1900	OLA1400
$\Delta C_p \left(\frac{\text{J}}{\text{g.K}}\right)$	0.51 ± 0.02	0.55 ± 0.03	0.57 ± 0.03	0.60 ± 0.03

Table3-1 Heat capacity step ΔC_p obtained from MDSC for all samples.

1-2 Thermal lag corrections in Flash DSC

In order to improve the accuracy of the fictive temperatures obtained by Flash DSC, the thermal lag correction is required⁸. The thermal lag is a shift of temperature due to the heat transfer delay between the heater and sample. It is caused by the high scanning rates used and the sample geometry (for ex. sample thickness)⁹. The thermal lag related to the sample thickness can be corrected by the melting of Indium piece or other materials (in our case it is Gallium) placed on the top of the sample⁹⁻¹². Schawe¹⁰ proposed two thermal lag corrections (static and dynamic) in order to measure the glass transition temperature accurately by Flash DSC experiments. The static thermal lag (ΔT_S) corresponds to a third of the difference between the onset melting points of an indium (or another material) piece placed on the sample specimen and another one placed directly on the reference chip sensor. The dynamic thermal lag (ΔT_D) corresponds to a half of the difference between the fictive temperatures determined from measurements upon heating and cooling. A total thermal lag values are calculated by following equation:

$$\Delta T_T = \Delta T_S + \Delta T_D \quad (3.2)$$

Figure3-3 depicts the procedure of the dynamic and static thermal lag determination for PDLLA. The different thermal lag values were summarized in **Table3-2** for all samples. The corrected fictive temperature is obtained by subtract the total thermal lag value from the fictive temperature (determined by area matching method).

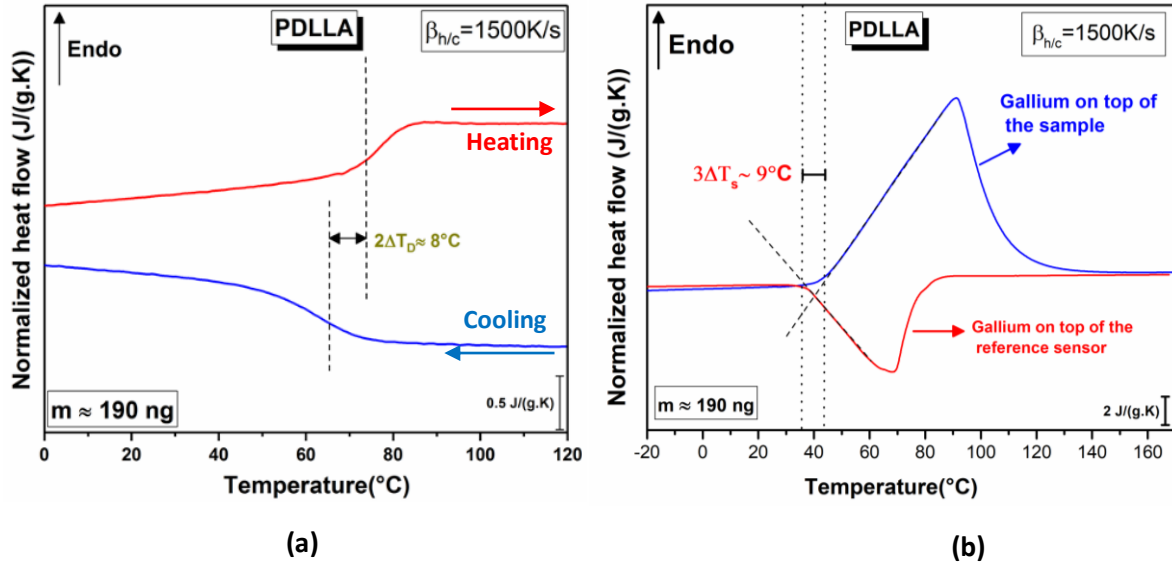


Figure3-3 (a) Estimation of dynamic thermal lag measured from a half of the difference of fictive temperatures T_f upon heating and cooling at $\beta_h = |\beta_c| = 1500\text{K/s}$ for PDLLA. **(b)** Estimation of static thermal lag measured from a third of the difference in the onset melting temperature of a Gallium placed on top of the PDLLA and another one on the reference sensor chip of Flash DSC.

Samples	ΔT_S (°C)	ΔT_D (°C)	ΔT_T (°C)
PDLLA	3	4	7
OLA2700	0	3	3
OLA1900	0	2	2
OLA1400	0	2	2

Table3-2 Dynamic ΔT_D , static ΔT_S and total thermal lag ΔT_T values estimated from Flash DSC for PDLLA and its OLAs at $\beta_h = |\beta_c| = 1500\text{K/s}$.

1-3 Non-Arrhenius behavior of fictive temperature's variation

Figure3-4 shows the variation of logarithm cooling rates with inverse fictive temperatures ($1/T_f$) after thermal lag corrections. As clearly shown in **Figure3-4**, when the cooling rate applied to form the glass increases, the fictive temperature increases by following a non-Arrhenius evolution. This curved evolution can be fitted with a modified version of VFT equation (**Eq.1.2 in Chapter1**)^{10,13}:

$$\log(|\beta_c|) = A - \frac{DT_V}{\ln_{10}(T_f - T_V)} \quad (3.3)$$

Where A is a constant, D and T_V are fitting parameters. T_V is the extrapolated temperature when relaxation times tends to infinite and is called Vogel temperature. By analogy to the

Eq.1.4 in Chapter1, the calorimetric fragility index can be defined through the following equation:

$$m = \left. \frac{d(\log \beta_c)}{d\left(\frac{T_g}{T_f}\right)} \right|_{T_f=T_g} = \frac{DT_V T_g}{\ln 10 (T_g - T_V)^2} \quad (3.4)$$

As shown in **Figure3-4**, experimental data fit well to VFT law. The glass transition temperature T_g at $\beta_h = |\beta_c| = 1500\text{K/s}$ and fragility indexes estimated from the slope of these fitting curves at T_g for $\beta_h = |\beta_c| = 1500\text{K/s}$ are shown in **Table3-3**. As expected T_g is shifted to higher temperature when the cooling rate increases (for ex. 1500K/s in Flash DSC in comparison with 10K/min in DSC)^{3,4,14,15}. According to **Eq.3.4** the fragility index is highly dependent on the temperature at which it is estimated. Since glass transition estimated from Flash DSC (at $\beta_h = |\beta_c| = 1500\text{K/s}$) is greater than the ones estimated from DSC, the value of $m_{\text{Flash DSC}}$ is much lower¹⁴. As is observed in **Figure3-4** and **Table3-3** the glass transition temperature T_g (T_f for $\beta_h = |\beta_c| = 1500\text{K/s}$) and fragility index decrease with decreasing molecular weight^{16,17}.

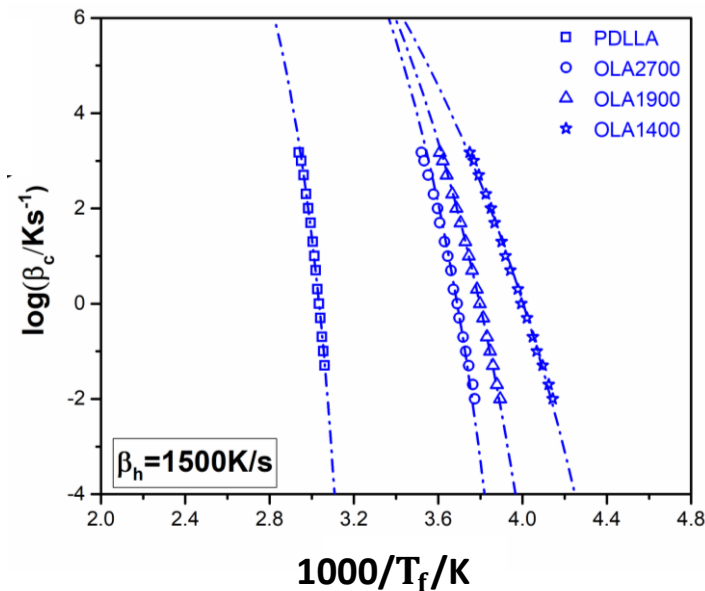


Figure3-4 Evolution of $\log(|\beta_c|)$ determined from Flash DSC experiments as a function of inverse fictive temperature for PDLLA and its OLAs. Dash-dot lines are VFT fits to Flash DSC data.

Samples	$T_g(\text{K})(\beta_c = \beta_h = 1500\text{K/s})$	$T_V(\text{K})$	$m_{\text{Flash DSC}}$
PDLLA	340.0	295.0	91
OLA2700	284.5	222.5	61
OLA1900	279.0	202.0	52
OLA1400	266.5	174.5	40

Table3-3 Glass transition temperatures and fragility indexes determined from Flash DSC data.

2- Dielectric relaxations in 3D curves

Figure3-5 shows dielectric relaxation maps of the imaginary part of permittivity (loss part) in 3D as a function of frequency and temperature for PDLLA and OLAs. In lower temperature range (-150°C to 0°C) PDLLA and all OLAs show secondary relaxations which shift to higher frequencies as the temperature increases. In higher temperature range the α -relaxation (which is more intense) takes place, associated to the structural relaxation (dynamic glass transition). The conductivity phenomenon at higher temperature than dynamic glass transition temperature (T_g) and lower frequency is also observed with large increment of ϵ'' for all samples. The appearance of this conductivity is related to the charge transport of free ions through the sample. In **Figure3-5** some parts of conductivity region have been cut to see better the relaxation processes.

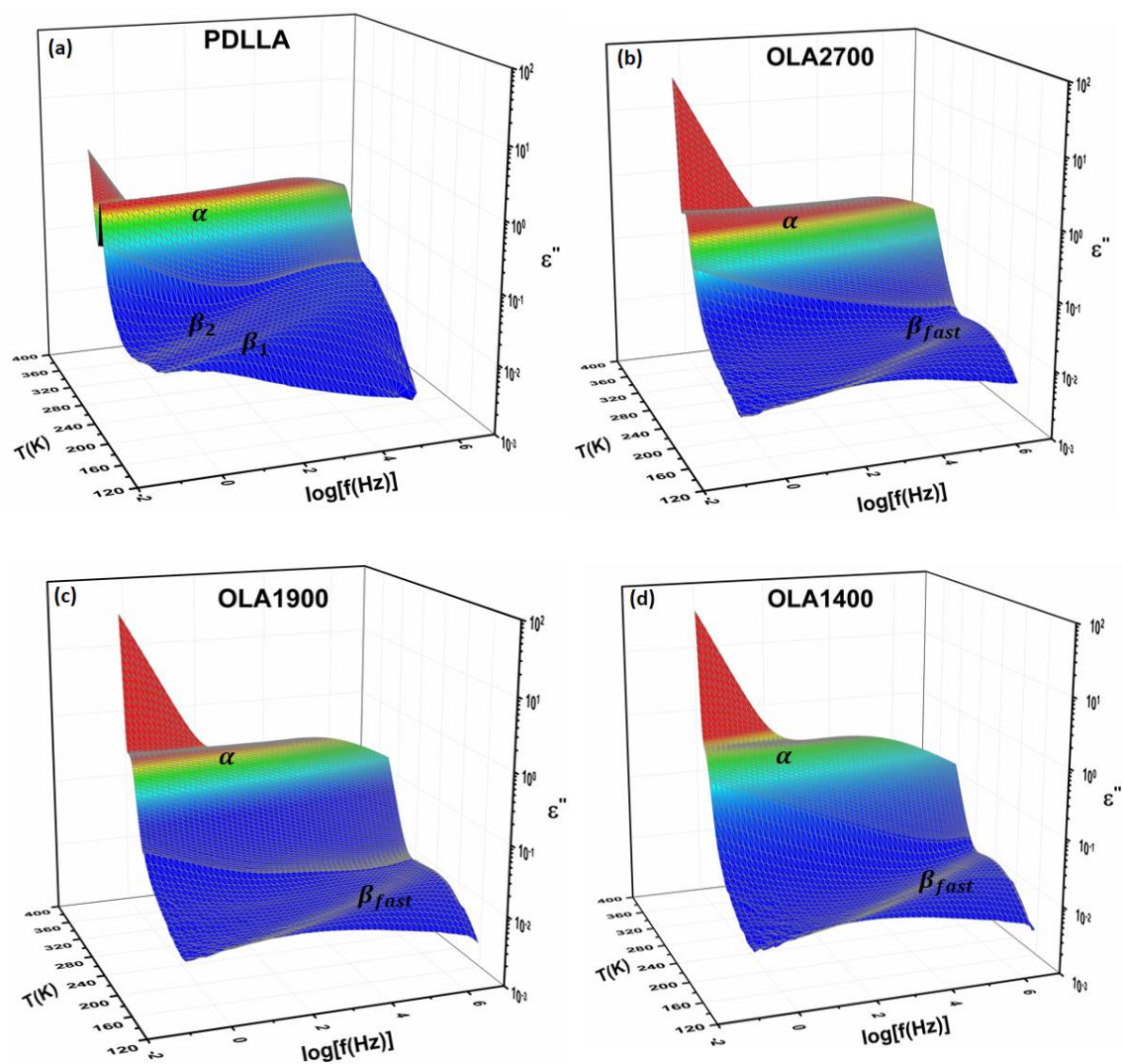


Figure3-5 Imaginary part of the complex dielectric permittivity ϵ'' vs frequency and temperature. The main relaxation process (structural relaxation) was indicated by α . Secondary relaxations were indicated by α . Secondary relaxations were indicated by β_1 and β_2 for PDLLA (β_1 is faster than β_2). There is only one observable secondary process in 3D relaxation map from DRS for OLAs indicated by β_{fast} .

3- Conduction effect in DRS data

As was mentioned in **chapter2**, relaxation processes are characterized by a peak in the imaginary part ϵ'' and a step-like decrease of the real part ϵ' of the complex dielectric function $\epsilon^*(\omega) = \epsilon'(\omega) - i\epsilon''(\omega)$ with increasing frequency. The conduction phenomena always shows an increase of imaginary part of the dielectric function with decreasing frequency¹⁸⁻²⁰. For pure ohmic conduction the real part of ϵ^* is independent of frequency while for non-ohmic conduction or polarization effects, the real part of ϵ^* increases with decreasing frequency²¹.

In these samples the separation of charges at interface gives rise to an additional polarization which is called electrode polarization²¹ (it was cut in **Figure3-5** to see better the relaxation processes). This is an unwanted parasitic effect during a dielectric experiment and takes place at the external electrodes containing the sample on a macroscopic scale that can mask the dielectric response of the sample. It occurs mainly for moderately to highly conducting samples and influences the dielectric properties at low frequencies. Both the magnitude and the frequency position of electrode polarization depend on conductivity of the sample and can result in extremely high values of real and imaginary part of the complex dielectric function. **Figure3-6** shows the real and imaginary part of the complex dielectric function of PDLLA and its OLAs at one example temperature where $\log(\epsilon')$ was increased at low frequencies that means the electrode polarization exists. High increase of $\log(\epsilon'')$ at low frequencies with slop equal to -1 shows the conductivity contribution.

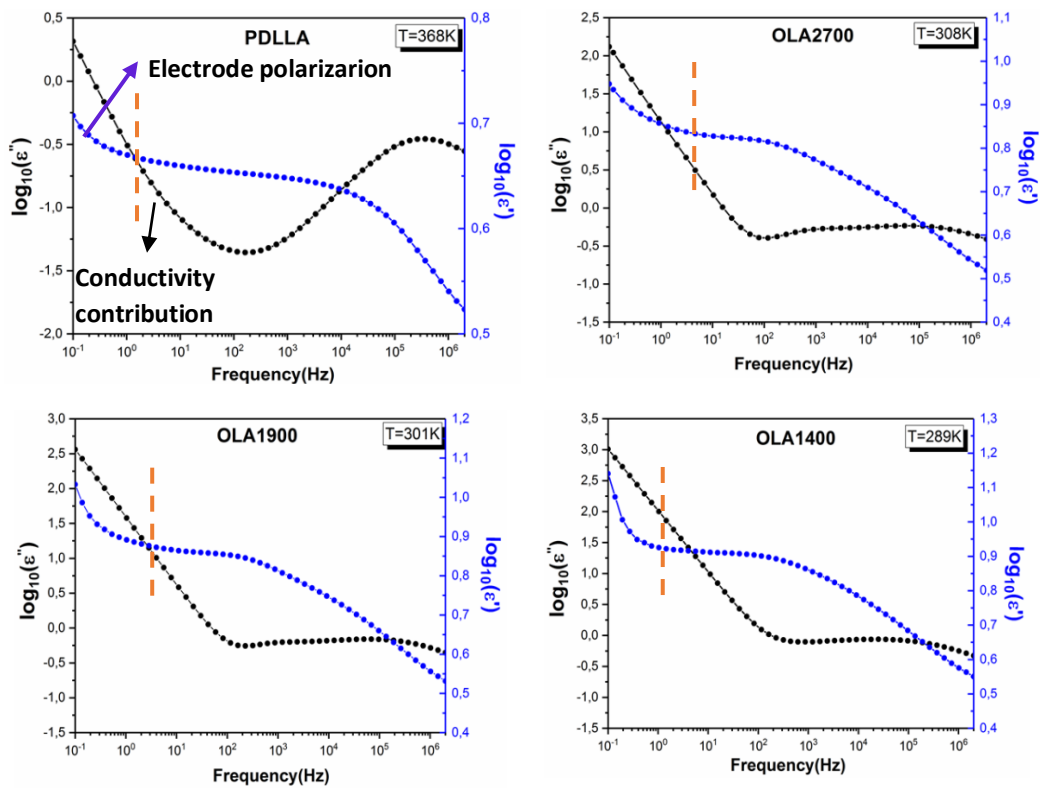


Figure3-6 The real and imaginary part of the complex dielectric function ϵ^* as a function of frequency at one example temperature for PDLLA and its OLAs to observe the conduction effect and electrode polarization.

4- Normal mode and α -relaxation

Figure3-7 shows the frequency dependence of $\log(\epsilon'')$ for PDLLA and different molecular weight of OLAs at different temperatures in α -relaxation range. Usually in a dielectric study, the frequency f_{\max} at which ϵ'' takes the maximum value shifts to higher frequency with increasing temperature which mainly shows the increasing mobility of molecules at higher temperature.

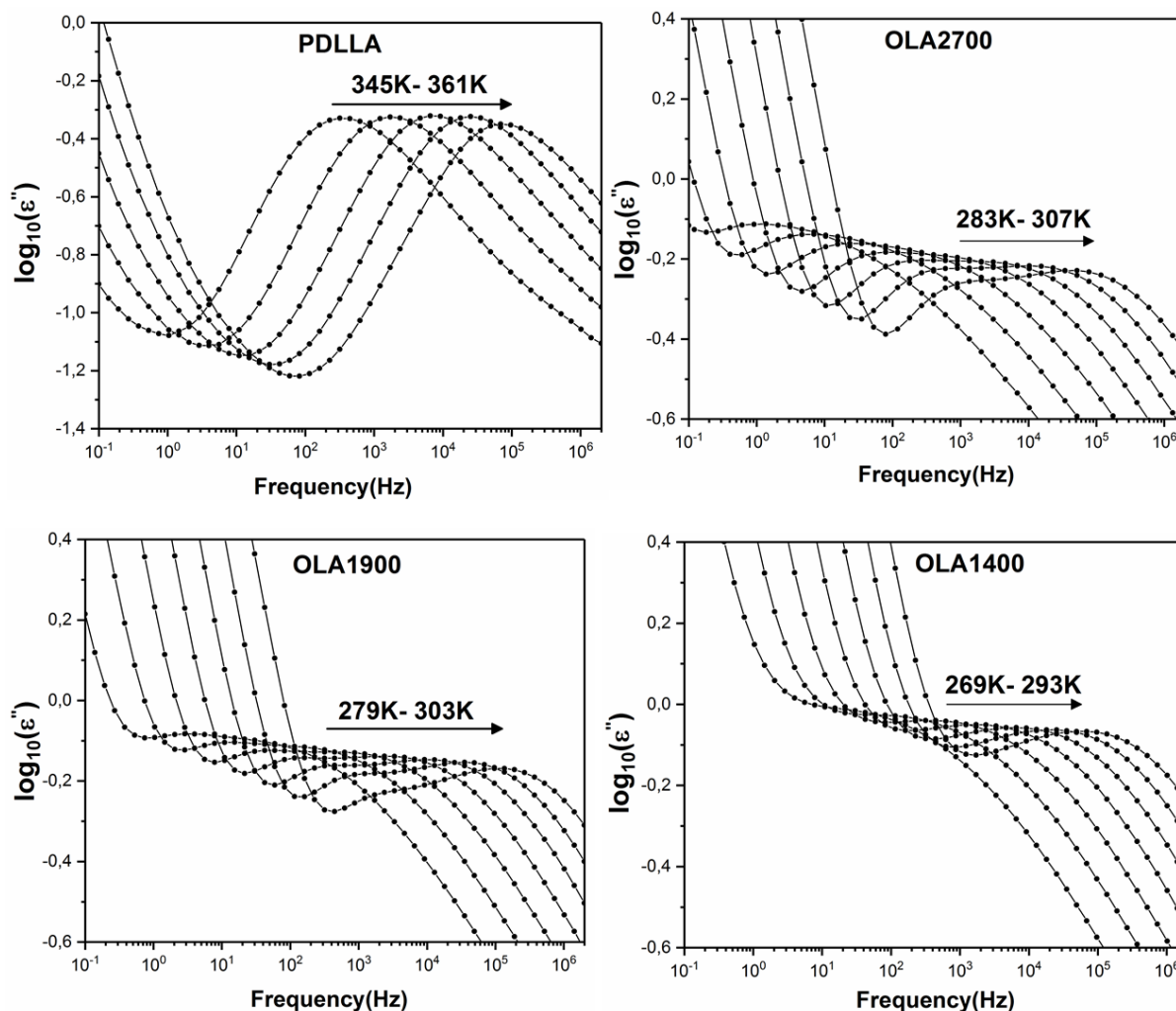


Figure3-7 Frequency dependence of dielectric loss factor ϵ'' (in logarithm) of normal mode and α -relaxation for PDLLA and OLAs at different temperatures.

In order to investigate the segmental relaxation phenomenon the isothermal dielectric loss spectra (**Figure3-7**) were fitted with a conductivity contribution and Havriliak- Negami (HN) complex functions²² in a range of α -process. According to 3D plots (**Figure3-5**), it seems only one HN function is needed to describe α -relaxation, whereas during fitting processes two HN functions are required for all samples. Two relaxation peaks are more clear in **Figure3-7** for OLA2700 and OLA1900 than PDLLA and OLA1400. Since PDLLA and OLAs are type-A polymers²³⁻²⁵ (Type-A polymers have a dipole moment parallel to the chain backbone), it is expected that another relaxation process at lower frequencies than

segmental relaxation exists which is called normal-mode relaxation²⁰ related to the overall chain dynamics.

Figure3-8 presents an example of fitting procedure for the imaginary part of the complex permittivity versus frequency for PDLLA and OLAs at selected temperatures. Two HN functions are required for fitting: one for normal-mode and another one for α -relaxation. The shape parameters (α_{HN} , β_{HN}) were reported for each sample at indicated temperature. These parameters for PDLLA are in good agreement with the thesis of B.Rijal²⁶.

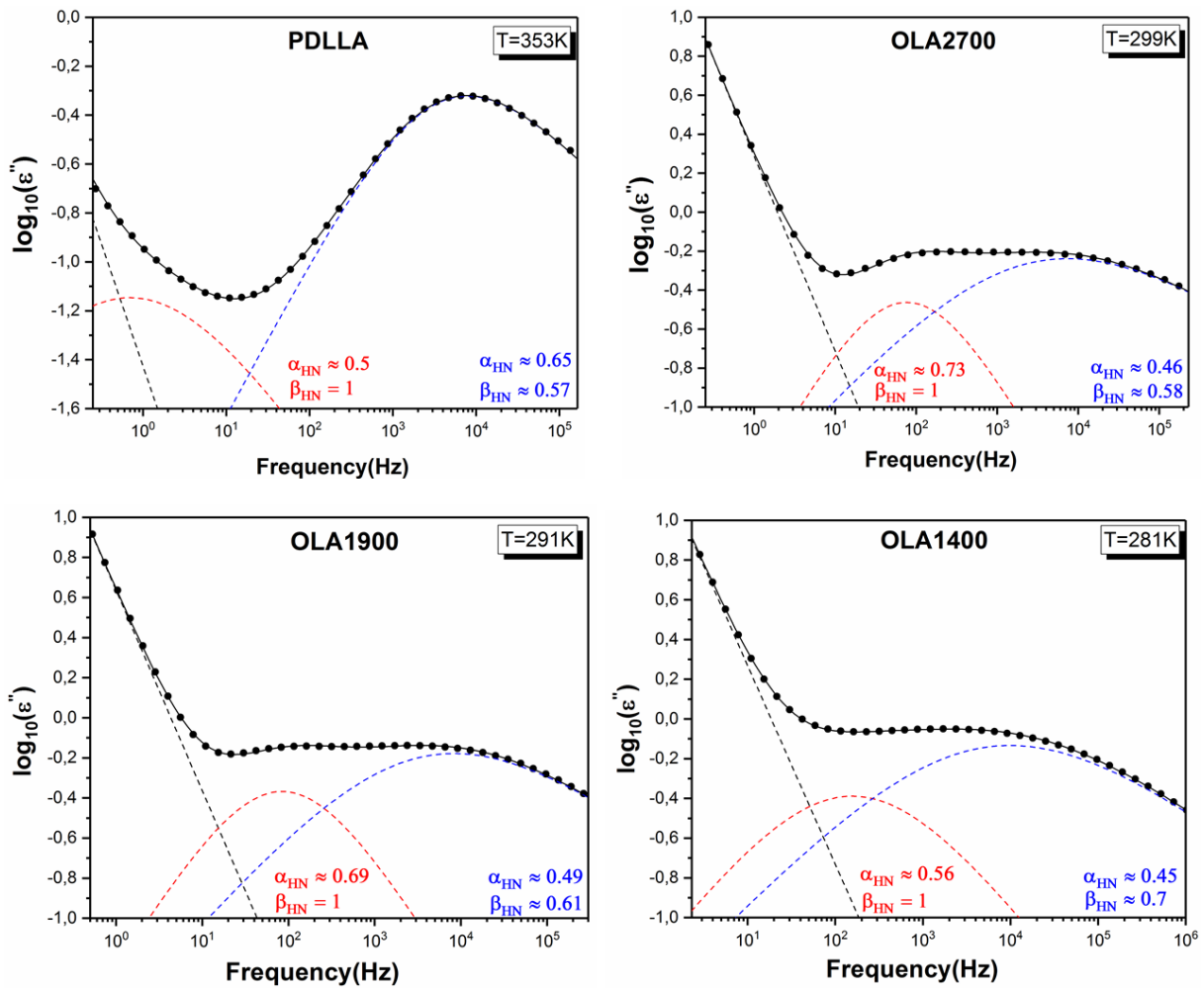


Figure3-8 Illustration of the analytical procedure used to investigate the relaxation phenomena in segmental relaxation region by fitting the isothermal dielectric loss with a conductivity contribution (black dashed line) and two Havriliak–Negami (HN) complex functions: one for normal mode relaxation (red dashed line) and another (blue dashed line) for α -relaxation. The black solid line is the final fitting. The shape HN parameters for both processes in amorphous state are also reported at temperature indicated for each sample.

4-1 Shape parameters α_{HN} , β_{HN}

As was discussed in **Chapter2**, these parameters describe the symmetric and asymmetric broadening of the complex dielectric function and founded less than 1²⁷. In **Figure3-9** the shape parameters obtained from HN fits (**Eq.3.5**) for α -relaxation process versus temperature were plotted for each sample. What can be observed is that for PDLLA, $\alpha_{HN} > \beta_{HN}$ but for OLAs it is vice versa.

$$\varepsilon^* = \varepsilon_\infty + \frac{\Delta\varepsilon_{HN}}{[1+(i\omega\tau_{HN})^{\alpha_{HN}}]^{\beta_{HN}}} \quad (3.5)$$

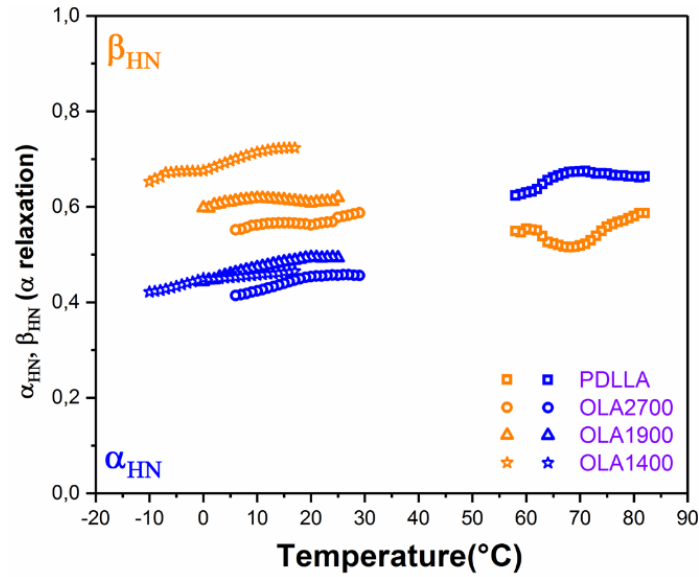


Figure3-9 Variation of shape parameters for α -relaxation as a function of temperature obtained by HN fitting procedure for PDLLA and different OLAs.

4-2 Dielectric relaxation strength $\Delta\varepsilon$

By fitting the experimental data with the HN function (**Eq3.5**), the dielectric strength $\Delta\varepsilon_\alpha$ is also obtained, which was defined (according to the generalized form of the Debye's theory) by Onsager, Fröhlich, and Kirkwood as²¹:

$$\Delta\varepsilon = \frac{1}{3\varepsilon_0} G_K \frac{\mu^2 N}{k_B T V} \quad (3.6)$$

Where ε_0 is the vacuum permittivity, G_K is the Kirkwood correlation factor, μ^2 is the time-correlation function of the total dipole moment, k_B is Boltzmann's constant, T is the temperature, and N/V is the volume density of dipoles. The temperature dependence of the dielectric strength $\Delta\varepsilon$ obtained from DRS experiment was demonstrated for α -relaxation for each amorphous sample in **Figure3-10**. According to **Eq.3.6** $\Delta\varepsilon_\alpha$ decreases with increasing temperature for different glass forming systems like polymers and thin polymer films²⁷⁻³⁰. As is observed in **Figure3-10** this value is also decreasing with increasing molecular weight which is in agreement with the work of Madhusudan.T et al. who compared the dynamics of poly (vinyl acetate) with its oligomer³¹. The lower $\Delta\varepsilon_\alpha$ in the case of PDLLA could be a direct consequence of its chain connectivity³¹. Usually in polymers only the component of the dipole moment perpendicular to the main chain contributes to the observed dielectric strength and since PDLLA is a type-A, the number of dipole moments perpendicular to the main chain is less compare to the parallel dipole moments^{20,27}. In the case of OLAs maybe the perpendicular dipole moments are more numerous or their density is higher³¹ so $\Delta\varepsilon_\alpha$ has higher value compare to PDLLA.

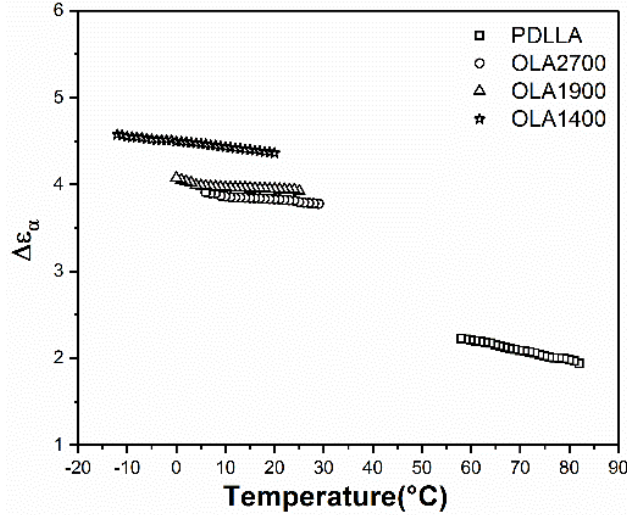


Figure3-10 Temperature dependence of the dielectric strength for α -relaxation $\Delta\epsilon_{\alpha}$ for all samples. PDLLA has lowest $\Delta\epsilon_{\alpha}$ compare to OLAs.

5- Relaxation map for α -relaxation

The fitting process of isothermal dielectric loss spectra by HN functions at each temperature in the range of structural relaxation allows obtaining the relaxation map on this range. **Figure3-11** shows the inverse of relaxation time as a function of the inverse temperature for PDLLA and OLAs. As we see, α -relaxation process of each sample occurs at higher temperature when molecular weight is increased, which is in good agreement with the work of Madhusudan.T et al³¹. It means that the glass transition temperature increases with increasing molecular weight.

The experimental data in the range of the α -relaxation can be fitted by a Vogel–Tamman–Fulcher (VFT) law^{13,27,32,33}. Usually the temperature dependence of the relaxation time for α -relaxation presents a non-Arrhenius behavior and is well described by VFT equation (**Eq.3.7**). The glass transition temperature (T_g) can be estimated by extrapolating VFT fit to the common convention, $\tau = 100s$ or $\log\left(\frac{1}{\tau}\right) = -2$. By putting VFT parameters in **Eq.3.8**, T_g can be obtained (all VFT parameters from fitting and T_g from DRS were reported in **Table3-4**). To correlate the dependence of the relaxation times to dynamic glass transitions, the MDSC data was added at $\tau \sim 10s$ ($\tau = \frac{P}{2\pi}$, $P = 60s$) for each sample. As shown in **Figure3-11** glass transition temperatures estimated from MDSC are in good agreement with dielectric relaxation spectroscopy (DRS) measurement.

$$\log\left(\frac{1}{\tau_{\max}}\right) = -\log(\tau_0) - \frac{DT_V}{\ln 10(T - T_V)} \quad (3.7)$$

$$T_g = T_V + \frac{DT_V}{\ln 10(2 - \log(\tau_0))} \quad (3.8)$$

Where τ_0 , T_V and D are VFT parameters obtained from **Eq.3.7**, D is the strength parameter (related to fragility, introduced in first chapter), when D increases the fragility index

decreases which means the material is more strong. T_V is a characteristic temperature below T_g which is called Vogel temperature. τ_0 is relaxation time at infinite temperature.

The fragility indexes are calculated at T_g with **Eq.3.9**. In general the fragility index is highly dependent on the temperature at which it is estimated. All fragility indexes related to PDLLA and OLAs from DRS were reported in **Table3-4**. Fragility indexes of OLAs reveal that amorphous OLAs can be classified as strong or intermediate glass forming liquids whereas PDLLA is classified as a fragile polymer.

$$m = \left. \frac{d(\log \tau)}{d\left(\frac{T_g}{T}\right)} \right|_{T=T_g} = \frac{DT_V T_g}{\ln 10 (T_g - T_V)^2} \quad (3.9)$$

	$\log(\tau_0)$	D	$T_V(K)$	$T_{g(DRS)}(K)$	m	$T_{g(MDSC)}(K)$
PDLLA	-13.43	4.28	291.5	327.0	145	330.0
OLA2700	-14.98	8.66	217.5	265.0	95	268.0
OLA1900	-16.40	12.61	198.5	257.5	81	259.5
OLA1400	-18.41	19.97	172.0	244.5	69	246.5

Table3-4 Fit parameters derived from VFT fits for PDLLA and OLAs. T_g ($\tau=100s$) and fragility indexes from DRS were indicated. T_g ($\tau\sim 10s$) were obtained from MDSC measurements.

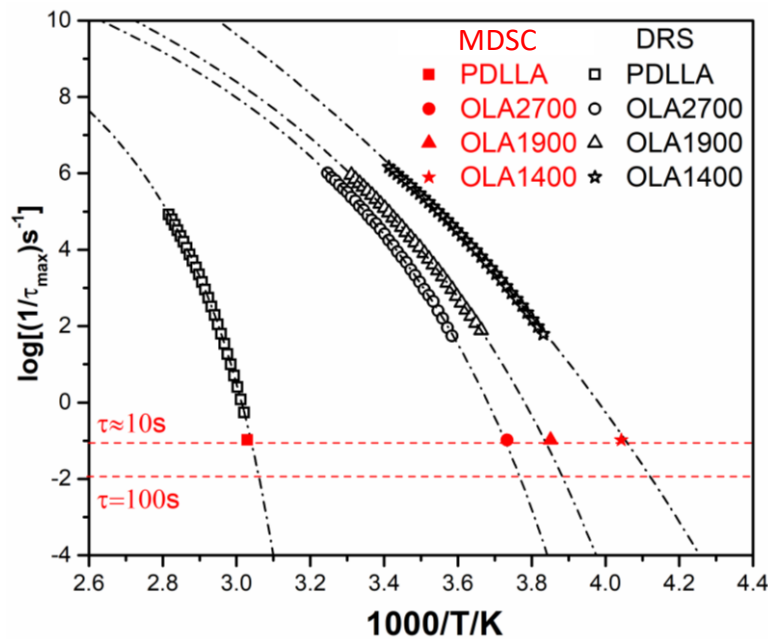


Figure3-11 Logarithmic plot of inverse relaxation time ($1/\tau_{max}$) for α -relaxation as a function of the inverse temperature for PDLLA and OLAs. Black hollow Symbols are from DRS experiments, red filled symbols are from MDSC experiments ($p=60s$, $\tau\sim 10s$) and dashed black lines represent VFT fits for each sample.

6- Combination of DRS and Flash DSC

The Temperature dependence of cooling rate can be correlated with the temperature dependence of relaxation rate of the structural relaxation. Superposition of dielectric relaxation rate noted $\log(\frac{1}{\tau})$ and Flash DSC cooling rates noted $\log(|\beta_c|)$ was plotted as a function of inverse temperature in **Figure3-12**.

The relationship between cooling rate and relaxation rate can be found as Frenkel-Kobeko-Reiner(FKR) relationship¹⁰ :

$$\beta_c \cdot \tau = \frac{\beta_c}{\omega} = C \quad (3.10)$$

Where C is constant.

According to FKR approach, a relationship between similar VFT equations should be used for glass transition temperature dependencies of the cooling rate and of the relaxation rate with same D and T_V constants and a simple constant logarithmic shift ($\log C$). From **Eq.3.3** and **Eq.3.7**:

$$\log(|\beta_c|) = \log\left(\frac{1}{\tau}\right) + \log C = \underbrace{-\log(\tau_0) + \log C}_A - \frac{DT_V}{\ln_{10}(T-T_V)} \quad (3.11)$$

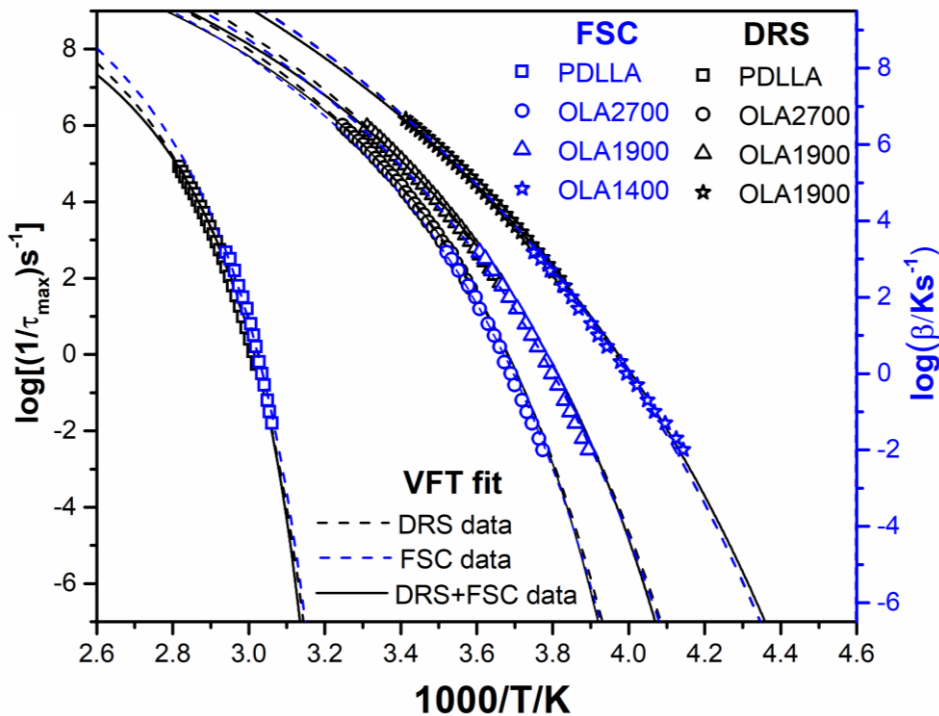


Figure3-12 Temperature dependence of the relaxation time (left coordinate) and cooling rate (right coordinate) as a function of inverse temperature determined from Flash DSC (blue symbols) and DRS (black symbols) for PDLLA and its OLAs. Blue and black dashed lines are VFT fits to Flash DSC and DRS data respectively. Solid black line is VFT fit to all data obtained from Flash DSC+DRS.

As reported in **Table3-4**, according to **Eq.3.7**, VFT parameters were extracted from DRS measurements. By putting T_V and D parameters obtained from VFT fitting of DRS data and

applying **Eq.3.11** to our Flash DSC results, we obtain $\log C = 0.87$ for PDLLA, $\log C = 0.30$ for OLA2700, $\log C = 0.35$ for OLA1900 and $\log C = 0.47$ for OLA1400.

As presented in **Figure3-12**, a shift of less than one decade ($\log C = 0.5$) of the right axis $\log(|\beta_c|)$ implies a very good superposition of DRS and Flash DSC data. In general, $\log C$ values can be obtained by correlating calorimetric dynamic spectroscopy measurement (AC-Chip calorimetry, HCS, MDSC, 3ω method, etc.) with DSC and Flash DSC data^{10,34}. These values are dispersed from values close to 0.3^{35} - $1.5^{36,37}$. In this idea, few studies compare systematically Flash DSC glass transition temperature dependencies of cooling rates with DRS structural relaxation temperature dependence for a set of samples (never done for oligomers).

In the past, studies of the cooling rate dependence of T_g were limited by the narrow range of rates available in DSC. This limited range led to Arrhenius-like dependencies of a broad family of strong and even fragile polymers³⁸⁻⁴¹. The determination of calorimetric fragility index in these constraining conditions had then significant uncertainties. Taking into account our results, the calculation of calorimetric fragility in order to be compared with dynamic fragility (at $\tau = 100$ s) has to be done using the logarithmic shift on the cooling rate dependence of T_g . Accepting VFT dependency of the logarithmic shift of the cooling rate, the calorimetric fragility can be written as **Eq.3.4** with T_g at cooling rate $|\beta_c| = \omega.C = 10^{-2}C$. For example, for PDLLA, this corresponds to T_g at $|\beta_c| = \beta_h = 0.079 \text{ Ks}^{-1}$, so a glass transition temperature of 327K identical to this obtained from DRS. Using the logarithmic shift on the cooling rate dependence of T_g , a new calculation to estimate fragility index (m) and glass transition temperature (T_g) from Flash DSC+DRS can be done. Since this calculation covers more data, it seems it will be more accurate (see **Table3-5**).

	Flash DSC					Flash DSC+DRS			
	PDLLA	2700	1900	1400		PDLLA	2700	1900	1400
A	14.30	15.28	16.75	18.88	$-\log(\tau_0)$	12.13	14.01	14.91	17.90
D	4.28	8.66	12.61	19.97	D	3.29	7.18	9.70	19.14
$T_V(\text{K})$	291.5	217.5	198.5	172.0	$T_V(\text{K})$	297.0	222.5	206.5	172.5
$T_g(\beta_c = 10^{-2}C)(\text{K})$	327.0	265.0	257.5	244.0	$T_g(\tau = 100\text{s})(\text{K})$	327.0	264.5	257.5	243.5
$m(T_g)$	145	95	81	69	$m(T_g)$	155	99	85	68

Table3-5 Fit parameters derived from VFT fits to data for PDLLA and its OLAs obtained from Flash DSC (with similar values of D and T_V , obtained from VFT fitting of DRS data) and from Flash DSC+DRS combination.

7- Variation of T_g and fragility with molecular weight

As mentioned in **Chapter1**, T_g of linear polymers increases with increasing molecular weight M_w and essentially saturates within an error at high M_w . Traditionally, variation in T_g as a function of molecular weight for polymers is described by using the Fox-Flory relation⁴²:

$$T_g = T_{g,\infty} - K/M_n \quad (3.12)$$

Where $T_{g,\infty}$ is T_g in the limit of infinite M_w , M_n is the number-average molecular weight and K is an empirical parameter for a particular polymer species.

This relation (as explained in **Chapter1**) often breaks down for oligomeric systems⁴³⁻⁴⁸. $T_g(M)$ reveals a noncontinuous M dependence with three distinct regimes especially for rigid polymers⁴⁸.

Figure3-13 shows the variation of T_g for different molecular weight (PDLLA and its OLAs) obtained from calorimetric technique (Flash DSC, MDSC) and Dielectric Relaxation Spectroscopy (DRS). There is a good agreement between the T_g derived from Flash DSC and DRS but the T_g obtained from MDSC is a little higher than others since in MDSC the relaxation time is about 10seconds which is different than the one chosen for defining T_g in DRS, meaning 100s. With increase in M_w , the restriction on segmental mobility increases, leading to an increase in T_g . However these data can be fitted satisfactorily by Fox-Flory relation but from the study of Baker L. et al.⁴⁸ since polylactic acid (PLA) is a rigid polymer, we expect to observe the complex behavior of $T_g(M)$ in three separated regimes as explained in **Chapter1**. We can assume that, lack of enough data especially in higher molecular weight than these oligomers leads to have invisible three distinguished regimes. If we consider three regions behavior for T_g , according to the recent study of Baker L. et al.⁴⁸, in region I and III, the α -relaxation is controlled by intermolecular interactions (regime III involved much less of structural units than regime I), whereas in region II, the α -relaxation arises from intramolecular dynamics.

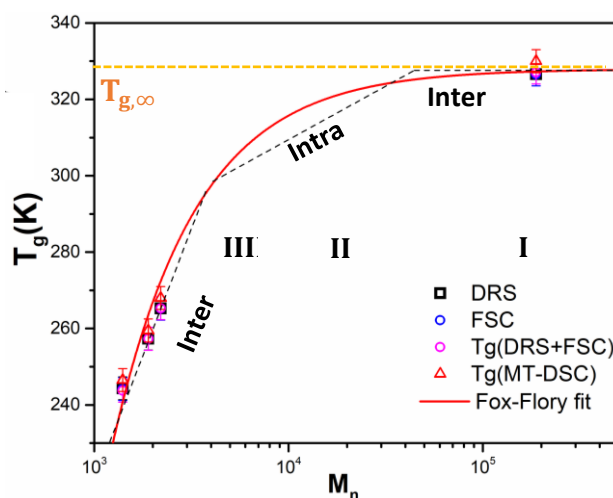


Figure3-13 The number-average molecular weight dependence of T_g for our samples with $T_{g,inf} = 328K \pm 1$ (obtained from Fox-Flory fit). The red line shows Fox-Flory fitting and the black dashed line separates three hypothetical regimes for $T_g(M)$.

The fragility index is also dependent on molecular weight, on **Figure3-14** we see this dependency for our set of samples. Most organic polymers with van der Waals interactions exhibit fragility much higher (over 100^{49,50}) than their small molecular weight counterparts. The fragility of most monomers or oligomers is within the range of 60-90⁵¹, similar to small molecules with Van der Waals interactions. Causes behind such large differences in the fragility of polymers versus small molecules or oligomers are not completely understood. As

we see in **Figure3-14**, the fragility indexes obtained from DRS and Flash DSC are in good agreement and also increase with increasing molecular weight (The fragility index obtained from DRS for PDLLA is similar to that reported by Rijal et al¹⁸), whereas the fragility indexes from DRS+ Flash DSC are a little higher. According to theoretical predictions⁵²⁻⁵⁴ T_g and fragility for linear monodisperse chains is only expected to increase with molecular weight.

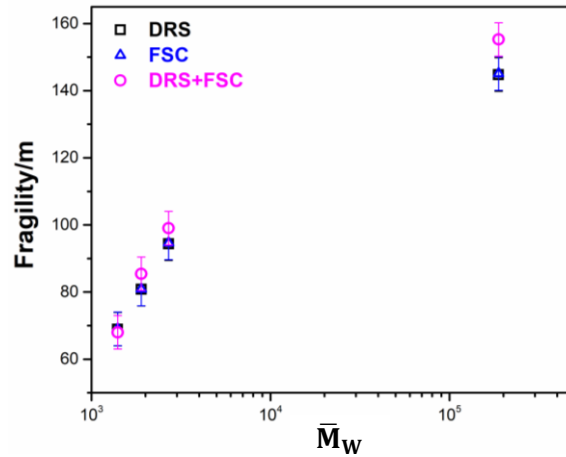


Figure3-14 The weight-average molecular weight dependency of fragility index (m) for our samples.

8- Activation energy of α -relaxation

Activation energy associated with the structural relaxation can be calculated by following equation:

$$E_{a,\alpha} = \frac{\partial \ln(\tau)}{\partial \left(\frac{1}{T}\right)} R \quad (3.13)$$

Where τ is the characteristic time of the structural relaxation at temperature T and R is the gas constant. Results of our samples are presented in **Figure3-15** in a normalized plot $\frac{T_g}{T}$. In liquid-like state, when approaching the glass transition, the activation energy increases because of the possibility that the structural relaxation mobilizes a higher number of structural units⁵⁵⁻⁵⁷.

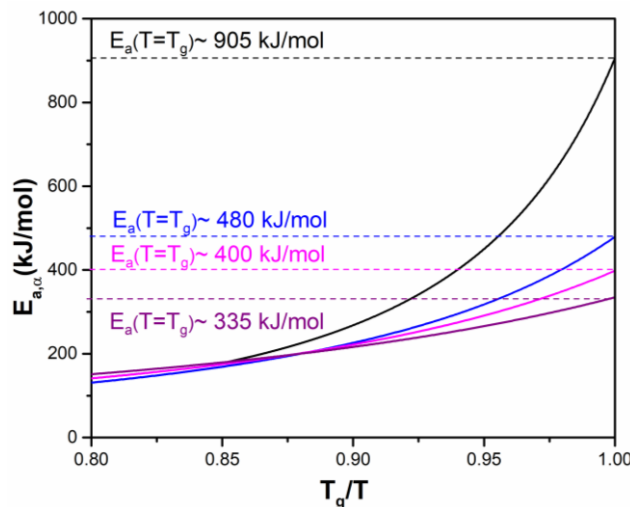


Figure3-15 Activation energy as a function of $\frac{T_g}{T}$ calculated from DRS results for PDLLA and OLAs.

Figure3-16 shows the dependency of activation energy associated to structural relaxation with molecular weight. As we see the activation energy $E_{a,\alpha}$ increases with increasing molecular weight.

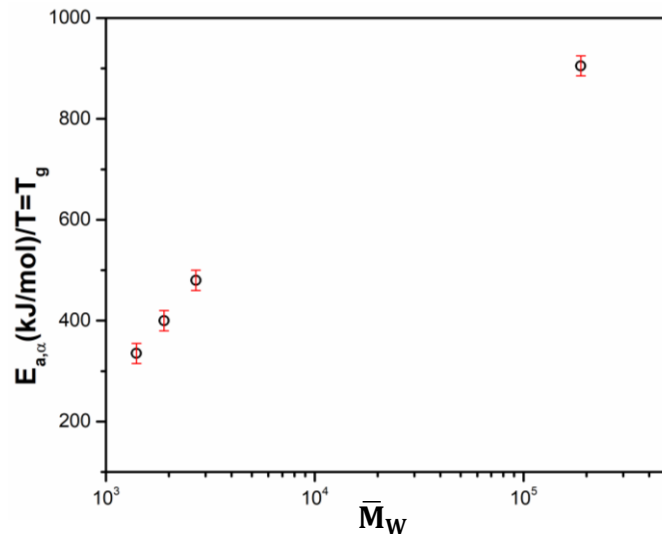
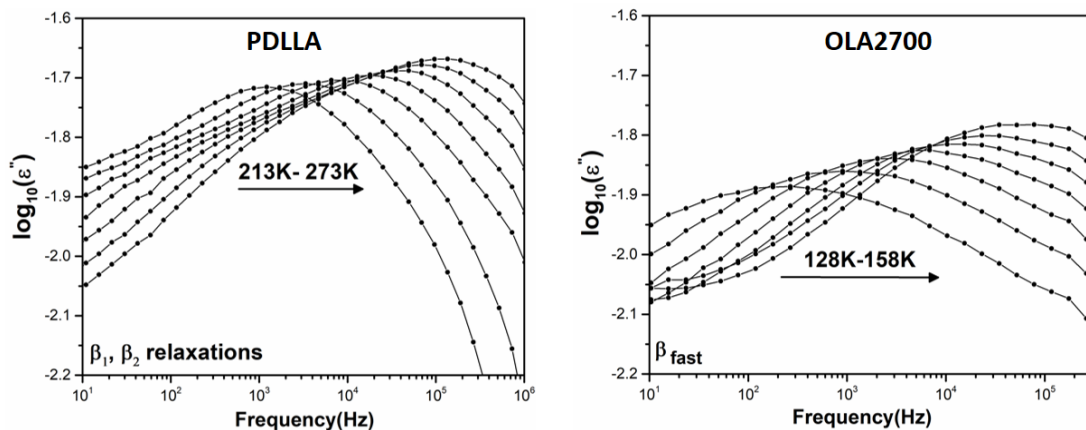


Figure3-16 The weight-average molecular weight dependency of activation energy calculated from DRS for our samples at T_g corresponding to $\tau=100s$.

9- Secondary relaxations

These processes are faster than α -relaxation, that appear in the supercooled liquid regime and persist at temperatures below glass transition. Secondary relaxation is considered as an inherent part of the glassy dynamics and so, its understanding can be very important to clarify the phenomenon of the glass transition⁵⁸. Most authors agree that β -relaxations of amorphous polymers arise from localized rotational fluctuations of the dipole vector^{59,60}. **Figure3-17** shows the frequency dependence of dielectric loss factor ϵ'' (in logarithm) of secondary relaxations at different temperatures for PDLLA and OLAs. As observed also in 3D curves (**Figure3-5**) for OLAs there is only one secondary relaxation which is almost in the same temperature range and has the same intensity (**Figure3-17**). For PDLLA there are two secondary relaxations which are very close together so we see a broad peak that was fitted by two HN functions in different temperature range of secondary relaxations of OLAs.



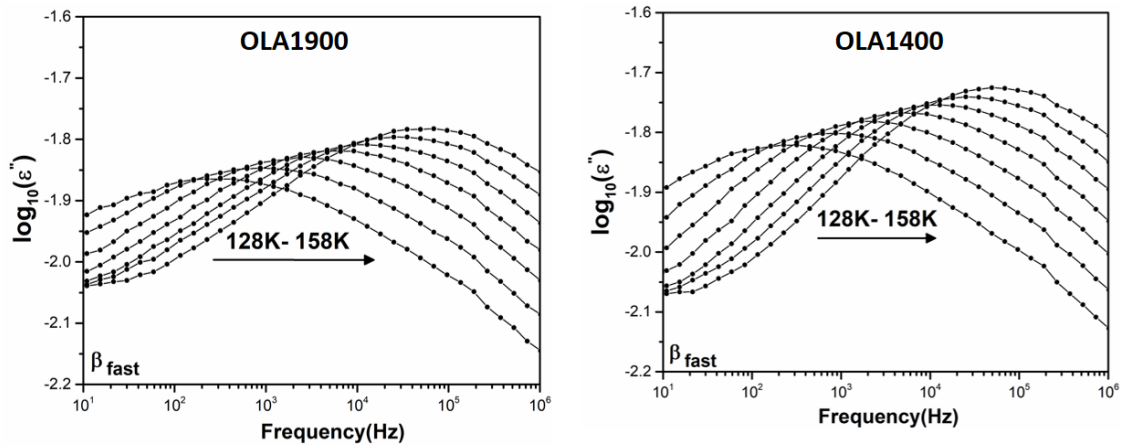


Figure3-17 Frequency dependence of dielectric loss factor (in logarithm) of β_1 , β_2 relaxations for PDLLA and fast β -relaxation (β_{fast}) for OLAs at different temperatures.

3D-images of dielectric relaxations in **Figure3-5** show that, there is only one secondary relaxation (β) for OLAs whereas for PDLLA there are two (β_1 , β_2). During fitting process of isothermal dielectric loss with HN functions in all temperature range (-145°C to 60°C) for OLA2700 and OLA1900, we observed that, there is another contribution near α -relaxation in higher frequency range which is not clear in 3D-images since its intensity and the range of temperature where it appears is small. This process could be considered as a secondary relaxation but it could also be attributed to Johary-Goldstein relaxation (β_{JG})^{61,62}. To be sure about this process we need more investigations.

Among glass-forming materials, the JG secondary relaxation is a universal feature of glass-forming liquids and polymers⁶³, and although it involves the motion of all atoms in the molecule or polymer repeat unit. Its limited amplitude results in faster dynamics than structural relaxation. This relaxation is an intermolecular secondary relaxation and is universally found in the amorphous states⁶⁴. For some years now, β_{JG} -relaxation is believed to be the precursor of the α -relaxation⁶⁵. **Figure3-18** show the slow β -relaxation (β_{slow}) of OLA2700 and OLA1900 at different temperatures (which could be attributed to β_{JG}). As is observed in **Figure3-18** β_{slow} -relaxation is almost in the same temperature and frequency range with same intensity.

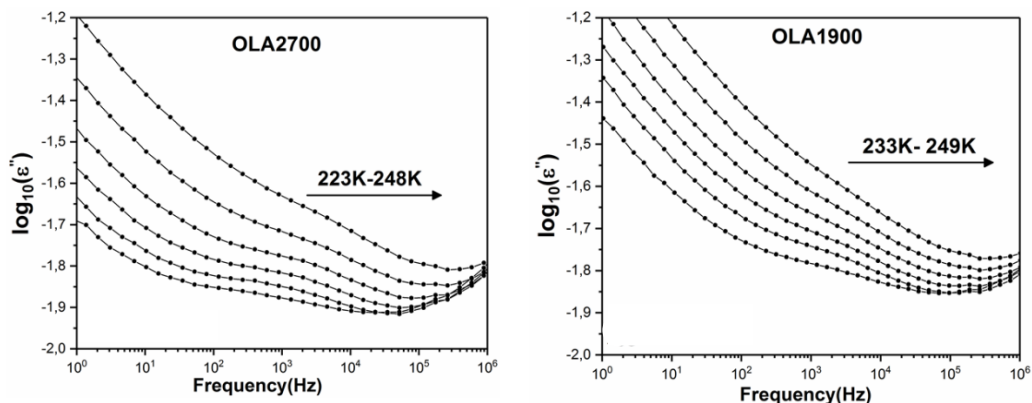


Figure3-18 Frequency dependence of dielectric loss factor (in logarithm) of slow β -relaxation (β_{slow}) for OLA2700 and OLA1900 at different temperatures.

9-1 Arrhenius behavior of secondary relaxations

The temperature dependence of the relaxation rate for secondary relaxations is shown in **Figure3-19** and relaxation time values were obtained from fitting procedure using HN equations. Values obtained from fitting can be well described by Arrhenius law with following equation which was explained in **Chapter1**:

$$\log\left(\frac{1}{\tau_{\max}}\right) = \frac{0.43E_a}{RT} - \log\tau_{\infty} \quad (3.14)$$

Where, τ_{∞} is the relaxation time at infinite temperature, E_a is the activation energy that depends on the internal rotation barriers as well as on the environment of a moving molecular unit and R is gas constant ($\approx 8.314 \text{ J} \cdot \text{K}^{-1} \cdot \text{mol}^{-1}$).

As we see clearly in **Figure3-19** secondary processes of OLAs are match well together, but they are different in frequency and temperature compared to PDLLA. It seems that β_{fast} of OLAs comes from the effect of hydroxyl and carboxyl group at the end chain of OLAs which is more dominant compared to PDLLA.

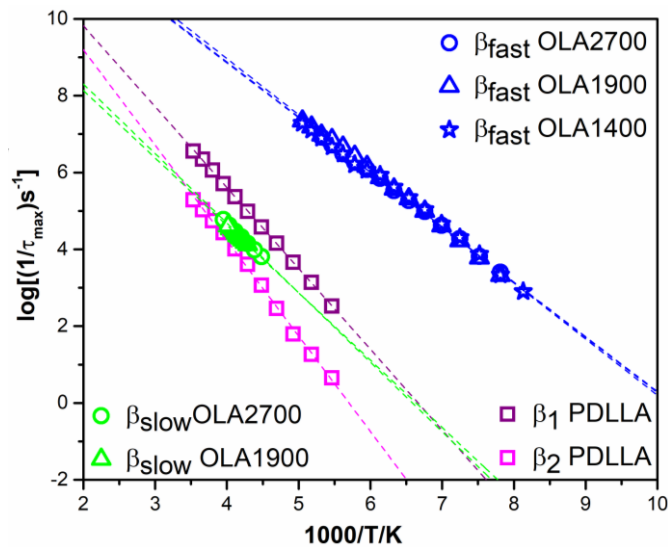


Figure3-19 Inverse of dielectric relaxation time ($1/\tau_{\max}$) for secondary relaxations as a function of the inverse temperature for PDLLA and OLAs with different molecular weight. Symbols are data obtained from DRS experiments and dashed lines represent fits by Arrhenius law.

9-2 Activation energy

By fitting the temperature dependence of the relaxation rate for secondary relaxations with Arrhenius law (**Eq.3.14**), the activation energy (E_a) is obtained. Typical values for E_a are in the range from 20-50 kJ/mol^{20,66}. Values of activation energy for PDLLA ($\beta_1 \approx 41 \text{ kJ/mol}$, $\beta_2 \approx 48 \text{ kJ/mol}$) are close to values provided by the literature (36-46 kJ/mol)⁶⁶. For OLAs there is no reference to compare the activation energies but in our case, E_a is almost the same for β_{slow} ($\approx 35 \text{ kJ/mol}$) and β_{fast} ($\approx 28 \text{ kJ/mol}$) relaxations (**Figure3-20**). In some oligomeric systems, the activation energy for β -relaxation depends on molecular weight⁴⁸. If β_{slow} relaxation could be attributed to β_{JG} , according to the literature of polymers^{62,67}, its activation energy should be much more (for ex. $\approx 80 \text{ kJ/mol}$). According to **Figure3-19**, we

observe that there is almost a superposition of the dielectric relaxation time for β_{slow} (in OLA2700 and OLA1900) and β_2 (in PDLLA), thus perhaps this relaxation is the same process with β_2 relaxation of PDLLA or maybe E_a for β_{JG} of oligomers is lower than polymers. However the precise interpretation needs much more investigations by more experimental techniques.

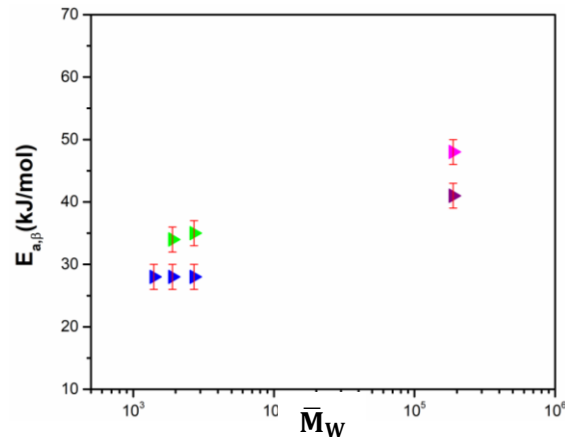


Figure3-20 Activation energies for secondary relaxations as a function of molecular weight. Blue triangle symbols correspond to β_{fast} relaxations for OLAs. Green triangle symbols correspond to β_{slow} relaxations for OLA2700 and OLA1900. Purple and magenta triangle symbols correspond to β_1 and β_2 relaxation for PDLLA respectively.

9-3 Shape parameters α_{HN} , $\beta_{\text{HN}} = 1$

Since the secondary relaxations come from local motions and they are symmetric, so the shape parameter (β_{HN}) is equal 1²⁷. The shape parameter (α_{HN}) obtained from HN fits for secondary processes versus temperature were plotted in **Figure3-21** for each sample. As observed for OLAs, the variation of α_{HN} for secondary relaxations is the same (higher than α_{HN} of β_1 and lower than α_{HN} of β_2 in PDLLA).

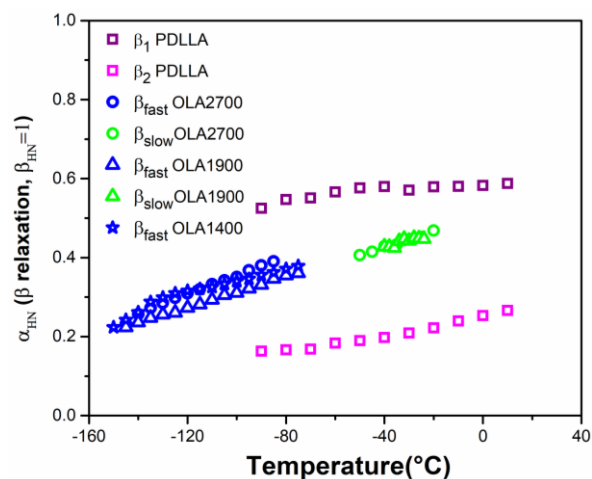


Figure3-21 Variation of shape parameter α_{HN} where $\beta_{\text{HN}} = 1$ for secondary relaxations as a function of temperature obtained by HN fitting procedure for PDLLA and different OLAs.

Conclusion

In this work, the fictive temperature and fragility index have been estimated from Flash DSC experiments and compared to values obtained from MDSC and DRS for PDLLA and its oligomers (OLAs) with different molecular weight. We have evidenced that DRS, MDSC and Flash DSC data match well together (**Figure3-11**, **Figure3-12**). The temperature dependence of the cooling rate obtained by calorimetric data has been compared to the temperature dependence of the relaxation times obtained on approximately 8-decades from DRS. This comparison shows that the calculation of calorimetric fragility in order to be compared with dynamic fragility ($\tau = 100\text{s}$) has to be done using a logarithmic shift on the cooling rate dependence of T_g .

Besides, from DRS and Flash DSC data we have observed that with increasing molecular weight the fragility index increases as well as the glass transition temperature (calorimetric and dynamic) which also matches with Fox-Flory law. However we can assume that by adding more samples with higher molecular weight than these OLAs maybe we will have three regimes for $T_g(M)$ behavior⁴⁸. We have also used DRS to investigate and compare the relaxation processes of PDLLA and OLAs over a broad range of temperature and frequency.

The dielectric spectra of α -relaxation and normal mode shifts to higher temperature range with increasing molecular weight whereas this shift is less evident for secondary relaxation processes for OLAs. We observed also, shape parameters for α -relaxation are changing with molecular weight whereas for secondary relaxations they are almost the same. As expected the dielectric strength $\Delta\epsilon_\alpha$ increases on average with decreasing \bar{M}_W and according to **Eq.3.6** this value decreases with increasing temperature for each amorphous sample. Secondary relaxations of OLAs are completely different with PDLLA and are not the same in shape and also in temperature and frequency ranges. In amorphous OLAs one secondary relaxation appeared at the end side of α -relaxation (in higher frequencies) for OLA2700 and OLA1900 (in the same temperature range), whereas for amorphous PDLLA and OLA1400 it did not appear (maybe because of its small intensity and narrow temperature range). This relaxation process could be called Johary-Goldstein relaxation but compare to the literature^{62,67} its activation energy is relatively small (≈ 35 kJ/mol) so we called it slow β -relaxation (β_{slow}). Secondary relaxations of OLAs have almost the same activation energy ($E_{a,\beta_{\text{fast}}} \approx 28$ kJ/mol, $E_{a,\beta_{\text{slow}}} \approx 35$ kJ/mol) whereas for α -relaxation, activation energy increases with increasing molecular weight. For PDLLA there are two secondary relaxations which are very close together and their activation energies are different from OLAs ($E_{a,\beta_1} \approx 41$ kJ/mol, $E_{a,\beta_2} \approx 48$ kJ/mol). All relaxation process for all samples are summarized in **Figure3-22**.

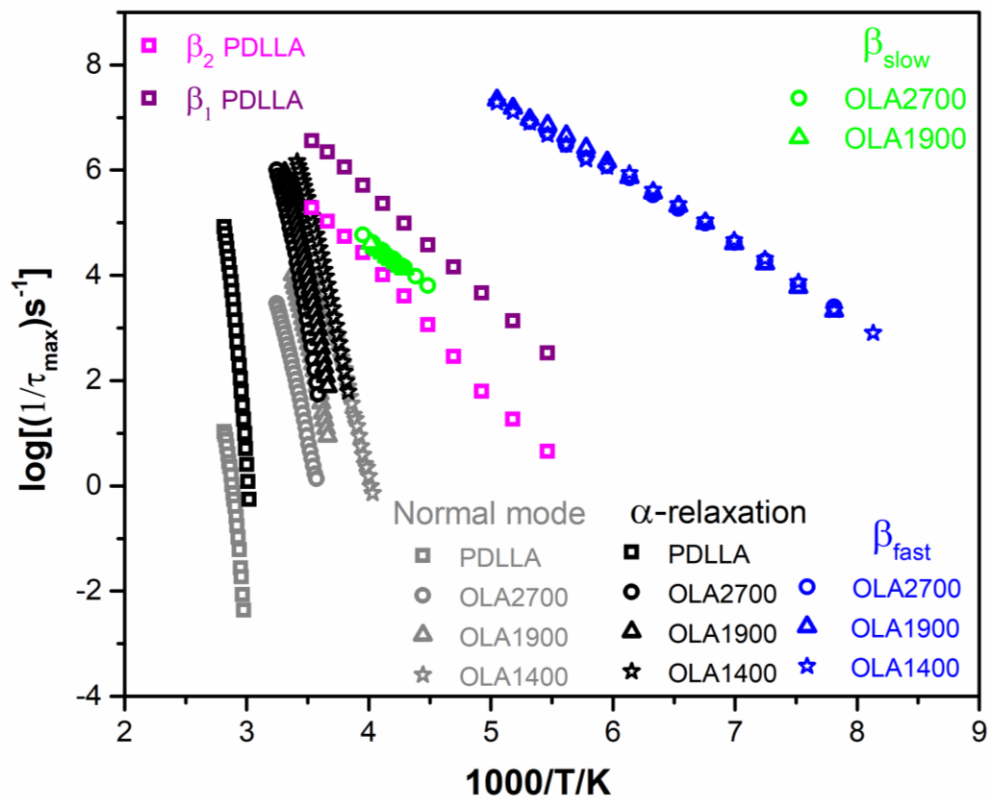


Figure3-22 Relaxation map of PDLLA and OLAs obtained by Dielectric Relaxation Spectroscopy (DRS).

Bibliography

- (1) Tool, A. Q.; Eicitlin, C. G. VARIATIONS CAUSED IN THE HEATING CURVES OF GLASS BY HEAT TREATMENT1. *J. Am. Ceram. Soc.* **1931**, *14* (4), 276–308. <https://doi.org/10.1111/j.1151-2916.1931.tb16602.x>.
- (2) Moynihan, C. T.; Macedo, P. B.; Montrose, C. J.; Montrose, C. J.; Gupta, P. K.; DeBolt, M. A.; Dill, J. F.; Dom, B. E.; Drake, P. W.; Easteal, A. J.; Elterman, P. B.; Moeller, R. P.; Sasabe, H.; Wilder, J. A. STRUCTURAL RELAXATION IN VITREOUS MATERIALS*. *Ann. N. Y. Acad. Sci.* **1976**, *279* (1), 15–35. <https://doi.org/10.1111/j.1749-6632.1976.tb39688.x>.
- (3) Cao, X.; Mohamed, A.; Gordon, S. H.; Willett, J. L.; Sessa, D. J. DSC Study of Biodegradable Poly(Lactic Acid) and Poly(Hydroxy Ester Ether) Blends. *Thermochim. Acta* **2003**, *406* (1–2), 115–127. [https://doi.org/10.1016/S0040-6031\(03\)00252-1](https://doi.org/10.1016/S0040-6031(03)00252-1).
- (4) Delpouve, N.; Saiter, A.; Dargent, E. Cooperativity Length Evolution during Crystallization of Poly(Lactic Acid). *Eur. Polym. J.* **2011**, *47* (12), 2414–2423. <https://doi.org/10.1016/j.eurpolymj.2011.09.027>.
- (5) Monnier, X. Molecular Dynamics in Complex Polymer Systems : From Anisotropy to Confinement Effects. phdthesis, Normandie Université, 2017.
- (6) Gao, S.; Simon, S. L. Measurement of the Limiting Fictive Temperature over Five Decades of Cooling and Heating Rates. *Thermochim. Acta* **2015**, *603*, 123–127. <https://doi.org/10.1016/j.tca.2014.08.019>.
- (7) Dhotel, A.; Rijal, B.; Delbreilh, L.; Dargent, E.; Saiter, A. Combining Flash DSC, DSC and Broadband Dielectric Spectroscopy to Determine Fragility. *J. Therm. Anal. Calorim.* **2015**, *121* (1), 453–461. <https://doi.org/10.1007/s10973-015-4650-9>.
- (8) *Fast Scanning Calorimetry*; Schick, C., Mathot, V., Eds.; Springer International Publishing: Cham, 2016. <https://doi.org/10.1007/978-3-319-31329-0>.
- (9) Poel, G. V.; Istrate, D.; Magon, A.; Mathot, V. Performance and Calibration of the Flash DSC 1, a New, MEMS-Based Fast Scanning Calorimeter. *J. Therm. Anal. Calorim.* **2012**, *110* (3), 1533–1546. <https://doi.org/10.1007/s10973-012-2722-7>.
- (10) Schawe, J. E. K. Measurement of the Thermal Glass Transition of Polystyrene in a Cooling Rate Range of More than Six Decades. *Thermochim. Acta* **2015**, *603*, 128–134. <https://doi.org/10.1016/j.tca.2014.05.025>.
- (11) Gao, S.; Koh, Y. P.; Simon, S. L. Calorimetric Glass Transition of Single Polystyrene Ultrathin Films. *Macromolecules* **2013**, *46* (2), 562–570. <https://doi.org/10.1021/ma3020036>.
- (12) Shamim, N.; Koh, Y. P.; Simon, S. L.; McKenna, G. B. Glass Transition Temperature of Thin Polycarbonate Films Measured by Flash Differential Scanning Calorimetry. *J. Polym. Sci. Part B Polym. Phys.* **2014**, *52* (22), 1462–1468. <https://doi.org/10.1002/polb.23583>.
- (13) Tammann, G.; Hesse, W. Die Abhängigkeit Der Viscosität von Der Temperatur Bie Unterkühlten Flüssigkeiten. *Z. Für Anorg. Allg. Chem.* **1926**, *156* (1), 245–257. <https://doi.org/10.1002/zaac.19261560121>.
- (14) Dhotel, A.; Rijal, B.; Delbreilh, L.; Dargent, E.; Saiter, A. Combining Flash DSC, DSC and Broadband Dielectric Spectroscopy to Determine Fragility. *J. Therm. Anal. Calorim.* **2015**, *121* (1), 453–461. <https://doi.org/10.1007/s10973-015-4650-9>.

- (15) Badrinarayanan, P.; Zheng, W.; Li, Q.; Simon, S. L. The Glass Transition Temperature versus the Fictive Temperature. *J. Non-Cryst. Solids* **2007**, *353* (26), 2603–2612. <https://doi.org/10.1016/j.jnoncrysol.2007.04.025>.
- (16) Forrest, J. A.; Dalnoki-Veress, K.; Dutcher, J. R. Interface and Chain Confinement Effects on the Glass Transition Temperature of Thin Polymer Films. *Phys. Rev. E* **1997**, *56* (5), 5705. <https://doi.org/10.1103/PhysRevE.56.5705>.
- (17) Sokolov, A. P.; Novikov, V. N.; Ding, Y. Why Many Polymers Are so Fragile. *J. Phys. Condens. Matter* **2007**, *19* (20), 205116. <https://doi.org/10.1088/0953-8984/19/20/205116>.
- (18) Rijal, B.; Delbreilh, L.; Saiter, A. Dynamic Heterogeneity and Cooperative Length Scale at Dynamic Glass Transition in Glass Forming Liquids. *Macromolecules* **2015**, *48* (22), 8219–8231. <https://doi.org/10.1021/acs.macromol.5b01152>.
- (19) Kremer, F. Dielectric Spectroscopy – Yesterday, Today and Tomorrow. *J. Non-Cryst. Solids* **2002**, *305* (1–3), 1–9. [https://doi.org/10.1016/S0022-3093\(02\)01083-9](https://doi.org/10.1016/S0022-3093(02)01083-9).
- (20) Schönhals, A. Dielectric Spectroscopy on the Dynamics of Amorphous Polymeric Systems. **1998**, *1*.
- (21) Analysis of Dielectric Spectra. In *Broadband Dielectric Spectroscopy*; Springer; Schönhals, A.; Kremer, F.: Berlin, 2003; pp 59–98.
- (22) Havriliak, S.; Negami, S. A Complex Plane Representation of Dielectric and Mechanical Relaxation Processes in Some Polymers. *Polymer* **1967**, *8*, 161–210. [https://doi.org/10.1016/0032-3861\(67\)90021-3](https://doi.org/10.1016/0032-3861(67)90021-3).
- (23) Stockmayer, W. H. Dielectric Dispersion in Solutions of Flexible Polymers. *Pure Appl. Chem.* **1967**, *15* (3–4), 539–554. <https://doi.org/10.1351/pac196715030539>.
- (24) Adachi, K.; Kotaka, T. Dielectric Normal Mode Relaxation. *Prog. Polym. Sci.* **1993**, *18* (3), 585–622. [https://doi.org/10.1016/0079-6700\(93\)90018-8](https://doi.org/10.1016/0079-6700(93)90018-8).
- (25) Boese, D.; Kremer, F. Molecular Dynamics in Bulk Cis-Polyisoprene as Studied by Dielectric Spectroscopy. *Macromolecules* **1990**, *23* (3), 829–835. <https://doi.org/10.1021/ma00205a023>.
- (26) Rijal, B. Study of Relaxation Phenomena at Dynamic Glass Transition and Cooperative Motion Length Scale in Glass-Forming Liquids. Thesis, Rouen, Normandy, France, 2015.
- (27) *Broadband Dielectric Spectroscopy*; Kremer, F., Schönhals, A., Eds.; Springer Berlin Heidelberg: Berlin, Heidelberg, 2003. <https://doi.org/10.1007/978-3-642-56120-7>.
- (28) Yin, H.; Napolitano, S.; Schönhals, A. Molecular Mobility and Glass Transition of Thin Films of Poly(Bisphenol A Carbonate). *Macromolecules* **2012**, *45* (3), 1652–1662. <https://doi.org/10.1021/ma202127p>.
- (29) Rotella, C.; Napolitano, S.; De Cremer, L.; Koeckelberghs, G.; Wübbenhorst, M. Distribution of Segmental Mobility in Ultrathin Polymer Films. *Macromolecules* **2010**, *43* (20), 8686–8691. <https://doi.org/10.1021/ma101695y>.
- (30) Pluta, M.; Jeszka, J. K.; Boiteux, G. Polylactide/Montmorillonite Nanocomposites: Structure, Dielectric, Viscoelastic and Thermal Properties. *Eur. Polym. J.* **2007**, *43* (7), 2819–2835. <https://doi.org/10.1016/j.eurpolymj.2007.04.009>.
- (31) Tyagi, M.; Alegría, A.; Colmenero, J. Broadband Dielectric Study of Oligomer of Poly(Vinyl Acetate): A Detailed Comparison of Dynamics with Its Polymer Analog. *Phys. Rev. E* **2007**, *75* (6). <https://doi.org/10.1103/PhysRevE.75.061805>.

- (32) Fulcher, G. S. ANALYSIS OF RECENT MEASUREMENTS OF THE VISCOSITY OF GLASSES. *J. Am. Ceram. Soc.* **1925**, *8* (6), 339–355. <https://doi.org/10.1111/j.1151-2916.1925.tb16731.x>.
- (33) A Possible Origin for the Vogel-Fulcher Law. *Phys. Lett. A* **1981**, *83* (6), 275–278. [https://doi.org/10.1016/0375-9601\(81\)90982-8](https://doi.org/10.1016/0375-9601(81)90982-8).
- (34) Hensel, A.; Schick, C. Relation between Freezing-in Due to Linear Cooling and the Dynamic Glass Transition Temperature by Temperature-Modulated DSC. *J. Non-Cryst. Solids* **1998**, *235–237*, 510–516. [https://doi.org/10.1016/S0022-3093\(98\)00607-3](https://doi.org/10.1016/S0022-3093(98)00607-3).
- (35) Morikawa, J.; Hashimoto, T. Estimation of Frequency from a Temperature Scanning Rate in Differential Scanning Calorimetry at the Glass Transition of Polystyrene. *Polymer* **2011**, *52* (18), 4129–4135. <https://doi.org/10.1016/j.polymer.2011.06.052>.
- (36) Adamovsky, S. A.; Minakov, A. A.; Schick, C. Scanning Microcalorimetry at High Cooling Rate. *Thermochim. Acta* **2003**, *403* (1), 55–63. [https://doi.org/10.1016/S0040-6031\(03\)00182-5](https://doi.org/10.1016/S0040-6031(03)00182-5).
- (37) Schawe, J. E. K. Vitrification in a Wide Cooling Rate Range: The Relations between Cooling Rate, Relaxation Time, Transition Width, and Fragility. *J. Chem. Phys.* **2014**, *141* (18), 184905. <https://doi.org/10.1063/1.4900961>.
- (38) Saiter, A.; Devallencourt, C.; Saiter, J. M.; Grenet, J. Thermodynamically “Strong” and Kinetically “Fragile” Polymeric Glass Exemplified by Melamine Formaldehyde Resins. *Eur. Polym. J.* **2001**, *37* (6), 1083–1090. [https://doi.org/10.1016/S0014-3057\(00\)00242-1](https://doi.org/10.1016/S0014-3057(00)00242-1).
- (39) Saiter, A.; Hess, M.; D’Souza, N. A.; Saiter, J. M. Entropy and Fragility in Vitreous Polymers. *Polymer* **2002**, *43* (26), 7497–7504. [https://doi.org/10.1016/S0032-3861\(02\)00631-6](https://doi.org/10.1016/S0032-3861(02)00631-6).
- (40) Delbreilh, L.; Negahban, M.; Benzohra, M.; Lacabanne, C.; Saiter, J. M. Glass Transition Investigated by a Combined Protocol Using Thermostimulated Depolarization Currents and Differential Scanning Calorimetry. *J. Therm. Anal. Calorim.* **2009**, *96* (3), 865–871. <https://doi.org/10.1007/s10973-009-0060-1>.
- (41) Arabeche, K.; Delbreilh, L.; Saiter, J.-M.; Michler, G. H.; Adhikari, R.; Baer, E. Fragility and Molecular Mobility in Micro- and Nano-Layered PC/PMMA Films. *Polymer* **2014**, *55* (6), 1546–1551. <https://doi.org/10.1016/j.polymer.2014.02.006>.
- (42) Fox, T. G.; Flory, P. J. Second-Order Transition Temperatures and Related Properties of Polystyrene. I. Influence of Molecular Weight. *J. Appl. Phys.* **1950**, *21* (6), 581–591. <https://doi.org/10.1063/1.1699711>.
- (43) Bershtein, V. A.; Egorov, V. M.; Podolsky, A. F.; Stepanov, V. A. Interrelationship and Common Nature of the β Relaxation and the Glass Transition in Polymers. *J. Polym. Sci. Polym. Lett. Ed.* **1985**, *23* (7), 371–377. <https://doi.org/10.1002/pol.1985.130230705>.
- (44) Beevers, R. B.; White, E. F. T. Physical Properties of Vinyl Polymers. Part 1.—Dependence of the Glass-Transition Temperature of Polymethylmethacrylate on Molecular Weight. *Trans Faraday Soc* **1960**, *56* (0), 744–752. <https://doi.org/10.1039/TF9605600744>.
- (45) Cown, J. M. G. Some General Features of Relations for Oligomers and Amorphous Polymers. *Eur. Polym. J.* **1975**, *11* (4), 297–300. [https://doi.org/10.1016/0014-3057\(75\)90037-3](https://doi.org/10.1016/0014-3057(75)90037-3).
- (46) Gibbs, J. H.; DiMarzio, E. A. Nature of the Glass Transition and the Glassy State. *J. Chem. Phys.* **1958**, *28* (3), 373–383. <https://doi.org/10.1063/1.1744141>.

- (47) Hintermeyer, J.; Herrmann, A.; Kahlau, R.; Goiceanu, C.; Rössler, E. A. Molecular Weight Dependence of Glassy Dynamics in Linear Polymers Revisited. *Macromolecules* **2008**, *41* (23), 9335–9344. <https://doi.org/10.1021/ma8016794>.
- (48) Baker, D. L.; Reynolds, M.; Masurel, R.; Olmsted, P. D.; Mattsson, J. Chain-Length, Flexibility and the Glass Transition of Polymers. *ArXiv191113278 Cond-Mat Physicsphysics* **2019**.
- (49) Huang, D.; McKenna, G. B. New Insights into the Fragility Dilemma in Liquids. *J. Chem. Phys.* **2001**, *114* (13), 5621–5630. <https://doi.org/10.1063/1.1348029>.
- (50) Böhmer, R.; Ngai, K. L.; Angell, C. A.; Plazek, D. J. Nonexponential Relaxations in Strong and Fragile Glass Formers. *J. Chem. Phys.* **1993**, *99* (5), 4201–4209. <https://doi.org/10.1063/1.466117>.
- (51) Ding, Y.; Novikov, V. N.; Sokolov, A. P.; Dalle-Ferrier, C.; Alba-Simionesco, C.; Frick, B. Influence of Molecular Weight on Fast Dynamics and Fragility of Polymers. *Macromolecules* **2004**, *37* (24), 9264–9272. <https://doi.org/10.1021/ma0492420>.
- (52) Dudowicz, J.; Freed, K. F.; Douglas, J. F. The Glass Transition Temperature of Polymer Melts [†]. *J. Phys. Chem. B* **2005**, *109* (45), 21285–21292. <https://doi.org/10.1021/jp0523266>.
- (53) Saltzman, E. J.; Schweizer, K. S. Universal Scaling, Dynamic Fragility, Segmental Relaxation, and Vitrification in Polymer Melts. *J. Chem. Phys.* **2004**, *121* (4), 2001–2009. <https://doi.org/10.1063/1.1756856>.
- (54) Andreatti, L.; Autiero, C.; Faetti, M.; Giordano, M.; Zulli, F. Dynamics, Fragility, and Glass Transition of Low-Molecular-Weight Linear Homopolymers. *Philos. Mag.* **2008**, *88* (33–35), 4151–4159. <https://doi.org/10.1080/14786430802468231>.
- (55) Araujo, S.; Delpouve, N.; Dhotel, A.; Domenek, S.; Guinault, A.; Delbreilh, L.; Dargent, E. Reducing the Gap between the Activation Energy Measured in the Liquid and the Glassy States by Adding a Plasticizer to Polylactide. *ACS Omega* **2018**, *3* (12), 17092–17099. <https://doi.org/10.1021/acsomega.8b02474>.
- (56) Hecksher, T.; Nielsen, A. I.; Olsen, N. B.; Dyre, J. C. Little Evidence for Dynamic Divergences in Ultraviscous Molecular Liquids. *Nat. Phys.* **2008**, *4* (9), 737–741. <https://doi.org/10.1038/nphys1033>.
- (57) Martinez-Garcia, J. C.; Rzoska, S. J.; Drozd-Rzoska, A.; Martinez-Garcia, J. A Universal Description of Ultraslow Glass Dynamics. *Nat. Commun.* **2013**, *4* (1), 1823. <https://doi.org/10.1038/ncomms2797>.
- (58) Murthy, S. S. N.; Sobhanadri, J.; Gangasharan; Sobhanadri, J. The Origin of β Relaxation in Organic Glasses. *J. Chem. Phys.* **1994**, *100* (6), 4601–4606. <https://doi.org/10.1063/1.466292>.
- (59) Buerger, D. E.; Boyd, R. H. Subglass Relaxation Processes: Dielectric Relaxation in Methyl Acrylate/Ethylene Copolymers. *Macromolecules* **1989**, *22* (6), 2694–2699. <https://doi.org/10.1021/ma00196a028>.
- (60) Katana, G.; Kremer, F.; Fischer, E. W.; Plaetschke, R. BROAD-BAND DIELECTRIC STUDY ON BINARY BLENDS OF BISPHENOL-A AND TETRAMETHYLBISPHENOL-A POLYCARBONATE. *Macromolecules* **1993**, *26* (12), 3075–3080. <https://doi.org/10.1021/ma00064a013>.
- (61) Ransom, T. C.; Fragiadakis, D.; Roland, C. M. The α and Johari–Goldstein Relaxations in 1,4-Polybutadiene: Breakdown of Isochronal Superpositioning. *Macromolecules* **2018**, *51* (12), 4694–4698. <https://doi.org/10.1021/acs.macromol.8b00664>.

- (62) Casalini, R.; Snow, A. W.; Roland, C. M. Temperature Dependence of the Johari–Goldstein Relaxation in Poly(Methyl Methacrylate) and Poly(Thiomethyl Methacrylate). *Macromolecules* **2013**, *46* (1), 330–334. <https://doi.org/10.1021/ma3021322>.
- (63) Ngai, K. L.; Paluch, M. Classification of Secondary Relaxation in Glass-Formers Based on Dynamic Properties. *J. Chem. Phys.* **2004**, *120* (2), 857–873. <https://doi.org/10.1063/1.1630295>.
- (64) Ngai, K. L. *Relaxation and Diffusion in Complex Systems; Partially Ordered Systems*; Springer New York: New York, NY, 2011. <https://doi.org/10.1007/978-1-4419-7649-9>.
- (65) Rodrigues, A. C.; Viciosa, M. T.; Danède, F.; Affouard, F.; Correia, N. T. Molecular Mobility of Amorphous S -Flurbiprofen: A Dielectric Relaxation Spectroscopy Approach. *Mol. Pharm.* **2014**, *11* (1), 112–130. <https://doi.org/10.1021/mp4002188>.
- (66) Starkweather, H. W.; Avakian, P.; Fontanella, J. J.; Wintersgill, M. C. Internal Motions in Polylactide and Related Polymers. *Macromolecules* **1993**, *26* (19), 5084–5087. <https://doi.org/10.1021/ma00071a016>.
- (67) Ngai, K.; Capaccioli, S. Relation between the Activation Energy of the Johari-Goldstein β Relaxation and $T_{\{g\}}$ of Glass Formers. *Phys. Rev. E* **2004**, *69* (3), 031501. <https://doi.org/10.1103/PhysRevE.69.031501>.

**Chapter4: Crystallization of OLA2700 investigated by
Flash DSC and Dielectric Relaxation Spectroscopy
(DRS)**

In this chapter, we study the molecular dynamics of crystallized oligomer of lactic acid with $\bar{M}_w = 2700 \text{ g.mol}^{-1}$ (OLA2700) by using Flash DSC and Dielectric Relaxation Spectroscopy (DRS) in order to compare with amorphous one. Properties of amorphous component in this oligomer, depends on its crystalline structure, it means, the presence of crystals have influence on the molecular dynamics of the mobile amorphous fraction (MAF). As it was explained in **Chapter1**, in semi-crystalline polymers, the amorphous phase appears to be constrained by the crystalline lamellae. This constraint is the effect of both a geometrical confinement and a covalent coupling between the lamellae and the non-crystalline regions through tie molecules. When this coupling is strong enough, a separate phase in nano-metric size can be created at the interface between the two phases^{1,2}. This low mobility non-crystalline interphase is called rigid amorphous fraction (RAF)³ which is a part of the amorphous phase that is not involved in glass transition, so it is necessary to describe most of semi-crystalline polymers with a three-phase model instead of two-phase model.

In this work, Flash DSC and DRS techniques were used to monitor isothermal crystallization of OLA2700. By Flash DSC the variation of glass transition temperature, melting temperature, melting enthalpy, heat capacity step and degree of crystallinity were studied for different crystallization temperatures. By using DRS, the constrained α -process present in crystallized material corresponding to the segmental motions of the amorphous phase were compared to the α -process of the amorphous material. Besides, the comparison of the features of β -relaxations in semi-crystalline and amorphous sample were done.

1-Flash DSC results

Flash DSC is used to attain unbiased information about the nature of crystalline phases generated before the measurement step, because any probable crystalline reorganization induced by the increasing temperature is strongly reduced⁴. Thus in this part, we study the crystallization of OLA2700 which is the oligomer of lactic acid by using Flash DSC at different crystallization temperatures (from 30°C to 80°C) and different crystallization times. This crystallization is called cold crystallization since the crystalline phase is generated during the heating from the glassy state.

1-1 Crystallization protocol

In order to study crystallization of OLA2700, we need to use appropriate protocol in Flash DSC. In first step we melt OLA2700 at 180°C with heating rate 1500K/s, then we cool it with same rate until -80°C to have the amorphous sample, after that we go to desired crystallization temperature and leave the sample at this temperature for various times, then in order to see the effect of crystallization process we heat the sample ($\beta_h=1500\text{K/s}$) up to 160°C (**Figure4-1**).

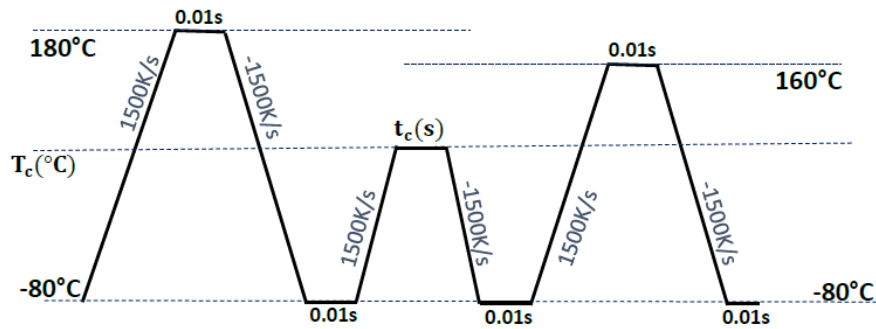
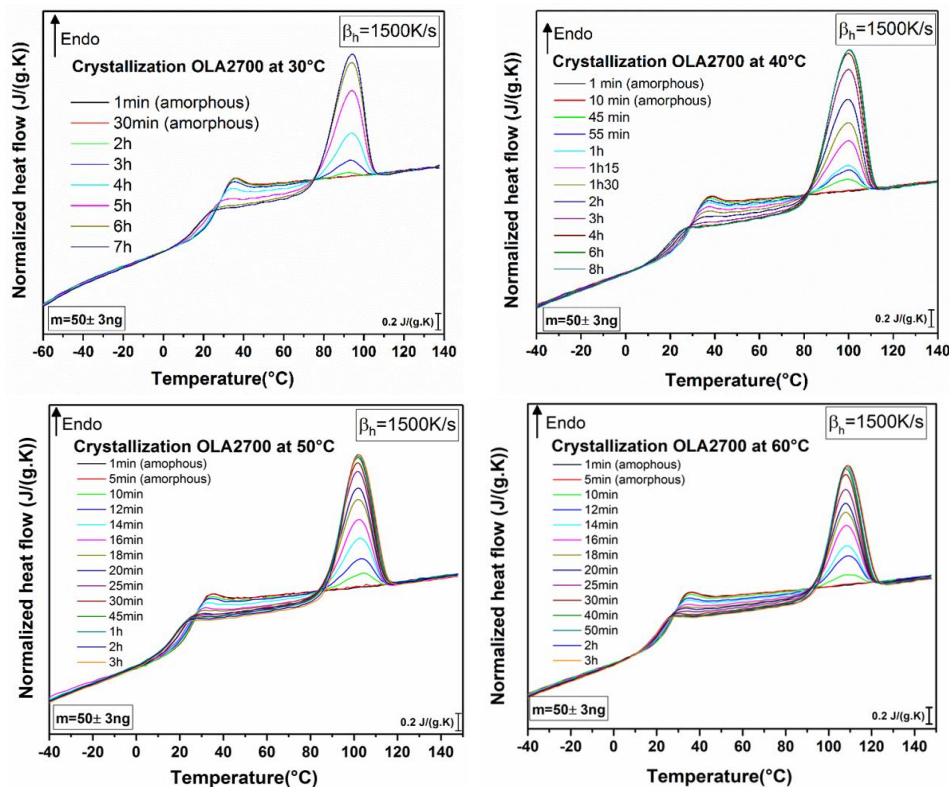


Figure4-1 schematic procedure illustrating how the heat flow curves related to crystallized sample are obtained in Flash DSC. T_c and t_c are crystallization temperature and time respectively.

1-2 Normalized heat flow of amorphous and semi-crystalline sample

In **Figure4-2** we observe the normalized heat flow obtained for different crystallization temperatures and times. On these curves we can see two thermal phenomena: **(i)** an endothermic heat flow step characteristic of glass transition, **(ii)** an endothermic peak due to the melting of the crystalline phase present in the sample. Focusing on **Figure4-2** shows clearly that for each crystallization temperature, the heat capacity step ΔC_p ($J \cdot g^{-1} \cdot K^{-1}$) decreases with increasing crystallization time. Besides the glass transition temperature (T_g) goes to lower values with increasing crystallization time with respect to amorphous sample (**Figure4-3**), which is in contrary with poly lactic acid (PLA) and some polymers since their glass transition temperature increases with increasing crystallization time⁵⁻⁸. According to the literature, these observations can be associated to confinement effect^{6,9}. The small overshoot at glass transition is related to fast relaxation processes inside the material⁶.



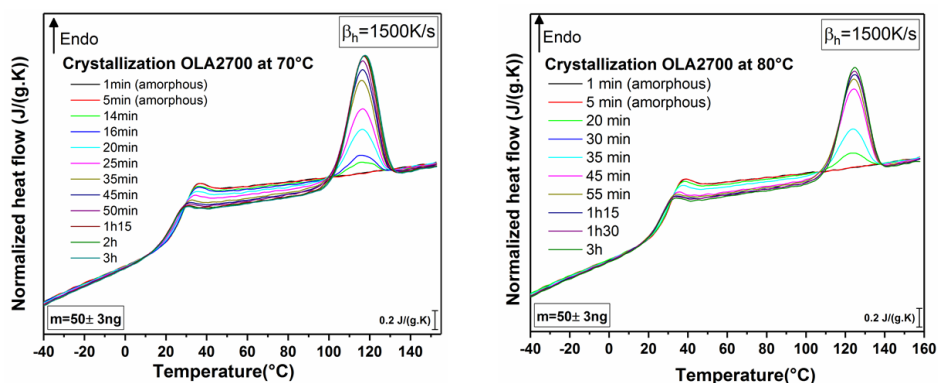


Figure4-2 Flash DSC Normalized heat flow of amorphous and crystallized OLA2700 (from $T_c = 30^\circ\text{C}$ to 80°C) as a function of temperature upon heating for scanning rate $\beta_h=1500\text{K/s}$.

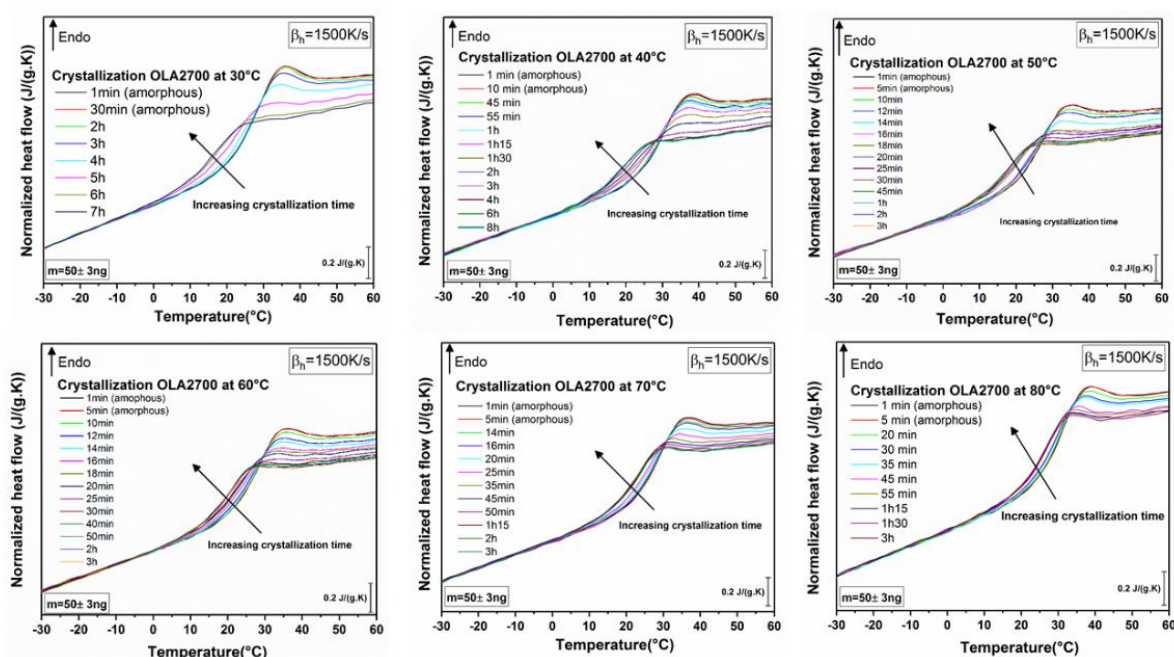


Figure4-3 Decreasing of glass transition temperature T_g and $\Delta C_p(T_g)$ with increasing crystallization time at different crystallization temperature for oligomer of lactic acid with $\bar{M}_W = 2700 \text{ g. mol}^{-1}$.

1-3 Variation of glass transition temperature T_g

Figure4-4 shows the variation of T_g with crystallization time (t_c) at different crystallization temperature (T_c) from 30°C to 80°C for OLA2700 with respect to T_g of amorphous OLA2700. We see, this variation $|\Delta T_g| = |T_g(t_c) - T_g(t_c = 0)|$ increases with increasing crystallization time at each crystallization temperature till reach a plateau where ΔT_g is constant and doesn't change with crystallization time. Reduction of T_g with crystallization time is a consequence of a change in the relaxation environment which can be related to confinement effect. According to statement of Schick C.¹⁰ in most cases, calorimetry shows only a weak dependence of the glass transition temperature on confinement as long as the confining dimensions are above 10nm. Here the maximum value

of $|\Delta T_g|$ which is related to maximum crystallized OLA2700 decreases with increasing crystallization temperature (**Table4-1**). We can say that, the influence of confinement at higher crystallization temperature is less (compared to crystallization at lower temperature). Different types of crystals were created in samples at different crystallization temperature and we observed the crystallization at 30°C is much slower than the crystallization at 80°C.

T_c	30°C	40°C	50°C	60°C	70°C	80°C
$ \Delta T_g $ (°C)	10	9.6	9.4	8.1	6.4	4.5

Table4-1 Maximum values of $|\Delta T_g|$ for different crystallization temperatures (T_c) for OLA2700.

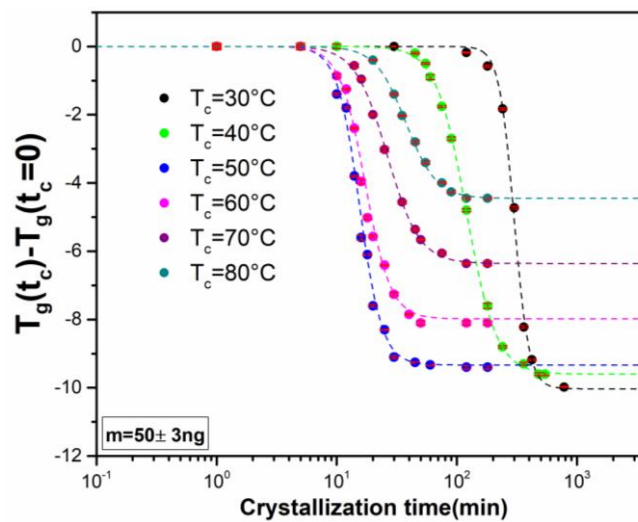


Figure4-4 Variation of glass transition temperature ΔT_g (respect to T_g of amorphous) with crystallization time (t_c) at different crystallization temperatures (T_c) for OLA2700. Dash lines are for following with eyes.

1-4 Variation of heat capacity step ΔC_p

Heat capacity in the glass transition temperature is linked to fluctuations¹¹, so in calorimetric curves only relaxation processes which are related to entropy fluctuations will be appeared. In general in calorimetric curves, the glass transition or the calorimetric α -relaxation is observed whereas the secondary relaxation processes are not visible, since the glass transition has a much larger calorimetric signature compared to secondary relaxation processes^{12,13}. In most studies on confinement effects on glass transition, they focus mostly on glass transition temperature, however calorimetry allows to determine other useful quantities such as the step height ΔC_p (relaxation strength)¹⁰. This quantity is important since it counts the degree of freedom going from a relaxed to a frozen state on cooling through the glass transition, besides it is also directly related to sample properties and linked to stability and order¹⁴⁻¹⁶.

As we see in **Figure4-3** the endothermic step at T_g , $\Delta C_p(T_g) = C_{p,liquid}(T_g) - C_{p,glass}(T_g)$ decreases with increasing crystallization time respect to amorphous sample until reaching a plateau for ΔC_p corresponding to the maximum of crystallinity. This reduction is attributed to a decrease of the quantity of amorphous phase in the material, that is to say a low content of amorphous phase constrained by a predominant crystallization phase^{5,6,17}. $\Delta C_p(T_g)$ characterizes the different degree of disorder available between the liquid-like state and the glassy state, so the lower $\Delta C_p(T_g)$ shows the lower level of disorder¹⁸.

Figure4-5 shows the variation of ΔC_p with crystallization time at different crystallization temperatures. Obviously, with increasing the crystallization temperature, the variation of $|\Delta C_p(t_c) - \Delta C_p(t_c = 0)|$ decreases so the value of ΔC_p for maximum crystallized sample increases due to the reduction of amount of crystals (or the crystallinity degree X_c) through the sample which is related to the formation of different crystals in shape and size at different crystallization temperatures. Values of ΔC_p for maximum crystallized sample and the variation of $|\Delta C_p(t_c) - \Delta C_p(t_c = 0)|$ were summarized in **Table4-2**.

T_c	30°C	40°C	50°C	60°C	70°C	80°C
$\Delta C_p(\text{J/g.K})[\text{at } X_c \text{ is maximum}]$	0.24	0.27	0.31	0.33	0.35	0.37
$ \Delta C_p(t_c) - \Delta C_p(t_c = 0) (\text{J/g.K})$	0.31	0.28	0.24	0.22	0.2	0.18

Table4-2 Values of ΔC_p when the sample is maximum crystallized and variation of $|\Delta C_p|$ (with respect to amorphous sample with $\Delta C_p(t_c = 0) \cong 0.55 \text{ J/g.K}$) for different crystallization temperature.

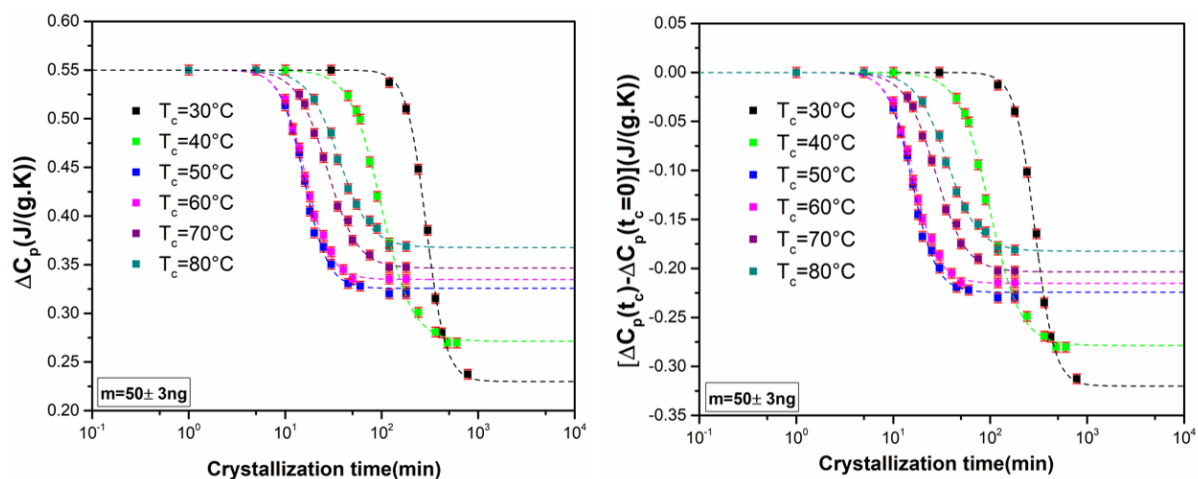


Figure4-5 Variation of (a) ΔC_p , (b) ΔC_p (respect to ΔC_p of amorphous) with crystallization time (t_c) at different crystallization temperatures (T_c) from 30°C to 80°C for oligomer of lactic acid with $\bar{M}_W = 2700 \text{ g.mol}^{-1}$. Dash lines are for following with eyes.

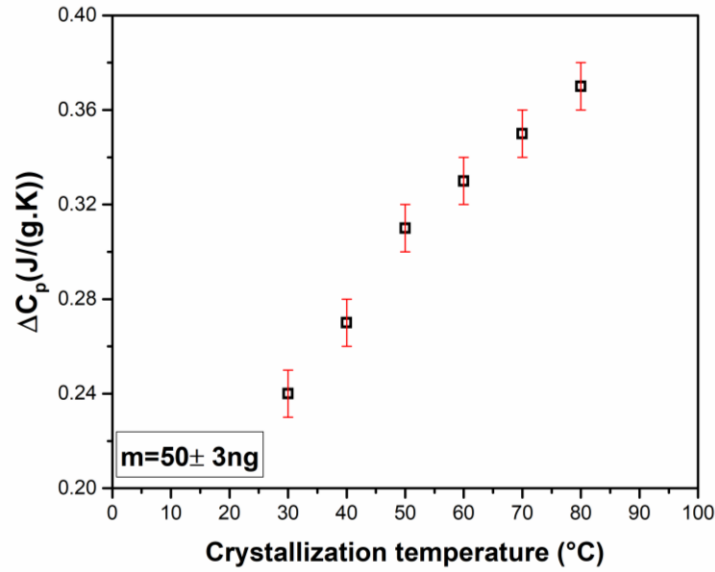


Figure4-6 Variation of ΔC_p of maximum crystallized OLA2700 as function of crystallization temperature. With increasing crystallization temperature (T_c) the ΔC_p of maximum crystallized sample increases in quasi linear behavior.

Now, in order to determine the quantity of material relaxing at the glass transition, the amorphous phase fraction X_{ma} (which is called also mobile amorphous fraction X_{MAF}) is calculated by following relation:

$$X_{ma} = \frac{\Delta C_p}{\Delta C_p^\circ} \quad (4.1)$$

Where, ΔC_p is the heat capacity step at T_g for crystallized sample and ΔC_p° for 100% amorphous one which was accurately measured by MT-DSC ($\Delta C_p^\circ = 0.55 \text{ J/(g.K)}$). The X_{ma} values for maximum crystallized sample at different crystallization temperatures from the glassy state are reported in **Table4-3**. As we see, since ΔC_p increases with increasing crystallization temperature the amorphous fraction also increases. The X_{ma} variation versus crystallization time is quasi sigmoidal for all crystallization temperatures (**Figure4-7**).

T_c	30°C	40°C	50°C	60°C	70°C	80°C
$X_{ma}(\%)$	44	49	56	60	64	67

Table4-3 Values of X_{ma} for maximum crystallized OLA2700 at different crystallization temperatures.

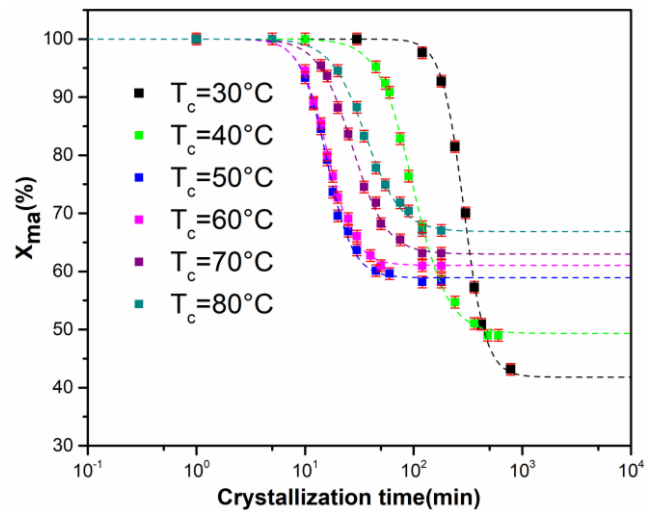


Figure4-7 Mobile amorphous phase degree evolution (X_{ma}) as a function of crystallization time (t_c) for OLA2700 at different crystallization temperatures.

1-5 Melting temperature T_m and melting enthalpy ΔH_m

According to **Figure4-2** when the crystallization temperature increases the endothermic peak related to the melting of the crystalline phase present in the sample shifts to higher temperature which can be related to the size and types of crystals with respect to the crystallization temperature by the Gibbs-Thomson law^{19,20}. **Figure4-8** shows that the melting temperature increases with increasing crystallization temperature (T_c) in linear behavior.

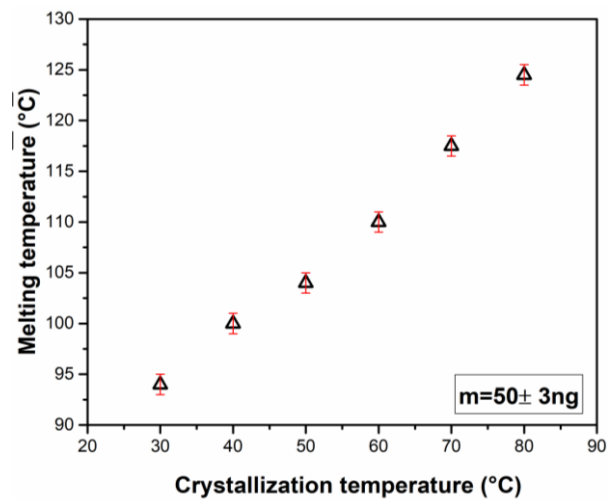


Figure4-8 Variation of melting temperature (related to the peak value) as a function of crystallization temperature.

The melting enthalpy ΔH_m can be calculated for different crystallization time at a specific crystallization temperature as shown in **Figure4-9**. The maximum value of ΔH_m (when the maximum crystallization is reached) is reduced with increasing crystallization temperature (**Figure4-10**).

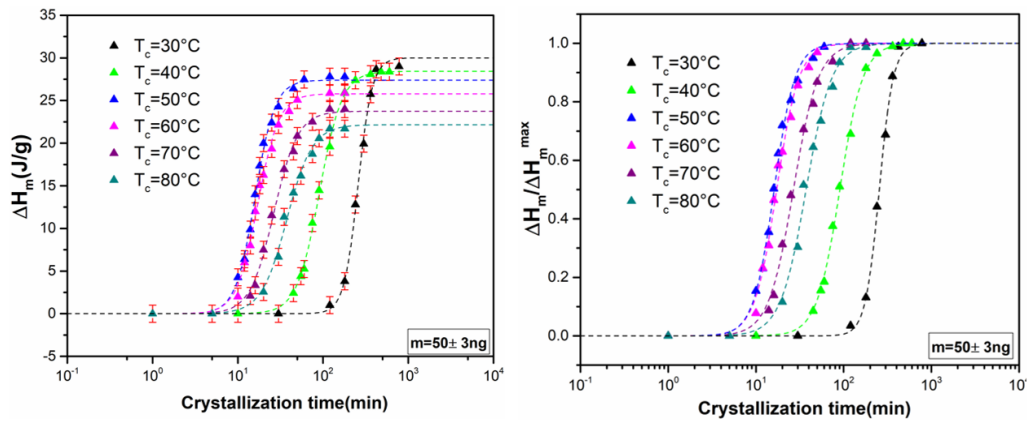


Figure4-9 (a) Variation of ΔH_m with crystallization time at different crystallization temperatures. There is a clear reduction of variation in ΔH_m with increasing crystallization temperature T_c . **(b)** Variation of ΔH_m respect to maximum value of melting enthalpy (when the maximum crystallization at different crystallization temperatures is reached). Dash lines are for following with eyes.

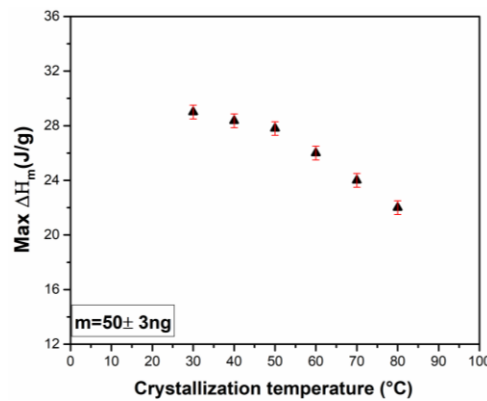


Figure4-10 The maximum value of ΔH_m for maximum crystallized sample as a function of crystallization temperature.

1-6 Two-phase and/or three-phase model

In order to calculate the crystallinity degree X_c we use the following equation:

$$X_c = \frac{\Delta H_m}{\Delta H_m^\circ} \quad (4.2)$$

Where, ΔH_m is the measured enthalpy of melting and ΔH_m° is the melting enthalpy of a wholly crystalline material obtained approximately with **Figure4-12** ($\Delta H_m^\circ \cong 70$ J/g). The X_c values for maximum crystallized sample at different crystallization temperatures from the glassy state are reported in **Table4-4**. As we see, with increasing crystallization temperature the crystallinity degree decreases. The X_c variation versus time is quasi sigmoidal for all the crystallization temperatures. After an induction time, X_c drastically increases to reach a maximum value (**Figure4-11**).

T_c	30°C	40°C	50°C	60°C	70°C	80°C
X_c (%)	41	40	39	37	34	31

Table4-4 Values of X_c for maximum crystallized OLA2700 at different crystallization temperatures.

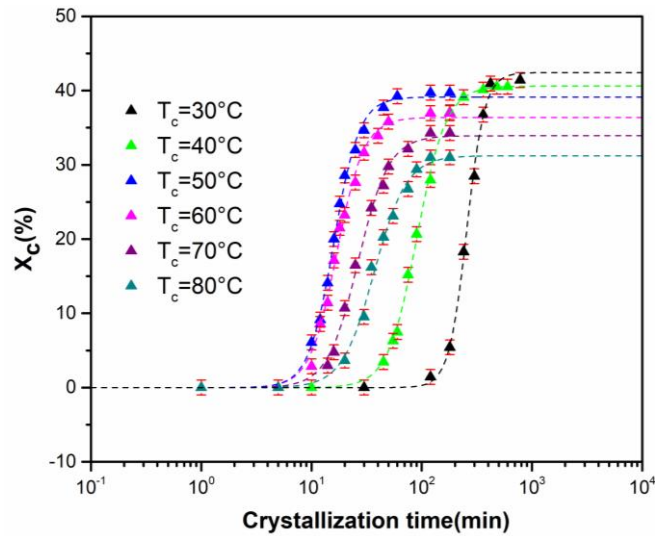


Figure4-11 Crystallinity degree evolution (X_c) as a function of crystallization time (t_c) for OLA2700 at different crystallization temperatures.

Evolution of ΔH_m as a function of ΔC_p for different crystallization temperatures from 30°C to 80°C for OLA2700 is shown in **Figure4-12**. We see approximately at $T_c = 30^\circ\text{C}$ and $T_c = 40^\circ\text{C}$ which are near glass transition's region the behavior is not linear after certain values of ΔC_p (**Figure4-12(a)**), it seems the value ΔH_m does not change drastically after certain values. It means that the reduction of ΔC_p (without changing ΔH_m) is related to increase of the Rigid Amorphous Fraction (RAF) which is not involved in melting enthalpy^{21,22}. According to **Figure4-12(a)** relaxation strength is smaller than expected from the fraction of the non-crystalline phase. Thus at these temperatures three-phase model can describe the crystallization phenomena. From $T_c = 50^\circ\text{C}$ to $T_c = 80^\circ\text{C}$ which are approaching to melting region the behavior is completely linear which can be described well by two-phase model (**Figure4-12(b)**). With linear fitting for $T_c = 50^\circ\text{C}$ to $T_c = 80^\circ\text{C}$, ΔH_m^0 can be estimated $70 \text{ J/g} \pm 1$.

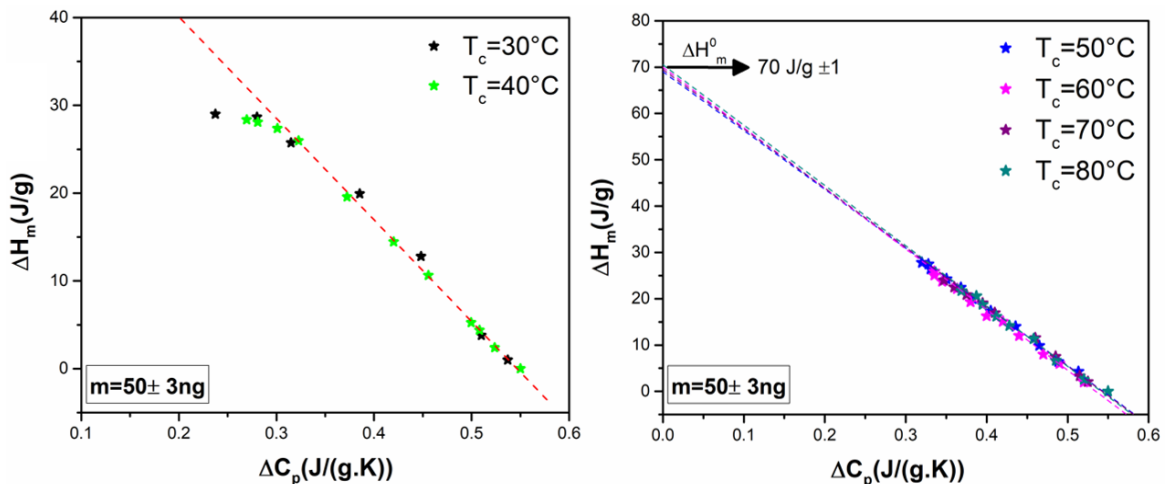


Figure4-12 Evolution of ΔH_m as a function of ΔC_p for OLA2700 **(a)** for $T_c = 30^\circ\text{C}$ and $T_c = 40^\circ\text{C}$ (There is a deviation from linear line) **(b)** from $T_c = 50^\circ\text{C}$ to $T_c = 80^\circ\text{C}$.

According to values of X_{ma} and X_c in **Table4-3** and **Table4-4**, we see that from $T_c = 50^\circ\text{C}$ to 80°C , $X_{ma} + X_c \cong 100\%$, whereas for $T_c = 30^\circ\text{C}$ and 40°C the $X_{ma} + X_c \neq 100\%$. Thus for crystallized sample at $T_c = 30^\circ\text{C}$ and 40°C , we observe a deviation from two-phase model which is caused by the incomplete decoupling between the crystalline and amorphous phases leading to create a non-crystalline interphase with low mobility called rigid amorphous fraction (RAF). In this three-phase model, a part of the amorphous phase does not participate to the glass transition. This part which describes the contribution of rigid amorphous fraction (RAF) must be taken into account as an additional element X_{ra} in following relation:

$$X_{ma} + X_c + X_{ra} = 100\% \quad (4.3)$$

For crystallized OLA2700 from $T_c = 50^\circ\text{C}$ up to 80°C , the two-phase model is appropriate to describe the material but at $T_c = 30^\circ\text{C}$ and 40°C , the crystallization procedure affects the amorphous phase by transforming a part of mobile amorphous phase into a rigid amorphous one^{6,23}. Values of rigid amorphous fraction were estimated by **Eq.4.3**, so for the maximum crystallized sample at 30°C and 40°C the RAF content is around 15% and 11% respectively. Several studies show the dependency of content of RAF on the chain mobility^{5,24-28}, it means that the probability that the RAF develops in parallel with the crystalline growth is higher when the mobility is lower, so the higher degree of RAF is observed when the OLA2700 is crystallizing at lower temperatures. **Figure4-13** shows the variation of mobile and rigid amorphous fraction with crystallinity degree for OLA2700 crystallized from 30°C up to 80°C . As we see in **Figure4-13(a)**, all data from $T_c = 50^\circ\text{C}$ up to 80°C are along the line $X_{ma} + X_c = 1$, whereas for $T_c = 30^\circ\text{C}$ and 40°C , data are really close to line up to $t_c \approx 300$ min but after that the mobile amorphous fraction decreases drastically. In **Figure4-13(b)**, the rigid amorphous fraction (X_{ra}) remains very weak (0-5%) up to $X_c \approx 40\%$, then increases strongly up to 15% of the material when the crystallization time increases.

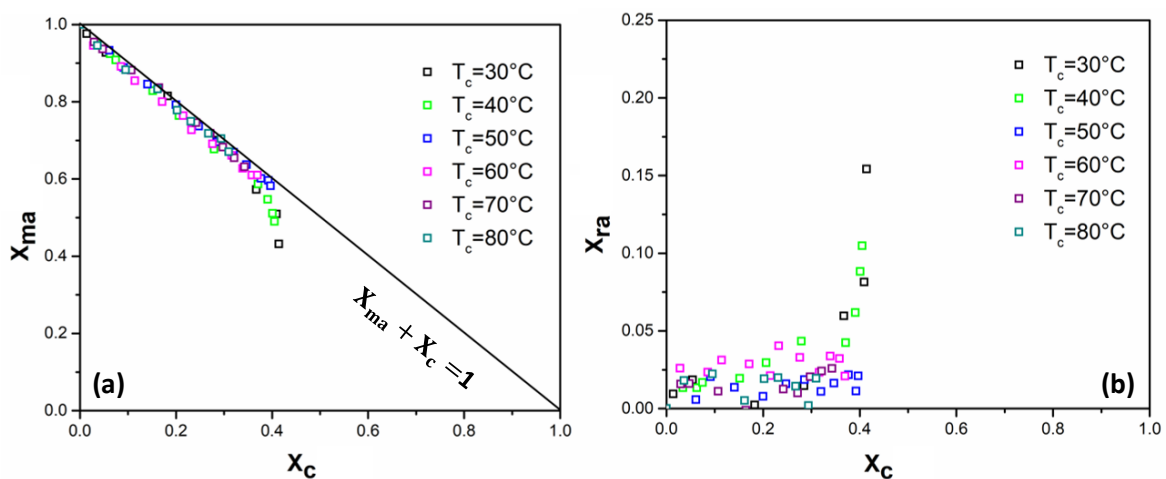


Figure4-13 (a) Variation of the mobile amorphous fraction as a function of crystallinity degree for OLA2700 crystallized at different temperatures and times. The line $X_{ma} + X_c = 1$ is theoretically related to two-phase model. **(b)** Variation of the rigid amorphous fraction as a function of crystallinity degree for OLA2700 crystallized at different temperatures and times.

Figure4-14 shows the pure confinement effect induced by crystals, since the value of T_g decreases with increasing crystallinity degree (or with decreasing mobile amorphous fraction). The reduction of T_g with confinement is extremely rare to observe after crystallization. Variation of T_g with respect to rigid amorphous fraction has been shown in **Figure4-15**. As we see the T_g decreases without changing rigid amorphous fraction ($\sim 0-5\%$) for T_c from 50°C to 80°C whereas for $T_c=30^\circ\text{C}, 40^\circ\text{C}$ this reduction will be of significantly weaker importance with increasing rigid amorphous fraction (up to 15%) after certain value of crystallization time.

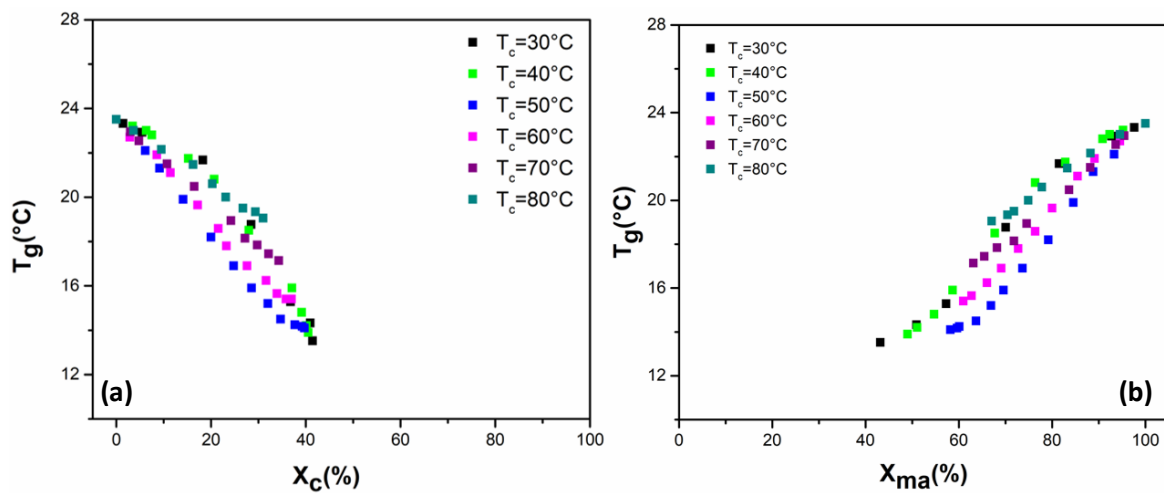


Figure4-14 Variation of the glass transition temperature as a function of (a) crystallinity degree and (b) mobile amorphous fraction for OLA2700 crystallized at different temperatures and times.

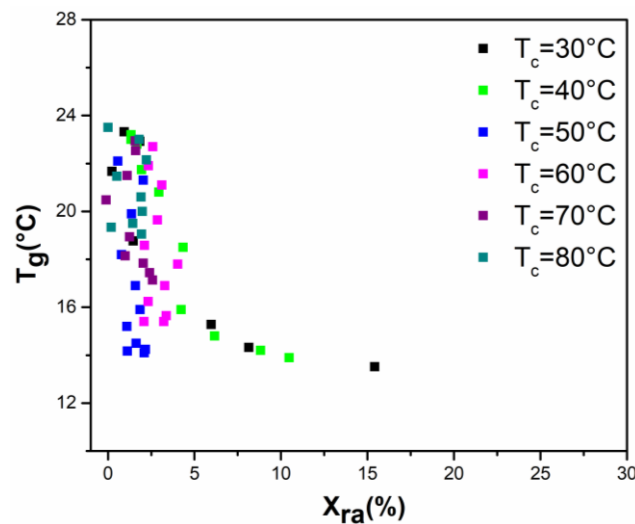


Figure4-15 Variation of the glass transition temperature as a function of rigid amorphous fraction for OLA2700 crystallized at different temperatures and times.

2-Dielectric Relaxation Spectroscopy (DRS) results

As was mentioned previously, Dielectric Relaxation Spectroscopy (DRS) is a suitable technique to study the molecular dynamics of polymers²⁹. The evolution of the dielectric α -relaxation, related to dipolar fluctuations from segmental motions along the chain backbone, has been used as a probe for the change in the glass transition dynamics upon crystallization^{30,31}. Depending on the type of polymer and crystallization conditions, loss peak position can be shifted to higher or lower frequencies during crystallization, however sometimes there is no change in the loss peak position³⁰⁻³². In most of polymeric systems, the features of the β -relaxation were found to be similar for amorphous and semicrystalline systems, indicating that it is not influenced by the crystallization. In this section we are interested in to investigate the effect of crystallization on α and β -relaxations in OLA2700.

2-1 Crystallization protocol

In this part, we will study the crystallization of an oligomer of lactic acid with $\bar{M}_w=2700$ g/mol by DRS at two different crystallization temperature (30°C and 80°C). For this purpose, first we put the sample in oven at 60°C in order to remove absorbed water for several hours. To crystallize at 30°C, we melt OLA2700 at 120°C in oven for several minutes on interdigitated electrodes (IE) of DRS, then we amorphize it by quenching with liquid nitrogen and put in oven at 30°C for several days to be sure it is fully crystallized. For crystallization at 80°C, after melting OLA2700 at 120°C on interdigitated electrodes (IE) of DRS, in order to avoid crystallization at room temperature, we put directly very fast in oven at 80°C for several days to have fully crystallized sample. Crystallization at 30°C is a cold crystallization and at 80°C is a melt crystallization (since the crystalline phase is generated from the melt). Finally the wholly crystallized sample was refrigerated to -145°C, and dielectric spectra were collected in increasing steps from -145°C to 60°C in the frequency range 0.1 to 2×10^6 Hz.

2-2 Dielectric relaxation in 3D curves

Figure4-16 shows dielectric relaxation maps of the imaginary part of permittivity (loss part) in 3D as a function of frequency and temperature for amorphous and crystallized OLA2700 at 30°C and 80°C. In lower temperature range (-145°C to 0°C) crystallized OLA2700 shows two secondary relaxations. In higher temperature range the α -relaxation takes place, associated to the segmental relaxation. The conductivity phenomenon at higher temperature than dynamic glass transition temperature (T_g) and lower frequency is also observed with large increment of ϵ'' for all samples. In **Figure4-16** some parts of conductivity region have been cut to see better the relaxation processes.

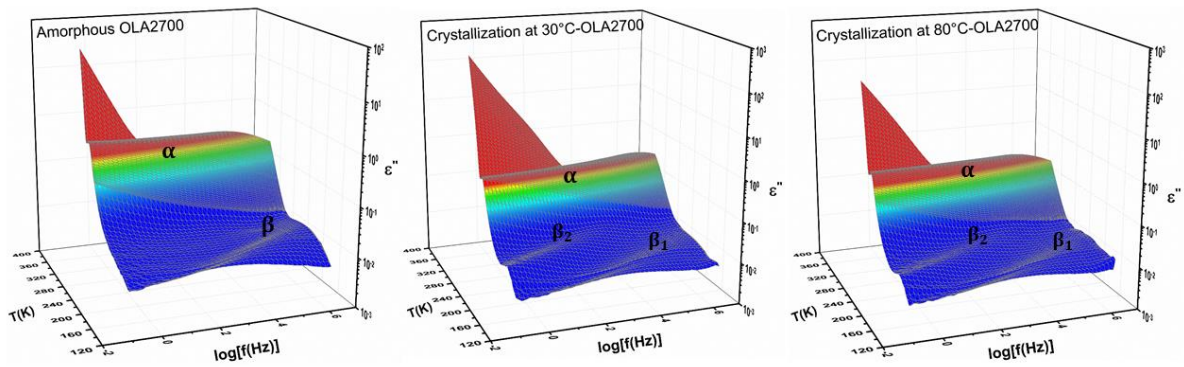


Figure4-16 Imaginary part of the complex dielectric permittivity ϵ'' vs frequency and temperature (in logarithm). The main relaxation process (segmental relaxation) was indicated by α . Secondary relaxations were indicated by β for amorphous OLA2700 and β_1 , β_2 for crystallized OLA2700 (β_1 is faster than β_2).

2-3 Segmental relaxation (α -relaxation)

Figure4-17 shows the frequency dependence of $\log(\epsilon'')$ for amorphous and crystallized OLA2700 at different temperatures in α -relaxation range. In order to investigate the segmental relaxation phenomenon the isothermal dielectric loss spectra were fitted with a conductivity contribution and two Havriliak- Negami (HN) complex functions in the range of α -process. One HN complex function for normal-mode at lower frequencies than α -relaxation (which was explained in more details in section4 of **Chapter3**) and another one for segmental relaxation.

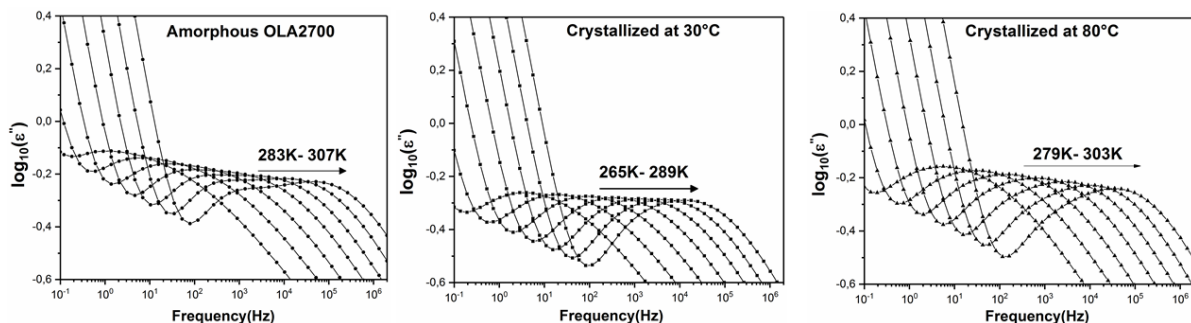


Figure4-17 Frequency dependence of dielectric loss factor ϵ'' (in logarithm) of normal mode and α -relaxation for amorphous and crystallized OLA2700 at different temperatures.

As we see in **Figure4-18** the position of the loss peak of crystallized sample shifts to higher frequencies compare to amorphous one, this is in contrary with amorphous and crystallized Poly (lactic acid) in the work of Brás A. et al³⁰, who observed the α -relaxation peak of crystallized PLLA at 80°C shifted to lower frequency for both melt and cold crystallization. The shifting for crystallized sample at 30°C is bigger than crystallized at 80°C. Thus, it is reasonable to assume that the relaxation kinetics of amorphous phase left after crystallization at 30°C is considerably faster than crystallization at 80°C due to the confinement effect induced by crystalline structure.

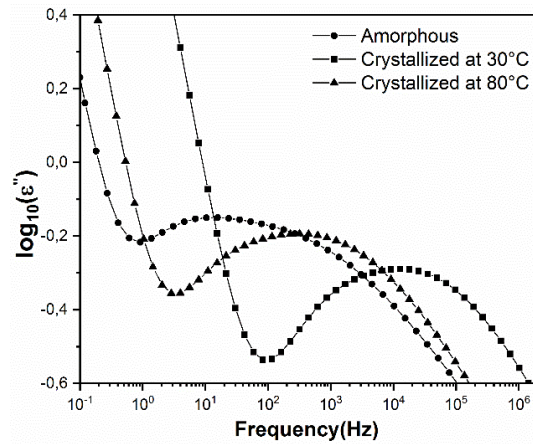


Figure4-18 Frequency dependence of dielectric loss factor ϵ'' (in logarithm) at 16°C (~289 K) of normal mode and α -relaxation for amorphous and crystallized OLA2700.

2-3-1 Fragility and glass transition

The fitting process of isothermal dielectric loss spectra by HN functions at each temperature in the range of segmental relaxation allows obtaining the relaxation map on this range. **Figure-4-19** shows the inverse of relaxation time as a function of the inverse temperature for amorphous and crystallized OLA2700 in the temperature range close to the glass transition. As we see, α -relaxation process of crystallized sample occurs at lower temperature range compare to amorphous OLA2700, it means the glass transition temperature is lower in crystalline sample than amorphous one. Moreover we see that the T_g for the sample crystallized at 30°C is lower than the sample crystallized at 80°C, which can be related to the influence of confinement on amorphous part which is less at higher crystallization temperature (compare to crystallization at lower temperature).

The variation of T_g with respect to amorphous OLA2700 $|\Delta T_g|$, obtained by DRS for crystallized sample at 30°C is much more than the $|\Delta T_g|$ obtained by Flash DSC, since the maximum degree of crystallinity is different depending on the crystallization conditions (for ex. in Flash DSC we used ~ 50 ng of sample, whereas in DRS the amount of sample was in grams). On the other hands, it seems the crystallization time applied in Flash DSC was not enough to maximum crystallize sample, or maximum crystallinity depends on sample shape, dimension and mass.

As was explained in section5 of **Chapter3**, The experimental data in the range of the α -relaxation can be fitted by a Vogel–Tamman–Fulcher (VFT) law. Usually the temperature dependence of the relaxation time for α -relaxation presents a non-Arrhenius behavior and is well described by VFT equation (**Eq.3.7**). The glass transition temperature (T_g) can be estimated by extrapolating VFT fit to the common convention, $\tau=100$ or $\log(1/\tau)=-2$. By putting VFT parameters in **Eq.3.8** and **Eq.3.9**, T_g and dynamic fragility index (m) can be obtained (All VFT parameters from fitting were reported in **Table4-5**). Similarly to the dynamic glass transition temperature, the dynamic fragility index is also sensitive to different microstructures. Fragility indexes for crystallized OLA2700 is smaller than amorphous one and, like T_g , for the sample crystallized at 30°C, m is lower than the sample crystallized at

80°C. The presence of crystals and subsequent organization of RAF, reduces the fragility index by approximately 44% for sample crystallized at 30°C. In semi-crystalline polymers, the discussion about the effect of the crystalline phase on the fragility index is still intense. Ngai et al.³³ showed that for various polymers the fragility index of the mobile amorphous fraction (MAF) is unchanged compare to complete amorphous state, however some studies show the variation of fragility in semi-crystalline polymers which establish the existence of rigid amorphous phase (RAF)²⁸. Napolitano and Wubbenhorst³⁴ assumed that the effect of the amorphous phase confinement on the fragility index depends on the chain flexibility. Generally, till now, there is no law for variation of fragility index with the crystallization, it means that the fragility index depends on crystallization condition and also on considered polymer³⁵⁻³⁷. However it has been evidenced that the relaxation dynamics can be severely affected by the crystallinity degree caused from the confinement effect induced by the crystalline phase directly on RAF and also the subsequent confinement effect of the latter on the MAF^{37,38}.

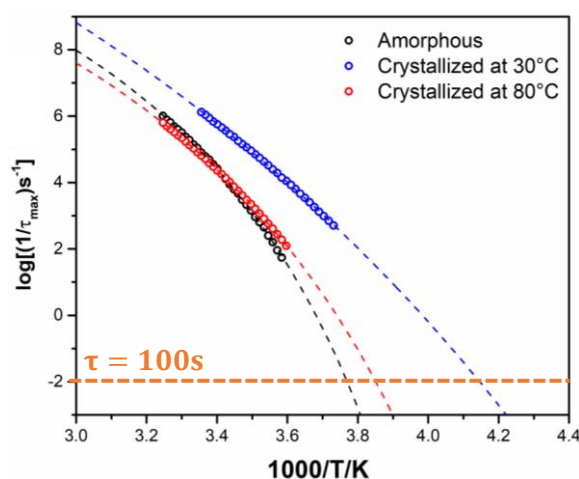


Figure4-19 Logarithmic plot of inverse relaxation time ($1/\tau_{\max}$) for α -relaxation as a function of the inverse temperature for amorphous and crystallized OLA2700. Dashed lines represent VFT fits.

OLA2700	$\log(\tau_0)$	D	$T_V(K)$	$T_g(K)$	m
Amorphous	-14.98	8.66	217.5	265	95
Crystallized at 30°C	-20.94	40	138	241.5	53
Crystallized at 80°C	-15.22	11.65	201	260	76

Table4-5 Fit parameters derived from VFT fits for amorphous and crystallized OLA2700. T_g ($\tau=100$) and fragility indexes from DRS were indicated.

2-3-2 Shape parameters α_{HN} , β_{HN}

In **Figure4-20** the shape parameters obtained from HN fits (**Eq.3.5**) for the constrained α -relaxation process versus temperature were plotted for fully amorphous and crystallized sample. What can be observed is that for both amorphous and crystallized OLA2700, $\beta_{HN} > \alpha_{HN}$. The shape parameters are approximately in the same range for amorphous and crystallized sample. In fact the crystallization didn't influence the shape of peak in α -relaxation.

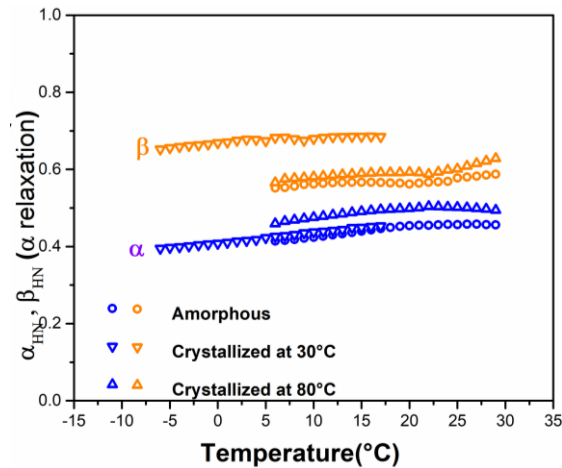


Figure4-20 Variation of shape parameters for α -relaxation as a function of temperature obtained by HN fitting procedure for amorphous and crystallized OLA2700.

2-3-3 Dielectric relaxation strength $\Delta\varepsilon_\alpha$

By fitting the experimental data with the HN function (Eq.3.5), the dielectric strength $\Delta\varepsilon_\alpha$ is also obtained. The temperature dependence of the dielectric strength for α -relaxation $\Delta\varepsilon_\alpha$ obtained from DRS experiment was demonstrated for amorphous and crystallized OLA2700 in **Figure4-21**. According to Eq.3.6, $\Delta\varepsilon_\alpha$ is directly proportional to the number of dipoles relaxing in the amorphous phase and since the volume density of dipoles (N/V) decreases with crystallization, for crystallized OLA2700, $\Delta\varepsilon_\alpha$ is much lower than amorphous one. $\Delta\varepsilon_\alpha$ decreases slightly for both amorphous and crystallized sample with increasing temperature (Eq.3.6). According to work of Esposito A. et al.¹, if we have RAF in crystallized sample, $\Delta\varepsilon_\alpha$ increases with temperature. Thus here it seems, the confinement effect comes more from crystalline part so it means there is no RAF or no strong coupling between crystalline and amorphous phase. Therefore, we may relate the change in fragility essentially to the confinement by crystals.

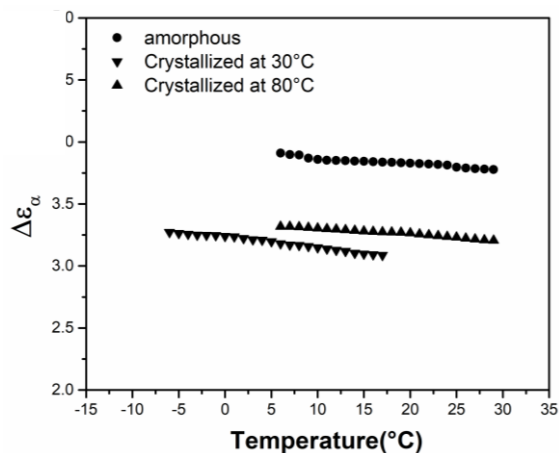


Figure4-21 Temperature dependence of the dielectric strength for α -relaxation $\Delta\varepsilon_\alpha$ for amorphous and crystallized OLA2700.

2-3-4 Activation energy of α -relaxation

As was explained in section 7 of **Chapter 3** the activation energy associated with the segmental relaxation can be calculated by **Eq. 3.13**. For crystallized sample, the evolution of activation energy associated with the segmental relaxation is different from amorphous one. **Figure 4-22** shows that the activation energy $E_{a,\alpha}$ for crystallized sample at glass transition temperature (T_g) is lower than amorphous one. Besides, the activation energy ($E_{a,\alpha}$) for the crystallized sample at lower crystallization temperature (30°C) is less than the activation energy ($E_{a,\alpha}$) for the sample crystallized at higher temperature (80°C) due to the confinement effect induced by crystals which is more dominant at lower crystallization temperature (30°C) and in consistence with the decrease of T_g . As discussed in previous section, there is a coupling between crystalline and amorphous phase in crystallized sample at 30°C which is low and leads to generate a separated phase called rigid amorphous fraction (RAF) but this RAF contain seems to have a negligible impact there.

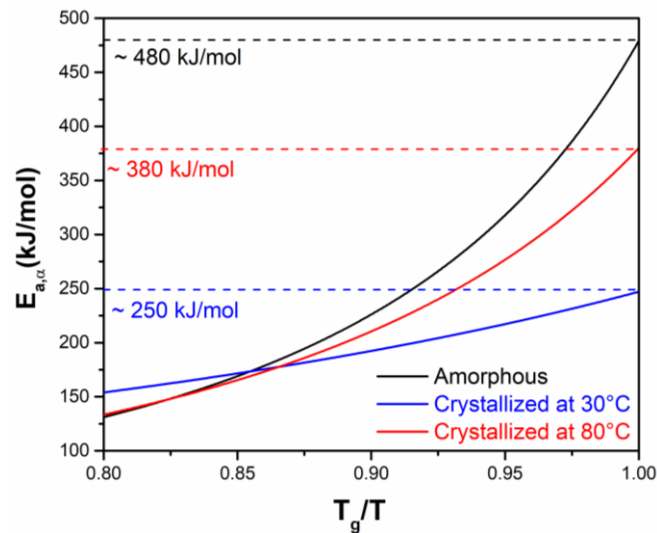


Figure 4-22 Activation energy as a function of $\frac{T_g}{T}$ calculated from DRS results for amorphous and crystallized OLA2700.

2-4 Secondary relaxations

As it is clear in 3D curves (**Figure 4-16**) there are two secondary relaxation when the sample is crystallized at 30°C and 80°C. According to results of **Chapter 3**, for amorphous OLA2700 there are two secondary relaxations, one at low temperatures and high frequencies which is called β_{fast} , another one which has low intensity, appears in small temperature range (223K to 248K), near α -relaxation which was considered as β_{slow} .

According to **Figure 4-23**, the secondary relaxations (β_1) for crystallized OLA2700 (crystallized at 30°C and 80°C) are approximately in same temperature and frequency range with same intensity and shape. Additionally, a superposition with the equivalent process detected in the amorphous sample which is β_{fast} is observed. β_2 relaxations for crystallized OLA2700 are also in same temperature and frequency range with almost the same shape and amplitude. These relaxations (β_2) appear in wider temperature range than β_{slow} of amorphous sample. The amplitude of β_2 for crystallized OLA2700 is higher than β_{slow} of

amorphous one. As was mentioned in **Chapter3** (section8-1), this relaxation might be considered as a Johary-Goldstein relaxation (β_{JG}) which is an intermolecular secondary relaxation.

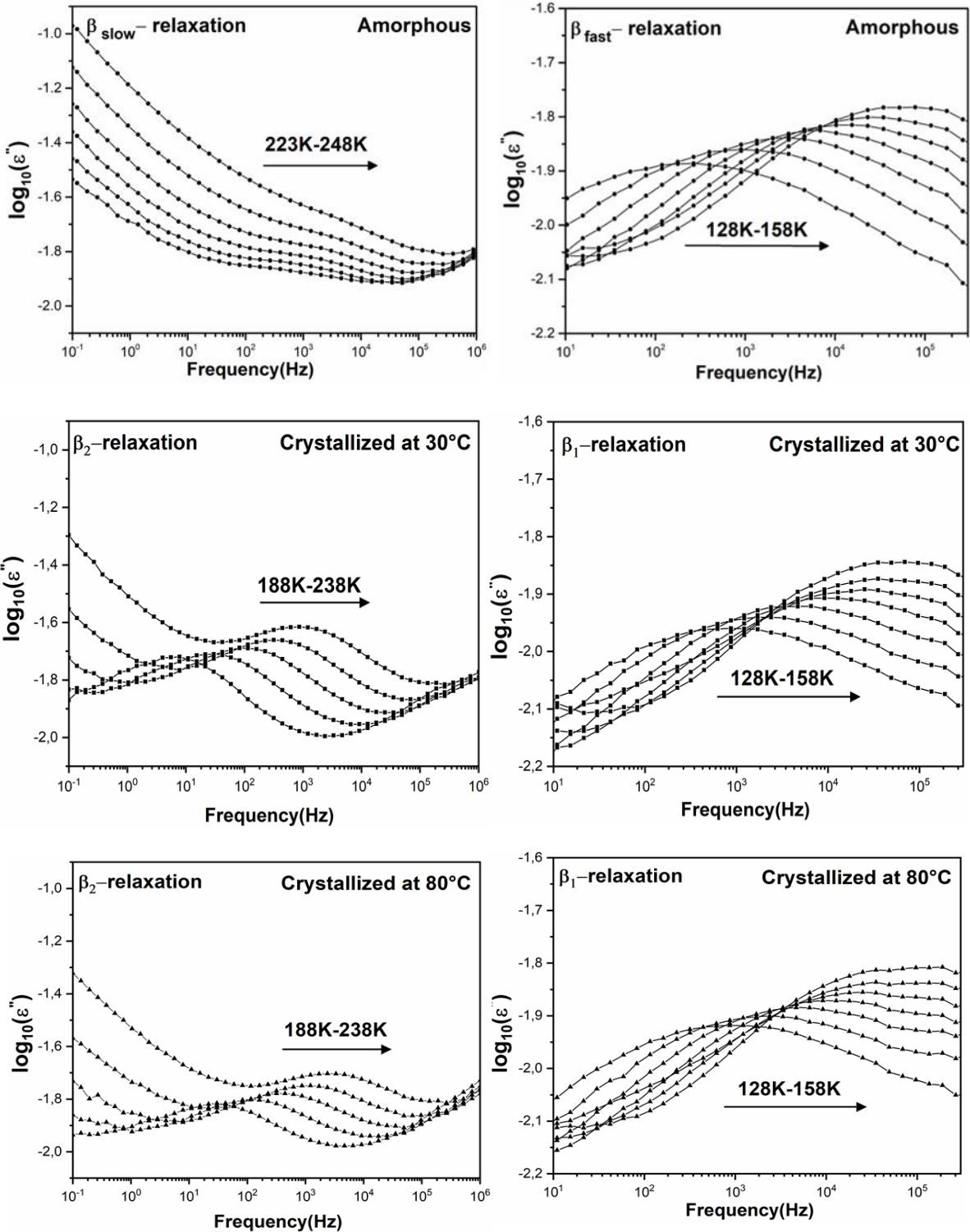


Figure4-23 Frequency dependence of dielectric loss factor (in logarithm) of secondary relaxations for amorphous and crystallized OLA2700 at different temperatures.

2-4-1 Activation energy of secondary relaxations

The temperature dependence of the relaxation time for secondary relaxations is shown in **Figure4-24** and relaxation time values were obtained from fitting procedure using HN equations. Values obtained from fitting can be well described by Arrhenius law with **Eq.3.14** in **Chapter3**. By using **Eq.3.14** we can obtain activation energy ($E_{a,\beta}$).

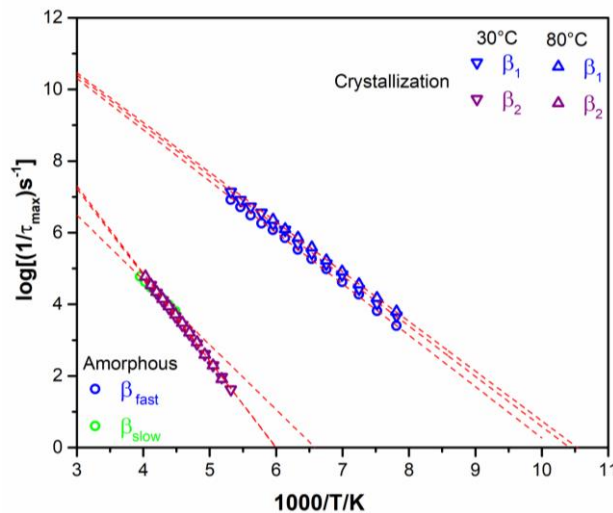


Figure4-24 Inverse of dielectric relaxation time ($1/\tau_{\max}$) for secondary relaxations as a function of the inverse temperature for amorphous and crystallized samples. Symbols were obtained from DRS experiments and red dashed lines represent fits by Arrhenius law.

As it is clear on **Figure4-24**, for OLA2700 crystallized at 30°C and 80°C, secondary processes superposed with amorphous one with almost the same activation energy, it means that the crystallization has no effect on secondary relaxations, which is in good agreement with literature³⁰. Values of activation energy for secondary relaxations were summarized in **Table4-6**.

OLA2700	Amorhous	Crystallized at 30°C	Crystallized at 80°C
E_a (kJ/mol)	$\beta_{\text{fast}}: 28 \pm 3$ $\beta_{\text{slow}}: 35 \pm 3$	$\beta_1: 27 \pm 3$ $\beta_2: 47 \pm 3$	$\beta_1: 27 \pm 3$ $\beta_2: 47 \pm 3$

Table4-6 Activation energy of secondary relaxations for amorphous and crystallized OLA2700.

2-4-2 Shape parameters α_{HN} , $\beta_{\text{HN}} = 1$

The shape parameter (α_{HN}) obtained from HN fits for secondary processes versus temperature were plotted in **Figure4-25** for amorphous and crystallized OLA2700. Since the secondary relaxations come from local motions and they are symmetric, so the shape parameter (β_{HN}) is equal 1²⁹. As is observed in **Figure4-25**, the variation of α_{HN} for β_1 -relaxations (for crystallized OLA2700) and β_{fast} -relaxation (for amorphous OLA2700) is almost the same. For β_2 -relaxations the variation of α_{HN} is the same for crystallized sample

at different temperatures but it is a little higher than the variation of α_{HN} for β_{slow} -relaxation in amorphous state.

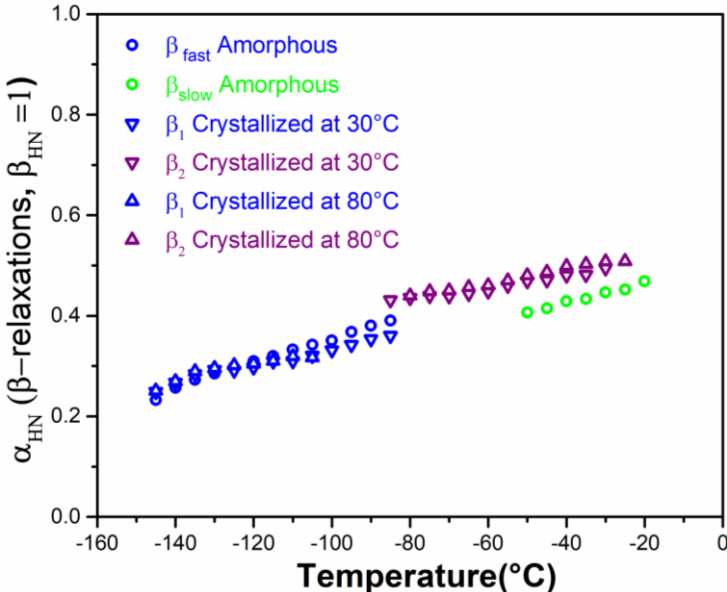


Figure4-25 Variation of shape parameter α_{HN} where $\beta_{HN} = 1$ for secondary relaxations as a function of temperature obtained by HN fitting procedure for amorphous and crystallized OLA2700.

Conclusion

In this work, the molecular dynamics of crystallized OLA2700 was investigated by using Flash DSC and DRS. We have evidenced that results obtained from both techniques almost match together. However the variation of T_g with respect to amorphous sample at $T_c = 30^\circ\text{C}$ obtained by DRS is much bigger than obtained by Flash DSC which can be related to the crystallization conditions.

According to results, we observed that the glass transition temperature (T_g), fragility index (m) and activation energy of segmental relaxation decreased with crystallization; this reduction is lower at higher crystallization temperature (T_c). We can attribute this phenomenon to the geometric confinement induced by crystals which reduces the chain mobility. This confinement effect is more dominant at lower crystallization temperature. Thus in oligomers, contrary to bulk PDLLA, it is possible to have semi-crystalline samples which do not have rigid amorphous fraction (RAF) from classical quiescent crystallization conditions.

Additionally, in what concerns in secondary relaxations, these processes were not affected by crystallization, since their relaxation time, the activation energy, the shape parameters and the intensity of dielectric loss spectra are almost the same, which means that the confinement induced by crystals has no effect on secondary processes.

Bibliography

- (1) Esposito, A.; Delpouve, N.; Causin, V.; Dhotel, A.; Delbreilh, L.; Dargent, E. From a Three-Phase Model to a Continuous Description of Molecular Mobility in Semicrystalline Poly(Hydroxybutyrate- Co -Hydroxyvalerate). *Macromolecules* **2016**, *49* (13), 4850–4861. <https://doi.org/10.1021/acs.macromol.6b00384>.
- (2) Androsch, R.; Wunderlich, B. The Link between Rigid Amorphous Fraction and Crystal Perfection in Cold-Crystallized Poly(Ethylene Terephthalate). *Polymer* **2005**, *46* (26), 12556–12566. <https://doi.org/10.1016/j.polymer.2005.10.099>.
- (3) Wunderlich, B. Reversible Crystallization and the Rigid–Amorphous Phase in Semicrystalline Macromolecules. *Progress in Polymer Science* **2003**, *28* (3), 383–450. [https://doi.org/10.1016/S0079-6700\(02\)00085-0](https://doi.org/10.1016/S0079-6700(02)00085-0).
- (4) *Fast Scanning Calorimetry*; Schick, C., Mathot, V., Eds.; Springer International Publishing: Cham, 2016. <https://doi.org/10.1007/978-3-319-31329-0>.
- (5) Saiter, A.; Delpouve, N.; Dargent, E.; Saiter, J. M. Cooperative Rearranging Region Size Determination by Temperature Modulated DSC in Semi-Crystalline Poly(l-Lactide Acid). *European Polymer Journal* **2007**, *43* (11), 4675–4682. <https://doi.org/10.1016/j.eurpolymj.2007.07.039>.
- (6) Delpouve, N.; Arnoult, M.; Saiter, A.; Dargent, E.; Saiter, J.-M. Evidence of Two Mobile Amorphous Phases in Semicrystalline Polylactide Observed from Calorimetric Investigations. *Polym Eng Sci* **2014**, *54* (5), 1144–1150. <https://doi.org/10.1002/pen.23657>.
- (7) Arnoult, M.; Dargent, E.; Mano, J. F. Mobile Amorphous Phase Fragility in Semi-Crystalline Polymers: Comparison of PET and PLLA. *Polymer* **2007**, *48* (4), 1012–1019. <https://doi.org/10.1016/j.polymer.2006.12.053>.
- (8) Saiter, A.; Delpouve, N.; Dargent, E.; Oberhauser, W.; Conzatti, L.; Cicogna, F.; Passaglia, E. Probing the Chain Segment Mobility at the Interface of Semi-Crystalline Polylactide/Clay Nanocomposites. *European Polymer Journal* **2016**, *78*, 274–289. <https://doi.org/10.1016/j.eurpolymj.2016.03.040>.
- (9) Schick, C.; Wurm, A.; Mohamed, A. Vitrification and Devitrification of the Rigid Amorphous Fraction of Semicrystalline Polymers Revealed from Frequency-Dependent Heat Capacity. *Colloid & Polymer Science* **2001**, *279* (8), 800–806. <https://doi.org/10.1007/s003960100507>.
- (10) Schick, C. Glass Transition under Confinement-What Can Be Learned from Calorimetry. *Eur. Phys. J. Spec. Top.* **2010**, *189* (1), 3–36. <https://doi.org/10.1140/epjst/e2010-01307-y>.
- (11) Donth, E.-J. *The Glass Transition: Relaxation Dynamics in Liquids and Disordered Materials*; Zunger, A., Osgood, R. M., Hull, R., Sakaki, H., Series Eds.; Springer Series in MATERIALS SCIENCE; Springer Berlin Heidelberg: Berlin, Heidelberg, 2001; Vol. 48. <https://doi.org/10.1007/978-3-662-04365-3>.
- (12) Suga, H. Adiabatic Calorimeter as an Ultra-Low Frequency Spectrometer: Interplay between Phase and Glass Transitions in Solids. *Thermochimica Acta* **2001**, *377* (1–2), 35–49. [https://doi.org/10.1016/S0040-6031\(01\)00540-8](https://doi.org/10.1016/S0040-6031(01)00540-8).
- (13) Kishimoto, K.; Suga, H.; Seki, S. Calorimetric Study of the Glassy State. VIII. Heat Capacity and Relaxational Phenomena of Isopropylbenzene. *BCSJ* **1973**, *46* (10), 3020–3031. <https://doi.org/10.1246/bcsj.46.3020>.

- (14) Hodge, I. M. Enthalpy Relaxation and Recovery in Amorphous Materials. *Journal of Non-Crystalline Solids* **1994**, *169* (3), 211–266. [https://doi.org/10.1016/0022-3093\(94\)90321-2](https://doi.org/10.1016/0022-3093(94)90321-2).
- (15) Hensel, A.; Schick, C. Relation between Freezing-in Due to Linear Cooling and the Dynamic Glass Transition Temperature by Temperature-Modulated DSC. *Journal of Non-Crystalline Solids* **1998**, *235–237*, 510–516. [https://doi.org/10.1016/S0022-3093\(98\)00607-3](https://doi.org/10.1016/S0022-3093(98)00607-3).
- (16) Schick, C. Differential Scanning Calorimetry (DSC) of Semicrystalline Polymers. *Anal Bioanal Chem* **2009**, *395* (6), 1589–1611. <https://doi.org/10.1007/s00216-009-3169-y>.
- (17) Delpouve, N.; Saiter, A.; Mano, J. F.; Dargent, E. Cooperative Rearranging Region Size in Semi-Crystalline Poly(L-Lactic Acid). *Polymer* **2008**, *49* (13–14), 3130–3135. <https://doi.org/10.1016/j.polymer.2008.04.045>.
- (18) Arabeche, K.; Delbreilh, L.; Saiter, J.-M.; Michler, G. H.; Adhikari, R.; Baer, E. Fragility and Molecular Mobility in Micro- and Nano-Layered PC/PMMA Films. *Polymer* **2014**, *55* (6), 1546–1551. <https://doi.org/10.1016/j.polymer.2014.02.006>.
- (19) Höhne, G. W. H. Another Approach to the Gibbs–Thomson Equation and the Melting Point of Polymers and Oligomers. *Polymer* **2002**, *43* (17), 4689–4698. [https://doi.org/10.1016/S0032-3861\(02\)00305-1](https://doi.org/10.1016/S0032-3861(02)00305-1).
- (20) Toda, A.; Taguchi, K.; Nozaki, K.; Konishi, M. Melting Behaviors of Polyethylene Crystals: An Application of Fast-Scan DSC. *Polymer* **2014**, *55* (14), 3186–3194. <https://doi.org/10.1016/j.polymer.2014.05.009>.
- (21) Gupta, V. B. Heat Setting. *J. Appl. Polym. Sci.* **2002**, *83* (3), 586–609. <https://doi.org/10.1002/app.2260>.
- (22) Suzuki, H.; Grebowicz, J.; Wunderlich, B. Heat Capacity of Semicrystalline: Linear Poly(Oxymethylene) and Poly(Oxyethylene). *Makromol. Chem.* **1985**, *186* (5), 1109–1119. <https://doi.org/10.1002/macp.1985.021860521>.
- (23) Delpouve, N.; Saiter, A.; Dargent, E. Cooperativity Length Evolution during Crystallization of Poly(Lactic Acid). *European Polymer Journal* **2011**, *47* (12), 2414–2423. <https://doi.org/10.1016/j.eurpolymj.2011.09.027>.
- (24) Righetti, M. C.; Tombari, E. Crystalline, Mobile Amorphous and Rigid Amorphous Fractions in Poly(L-Lactic Acid) by TMDSC. *Thermochimica Acta* **2011**, *522* (1–2), 118–127. <https://doi.org/10.1016/j.tca.2010.12.024>.
- (25) Kattan, M.; Dargent, E.; Grenet, J. Three Phase Model in Drawn Thermoplastic Polyesters: Comparison of Differential Scanning Calorimetry and Thermally Stimulated Depolarisation Current Experiments. *Polymer* **2002**, *43* (4), 1399–1405. [https://doi.org/10.1016/S0032-3861\(01\)00719-4](https://doi.org/10.1016/S0032-3861(01)00719-4).
- (26) Kattan, M.; Dargent, E.; Grenet, J. Microstructural Modifications in Uniaxially Hot-Drawn Polycyclohexylene Terephthalate Films. *Polym Eng Sci* **2004**, *44* (3), 509–517. <https://doi.org/10.1002/pen.20045>.
- (27) del Río, J.; Etxeberria, A.; López-Rodríguez, N.; Lizundia, E.; Sarasua, J. R. A PALS Contribution to the Supramolecular Structure of Poly(L-Lactide). *Macromolecules* **2010**, *43* (10), 4698–4707. <https://doi.org/10.1021/ma902247y>.
- (28) Brás, A. R.; Malik, P.; Dionísio, M.; Mano, J. F. Influence of Crystallinity in Molecular Motions of Poly(L-Lactic Acid) Investigated by Dielectric Relaxation Spectroscopy. *Macromolecules* **2008**, *41* (17), 6419–6430. <https://doi.org/10.1021/ma800842a>.

- (29) *Broadband Dielectric Spectroscopy*; Kremer, F., Schönhals, A., Eds.; Springer Berlin Heidelberg: Berlin, Heidelberg, 2003. <https://doi.org/10.1007/978-3-642-56120-7>.
- (30) Brás, A. R.; Viciosa, M. T.; Wang, Y.; Dionísio, M.; Mano, J. F. Crystallization of Poly(L-Lactic Acid) Probed with Dielectric Relaxation Spectroscopy. *Macromolecules* **2006**, *39* (19), 6513–6520. <https://doi.org/10.1021/ma061148r>.
- (31) Dionísio, M.; Viciosa, M. T.; Wang, Y.; Mano, J. F. Glass Transition Dynamics of Poly(L-Lactic Acid) during Isothermal Crystallisation Monitored by Real-Time Dielectric Relaxation Spectroscopy Measurements. *Macromol. Rapid Commun.* **2005**, *26* (17), 1423–1427. <https://doi.org/10.1002/marc.200500319>.
- (32) Mijović, J.; Sy, J.-W. Molecular Dynamics during Crystallization of Poly(L-Lactic Acid) As Studied by Broad-Band Dielectric Relaxation Spectroscopy. *Macromolecules* **2002**, *35* (16), 6370–6376. <https://doi.org/10.1021/ma0203647>.
- (33) Ngai, K. L.; Roland, C. M. Intermolecular Cooperativity and the Temperature Dependence of Segmental Relaxation in Semicrystalline Polymers. *Macromolecules* **1993**, *26* (11), 2688–2690. <https://doi.org/10.1021/ma00063a008>.
- (34) Napolitano, S.; Wübbenhorst, M. Slowing Down of the Crystallization Kinetics in Ultrathin Polymer Films: A Size or an Interface Effect? *Macromolecules* **2006**, *39* (18), 5967–5970. <https://doi.org/10.1021/ma061304u>.
- (35) Hamonic, F.; Miri, V.; Saiter, A.; Dargent, E. Rigid Amorphous Fraction versus Oriented Amorphous Fraction in Uniaxially Drawn Polyesters. *European Polymer Journal* **2014**, *58*, 233–244. <https://doi.org/10.1016/j.eurpolymj.2014.06.014>.
- (36) Hamonic, F.; Prevosto, D.; Dargent, E.; Saiter, A. Contribution of Chain Alignment and Crystallization in the Evolution of Cooperativity in Drawn Polymers. *Polymer* **2014**, *55* (12), 2882–2889. <https://doi.org/10.1016/j.polymer.2014.04.030>.
- (37) Delpouve, N.; Delbreilh, L.; Stoclet, G.; Saiter, A.; Dargent, E. Structural Dependence of the Molecular Mobility in the Amorphous Fractions of Polylactide. *Macromolecules* **2014**, *47* (15), 5186–5197. <https://doi.org/10.1021/ma500839p>.
- (38) Dobbertin, J.; Hensel, A.; Schick, C. Dielectric Spectroscopy and Calorimetry in the Glass Transition Region of Semi-Crystalline Poly(Ethylene Terephthalate). *Journal of Thermal Analysis* **1996**, *47* (4), 1027–1040. <https://doi.org/10.1007/BF01979446>.
- (39) Ngai, K. L. *Relaxation and Diffusion in Complex Systems; Partially Ordered Systems*; Springer New York: New York, NY, 2011. <https://doi.org/10.1007/978-1-4419-7649-9>.

Conclusion and perspectives

This research work was conducted to investigate the effect of molecular weight in amorphous samples and also the effect of different crystallization conditions on the dynamics of an oligomer of lactic acid, that has been compared with the dynamics of PLA, especially on glass transition temperature and fragility index.

According to results of **Chapter3**, the fictive temperature (associated to glass transition temperature) and fragility index decreased with the reduction of molecular weight and match well with Fox-Flory law. However, it seems that considering more samples with higher molecular weight than these OLAs, it is more probable to have three regimes for variation of glass transition with molecular weight $T_g(M)$ behavior instead of two regimes. We should also determine, whether these three regimes are also apparent when investigating other parameters such as fragility. Besides, in following work, we could carry DRS measurements under pressure to see whether the reducing the chain length reduces the volume engaged in the α -relaxation. Doing DRS measurements under pressure give access to an isochoric fragility which differs from the fragility calculated under isobaric conditions. Some authors have proposed that there are two components of fragility: thermal and volumic. The thermal one being the isochoric fragility, and the volumic one giving access to the volume engaged in the relaxation process, being proportional to the Cooperative rearranging Region (CRR) size.

Besides, we deduced that the results estimated from Flash DSC, MT-DSC and DRS experiments matched well together. The comparison between the temperature dependence of the cooling rate obtained by calorimetric data and the temperature dependence of the relaxation times obtained from DRS shows that the calculation of calorimetric fragility in order to be compared with dynamic fragility ($\tau = 100s$) has to be done using a logarithmic shift on the cooling rate dependence of T_g . According to our results the T_g and the fragility index reduced with decreasing molecular weight. We can observe that there is some similarities with free surface effect which is often described as the free confinement.

In the following, we evidenced secondary relaxations of OLAs (observed from DRS) are completely different with PDLLA in shape, temperature and frequency ranges, whereas in amorphous OLAs the reduction of molecular weight had no effect on the fast secondary relaxation (β_{fast}) appearing in higher frequencies. We observed the shape parameters for α -relaxation is changing with molecular weight whereas for secondary relaxations it is almost the same. The dielectric strength ($\Delta\epsilon_\alpha$) associated to for α -relaxation increases on average with decreasing molecular weight and this value decreases with increasing temperature for each amorphous sample. Besides the activation energy associated to α -relaxation decreases with decreasing molecular weight.

We studied also the crystallization behavior for OLA2700 at different crystallization temperatures and annealing times in **Chapter4**, in order to see the evolution of glass transition and melting temperature during the crystallization and obtain the crystallinity degree. The molecular dynamics of crystallized OLA2700 was investigated by using Flash DSC and DRS. Results obtained from both techniques almost match together. We observed the geometric confinement induced by crystals reduces the glass transition temperature,

fragility index and activation energy associated to α -relaxation. This reduction is more dominant at lower crystallization temperatures. According to our results, compared to the bulk PDLLA the Rigid Amorphous Fraction (RAF) is very small. At lower crystallization temperatures (which are near to the glass transition temperature) after a very long crystallization time the RAF reaches up to 15% and at higher crystallization temperatures (near to the melting temperature) the RAF is between 0-5%. Thus, in perspective, it will be interesting if we ask is there any connection between the aptitude of the system to form RAF and the existence of the three regimes in the T_g versus molecular weight curve? Generally in this work we could create crystals in our system with a very small amount of RAF compare to other polymers. Thus we could observe the effect of crystals in molecular dynamics separately without the disturbance of RAF.

Furthermore, we observed the secondary relaxations of crystallized OLA2700 were not affected by different crystallization temperatures.

With regard to polymer science, various investigations have been done to characterize the molecular mobility as a function of time and temperature at different scales. To go further in following researches, in order to investigate the α -relaxation at the minimum scale (from one to ten repeating monomer units), several simulation techniques can be done. Density Functional Theory (DFT) offers the opportunity to describe the motions occurring at the very fast scale and provides dataset that could be implemented in molecular dynamics approach to be able describing the molecular motions occurring at significantly slower scale (such as the α -relaxation).

Abbreviations List

M_W : Molecular weight	DRS: Dielectric Relaxation Spectroscopy
\bar{M}_n : Number average molecular weight	DSC: Differential Scanning Calorimetry
\bar{M}_W : Weight-average molecular weight	MT-DSC : Modulated Temperature DSC
K_{Cp} : Calibration factor	FSC : Fast Scanning Calorimetry
σ_0 : Ohmic conduction	TGA: ThermoGravimetric Analysis
$Z^*(\omega)$: Complex impedance	S_c : Configurational entropy
$\sigma^*(\omega)$: Electrical conductivity	VFT: Vogel-Fulcher-Tammann
$R^*(\omega)$: Electrical resistivity	$\varepsilon'(\omega)$: Real part of the permittivity
$M^*(\omega)$: Electrical modulus	$\varepsilon''(\omega)$: Imaginary part of the permittivity
$\Delta\mu$: Energy barrier	ΔS_{ex} : Excess entropy
T_g : Glass transition temperature	β_c : Cooling rate
T_f : Fictive temperature	β_h : Heating rate
T'_f : Limiting fictive temperature	E_a : Activation energy
T_α : Dynamic glass transition temperature	ξ_α : Characteristic length of α -relaxation
T_M : Melting temperature	D : Strength parameter
T_K : Kauzmann's temperature	β, γ, δ : Secondary processes
T_c : Crystallization temperature	α : Segmental relaxation
T_V : Vogel temperature	OLA : Oligomer of Lacric Acid
T_{ag} : Aging temperature	ξ : Cooperative length
t_c : Crystallization time	η : Viscosity
τ : Relaxation time	V_f : Free volume
τ_D : Debye relaxation time	ΔT_S : Static thermal lag
τ_{CC} : Cole/Cole relaxation time	ΔT_D : Dynamics thermal lag
τ_{CD} : Cole/Davidson relaxation time	R: Gas constant
τ_∞ : Relaxation time at infinite temperature	β_{JG} : Johary-Goldstein relaxation
τ_α : Relaxation time of α -relaxation	β_{fast} : Fast secondary relaxation
k_B : Boltzmann constant	β_{slow} : Slow secondary relaxation

CRR: Cooperative rearranging region	m : Fragility index
ΔC_p : Heat capacity step at a constant pressure	N_A : Avogadro number
C_p : Heat capacity at a constant pressure	ρ : Density
$C_{p,g}$: Heat capacity of the glass	ΔV^* : Activation volume
$C_{p,l}$: Heat capacity of the liquid	β_{KWW} : Stretch exponent
α_T : coefficient of thermal expansion	ε^* : Complex dielectric permittivity
κ : Compressibility	V_α : Cooperative volume at α -relaxation
RAF: Rigid Amorphous Fraction	N_α : Number of structural units in an average CRR
MAF: Rigid Amorphous Fraction	α_{HN} : Shape parameter describing the symmetric broadening factors of the dielectric spectra
CRF: Crystalline Rigid Fraction	β_{HN} : Shape parameter describing the asymmetric broadening factors of the dielectric spectra
ω : Angular frequency	X_{ma} : Amorphous phase fraction
PLA: Poly (lactic acid)	X_{ra} : Rigid amorphous fraction
R_{EE} : Root mean square end-to-end distance	X_C : Crystallinity degree
$E(\omega)$: Electric field	ΔH_m : Melting enthalpy
G_K : Kirkwood correlation factor	ΔH_m° : Melting enthalpy of a wholly crystalline material
$C_m^*(\omega)$: Complex capacity of the electrode	P: Period of oscillation
$\varepsilon_s^*(\omega)$: Complex permittivity of the sample	β : Scanning rate
$\varepsilon_{su}^*(\omega)$: Complex permittivity of the substrate	q: Heating rate
$\Delta\varepsilon$: Dielectric relaxation strength	m_T : Thermodynamic fragility
A: Modulation amplitude	
μ : Time-correlation function	
ε_∞ : Dielectric permittivity at high frequency limit	
ε_0 : Dielectric permittivity of vacuum	
$E_{\alpha,\alpha}$: Activation energy associated to the α -relaxation	

Résumé

Ce travail s'est concentré sur deux façons d'influencer les dynamiques moléculaires. Une façon était la modification de l'interaction intermoléculaire en réduisant la masse moléculaire moyenne en poids et une autre était la création de confinement par des cristaux dans un oligomère d'acide lactique. Ces voies ont conduit à diminuer la température de transition vitreuse, la fragilité et les énergies d'activation (associées à la transition vitreuse). Dans un oligomère d'acide lactique nous avons réussi à former des cristaux avec une très petite quantité de fraction amorphe rigide (RAF) ce qui nous a donné l'occasion d'observer l'effet de confinement pur induit par les cristaux en mobilité moléculaire (sans perturbation causée par la RAF).

Les dynamiques de la relaxation moléculaire en phase amorphe libre ou confinée par la phase cristalline, aussi bien localisées que coopératives, ont été étudiées sur une large gamme de fréquences et de températures, selon les approches typiquement utilisées pour étudier les liquides formateurs de verre.

Dans ce travail, plusieurs techniques expérimentales ont été utilisées: calorimétrie différentielle à balayage (DSC), calorimétrie à balayage différentiel avec modulation de température (MT-DSC), calorimétrie à balayage rapide (FSC) et spectroscopie de relaxation diélectrique (DRS).

Mots clés: dynamiques moléculaires, masse molaire, oligomères d'acide lactique, cristallisation, fraction amorphe rigide (RAF), confinement.

Abstract

This work focused on two ways to impact the molecular dynamics. One way was the changing intermolecular interaction by reduction the weight-average molecular weight (\bar{M}_w) and another way was the creation confinement by crystals in an oligomer of lactic acid. These ways led to decrease the glass transition temperature, fragility and activation energies (associated to glass transition). In an oligomer of lactic acid we succeeded to form crystals with a very small amount of Rigid amorphous Fraction (RAF) which gave us an opportunity to observe the pure confinement effect induced by crystals in molecular mobility (without disturbance of RAF).

The dynamics of molecular relaxation in the amorphous and crystalline phase, for both localized and cooperative, have been studied over a wide range of frequencies and temperatures, according to approaches typically used to study glass-forming liquids.

In this work, several experimental techniques have been used: Differential Scanning Calorimetry (DSC), Modulate-Temperature Differential Scanning Calorimetry (MT-DSC), Fast Scanning Calorimetry (FSC) and dielectric relaxation spectroscopy (DRS).

Keywords: molecular dynamics, molecular weight, oligomers of lactic acid, crystallization, Rigid Amorphous Fraction (RAF), confinement.

